UNIVERSITA' DEGLI STUDI DI NAPOLI FEDERICO II

SCUOLA DI MEDICINA E CHIRUGIA
AREA DIDATTICA DI FARMACIA E BIOTECNOLOGIE PER LA SALUTE

DOTTORATO IN SCIENZA DEL FARMACO

XXXIII CICLO 2018/2020

"CHEMISTRY AND PHARMACOLOGY OF STEROIDAL AND NON-STEROIDAL MODULATORS OF HUMAN RECEPTORS"

Dott.ssa Giuliana Baronissi

Tutor

Prof.ssa Simona De Marino

Coordinator

Prof.ssa Maria Valeria D'Auria

COLLABORATION

My research project was carried out under the supervision of Prof. Simona De Marino and Prof. Valentina Sepe.

The pharmacological evaluations were performed thanks to the collaboration with the group of Prof. Stefano Fiorucci (Department of Surgery and Biomedical Sciences, Perugia) whereas the computational studies thanks to the collaboration with the group of Prof. Vittorio Limongelli (Institute of Computational Science Center for Computational Medicine in Cardiology, Università della Svizzera Italiana)

Index

INDEX

ABSTRACT

Metabolic and inflammatory diseases, affecting the liver and gastrointestinal system, are very widespread and often their pathogenesis is still unknown. Because these disorders represent a growing global public health problem and the present therapies expose the patients to several side effects, there is increased interest in the development of new pharmacological tools that could provide new opportunities in the treatment of complex metabolic disorders in which several target pathways are involved. The main liver manifestation of metabolic disorders are: **NASH** (Non-Alcoholic SteatoHepatitis), caused by the accumulation of fat in the liver, and **PBC** (Primary Biliary Cholangitis) an autoimmune disease that causes damage to the small bile ducts.

In these pathologies, alterations of bile acid pool regulation have revealed a link between bile acid and metabolic homeostasis. The bile acid receptors farnesoid X receptor (FXR) and GPBAR1 both regulating lipid, glucose and energy metabolism, are today recognized promising targets for NASH and PBC. My research project was mainly focused on the design, synthesis and biological evaluation of small molecules as new modulators of human receptors involved in hepatic and metabolic diseases. Specifically, my research activity was addressed to the investigation of three major targets: the bile acids receptors (FXR and GPBAR1) and the cysteinyl leukotriene receptor 1 (CysLT$_1$R).

The obtained results can be summarized in the three main sections reported below according to the target of interest:

> **Discovery of 6-ethylcholane derivatives as potent bile acid receptor agonists with improved pharmacokinetic properties**

The nuclear receptor FXR has been proposed as a potential target for the treatment of various pathologies, such as cholestasis, hepatic steatosis, atherosclerosis,

dyslipidaemias, type 2 diabetes, non-alcoholic fatty liver disease (NAFLD) and non-alcoholic steatohepatitis (NASH).

Based on the previous results, extensive ligand/receptor binding studies, using the hGPBAR1 homology model and FXR crystal structure, allowed to elucidate the structural requirements for GPBAR1 and FXR recognition. These outcomes have paved the way for the rational design of a new generation of potent FXR ligands.

GPBAR1 has been recently demonstrated the physiological mediator of itching, a common symptom observed in cholestasis and the severity of this side effect limits the pharmacological utility of dual FXR/GPBAR1 agonists in the treatment of different cholestatic disorders. In this context, the discovery of new chemical entities endowed with selective agonistic activity on FXR represents a promising approach in the identification of new pharmacological protocols for the treatment of metabolic disorders. My project concerned the synthesis, starting from the 6-ethylcholane scaffold, of new small molecules as modulators of the nuclear receptor FXR.

These studies led us to identify compound **6** as a selective FXR agonist even if with reduced potency respect to 6-ECDCA (EC$_{50}$=0.5 μM) and compounds **1** and **3** which showed a dual activity (FXR/GPBAR1) but with improved pharmacodynamic and pharmacokinetic capabilities.

➤ **Synthesis of novel isoxazole derivatives with FXR agonistic activity**

In *vivo* acetaminophen (APAP) is one of the most prescribed drugs worldwide, but the misuse causes acute liver failure. Since FXR ligands have shown effective in reducing liver injury in some experimental, I have decided to elaborate the chemical structure of GW4064, the first non-steroidal agonist for FXR, in order to obtain a new library of isoxazoles endowed with FXR agonistic activity.

Compound **28** was the most effective FXR agonist of the library (EC_{50} = 0.30 ± 0.006 µM). This compound was orally active and rescued mice from acute liver toxicity caused by APAP overdose.

> ➢ **Development of dual CysLT$_1$R and GPBAR1 modulators**

In order to develop multitarget drugs for the treatment of various metabolic diseases such as type 2 diabetes, fatty liver disease, dyslipidemia and inflammatory states affecting the enterohepatic system, we have decided to explore if there is a possible cross-talk between CysLT$_1$R antagonists and the two bile acid receptors FXR and GPBAR1. New evidence suggests that cysteinyl leukotriene receptor type 1 (CysLT$_1$R) is a critical signaling molecules implicated in the immune response, cell proliferation, inflammation regulation and intestinal barrier maintenance. Recently, a selected group of CysLT$_1$R antagonists was tested on FXR and GPBAR1 by my research group. Results showed that REV5901 was effective as GPBAR1 agonist attenuating inflammation and immune dysfunction with an EC_{50} of 2.5 µM. None of the tested compounds exhibited activity on FXR. Therefore, in order to obtain a new library of compounds with improving CysLT$_1$R antagonist/GPBAR1 agonist dual modulation, we have decided to synthetize a new library of compounds preserving the quinoline ring of REV5901 and modifying the substituents on the benzene ring. In *vitro* and in *vivo* assays showed that the most effective in modulating the two receptors, were compounds **44** (IC_{50} = 2.8µM and EC_{50} = 3µM, respectively) and **45** (IC_{50} = 1.2µM and EC_{50} = 7.4µM, respectively).

These results could be a starting point for the development of new drugs for the treatment of metabolic and inflammatory diseases.

CHAPTER 1

INTRODUCTION

1.1. Drug Discovery

For centuries, the main objectives of the human being have been the survival of the species and the cure of the pathologies that can afflict it. For this reason, herbs and natural extracts have always been used for healing purposes. Over the centuries, improved techniques and technologies allowed not only to discover new molecules, but also to synthesize new ones from scratch. The process that has been used to identify new compounds useful for the cure and the treatment of various pathologies is called "drug discovery".[1] (Figure 1)

The whole process starts by studying a disease-related target molecule, then it proceeds by designing a molecule able to interact with the identified target, and thus able to possibly cure the pathology. The identification of the type of interaction between two chemical structures (a ligand or small molecule and a protein) is essential to correctly design and develop a new drug.
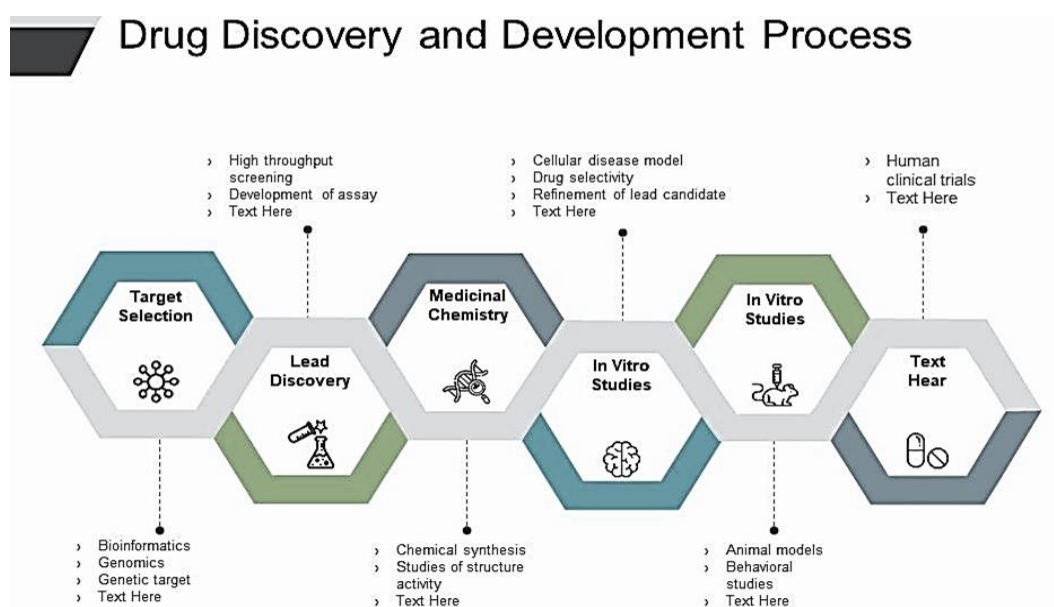

Figure 1. Drug discovery process

The process consists of several stages:

- Target identification and validation

- HIT and lead identification.

- Synthesis and Lead optimization

- Pre-Clinical testing (*in vitro* and *in vivo* assays)

- Clinical testing (on human)

Target identification begins with the discovery of a possible therapeutic drug target and understanding its role in the pathogenesis. Typically, a potential target is a single molecule such as a gene or protein that is involved in a particular physio-pathological pathway. Once the target is identified, one must always assess its role in a specific disease to demonstrate its potential therapeutic value.

Drug design is a very useful approach for the creation of a drug, which is designed, on the basis of its biological target, generally a key molecule of the process that must be stopped or regulated or, in the case of an infectious disease, an essential element for the replication of the bacterium or virus.

There are two types of drug design approaches; one is called "rational drug design" and the second is called "structure-based drug design"[2].

Rational drug design (RDD) is a method utilized in biopharmaceutical to find and develop new drug compounds. RDD employs several computational methods to spot novel compounds. Computational chemistry is a branch of chemistry that assists and tries to solve chemical problems through software and computer simulation. This branch uses theoretical chemistry together with softwares to calculate and predict the structures and interactions of molecules with the receptors, in order to identify small library of compounds, which can be possible ligands of that receptor.[2]

Structure-based drug design (SBDD) is one of the primary techniques to be utilized in drug design. Drug targets are, usually, proteins and enzymes involved in specific metabolic pathway; therefore SBDD allows the development of new compounds via the prediction of a 3D structure of the targets.[2]

The next phase, the HIT and lead identification, consists in the discovery of a small molecule that can modulate the functions of the chosen target. This phase is followed by the synthesis and optimization of the identified LEAs (third stage).

The optimization mainly concerns the improvement of properties including selectivity and affinity towards the target and synthetic feasibility. Docking techniques could facilitate the understanding and the prediction of the pharmacodynamic and pharmacokinetic parameters, such as absorption, distribution, metabolism, and excretion (ADME). The lead must be evaluated using specific animal/cellular models for the pathology under study. *In vitro* studies are carried out using cellular models, and subsequently *in vivo*, thanks to the use of animal models. (usually guinea pigs and mice)[2]

In clinical trial human volunteers participate in tests on a particular drug. During the clinical phase, the investigators called patients with certain prerequisites, administer the treatment(s), and gather information on the patients' health for a precise period. If the drug overcomes all these phases and receives permission from the food and drug administration (FDA), it will be introduced on the market while the pharmacovigilance phase begins. All adverse and non-adverse effects that were not foreseen during the clinical phases are recorded. The drug is taken off the market whether its side effect proved to be severe and dangerous.

1.2. Metabolic and inflammatory diseases and their targets

1.2.1. PBC and NASH

The metabolic syndrome is not a disease with an unifactorial etiology, but a clinical condition characterized by several predisposing elements that greatly increase an individual's probability for developing non-alcoholic steatohepatitis, type 2 diabetes, atherosclerotic cardiovascular disease, as well as other liver conditions. **NASH** (Non-Alcoholic SteatoHepatitis) and **PBC** (Primary Biliary Cholangitis) could be defined as the liver manifestation of a metabolic disorder and similarly to metabolic syndrome, many targets are involved in the pathogenesis of the disease. Currently, the therapies must aim to interrupt one or more processes involved in the progression of the disease.

Primary biliary cholangitis (PBC), known as primary biliary cirrhosis, is a liver autoimmune disease[3,4,5] caused by a progressive deterioration of the small bile ducts, that determines bile accumulation in the liver (cholestasis). Further slow damage tissue can lead to fibrosis, and eventually cirrhosis. The most common symptoms are pruritus, which can become so severe as to invalidate the patient, and fatigue, which however is not a specific symptom. More severe stages of the disease can lead to jaundice (yellow eyes and skin).[6] However, some patients could be asymptomatic. Sometimes people with PBC could also show signs of extrahepatic autoimmune disorder such as thyroid disease or rheumatoid arthritis or Sjögren's syndrome.[7,8] PBC is a quite rare disease and can affect up to 1 in 3,000–4,000 people.[9,10] The condition has been discovered since 1851,[11] but only in 2014 the name was changed to "primary biliary cholangitis", because it emerged in advanced disease cirrhosis.[12,13]

PBC stages	Histological findings
Stage 1	Connective tissue abnormality and/or inflammation restricted to the portal areas
Stage 2	Fibrosis and/or inflammation restricted to the portal and periportal areas
Stage 3	Bridging fibrosis
Stage 4	Cirrhosis

Figure 2. Stages of PBC

Several studies have demonstrated the role of IL12 signaling cascade in the manifestation of the disease, and of several genes in the regulation of cytokines such as TYK2, SH2B3 and TNFSF11.[14,15]

A genetic predisposition to PBC has been demonstrated to be an important factor; indeed, cases of PBC in family members and identical twins are very common. A study identified a gene -POGLUT1- that seems to be associated with this pathology.[16] Its pathogenesis is still unknown and for this reason is very difficult to find a specific treatment. Currently, treatments for PBC are still in development.

Non-alcoholic steatohepatitis (NASH), is a type of non-alcoholic fatty liver disease (NAFLD) associated to liver inflammation.[17,18,19] The primary characteristic of NAFLD and NASH is the accumulation of lipids in the liver.[20] However, the mechanisms are complex and incompletely understood.[20,21,22,23] NAFLD and NASH are the most common liver diseases worldwide and are present in 25% of population.[20] In Europe, these pathologies, affected, approximately, about 20% to 25% of people.[23] Obesity and unhealthy lifestyle are considered a high risk factor for NASH.[19,24]

People suffering from this disease may be asymptomatic,[18,25] anyhow there can be some cases manifesting fatigue, steatosis, malaise, liver injury and abdominal pain and in advanced cases it can include portal inflammation, polymorphonuclear cell infiltrates,

Mallory bodies, apoptotic bodies, clear vacuolated nuclei, microvesicular steatosis, megamitochondria, and perisinusoidal fibrosis.[26] (Figure 3)
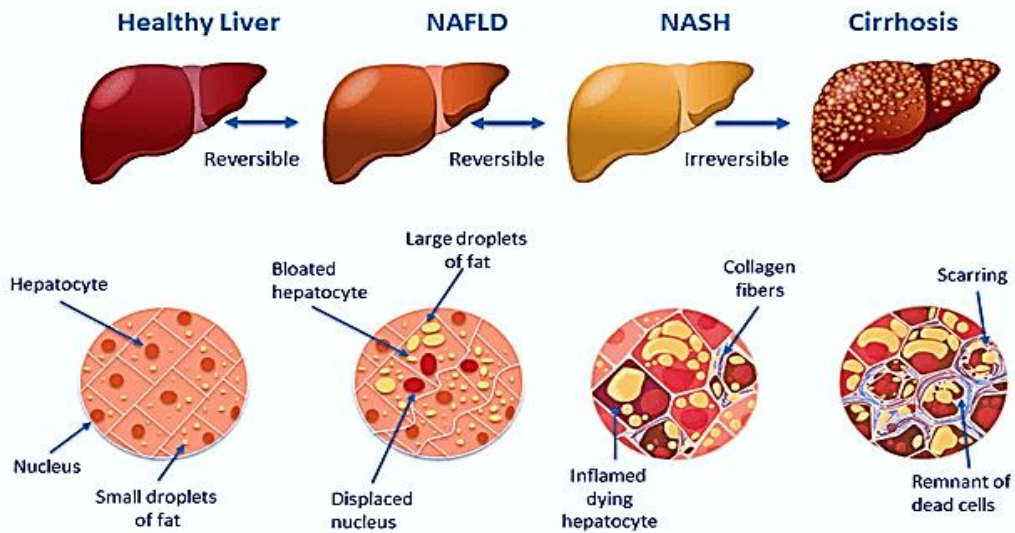

Figure 3. Stages of NAFLD

NASH increases hepatocyte death via apoptosis and is also associated with, or could cause, type 2 diabetes, insulin resistance, metabolic syndrome and hormonal disorders.[27,28,29,30,31,32,33]
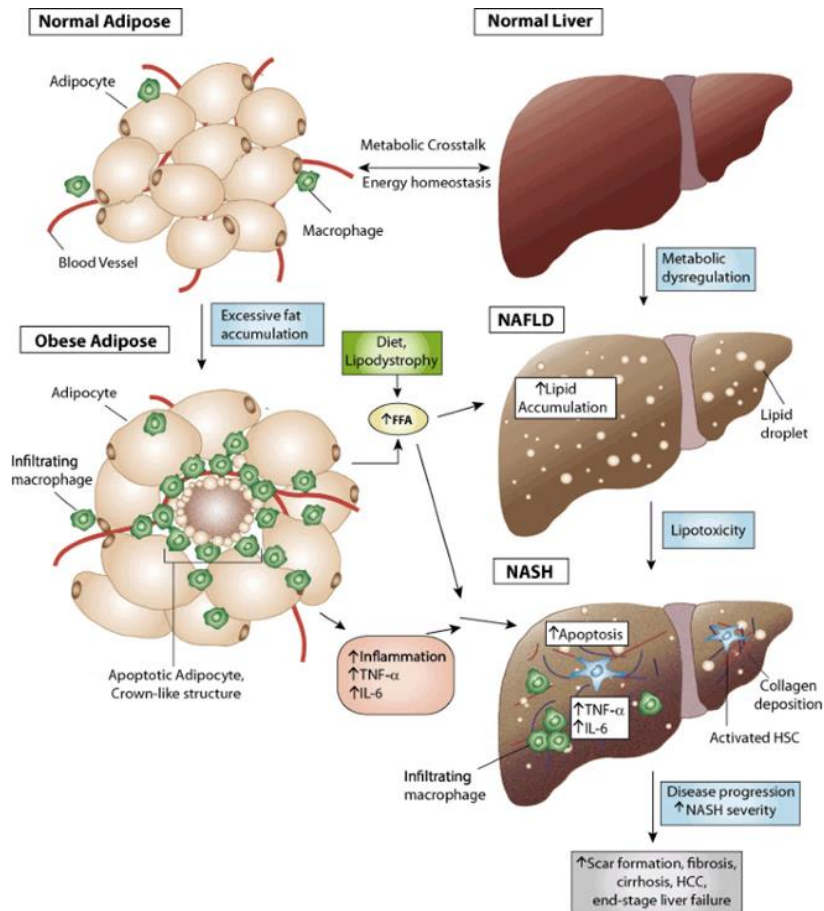
Figure 4. Mechanisms that cause NASH[34]

This disease has a genetic component; indeed, members of a family with a NASH patient have a higher risk of fibrosis.[35] Two genetic variations are associated with NASH: non-synonymous single-nucleotide polymorphisms (SNPs) in PNPLA3 and TM6SF2. Their presence is not only related to the manifestation of the disease but also to its severity. However, their role in the pathogenesis remains unclear.[32,36] It would appear that NASH is caused by the accumulation of fat in the liver in patients with Non-alcoholic fatty liver (NALF), which causes the production of cytotoxic lipid derivatives that cause a toxic necrotizing inflammation typical of NASH. This inflammation, in turn, causes scar tissue to appear on the liver (fibrosis), which can, then, lead to cirrhosis and irreversible liver damage.[37] (Figure 4)

The main drugs used in these pathologies improve metabolic functions, reduce steatosis, decrease inflammation, and stop or reverse the progression of fibrosis. However, the use

of therapies that act on several fronts is expected to be the most useful in these diseases, intervening on different pathways in order to slow down or reverse the progression of the disease.

For the treatment of NASH and PBC, many types of targets have been studied and are still being studied, such as Farnesoid-X-Receptor, GPBAR1/TGR5, PPARs, Glucagon-like Peptide-1 Receptor or Apoptosis Signal-Regulating Kinase 1.[38] (Figure 5)

- Glucagon-like peptide-1 receptor (GLP1R) involved in the metabolism of sugars

- Peroxisome proliferator-activated receptor (PPARs) implicated in lipids metabolism

- Apoptosis signal-regulating kinase 1 (ASK1) involved in inflammation and fibrosis

- The bile acid receptors: Farnesoid-X-Receptor (FXR) and Type 1 bile acid receptor coupled to G protein (GPBAR1) implicated in cholesterol, glucose metabolism and inflammation.
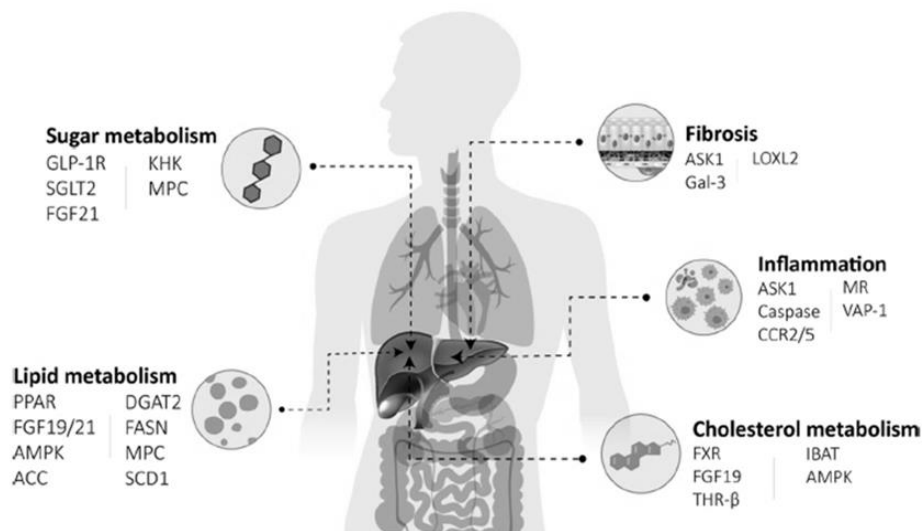

Figure 5. Targets involved in liver diseases[51]

The glucagon-like peptide-1 receptor (GLP1R), protein expressed by pancreatic beta cells and neurons, controls blood sugar level by stimulating insulin secretion. The gene

GLP1R on chromosome 6 is responsible for expression of this protein.[39,40] GLP1R is a G protein-coupled receptor[41] and consists of two domains, one extracellular (ECD)[42] and one transmembrane (TMD).[43,44,45,46] On the TMD domain there is a polar residue that regulates the signalling of the receptor[44] while the transmembrane helical boundaries[47] and extracellular surface are a trigger factors for agonism.[45]

GLP1R is expressed in pancreas beta cells and his activation stimulates the adenyl cyclase pathway which leads to the increase of the insulin synthesis and his release in the blood circle.[48] Consequently, GLP1R has been a target for the development of drugs for the treatment of diabetes mellitus.[49]

The peroxisome proliferator-activated receptors (PPARs) are a family of nuclear receptors that work as transcription factors.[50] PPARs are very important in cellular differentiation, development, and metabolism of carbohydrate, lipid and protein[51] and tumorigenesis.[52,53,54]

All PPARs heterodimerize with the Retinoid-X-Receptor (RXR) and bind to specific DNA sequences, named PPREs (peroxisome proliferator hormone response elements). These sequences are in the promoter region of a gene, and, when the PPAR binds its ligand, the transcription of the targeted genes is increased or decreased. The function of PPARs depend on their ligand-binding domain shape, on several coactivator and corepressor proteins.[55] Endogenous ligands of PPARs are free fatty acids and Vitamin B3.

Apoptosis signal-regulating kinase 1 (ASK1) known as mitogen-activated protein kinase-kinase-kinase 5 (MAP3K5) is a kinase belonging to the group of MAP. In response to a stress, such as oxidative stress or calcium influx c-Jun N-terminal kinase (JNK) and p38 mitogen-activated, protein kinases are activated. ASK1 seems to be involved in cancer, diabetes, rheumatoid arthritis, cardiovascular and neurodegenerative diseases.[56,57]

Under physiological conditions, ASK1 is oligomerized, through its C-terminal coiled-coil domain (CCC) but remains in an inactive form thanks to the reduction of thioredoxin (Trx), calcium and integrin binding protein 1 (CIB1).[58] Trx inhibits ASK1 kinase activity directing the bonds towards its N-terminal coiled-coil domain (NCC). Trx and CIB1 regulate ASK1 activation through a redox- or calcium-reaction, respectively. Both seems to compete with TNF-α receptor-associated factor 2 (TRAF2), an activator of ASK1. ASK1 gene transcription can be induced by inflammatory cytokines such as IL-1 and TNF-α.[57]

Bile acid receptors: FXR and GPBAR1. As concerning the nuclear receptor FXR and the membrane receptor GPBAR1, a detailed description is reported in the next chapter, since these receptors are the main targets of the first part of my PhD project.

1.2.2. Inflammatory Bowel Disease (IBD)

The gastrointestinal tract is always exposed to a vast number of antigens present in food or bacteria. In physiological condition, the homeostasis is maintained by suppressing the immune responses to this type of antigens. Among the many pathologies that can affect the gastrointestinal tract, the object of my research was the inflammatory bowel disease. **Inflammatory bowel disease** (IBD) is an idiopathic disease caused by chronic inflammation of the gastrointestinal tract, that can lead to rectal bleeding and weight loss. The two major forms of IBD are **ulcerative colitis** (UC) and **Crohn's disease** (CD).[59] (Figure 6)
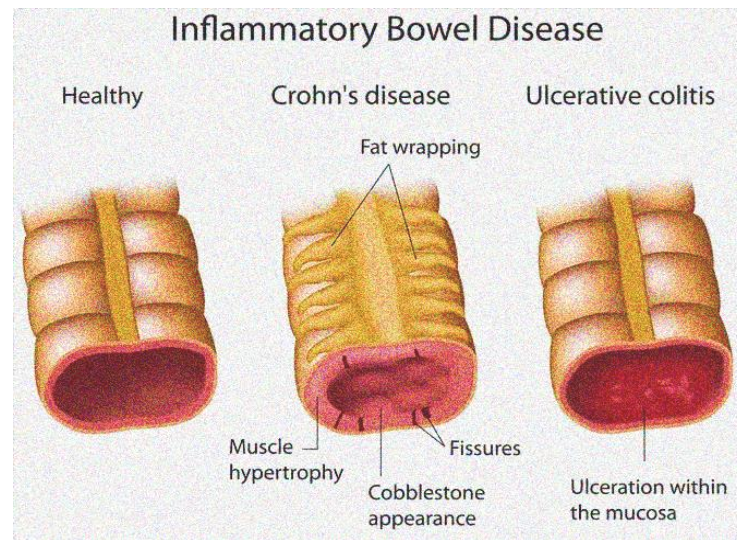

Figure 6. Tissues damage in IBD[60]

These chronic intestinal diseases are characterized by strong inflammation that can cause the destruction of the organ tissue. Over recent decades the incidence of IBD has been rising and it has become increasingly common in Asia, Europe and North America[61]. The pathological process of IBD doubtless involves complex interactions among genetic factors, immunological factors and environmental triggers[62]. Recent study suggests that a pathologic activation of the mucosal system in response to antigens may be a key issue in the pathological process of IBD. In patients with IBD, a loss of immune tolerance happens to some commensal bacterial antigens including

alterations in T-cell regulation that leads to backsliding chronic inflammation[63,64]. There seem to be distinct pathways of inflammation in Crohn's disease and ulcerative colitis.
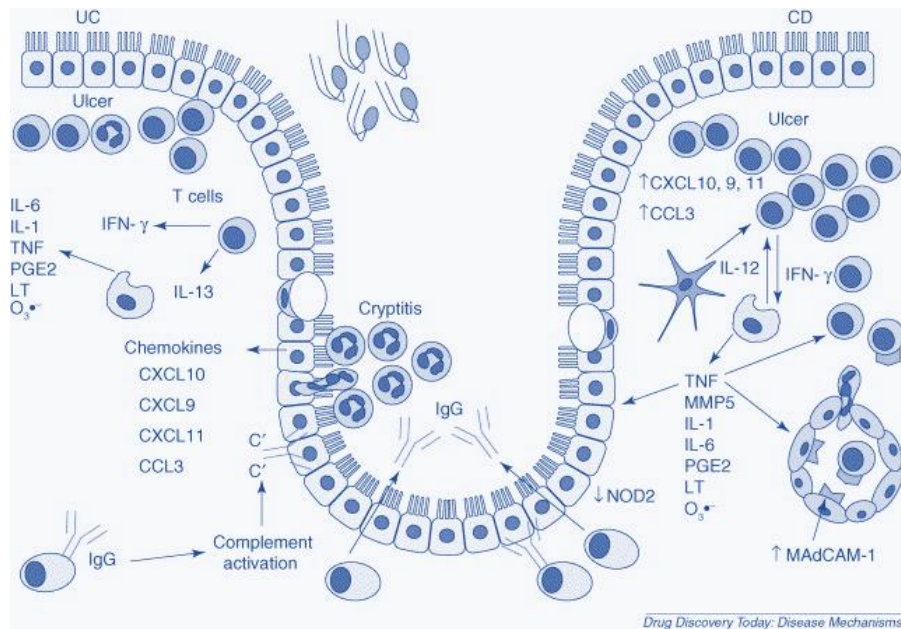

Figure 7. Mechanism of IBD[65]

As shown in Figure 7 in patients with Crohn's disease, protein models expressed by tissue layer lymphocytes tend to be in line with a T-helper-1 (Th1) response, together with associate early increase within the expression of antiviral (IFN), IL-2 and IL-12, followed by a succeeding increase in mortification tumor factor-α (TNF-α) and IL-18[66]. Moreover, there additionally seems to be a compensative increase in IL-10 and transformation levels of protein β (TGF-β). In patients with ulcerative colitis, the protein expression pattern differs from that seen in inflammatory bowel disease, with inflated expression of IL-5, IL-6, IL-10 and IL-13[65]. Although many studies have been performed to identify the factors that cause IBD, its pathogenesis is still unclear. Current medical care of IBD is neither sufficient nor disease-modifying. Long-term treatment with non-specific anti-inflammatory drugs is often associated to serious side effects[67].

However, the homeostasis of the gastrointestinal tract is regulated by several receptors, that play a large number of roles stretching from nutrient uptake, regulation of epithelial intestinal cell integrity to shaping of the intestinal immune cell repertory.[68,69] Recently many receptors have been confirmed as potential targets for the treatment of these pathologies. Some studies have shown that G-protein coupled receptors may play a role in the treatment of IBD. In fact, all G protein coupled receptors are a critical signaling receptors implicated in the immune response, cell proliferation, regulation of inflammation and intestinal barrier maintenance.[70,71]

Some studies have shown that many receptors involved in inflammatory process, could be potential targets for the treatment of IBD.

In particular, the **cysteinyl leukotriene receptor 1** (**CysLT$_1$R**), belonging to the G-protein-coupled receptor family, was shown to be involved in the inflammatory process and therefore useful for the treatment of IBD.

1.3. Bile acids receptors: FXR and GPBAR1

The **Farnesoid X Receptor** (FXR) (Figure 8) is a nuclear hormone receptor isolated for the first time in 1995[72] through the YAC (Yeast Artificial Chromosome) cloning system and subsequently identified, together with the GPBAR1 receptor, as a bile acid receptor. It is coded in humans by the NR1HA gene and is particularly expressed in the liver, intestine and adrenal tissues.

Figure 8. Farnesoid-X-Receptor (FXR)
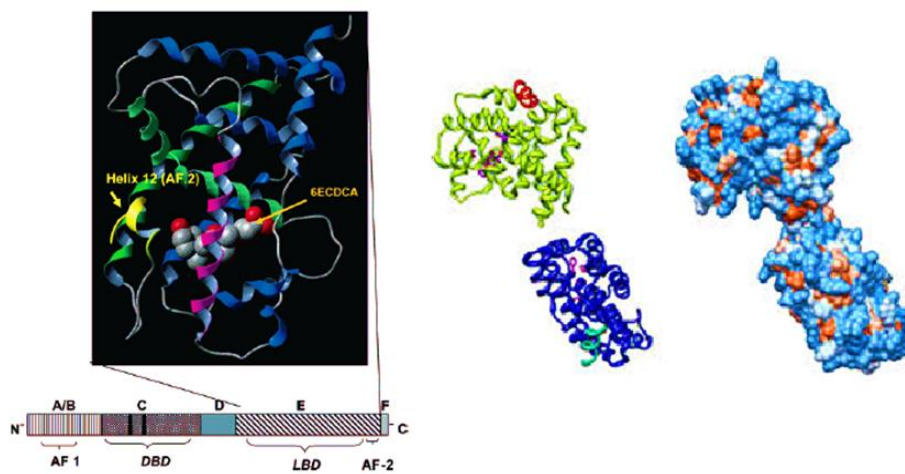
Currently two FXR genes have been identified: FXRα which in humans encodes four receptor isoforms that differ for the promoter and FXRβ which in humans is a pseudogene but has a role as a sensor of lanosterol levels in rabbits and dogs.[73]

FXR is a hetero-dimeric receptor and binds to specific DNA responsive elements (FXRE) in complex with the Retinoic-X-receptor (RXR). (Figure 9)
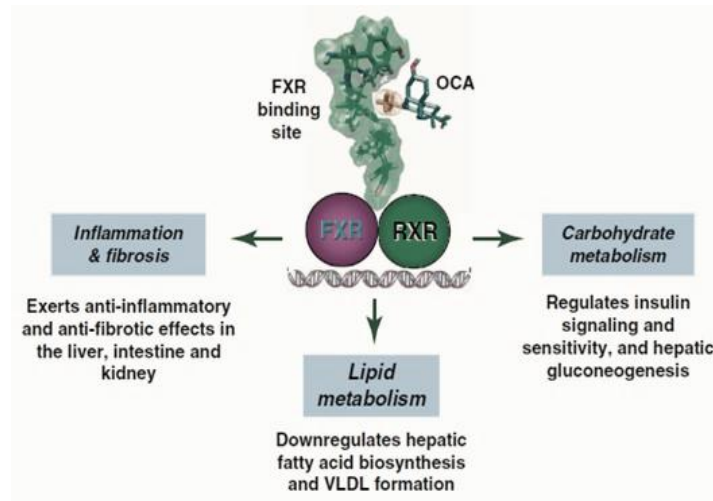
Figure 9. FXR activity

In the absence of a ligand this complex is associated with several co-repressors (such as N-CoR). In the presence of an endogenous ligand, i.e., a bile acid, a conformational change allows the release of co-repressors and the recruitment of co-activators such as the coactivator-1 (SRC-1) with consequent recognition of sequences on the promoter of specific genes (Figure 10). FXR is a very interesting and promising target being involved in many patho-physiological processes. Its main activity is to inhibit, once activated, the synthesis of bile acids through the indirect inhibition of the expression of the enzyme CYP7A1, which catalyses the reaction limiting the cholesterol metabolism.

The inhibition of the CYP7A1 enzyme is indirect, because the activation of FXR induces the expression of another nuclear receptor, small heterodimer partner (SHP),[74] an atypical NR lacking a DNA-binding domain, which induces a decrease of CYP7A1 expression/function and the repression of bile acid synthesis. SHP interacts with the LRH-1 (Liver Homolog Receptor-1) and HNF4α receptors in heterodimeric form, preventing their interaction with the consensus sequences in the CYP7A1 gene promoter, and inhibiting the basal transcription of the target gene.

The intestinal activation of FXR increases the expression and the release of fibroblast growth factor (FGF-19)[75] which binds FGF-R4 (FGF receptor) receptor with consequent

inhibition, in the hepatocytes, of CYP7A1 gene and therefore a subsequent reduction of bile acid synthesis, circulation of cholesterol, glucose and triglycerides (Figure. 10).
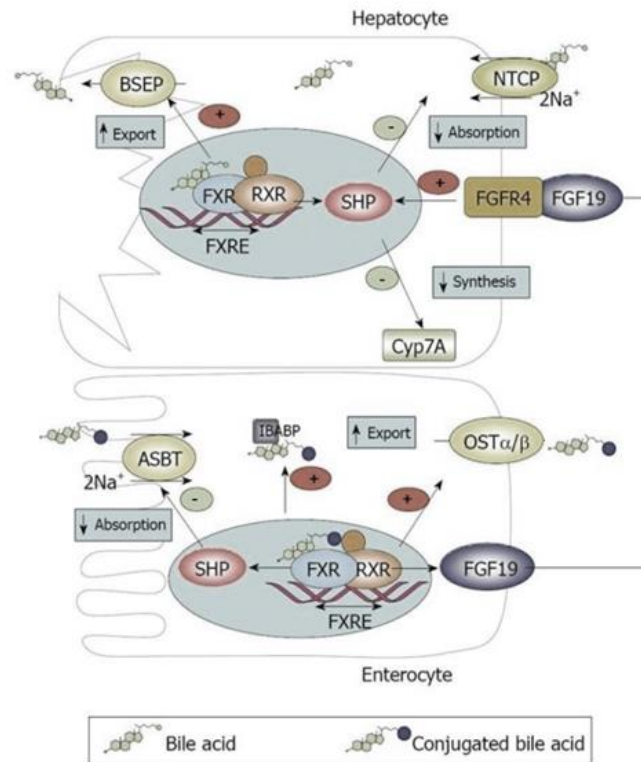

Figure 10. FXR mechanism of action

FXR is involved in cholesterol homeostasis by reducing the amount of circulating HDL by inhibiting the membrane transporter called ATP-binding cassette-A1 (ABCA1) through post-transcriptional modifications mediated by non-coding RNA segments called micro-RNA, thanks to the intervention of miR-144. FXR ligands induce overexpression of these micro-RNAs which reduce the expression of ACAB1 and consequently the transfer of cholesterol to apoproteins, with ApoA-I, to decrease the blood circulation of HDL. Therefore, FXR activation could exert benefic effects in the treatment of atherosclerosis and liver diseases such as liver steatosis.[76]

FXR is also involved in the regulation of the enterohepatic circulation of bile acids to prevent their accumulation in the cells. When activated it stimulates the transcription of proteins involved in the transport of bile acids from the inside to the outside of the cell

(BSEP and OSTα-OSTβ)[77] and simultaneously inhibits the synthesis of proteins that instead stimulate their uptake (NTPC, ABST, OATPs)[78]. FXR ligands have shown positive effects in the treatment of cholestasis.

In addition, many studies have shown that FXR is involved in the hepatic metabolism of carbohydrates[79], in the inhibition of the synthesis of pro-inflammatory cytokines[80] and also in tumorigenesis, both as a tumour suppressor and as an oncogene[81]. Due to its different physiological effects, FXR has been proposed as a potential target for the treatment of various pathologies, such as cholestasis, hepatic steatosis, atherosclerosis, dyslipidaemias, type 2 diabetes, non-alcoholic fatty liver disease (NAFLD) and non-alcoholic steatohepatitis (NASH)[82,83]. FXR can inhibit the transcription of the gene of NF-κB (nuclear factor kappa-light-chain-enhancer of activated B cells) and for various pro-inflammatory cytokines. Therefore, FXR has been identified as a target for the treatment of liver and intestinal inflammation and liver fibrosis.[80,84]

For these reasons, FXR ligands have demonstrated beneficial effects in the treatment of several liver disorders, including various types of cholestasis and steatosis due to his role in the regulation of glucose homeostasis, through regulation of gluconeogenesis and glycogenolysis.[51]

The **GPBAR1** receptor (Type 1 bile acid receptor coupled to G proteins) (Figure 11), also known as TGR5, is a seven transmembrane metabotropic receptor. It is mainly expressed in the spleen, gallbladder, liver, kidney, small intestine and adipose tissue.[85]

It pairs with a G protein and the binding of a ligand resulting in the activation of the adenylate cyclase with a subsequent increase of intracellular concentration of cAMP.
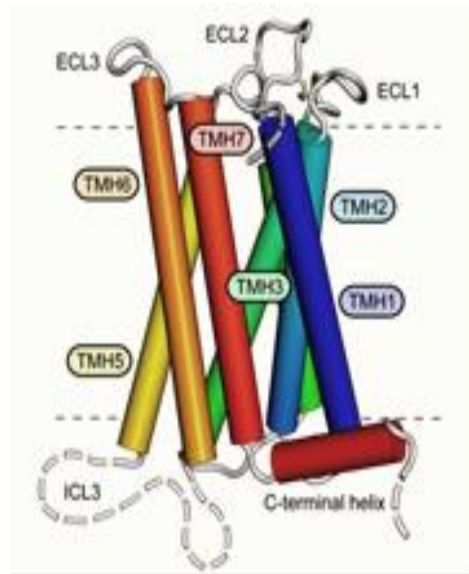
Figure 11. GPBAR1-TGR5

The cAMP activates the protein kinase A (PKA), a kinase capable of phosphorylating various substrates including the transcription factor CREB which in turn transmigrates in the nucleus where regulates the expression of specific genes involved in lipid and glucidic homeostasis and in inflammatory processes (Figure 12).

Figure 12. GPBAR1 activity[86]

In the intestine, GPBAR1 is highly expressed in entero-endocrine L-type cells, where induces the release of glucagon-like hormone (GLP-1), an incretin that binds a specific

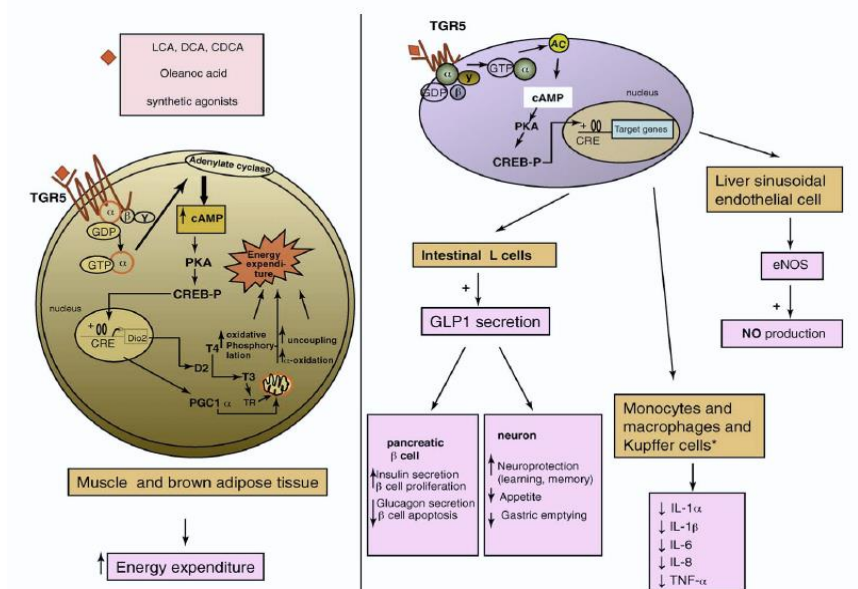receptor of β-pancreatic cells and determines the release of insulin, thus controlling post-prandial blood sugar.[87] In the brown adipose tissue and skeletal muscle, GPBAR1 controls the energy expenditure and cellular metabolism by stimulating the activity of iodothyronine deiodinase enzyme (D2), an enzyme that induce the T4 hormone conversion in corresponding activated form (T3).[88]

In the liver GPBAR1 is not directly expressed by the hepatocytes but is localized in the sinusoidal endothelial cells and in the Kupffer cells.[89] In the endothelial cells, this receptor is able to stimulate the activity of the endothelial nitric oxide synthase enzyme (eNOS) which converts L-arginine to L-citrulline with the release of nitrogen monoxide that induces vasodilatation regulating blood pressure. It is also involved in inflammatory processes, regulating vascular permeability and the expression of adhesion molecules on the endothelial surface, such as the ICAM-1 protein.[90] It has been suggested that GPBAR1 stimulates the activity of eNOS enzyme through a cAMP / PKA-dependent intracellular pathway.[91] More recently, different studies have demonstrated that the activation of the enzyme takes place through an intracellular Akt/Ca^{2+}-dependent pathway.[89]

In Kupffer cells, the hepatic macrophages, GPBAR1 reduces cellular reactivity and the production of pro-inflammatory cytokines (IL-6, IL-8 and TNF-α).[89] It is also able to inhibit the biosynthesis of bile acids and the accumulation of triglycerides in the liver[88] and the synthesis of important inflammatory mediators such as the NF-κB factor, which is involved in liver inflammation.[92]

GPBAR1 is localized in peptidergic neurons of the dorsal ganglion, where it appears to be involved in the regulation of itching and analgesia.[93]

Collectively, these findings have prompted the development of dual GPBAR1/FXR agonists as a new frontier in the pharmacological treatment of liver diseases, hyperlipidemia, and diabetes mellitus type 2. However, the concomitant activation of both

receptors endorses with potential side effects, and therefore, the discovery of highly selective FXR or GPBAR1 agonists is therapeutically attractive for a large cluster of human diseases.

1.4. Cystenil Leukotriene Receptors

$CysLT_1R$ and $CysLT_2R$, the two isoforms of the CysLT receptor, are metabotropic receptors coupled with G protein with seven transmembrane domains. The affinity scale for leukotrienes is different for the two receptor subtypes: LTD4 >> LTE4 = LTC4 for $CysLT_1R$[94] and LTC4 ≥ LTD4 = LTE4 for $CysLT_2R$.[95] The G protein coupled to $CysLT_2$ is a Gq protein, whereby the activation of the receptor determines an increase in the intracellular concentration of Ca^{2+} ions. On the other hand, the G protein coupled to $CysLT_1$ is tissue-dependent determining different intracellular signalling pathways and can be a Gq protein, causing an increase in the intracellular concentration of Ca^{2+} ions, or a Gi protein, determining a cAMP intracellular level reduction.[96] The $CysLT_1$ receptor (Figure 13) is particularly expressed in the lung, pancreas, colon, liver, intestine and heart and lymphocytes[94] whereas the $CysLT_2$ is expressed in the lung, brain, heart, kidney and adrenal glands.[97]
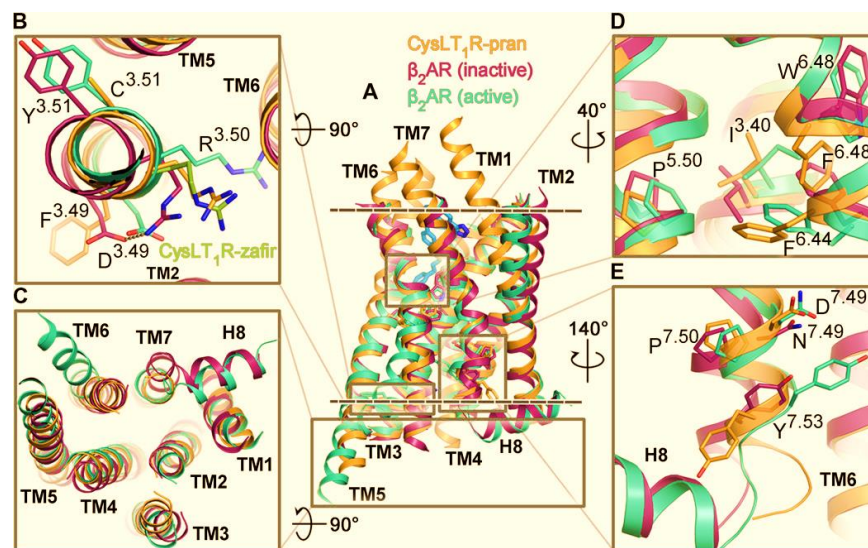

Figure 13. $CysLT_1R$ structure[98]

These receptors perform different biological functions and are involved in various chronic inflammatory diseases. $CysLT_1$ receptor has a bronchoconstrictor action, stimulates the secretion of the exocrine glands, induces contraction of the gastrointestinal and is

involved in chemotaxis, while $CysLT_2$ mainly performs a vasoconstrictor action and increases vascular permeability with consequent development of the oedema. An interesting effect of the $CysLT_1$ receptor is represented by the involvement in inflammation and intestinal carcinogenesis.

Activation of $CysLT_1$ by leukotrienes (Figure 14), especially by LTD_4, leads to the activation of Akt / PKB and the small GTPases Rho and Rac, which inhibits the glycogen synthase kinase-3β (GSK-3β). Consequently, the GSK-3β, APC, axin and cytosolic β-catenin complex is degraded. The β-catenin free, thus, enters the nucleus and activates the gene expression of different targets such as COX-2, and in the progression of the cell cycle, such as c-Myc and cyclin D1. Moreover, the $CysLT_1$ receptor regulates cell proliferation thanks to the activation of a protein kinase Cα (PKCα) and simultaneous activation of the mitogen-activated protein kinase (MAPK)/extracellular signal-regulated kinase (Erk) pathways, which activate different transcription processes. (Figure 14)[99]

CysLT receptors are already used as a target for the treatment of chronic inflammatory diseases such as asthma and have also been identified as potential targets for the treatment of intestinal and liver inflammation.[95,100]
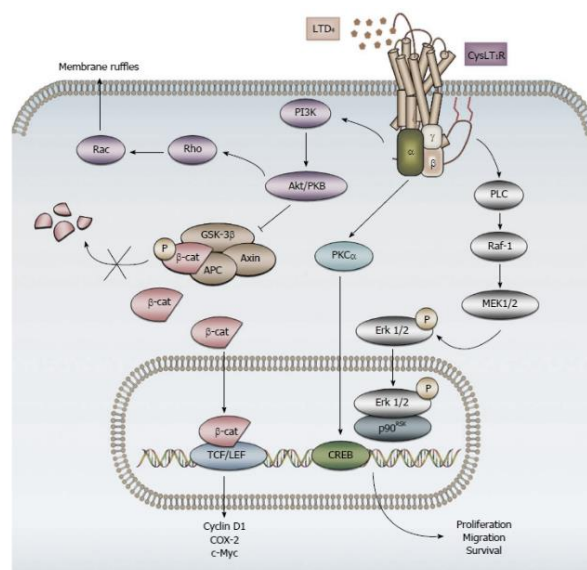

Figure 14. Mechanism of activation of $CysLT_1R$ by LTD_4[100]

1.5. Ligands of FXR and GPBAR1 Receptors

1.5.1. Steroidal Ligands

Bile Acids (BAs) are the endogenous ligands of FXR and GPBAR1 receptors.

They are polar molecules produced by cholesterol and represent about 12% of bile.

From a structural point of view, they are characterized by a cyclopentanoperhydrophenanthrene core (Figure 15a) with two methyl groups at positions 10β and 13β and a truncated side chain at C17 ending with a carboxylic group, generally ionized at pH 7.[101] All bile acids possess, on the tetracyclic nucleus, one or more hydroxyl groups at C-3, C-6, C-7 or C-12 position (Figure 15a).

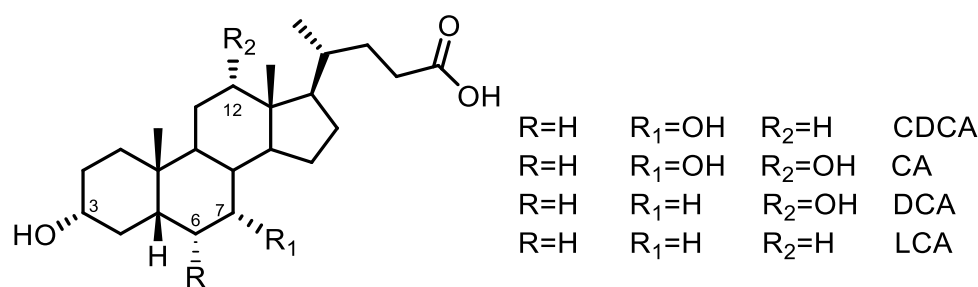|			
R=H	R_1=OH	R_2=H	CDCA
R=H	R_1=OH	R_2=OH	CA
R=H	R_1=H	R_2=OH	DCA
R=H	R_1=H	R_2=H	LCA

Figure 15a. Structures of endogenous bile acids

BAs differ from natural steroids for the presence of a *cis* junction between the A and B rings. This structural feature confers a "bent form" to the ring A which is not coplanar with rings B-C and D.[102]

Therefore, is possible to identify two faces: a hydrophilic face, in which the hydroxyl groups and the carboxylic group are on the same side (Face α), and a hydrophobic face in which we find the methyl groups (Face β) (Figure. 15b).
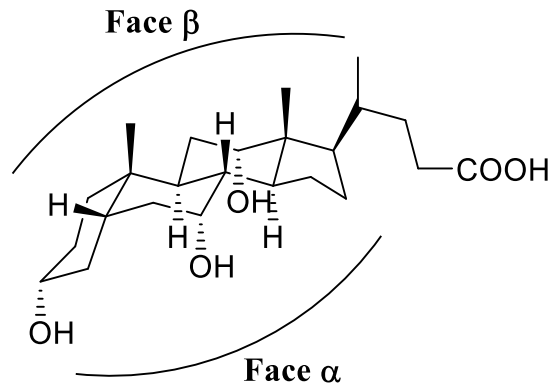
Figure 15b. Three-dimensional arrangement of bile acids

In aqueous solution, due to their amphipathic nature, they are organized in structures called micelles (Figure. 16) composed by a hydrophilic head positioned outside in contact with the aqueous solution and a hydrophobic tail positioned inside so that hydrophobic molecules can be solubilized.

Indeed, the bile acids allow the absorption in the intestine of fat-soluble vitamins, such as vitamin A, D, E and K[103,104] and lipids ingested from the diet. In the gallbladder the micelles help to solubilize the cholesterol avoiding the formation of stones.
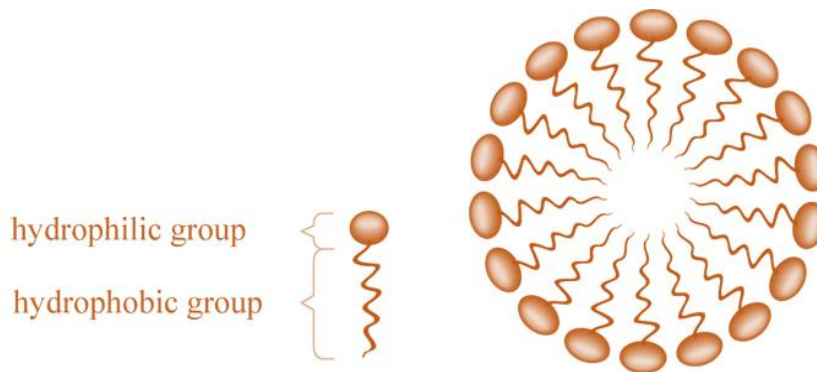

Figure 16. Micelles

At pH 7 bile acids are present as soluble potassium and sodium salts due to the alkaline environment of the bile. Over 99% of BAs in bile are conjugated with the amino acids glycine and taurine. The conjugation (N-acylamidation), which occurs at C-24, is catalyzed by the N-acetyltransferase enzyme. The conjugated molecules are endowed

with a greater hydrophilicity, which gives them a greater emulsifying capacity and a reduction in the value of pKa, which promotes the ionized form and, therefore, the solubility in bile.

About 95% of bile salts are recovered from the enterohepatic circulation to reach the liver where they are metabolized and reused. In this way the hepatocytes will have to synthesize from scratch only 5% of the total bile acids. On the other hand, the excess, reaches the intestine and then is eliminated in the faeces.

Cholesterol is the precursor of all bile acids. In mammals, the synthesis of bile acids is the main path of cholesterol catabolism. Although many of the enzymes involved in the synthesis of bile acids are active in cells of different tissues, the liver is the only organ responsible for their biosynthesis.

The synthesis requires seventeen enzymes and occurs in multiple cellular compartments. The synthesis can take place through two main metabolic pathways: the "classic way" also called the "neutral way" that takes place in the liver and produces 90% of the total pool of primary bile acids[105] and the "alternative way" (Figure 17).

Cholesterol is firstly converted by the liver in primary bile acids, cholic acid (CA) and chenodeoxycholic acid (CDCA) which are then metabolized by intestinal microbiota in secondary bile acids, deoxycholic (DCA), lithocholic (LCA) and ursodeoxycholic acid (UDCA) as well as in their glycine (Human) and taurine (mouse) conjugated forms.

The first step in the synthesis of these molecules is catalysed by the enzyme 7α-hydroxylase (CYP7A1), a microsomal P450 cytochrome enzyme, which converts cholesterol into 7α-hydroxycholesterol. This conversion represents the rate-limiting step of the synthesis and influences the kinetics of the reaction.[105]

After the hydroxylation at C-7, an oxide-reductase (HSD3B7) catalyses the oxidation of the hydroxyl group at C-3 and the isomerization of the double bond C-5/C-6 to C-4/C-5

providing the 7α-hydroxy-4-cholesten-3-one This intermediate, which is common to the synthesis of both cholic acid (CA) and chenodeoxycholic acid (CDCA), can be hydrolysed at C-12, by the sterol 12α-hydroxylase, and oxidized in the side chain by the enzyme CYP27A1-to furnish the cholic acid and can be reduced by the 3-oxo-Δ^4-steroid 5β-reductase or AKR1D1 to chenodeoxycholic acid (CDCA).

In alternative way, also called the "acidic way", the first step concerns the conversion of cholesterol into 27-hydroxycholesterol catalysed by the sterol 27-hydroxylase (CYP27A1).

CYP27A1 catalyses other oxidation reactions of the side chain that lead to the formation of 3β-hydroxy-5-cholestenoic acid. The acid intermediate will be hydroxylated in 7α by the enzyme oxysterol-7α-hydroxylase (CYP7B1). Then, the intermediate is oxidized in C-3 and undergoes the isomerization of the double bond by the microsomal enzyme HSD3B7, leading to the formation of 7α-hydroxy-3-oxo-4-cholestanoic acid which will proceed along the metabolic pathway leading to chenodeoxycholic acid as the final product.

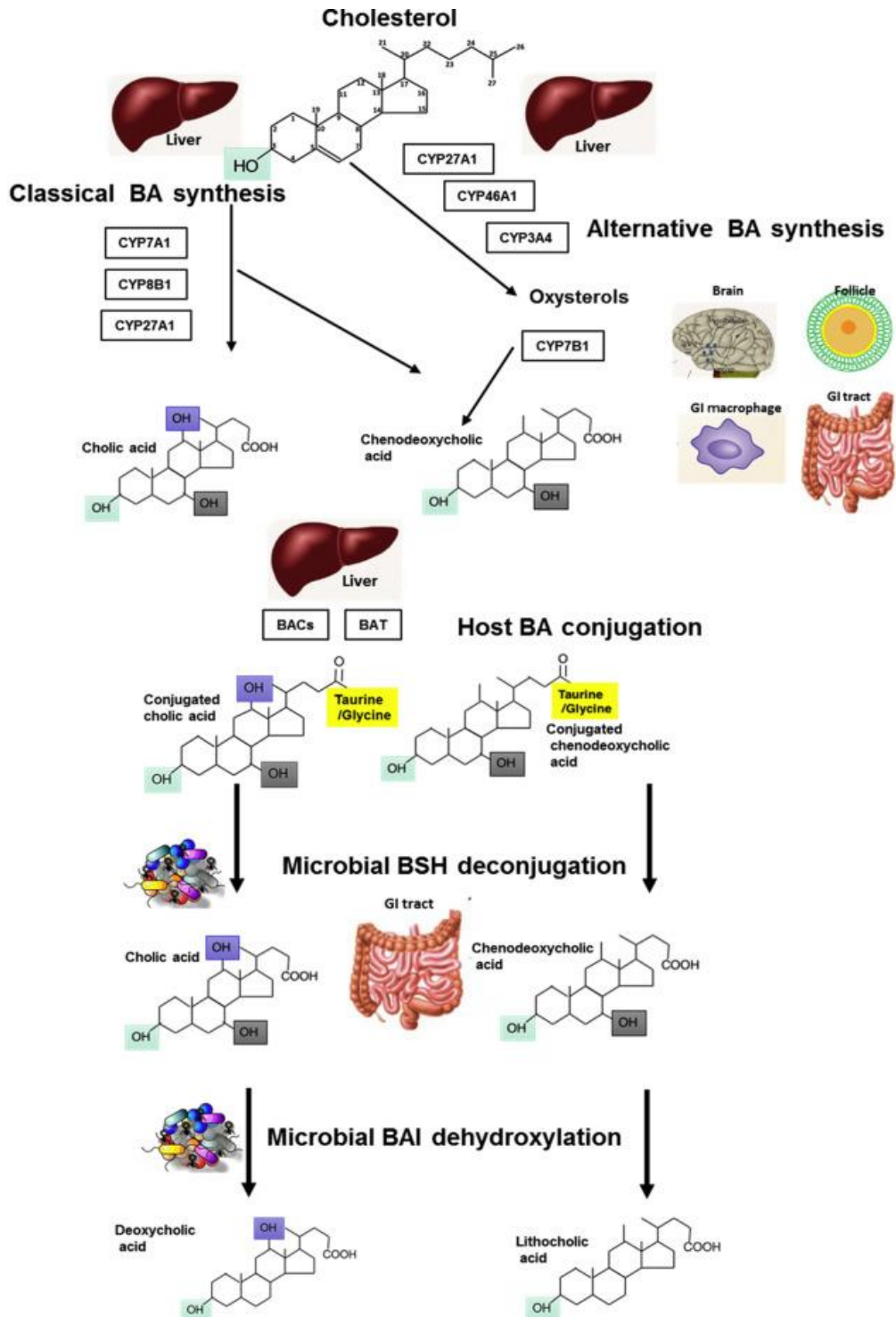**Figure 17.** Synthesis and metabolism of bile acids[106]

Therefore, bile acids can be divided in:

- primary bile acids, such as cholic acid (CA) and chenodeoxycholic acid (CDCA), which are synthesized in the liver directly from cholesterol

- secondary bile acids, such as deoxycholic acid (DCA), lithocholic acid (LCA) and ursodeoxycholic acid (UDCA), which are synthesized in the intestine from primary bile acids.[105]
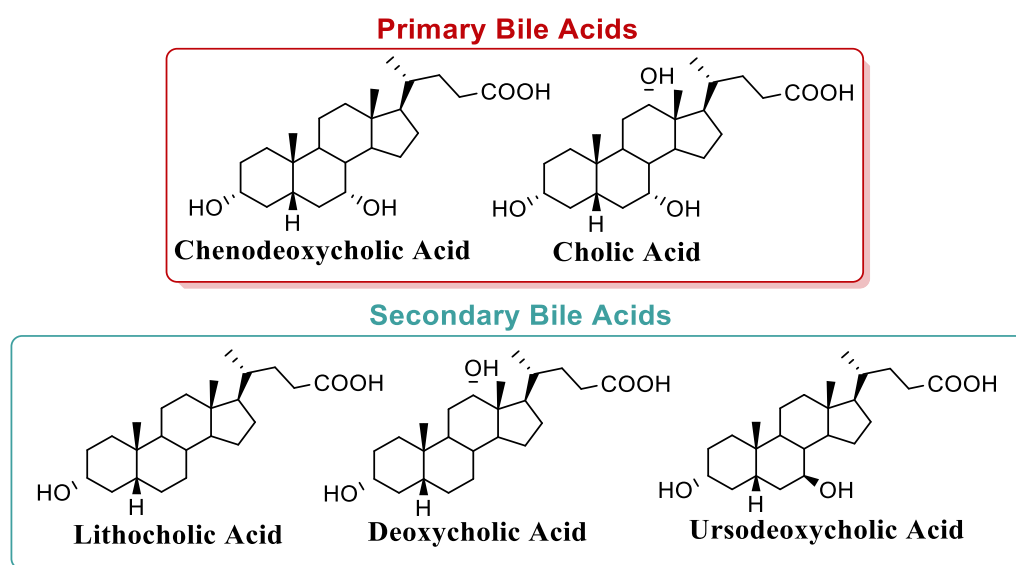

Figure 18. Primary and secondary bile acids

In addition to their primitive role in lipid digestion, solubilisation, and absorption of nutrients, nowadays, bile acids are considered signalling molecules able to interact with different receptors included the previously mentioned FXR and GPBAR1.

In particular, the primary bile acid, chenodeoxycholic acid (CDCA) represents the most powerful endogenous ligand (EC_{50}= 10mM) of FXR[107] while the GPBAR1 receptor is activated by both primary and secondary bile acids although lithocholic acid (LCA) and its taurine conjugated form (TLCA, taurolithocholic acid) are the main ligands (EC_{50}= 0.53µM and EC_{50} = 0.33 µM respectively) (Figure 19).[108]
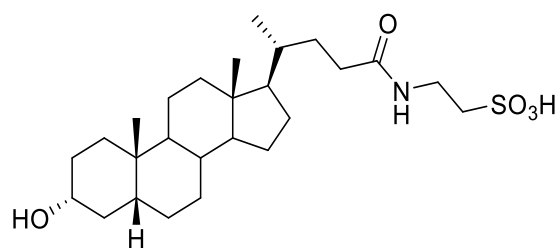

Figure 19. Taurolithocholic Acid (TLCA)

1.5.2. Semisynthetic Steroidal ligands

The chemical manipulation of bile acids scaffold, with the purpose of improving potency, efficacy and metabolic stability, allowed to obtain a large number of derivatives with promising pharmacological profiles.

In 2016, the introduction of an ethyl group at C-6 on the CDCA ring B, led to the discovery of 6-ethylchenodeoxycholic acid (6-ECDCA or INT-747 or obeticholic acid or OCA or OCAliva) with an increased FXR agonistic activity (EC_{50} of 0.099 µM) (Figure 20).[104]
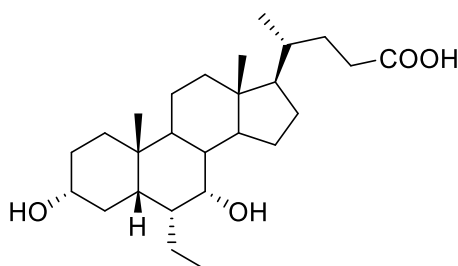

Figure 20. 6-ECDCA

6-ECDCA is a optimal candidate for the treatment of NASH. It has been widely tested *in vitro* and *in vivo*. In phase III of clinical trials in patients with non-alcoholic steatohepatitis (NASH), 6-ECDCA improved several features of NASH; indeed, the group of patients treated with the daily dose of 25 mg recorded an improvement in liver histology, with a reduction in fibrosis, steatosis, and lobular inflammation.[109] Recently, the promising experimental therapy for the treatment of NASH suffered a setback after the FDA turned down an accelerated approval request filed by a US company. This refusal could be due to side effect that occurs during clinical tests such as the increase in blood levels of LDL lipoproteins, which is an important cardiovascular risk factor. Furthermore, in 23% of

patients appeared an increase of cholestatic itching. This effect was unsustainable enough to induce drug discontinuation in 40% of patients.

Indeed, 6-ECDCA causes severe itching, probably due to its interaction with FXR and GPBAR1 receptor.[110]

6-ECDCA has been examined also for the treatment of PBC in patients that responded inadequately to ursodeoxycholic acid (UDCA),[111] the only endogenous bile acid used in the therapy of cholestasis.[112] Specifically, 6-ECDCA decreases all markers of cholestasis: ALP, GGTP, aminotransferases, C-reactive protein and immunoglobulin M.

In the last few years many research groups have focused their attention on the identification and development of new libraries of 6-ECDCA derivatives, obtaining a rational modulation of nuclear and membrane receptors.

It is important to remember that bile acids, covering the same chemical space, are promiscuous molecules towards FXR and GPBAR1, also considering that the receptor pockets have common structural motifs in the ligand binding domain (LDB). Therefore, medicinal chemistry on bile acids scaffold is very difficult since it could lead to non-selective modulators.

In previous studies of the research group in which I carried out my doctoral period, large libraries of steroid-structured compounds have been synthesized modifying the length and the functionalization of the side chain and the tetracyclic core that have shown interesting pharmacological profiles.[113,114,115,116,117,118,119,120,121,122,123] Among these extensive libraries, many derivatives of 6-ECDCA were found to be very interesting and were subjected to international patents. In detail, 6β-ethyl-3α,7β-dihydroxy-5β-cholan-24-ol, patented with the name of **BAR501**[122] and 6α-ethyl-3α, 7α-dihydroxy-24-*nor*-5β-cholan-23-ol, known with the name **BAR502**[114], which differ each other for the length of

the side chain and for the stereochemistry of the ethyl group at C-6 and of the hydroxyl

group at C-7, are currently in advanced clinical trials for the treatment of liver pathology.
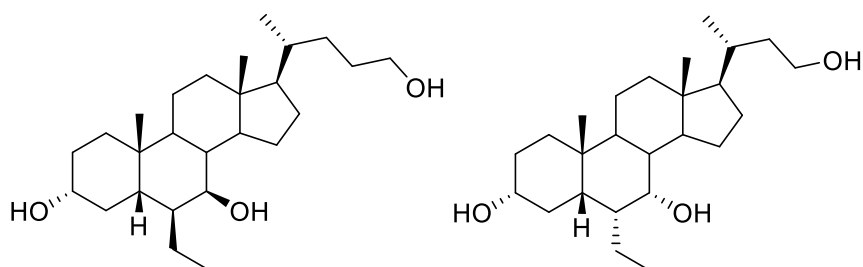

Figure 21. BAR501/EUDCOH and **BAR502**/NorECDCOH

The abbreviation BAR is due to the "BAR Pharmaceuticals" a company that was attracted

by these promising molecules and is currently involved in the large-scale synthesis.

BAR501 was found to be a selective GPBAR1 agonist with an EC_{50} of 1.03 µM. It has

demonstrated beneficial effects on portal hypertension in a rodent model of liver cirrhosis,

by exerting genomic and non-genomic effects on cystathione-γ-lyase (CSE), nitric oxide

synthase (eNOS) and endothelin (ET) -1, in liver sinusoidal cells.[122] Portal hypertension

is a common symptom of liver cirrhosis, in which the fibrosis combined with a

vasculogenic component contributes to an endothelial dysfunction. Because GPBAR1

expression is limited only to Kupffer and sinusoidal (LSEC) hepatic cells, whose

activation regulates the endothelial nitric oxide (NO) synthase (eNOS) activity,[121] this

suggests the effective role of GPBAR1 in the treatment of endothelial dysfunction in

presence of liver cirrhosis. Moreover, BAR501 effectively reduced hepatic perfusion

pressure in naïve rats and contrasted the vasoconstriction activity of norepinephrine (NE)

and of methoxamine, two α1-adrenergic receptor agonists, but was unable to improve

fibrosis developed in mice model of CCl_4.[124]

The second compound, **BAR502**, was found to be a dual modulator of FXR and GPBAR1

with EC_{50} of 2 µM and 0.4 µM, respectively. It was able to reverse the steatohepatitis and

fibrosis in mice subjected to HFD, to reduce liver cholesterol and to slightly increase HDL levels, indicating a benefic effect in the control of hepatic cholesterol homeostasis. **BAR502** protected against portal hypertension caused by CCl_4 administration and resulted able to exert protective effects against NASH-features, induced in a mice model of HFD. The absence of the common side effect (the cholestatic itching) linked to the use of 6-ECDCA, dual FXR/GPBAR1 modulator is worth to mention. Collectively these data suggest that **BAR502** could be a promising candidate in treating NASH.[125]

1.6. Non-steroidal FXR agonists

1.6.1. GW4064 and its derivatives

Since steroidal ligands cover the same chemical space of BAs, they are intrinsically promiscuous towards FXR and GPBAR1 receptors and, with few exceptions, it is very difficult to obtain selectivity towards one or the other receptor.

Looking the literature, several pharmaceutical companies have focused their attention on non-steroidal compounds able to selectively bind the bile acid receptors. In particular, the researchers, have turned their attention to the discovery of new selective FXR agonists since, as previously mentioned, in PBC the concomitant activation of GPBAR1 is associated with severe side effects such as the cholestatic itching.

Among the many synthesized and tested compounds, a milestone was the discovery of **GW4064**, whose structure is shown below. It represents one of the first compounds with isoxazole nucleus to be active as an FXR agonist with a potency of 70 nM and an efficacy of 166% compared to CDCA, the endogenous ligand.[126] (Figure 22)
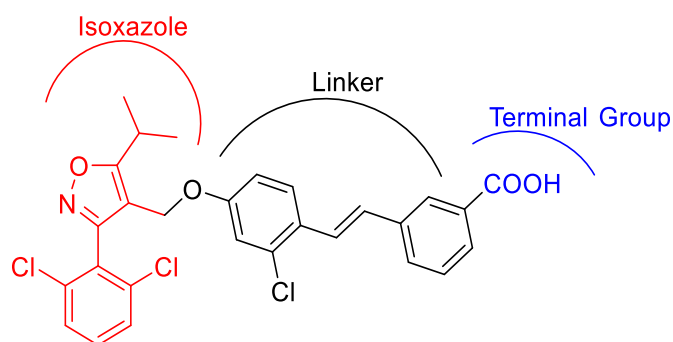

Figure 22. GW4064 structure

Since its discovery in 2000, a large number of modifications have been made, disclosed in patents and literature, around its scaffold with the aim of overcoming the limits shown, i.e. its limited intestinal absorption (<10%) and the presence of the stilbene-system widely delocalized electron associated with intrinsic photo instability and potential cellular

toxicity. For these reasons, **GW4064** has not entered the market as a real drug for the treatment of metabolic and liver diseases.[127] So, different research groups, keeping the trisubstituted isoxazole core unchanged, have explored the chemical space around the stilbene portion.

These modifications have led to the identification of **Px-102** and **LJN452** (Tropifexor, LMB763),[127] featuring a trans-cyclopropyl group and an 8-azabicycle [3.2.1]-octane as linker, respectively (Figure 23).
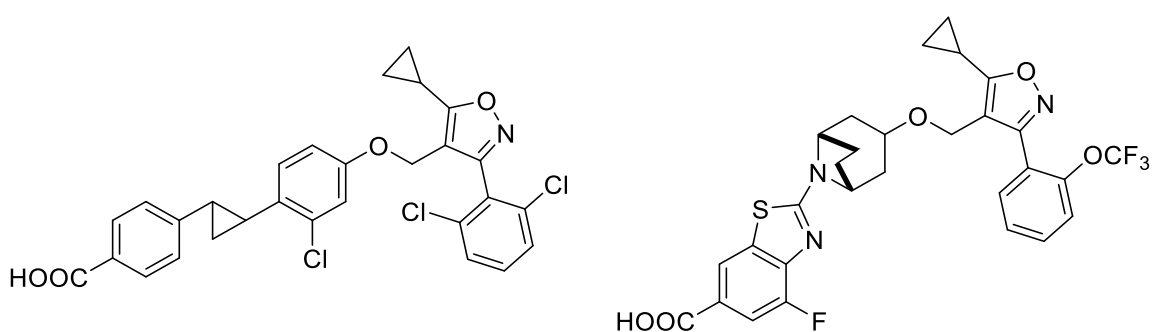

Figure 23. Px102 and **LJN452** structures

Compared to **GW4064**, **Px-102** showed an effectiveness of 103% by FRET and 80% in a GAL4-based assay and an increased solubility in water and a greater bioavailability. This compound has shown a significant ability to lower cholesterol and triglycerides present in the blood and liver. Indeed, it reduced the expression of the SREBP-1c protein and the malic enzyme, both of which are involved in the *ex novo* lipogenesis that occurs in the liver.[128,129,130,131,132] In summary, **Px-102**, a new synthetic FXR agonist, improves hepatic steatosis associated with metabolic syndrome and could be a good candidate for the treatment of human NAFLD. It is currently tested in a phase II study in patients with non-alcoholic steatohepatitis (NASH).[133]

Instead, the idea of inserting the 8-azabicycle [3.2.1]-octane as a linker, characteristic of nortropin, led to the identification of **LJN452** or Tropiferox, an extraordinarily potent

FXR agonist (EC_{50} = 0.20 nM in FRET and EC_{50} = 0.26 nM in transactivation assays, respectively) discovered by Novartis 2017[134].

Preclinical studies were conducted using two different mice models for NASH. Following treatment with **LJN452** (Figure 23), the liver transcriptome of a single type of mouse model was analysed and a different expression of 461 genes was recorded, resulting in a reduction in oxidative stress, fibrogenesis and inflammation.[134] Based on preclinical validation in animal models, **LJN452** is currently in phase II clinical trials for the treatment of patients with PBC and NASH.

Recently, the results of a first study in healthy volunteers, administered with single and multiple increasing doses of **LJN452** (SAD/MAD) have been published. **LJN452** was well tolerated up to 3000 µg and 100 µg in the SAD and MAD studies, respectively. However, two subjects discontinued the MAD study due to the asymptomatic elevation of liver transaminases. In single doses, **LJN452** showed a moderate level of absorption (maximum concentration four hours after intake) and a half-life of between 14 and 22 hours. With multiple doses, however, steady state was reached on the fourth day. In both studies there was a dose-dependent increase in fibroblast growth factor 19 (FGF19).[135] In conclusion, **LJN452** was well tolerated and the results obtained are promising.

1.7. Ligands of CysLT Receptor

1.7.1. Endogenous Ligands: Leukotrienes

Leukotrienes are lipid mediators that perform function like autocrine or paracrine hormones. The name "leukotriene" is due to their discover in leukocytes and because they have three conjugated double bonds. They belong to the class of eicosanoids originating from arachidonic acid.

There are six different leukotrienes, called LTA_4, LTB_4, LTC_4, LTD_4, LTE_4 and LTF_4.

The leukotrienes are involved in inflammatory and allergic processes, because activate the CysLT receptors. Their production is always accompanied by the release of histamine, which is also involved in these processes.

They are produced through the cascade of arachidonic acid (Figure 24) with the path of lipoxygenases (LO), enzymes capable of oxidizing arachidonic acid and hydroperoxyl-eicosatetraenoic acid (HPETE).
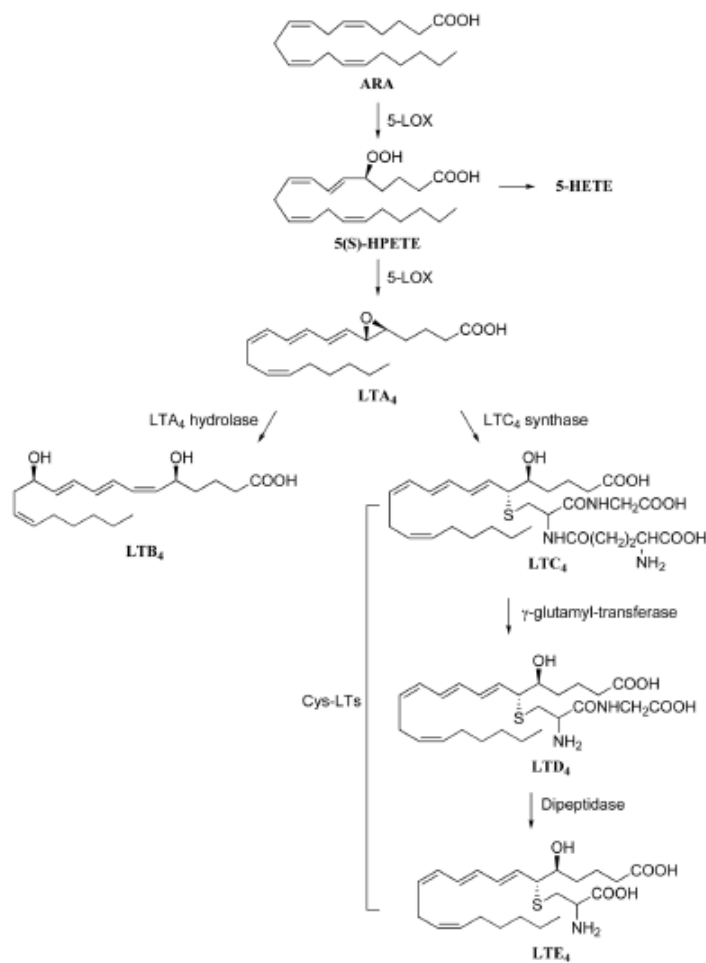
Figure 24. Cysteinyl-Leukotriene Synthesis

Currently three different lipoxygenases (5-LO, 12-LO, 15-LO) have been identified which differ in their ability to oxidize different positions of the endogenous substrate. 5-LO is able to oxidize arachidonic acid to 5-hydroperoxieicosatetraenoic acid (5-HPETE) in the presence of the activating protein 5-LO (FLAP) and cofactors such as calcium Ca^{2+} and ATP. The 5-HPETE can be reduced using a Arachidonate 5-lipoxygenase, a non-heme iron-containing enzyme, to 5-hydroxyheicosatetraenoic acid (5-HETE) or it can be converted, thanks to the 5-LO, into LTA_4, featuring an unstable epoxy function. In turn, LTA_4 can be converted into LTB_4 thanks to the Lima4 LTA_4 hydrolase or into LTC_4 thanks to the LTC_4 enzyme synthase using the combination with glutathione.[136] LTC_4 is

transformed into LTD$_4$ by a γ-glutamyl-transpeptidase which in turn is converted into LTE$_4$ by a glycinase. LTC$_4$, LTD$_4$ and LTE$_4$ are also defined as "cysteyl-leukotrienes" due to the presence in their structure of a cysteine residue (Figure 24).[94]

1.7.2. Synthetic CysLTR₁ Antagonists

Several CysLT receptor antagonists have been developed, some of which have a consolidated use in therapy. Figure 25 shows some examples of antagonists: **REV5901**, pranlukast, montelukast, zafirlukast, that are used specially for the management of asthma or in seasonal allergies.
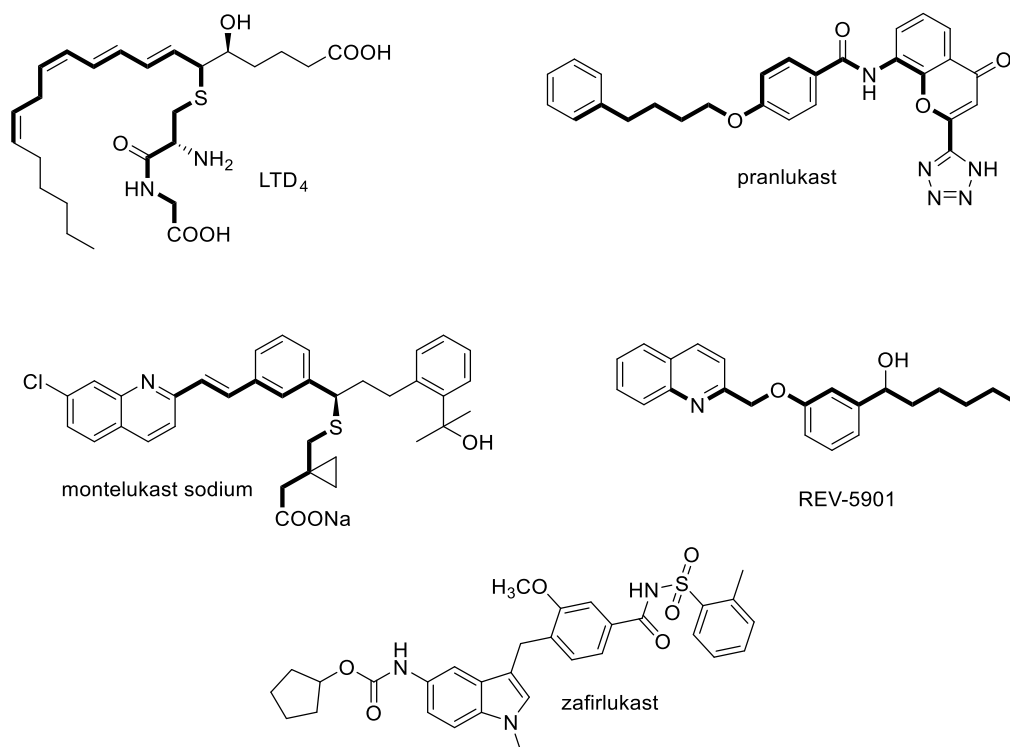

Figure 25. Synthetic Cysteinyl Leukotriene antagonists

Recent studies have shown that zafirlukast is a potent CysLT antagonist, useful in the treatment of asthma due to its capability to deal with LTD-mediated bronchoconstriction.[137]

Pranlukast drastically reduces bronchial constriction due to human antigens and is much more effective than pyrilamine, a well-known antihistamine. This molecule is able to inhibit bronchoconstriction within 100 min from the administration of the antigens unlike pyrilamine (60 min); therefore, it can be effective in both the treatment and prophylaxis of asthma.[138]

Montelukast has been shown to be an effective asthma drug.[139a,b] It acts also as antioxidant in intestinal ischemia–reperfusion injury reducing hepatic and kidney damages.[139a,b] Pranlukast and montelukast as shown in Figure 25 are featured by structural motif of LTD$_4$ which is also present in **REV5901.**[140]
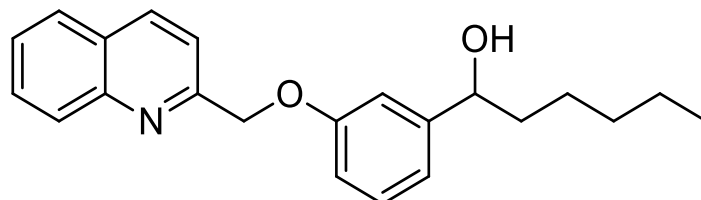

Figure 26. REV5901

REV5901 is a quinolinic derivative primarily developed to be a 5-LO enzyme inhibitor. It was later identified as a neutral CysLT$_1$ receptor antagonist.[141] Structurally it is a quinoline substituted in C2 with an aromatic moiety linked to an alkyl chain.

Research on **REV5901** has shown its ability to protect and reduce ethanol-induced gastric lesions in rat models. Moreover, the administration of ethanol induces the production of LTC$_4$, which increases in relation to the severity of the lesions. **REV5901** has been shown to be able to reduce its production and consequently increase its ability to protect gastric tissue from damage.[142] This compound has attracted the interest of the scientific community because it represents the only neutral derivative capable of acting as an antagonist of the CysLT$_1$ receptor.

CHAPTER 2

PROJECT PRESENTATION

2.1. Steroidal FXR agonists

A part of my PhD project was devoted to the identification of potential selective steroidal FXR modulators. The FXR nuclear receptor has been proposed as a potential target for the treatment of various pathologies, such as cholestasis, hepatic steatosis, atherosclerosis, dyslipidaemias, type 2 diabetes, non-alcoholic fatty liver disease (NAFLD) and non-alcoholic steatohepatitis (NASH).

BAs are able to interact with nuclear and membrane endogenous receptors. Two well-known targets of BAs are the nuclear receptor FXR and the membrane receptor GPBAR1. Through several modifications on bile acid scaffolds, we obtained a large number of derivatives with different pharmacological profiles, useful in the treatment of metabolic and enterohepatic disorders.

A comprehensive understanding of the effects of BAs modifications on the activity and selectivity towards FXR and GPBAR1 receptors is possible only if the binding mode of the ligands to the two receptors is elucidated.

Therefore, all kind of modifications on BA scaffold, have been designed by computational chemistry using the hGPBAR1 homology model[143] and the available rFXR crystal structure[145] It is important to remember that BAs are promiscuous molecules, capable of binding to multiple receptors, therefore the medicinal chemistry is very difficult because you can get dual agonist but it is also very important to obtain selective agonist towards one or the other receptor.

The dual activation can lead to several side effects, such as, increasing low-density lipoprotein cholesterol and total cholesterol, decreasing high-density lipoprotein cholesterol and pruritus.[112]

Few differences could be highlighted inside the binding mode of BA at the two receptors. For example, in FXR the carboxyl group on the side chain salt-bridges with the Arg328 guanidinium group; in GPBAR1 the pocket where the side chain is placed is more amphipathic and the carboxyl group H-bond with three serine residues. More important of all, it was found that in GPBAR1 the 3α-OH forms a stable H-bonds with the negatively charged side chain of glutamic acid (Glu169) on the transmembrane helix TM-5, while the same group in FXR H-bonds with the side chains of Tyr358 and a positively charged residue of His444 on helix H12. (Figure 27)
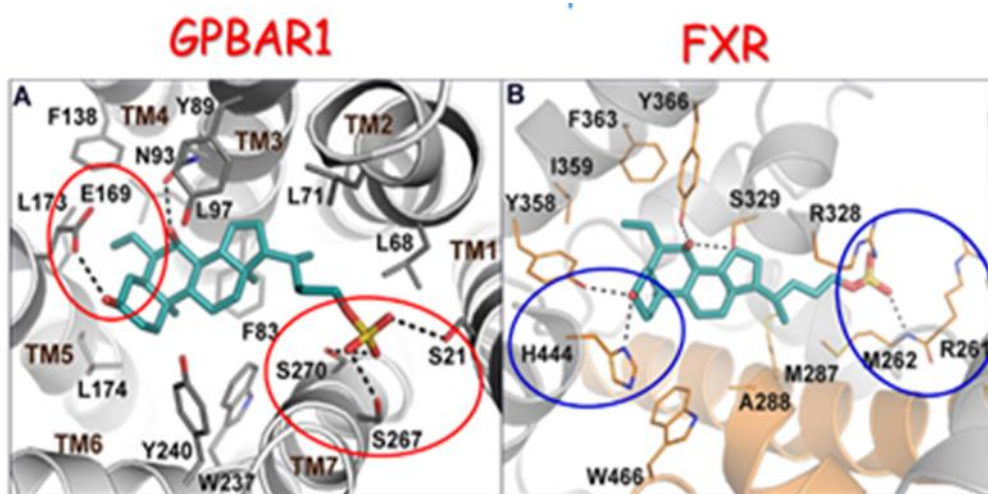

Figure 27. Interaction of 6-ECDCA on GPBAR1 and FXR[145]

The research group in which I have carried out my doctorate over the years has synthesized different steroidal compounds of great pharmacological interest. For example, the **norECDCOH** (**BAR502**)[121] a 6-ECDCA derivative actually in advanced clinical trials for the treatment of liver pathology, having an alcoholic function on a

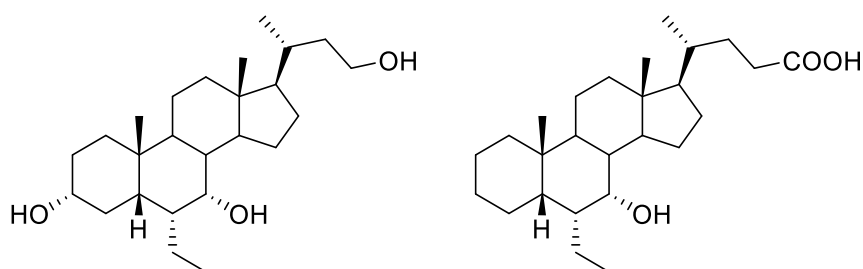truncated side chain, and the **3-deoxy 6-ECDCA** a potent and selective FXR agonist[115]. (Figure 28)

Figure 28. *nor*ECDCOH (BAR502) and **3-deoxy-6-ECDCA** structure

Therefore, starting from these encouraging results, my project concerned the synthesis of new steroidal derivatives, in order to obtain new selective agonists of FXR with improved potency and pharmacokinetic properties and therefore useful for the treatment of metabolic disorders.[145]

We have made modifications on 6-ethylcholane scaffold, manipulating (Figure 29):

✓ the tetracyclic core with the elimination of the 3-OH group on ring A which is essential for the activation of GPBAR1 and to obtain selective FXR agonists

✓ the side chain with the introduction of non-acidic side chain in order to obtain molecules unable to form insoluble metabolites that could accumulate in the organism.[116 he] The carboxylic group on 6-ECDCA side chain undergo extensive metabolization after conjugation with taurine in mice and glycine in human, leading to enterohepatic circulation and a subsequent drug accumulation in the liver.

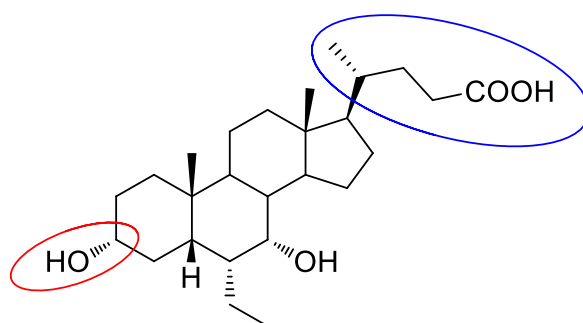**Figure 29.** Modifications on the 6-ECDCA scaffold

The workflow followed in the research of potential selective FXR binders was based on an integrated approach including design, synthesis, investigation of ligand/receptor molecular interaction and pharmacological *in vitro* and *in vivo* evaluation.

2.1.1. Synthesis of 6-ECDCA derivatives

A small library of compounds was synthesized through modifications of the 6-ethylcholane scaffold.[146]

In particular, the introduction of a shortened non-acidic side chain led to derivatives **1**-**3**.

The simultaneous modification of the side chains and the elimination of the 3α-OH group

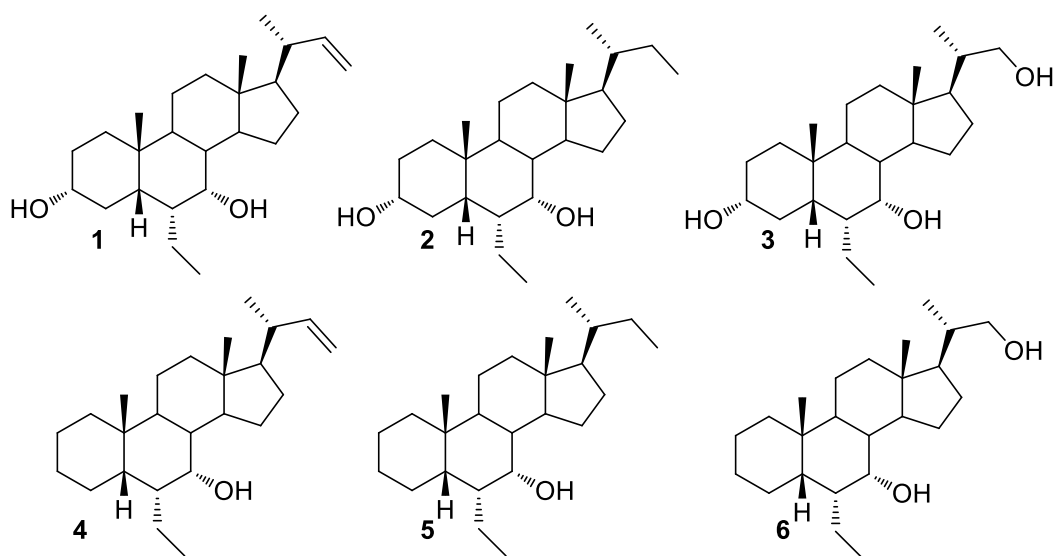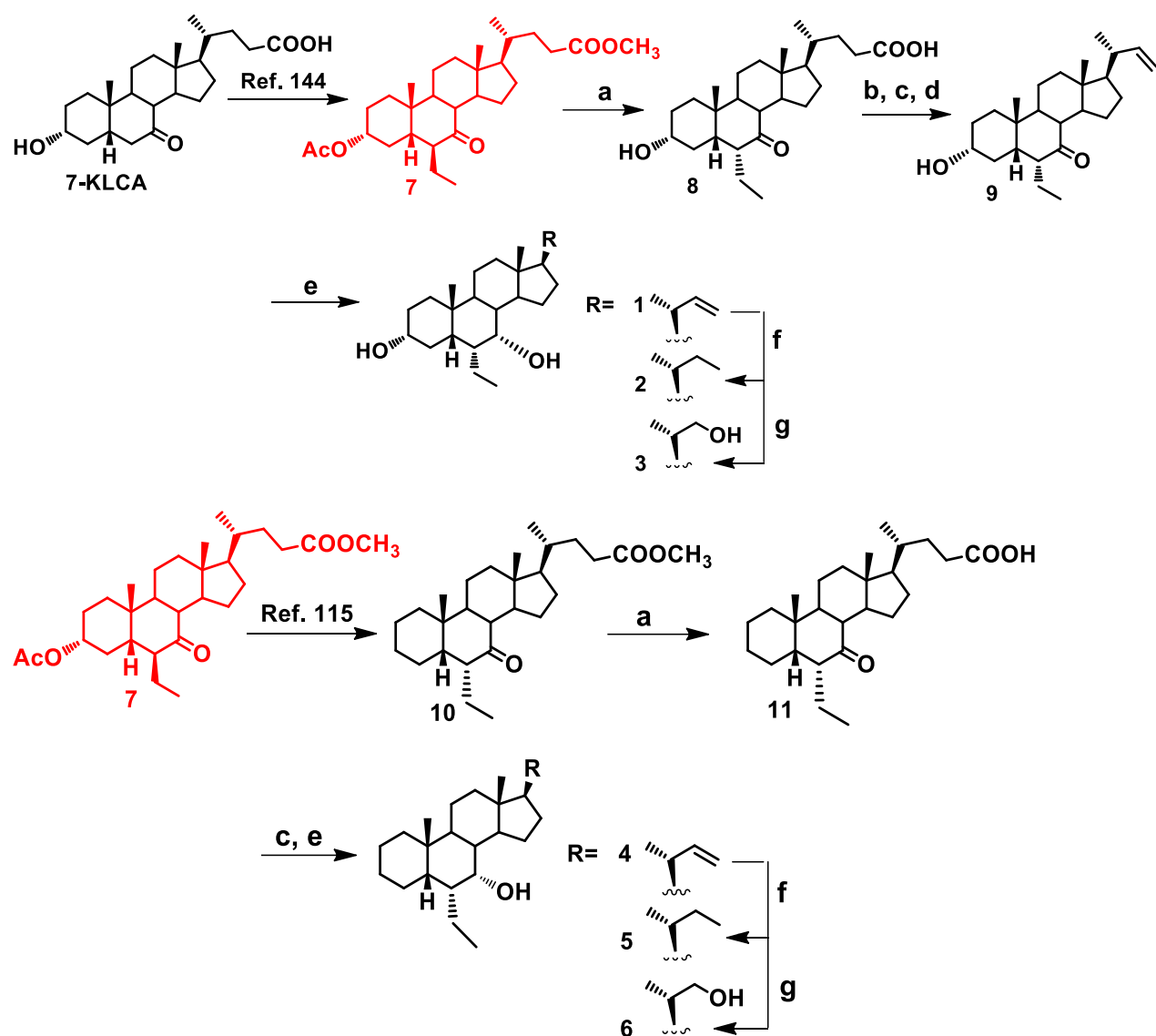on the ring A, led to compounds **4**-**6**.[146]

Figure 30. Library of Compounds

The synthesis of derivatives **1**-**6** is shown in **Scheme 1**. The first step of the synthetic

scheme, which lead to the formation of derivative **7,** have been described in a previous

paper.[114,147]

Scheme 1: *Reagents and conditions:* **(Ref.144)(Ref.115) (a)** NaOH, MeOH:H_2O 1:1 v/v; **(b)** acetic anhydride, pyridine dry, 84% yield over two steps; **(c)** $Cu(OAc)_2 \cdot H_2O$, $Pb(Oac)_4$, toluene/pyridine 10:1 v/v; **(d)** NaOMe, MeOH; **e)** $LiBH_4$, MeOH/THF dry; **(f)** H_2, $Pd(OH)_2/C$, THF/MeOH 1:1; **(l)** LiBr, Li_2CO_3, DMF, reflux.

The synthesis starts with the 7-ketolithocholic acid (7-KLCA), which after the esterification at the side chain and the acetylation at position C-3 (87% yield over two steps), undergoes an aldol addition to a silyl enol ether and finally hydrogenation (80% yield over three steps), to obtain derivative **7**. [144]

The 6β-configuration of the ethyl group in compound **7** after catalytic hydrogenation depend on the presence of a *cis* junction between the rings A and B, which induce the

molecule to assume a bent form; thus, the C-19 methyl group causes a steric hindrance that force the attack of the hydrogen on the α face of the double bond and gives the β-configuration of the ethyl group.[114,144,147]
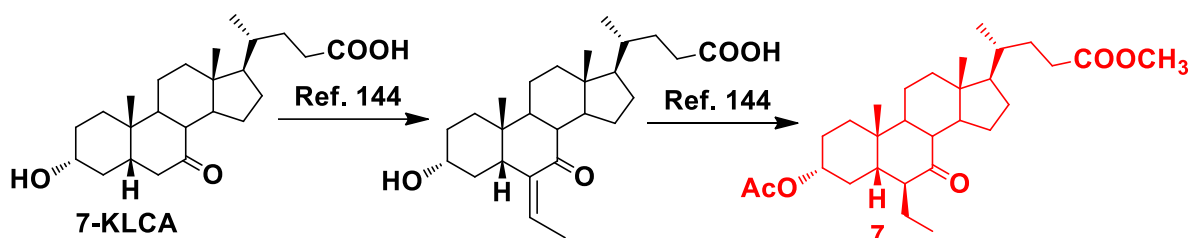

Figure 31. Formation of derivative **7** *Reagents and conditions:* (**Ref.144**)

Derivative **7** is the key intermediate for the synthesis of the entire library of compounds. Treatment with NaOH in MeOH afforded the concomitant hydrolysis of the methyl ester, deprotection at C-3 and inversion of the configuration of the ethyl group in C-6, giving compound **8**. (Scheme 1)

C-3 OH acetylation followed by the oxidative decarboxylation with $Cu(Oac)_2$ H_2O and $Pb(Oac)_4$ in toluene/pyridine dry gave a shorter side chain. Then, deacetylation gave intermediate **9** in 58% yield over three steps. Reduction at C-7 with $LiBH_4$ in MeOH and THF dry generate compound **1** in quantitative yield

Hydrogenation with H_2 and $Pd(OH)_2/C$ of compound **1** afforded compound **2** while reductive ozonolysis with O_3 give compound **3**.[145]

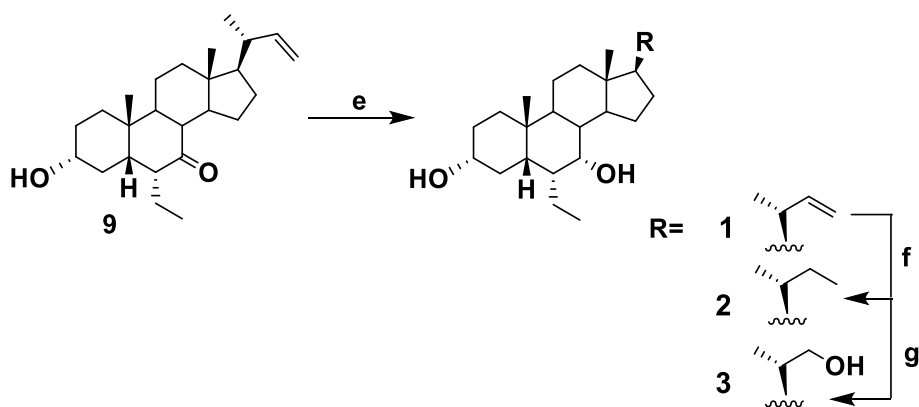**Figure 32.** *Reagents and conditions:* (**e**) $LiBH_4$, MeOH/THF dry, 98% yield; (**f**) H_2, $Pd(OH)_2$, THF/MeOH 1:1, quantitative yield; (**g**) O_3, CH_2Cl_2, −78 °C, then MeOH and $NaBH_4$ in excess, quantitative yield.

Preparation of 3-deoxy-6-ethylcholane derivatives **4-6** start with deacetylation at C-3 of intermediate **7** with MeONa in MeOH dry and then tosylated (quantitative yield over two steps). Elimination with $LiBr/LiCO_3$ and hydrogenation of the transient double bond furnished the key derivative **10** (88% yield over two steps).[115]
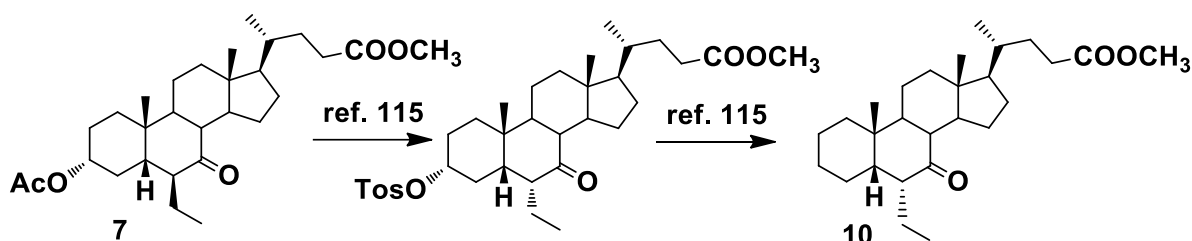
Figure 33. Formation of derivative **10** *Reagents and conditions:* **(Ref.115)**

Hydrolysis of compound **10** followed by oxidative decarboxylation, as described for compound **8,** furnished compound **11** in quantitative yield. Reduction with $LiBH_4$ give compound **4** (91% yield).
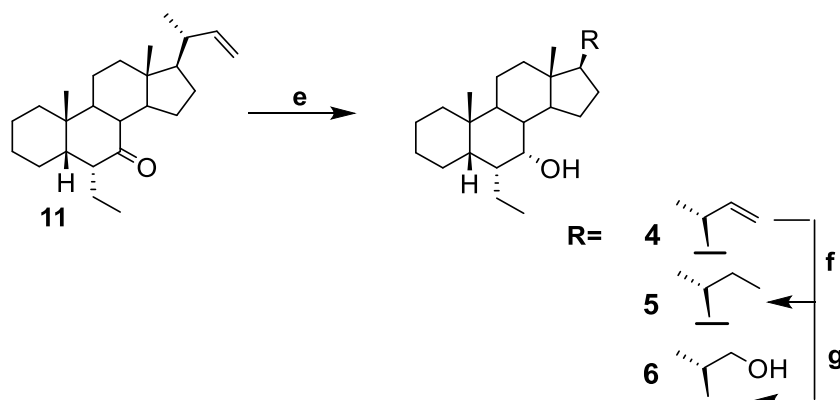
Figure 34. *Reagents and conditions:* **(e)** $LiBH_4$, MeOH/THF dry 91% yield; **(f)** H_2, $Pd(OH)_2$, THF/MeOH 1:1 v/v, quantitative yield;; **(g)** O_3, CH_2Cl_2, −78 °C, 95% yield.

Compound **4** was hydrogenated and then subjected to a reductive ozonolysis to obtain compounds **5** and **6**, respectively (quantitative yield and 95% yield, respectively), as described for compounds **2** and **3**.[146]

2.1.2. In *vitro* and in *vivo* assays

Thanks to the collaboration with Professor Fiorucci's Group, compounds **1**-**6** were evaluated on FXR and GPBAR1 receptors in a luciferase reporter assay on HepG2 and HEK-293T cells, previously transfected with responsive elements for the two receptors. **Table 1** displays the efficacy and potency of compounds **1**-**6**. Compounds **1**, **2** and **3** were the most effective FXR agonists, thus suggesting that the introduction of a nonacidic side chin on the 6-ethylchenodeoxycholic scaffold produced a positive effect on FXR activation.

Furthermore, compounds **1, 2** and **3** were less effective in GPBAR1 transactivation but in term of potency, compounds **1** and **3** proved to be promising GPBAR1 agonists. Consequently, compounds **1**, **2** and **3** can be considered dual agonists. The aim of the project, nevertheless, was to find selective steroidal FXR agonists. FXR selectivity is an important point in the treatment of cholestasis disorders, because the dual activity on GPBAR1, has shown to led itching in mice [93] as side effect, limiting the use of dual modulators as drugs.

As I described before, the elimination of the hydroxyl group at C-3, which is essential for the activation of GPBAR1, leads to **3-deoxy-6-ECDCA** a potent and selective FXR agonist.[114] Therefore, the idea of my medicinal chemistry strategy was to modify the C-3 position of 6-ECDCA, eliminating the OH group to get best selectivity to FXR.

Table 1. Efficacy and potency of compounds **1-6**

Compound	R	R₁	FXRᵃ			GPBAR1ᵃ		
			Eff%ᵇ		EC₅₀	Eff%ᶜ		EC₅₀
			Vs CDCA	Vs 6-ECDCA		Vs TLCA	Vs 6-ECDCA	
CDCA	-	-	-	-	20	-	-	-
TLCA	-	-	-	-	-	-	-	0.33
6-ECDCA	-	-	-	-	0.5	-	-	0.9
1	OH	(structure)	252	45.6	1.8±0.5	79	367.1	0.14±0.032
2	OH	(structure)	249	46.5	1.3±0.12	53	255.2	1.5±0.29
3	OH	(structure)	257	45	2.8±0.45	55	243.4	0.43±0.015
4	H	(structure)	17	3.1	ND	15	68.8	ND
5	H	(structure)	14	2.5	ND	12	53.4	ND
6	H	(structure)	185	33.4	13.7±2.05	19	87.5	ND

a Results are the mean of at two experiments or more. **b** Eff (%) is the maximum efficacy of the compound (10 μM) in comparison to CDCA (10 _M) or 6-ECDCA (1 μM) set as 100% in FRE (FXR responsive element) on HepG2 cells; results are the mean of two experiments or more ± SD. **c** Eff (%) is the maximum efficacy of the compound in comparison to TLCA (10 μM) or 6-ECDCA (1 μM) set as 100 in CRE (transactivation of a cAMP responsive element) on HEK293T cells; results are mean of at least two experiments ± SD. ND, not determined.

CREB (cAMP response element-binding protein) transactivation in HEK293T, transfected with GPBAR1, showed that the elimination of the 3-OH leads to inactive derivatives at 10μM. Surprisingly, the removal of the C-3 hydroxyl group in the

nonacidic side chain derivatives also negatively affects the FXR agonism with loss in efficacy and potency. Only compound **6** shown interesting efficacy when tested at 10 μM, even if the potency (EC_{50}= 13.7 μM) turn out to be reduced. The lack of the OH at C-3 and the introduction of a nonacidic group in the side chain, however, produces improvement in metabolic stability as shown in Table 2, justified by the loss of the two most important point of metabolization of the cyclopentanoperhydrophenanthrene scaffold. [148]

Table 2. Physiochemical properties of selected compounds

Compound	Solubility[a] (nM)	Cl_{int}[b]	$t_{1/2}$ (min)	%[c]
6-ECDCA	195	109.0	21.1	26.9
1	201	52.6	43.8	42.2
2	176	25.0	92.4	72.8
3	210	36.6	63.0	60.6
6	162	19.7	117.4	79.2

a Aqueous solubility at pH 7.4; **b** Reported as _L/min/mg protein; **c** % of compound that remain in solution after 40 min. Each measurement has been repeated three times and SD < 5%; **d** Synthesized as previously reported[118]

In **Table 2**, the most active derivatives prepared (**1-3** and **6**), showed a similar aqueous solubility to the 6-ECDCA, whereas they are endowed with better metabolic stability. As a matter of fact, the drug metabolization rate by liver enzymes and its elimination are evaluated through the Cl_{int} (intrinsic clearance) and $t_{1/2}$ (half-life). Compounds **3** and **6** showed promising results.

We have also analysed if compounds **1**-**3** and **6** regulate canonical functions employed by FXR and GPBAR1, by RT-PCR (reverse transcriptase-polymerase chain reaction) analysis. As shown in figure 12, compounds **1**, **2** and **3** are capable to induce the

expression in GLUTag cells of the pro-glucagon mRNA, while compond **6** was unable to regulate this function. (Figure 35 A)
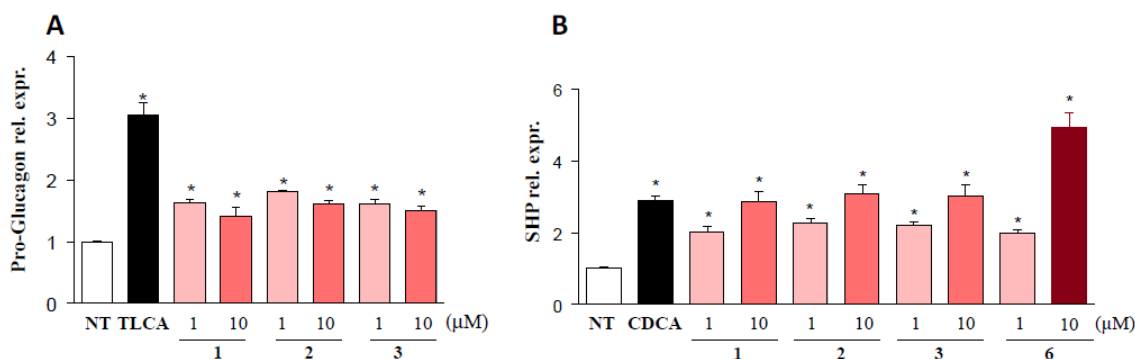

Figure 35. RT-PCR of mRNA expression on (**A**) GPBAR1 target gene *proglucagon* and (**B**) on FXR target gene *SHP* in murine GLUTag cells and human HepG2 cells, respectively. In panel **A** cells were setted with TLCA (10 μM), or with increasing dose of compounds **1**–**3** (1 and 10 μM), or with vehicle (DMSO) alone. In panel **B**, cells were setted with CDCA (10 μM), or with increasing dose of compounds **1**–**3**, and **6** (1 and 10 μM), or with vehicle (DMSO) alone. Values are normalized to GAPDH. The relative mRNA expression is analyzed in step with the CT technique. Data were calculated from a minimum of three experiments. Results are expressed as mean ± SEM * p < 0.05 versus not treated cells (NT), indiscriminately settled as 1.

As illustrated in Figure 35B, compounds **1-3** and **6** were able *in vitro*, to induce the small heterodimer partner (SHP) mRNA, a FXR target gene. Compound **6** was the most potent in the induction of expression when administrated at 10μM. (Figure 35 B) These results showed the dual nature as FXR/GPBAR1 agonists of compounds **1-3**, and the nature of compound **6** as selective FXR agonist.

To understand the binding mode of the synthesized 6-ECDCA derivatives, thanks to the collaboration with Professor Limongelli's Group, molecular docking studies were performed.[149,150,151] In particular, the docking calculations were performed on the dual agonist **3** with the purpose to elucidate the binding mode to FXR and GPBAR1. (Figure 36 A). In FXR the best docking pose, reveal that **3** established favourable hydrophobic interactions with the side chains of Leu284, Met287, Ala288, Met325, Phe333, Leu345 and Ile349. The alcoholic side chain positioned itself in an amphipathic region of the

FXR-LDB (ligand bind domain), where it forms water-mediated hydrogen bonds with His291, Arg328 and Ser329. The formation of these polar interactions can contribute to FXR activation.[144] On the other side, the 3α-OH engages hydrogens bonds with the side chains of Tyr358 and His444. The formation of the H-bond with His444, reinforce the cation-π interaction between His444 and Trp466 which in turn stabilizes the receptor agonist conformation.[144] Finally, the 7α-OH group forms H-bonds with Ser329 and Tyr366, while the 6α-ethyl group interacts with Tyr 358, Ile359 and Phe363. The binding pose of compound **3** is very similar to the parent compound 6-ECDCA, but the latter can form a salt bridge through the carboxylic side chain with Arg328. (Figure 36 A)
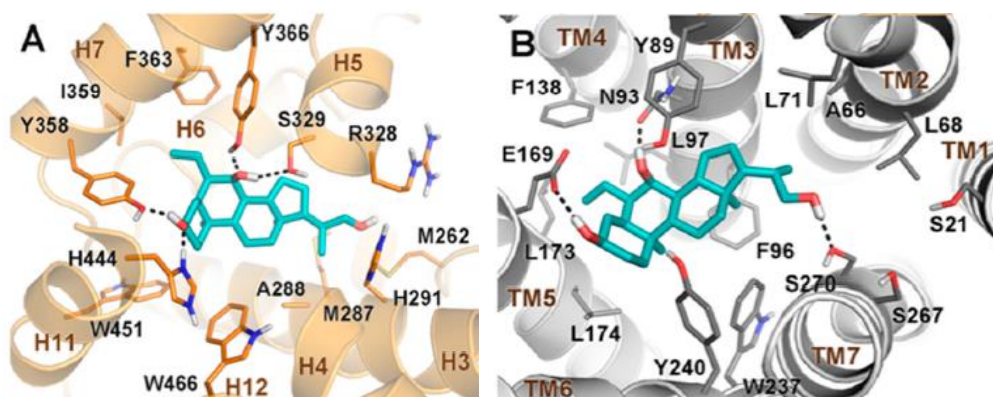

Figure 36. Docking study of compound **3** in the crystal structure of FXR and (**B**) in the homology model of GPBAR1. The ligand is shown as cyan sticks. FXR and GPBAR1 are depicted as orange and cartoons, respectively. Important amino acids are shown as sticks. Nonpolar hydrogens are omitted for clarity. Hydrogen bonds are depicted as dashed black lines.

Compounds **1** and **2** shown an FXR agonist profile like compound **3**, although they have a hydrophilic side chain that cannot form polar contacts with Arg328. Compound **6** shown an efficacy like **3**, even if cannot form H-bond with His444, due to the lack of the 3α-OH group. This confirms that bile acids lacking the 3α-OH can stabilize the cation-π interaction between His444 and Trp466 through hydrophobic contacts.[146] However, compounds missing the 3α-OH and a polar side chain (**4** and **5**) cannot interact with Arg328 or with His444, resulting unable to activate FXR. In conclusion, the 3α-OH group

or a polar side chain are two structural features necessary for the activation of the FXR receptor.

In GPBAR1, the best docking pose (Figure 36 B) shows that **3** binds with GPBAR1 similarly to other bile acid agonists of this receptor previously reported.[121,143,152] The ligand's steroidal scaffold forms a hydrophobics interactions with the side chains of Leu71, Phe96, Leu174 and Trp237, while the 3α and 7α-OH groups establish H-bonds with Glu169 and Ans93, respectively. Particularly, the bond with the 3α-OH is necessary for the activation of the receptor; indeed, compounds **4-6,** which missing the hydroxyl group at C-3, are inactive towards GPBAR1. The hydroxyl side chain of compound **3** is directed towards a polar cavity formed by transmembrane™ helices 1,2 and 7 and where establish H-bond with Ser270. Compounds **1** and **2** form favourable interaction with Ala66, Leu68 and Leu71 on TM2 for the presence of a hydrophobic side chain. These interactions stabilize the binding of these compounds, which show an efficacy comparable to **3**.
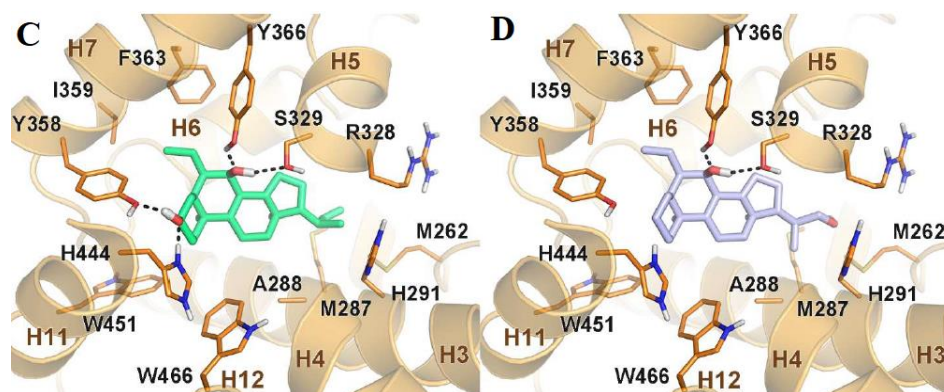

Figure 37. Docking model of **1** (**C**) and **6** (**D**) at the FXR LBD. Compounds **1** and **6** are shown as green and light blue sticks, respectively. FXR is depicted as orange cartoons. Important amino acids are shown as sticks. Non-polar hydrogens are omitted for clarity. Hydrogen bonds are depicted as dashed black lines.

In conclusion, a series of non-acidic 6-ethylcholane derivatives has been designed and synthetized and their *in vitro* activities on FXR and GPBAR1 were assayed. This study resulted within the identification of compound **6**, as a selective FXR agonist with

improved metabolic stability *in vitro*, and the discovery of some derivatives showing dual agonistic activity. Interestingly, the lack of acidic side chains, which preserve their specificity on different off-target targets, as well as improved ADME profiles make compounds **1**-**3** and **6** appropriate for further investigation.

CHAPTER 3

PROJECT PRESENTATION

3.1. Non-steroidal FXR agonists

In recent years, many research groups have focused their attention on non-steroidal bile acids of Nuclear Receptor.

While the **6-ECDCA** represents the first-in-class of steroidal FXR ligands, **GW4064** is the best representative of non-steroidal FXR ligands. The latter presents an isoxazole core and is endowed with an efficacy of 140% versus CDCA, the FXR endogenous ligand. It proved unsuitable for advanced clinical trials due to its poor intestinal absorption and stilbene mediated photosensitivity, anyway its discovery led to the identification of a new prototype of FXR agonists featuring an isoxazole core. In literature many papers reported the elaboration on the **GW4064** chemical space in order to limit these two adverse effects.
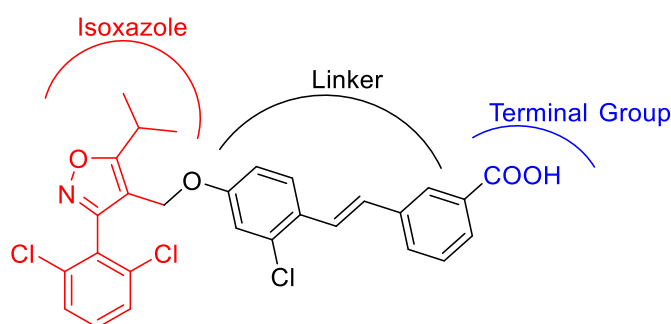

Figure 38. GW4064 structure

A part of my PhD project was devoted to the synthesis of derivatives of **GW4064** derivatives, keeping unchanged the isoxazole core with the isopropyl group at C-5 and the 2,6-dichloro-substituted phenyl at C-3 and modifying the linker between the trisubstituted isoxazole core and the terminal entity at C-4, thus eliminating the stilbene group, which causes the adverse effects of **GW4064**.

3.1.1. Synthesis of GW4064 derivatives

To synthesize compounds with improved efficacy and stability, we have introduced on the oxymethylene function at C-4 various phenyl rings differently decorated. The structures of the compounds are shown in Figure 39. [153]
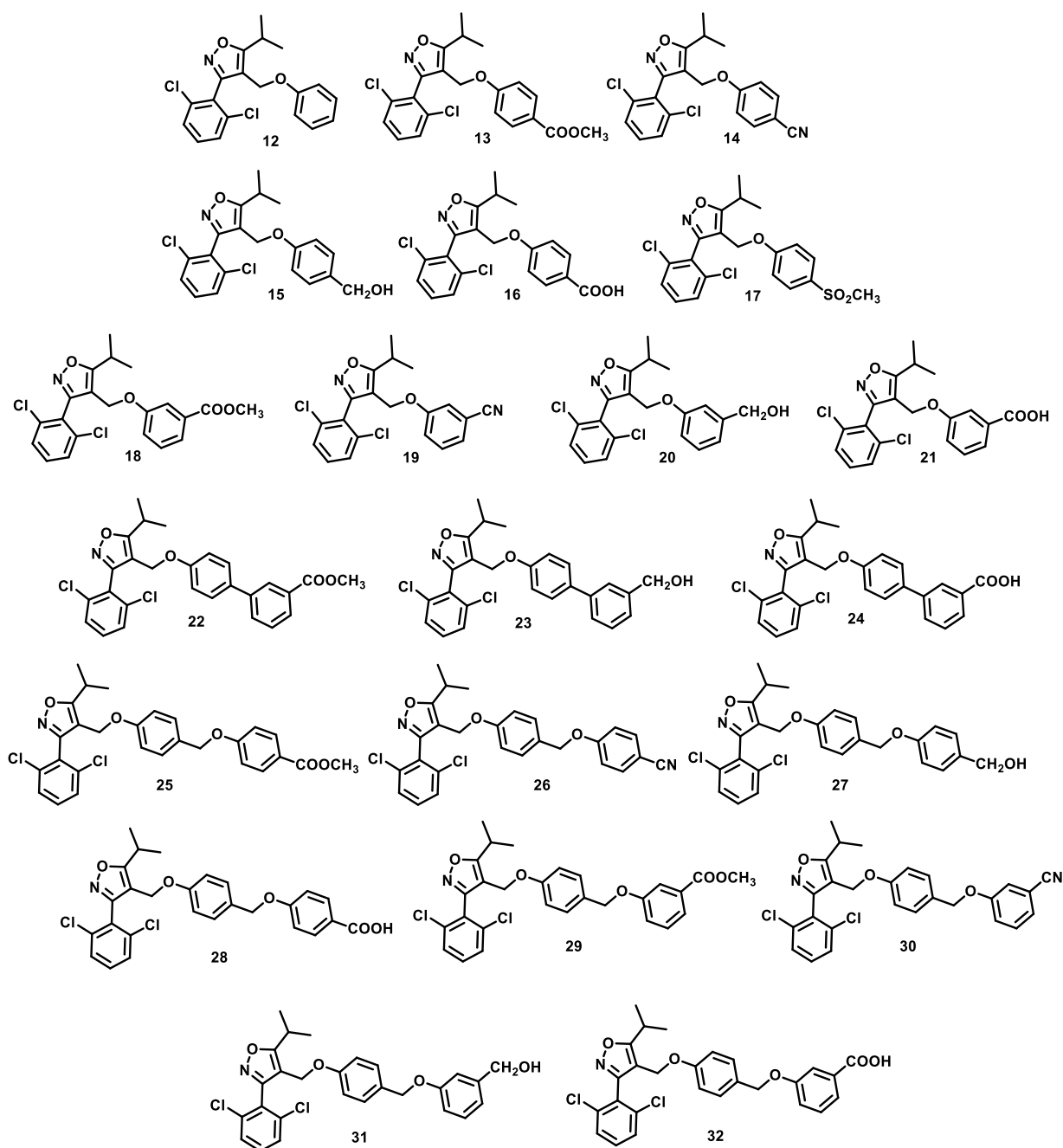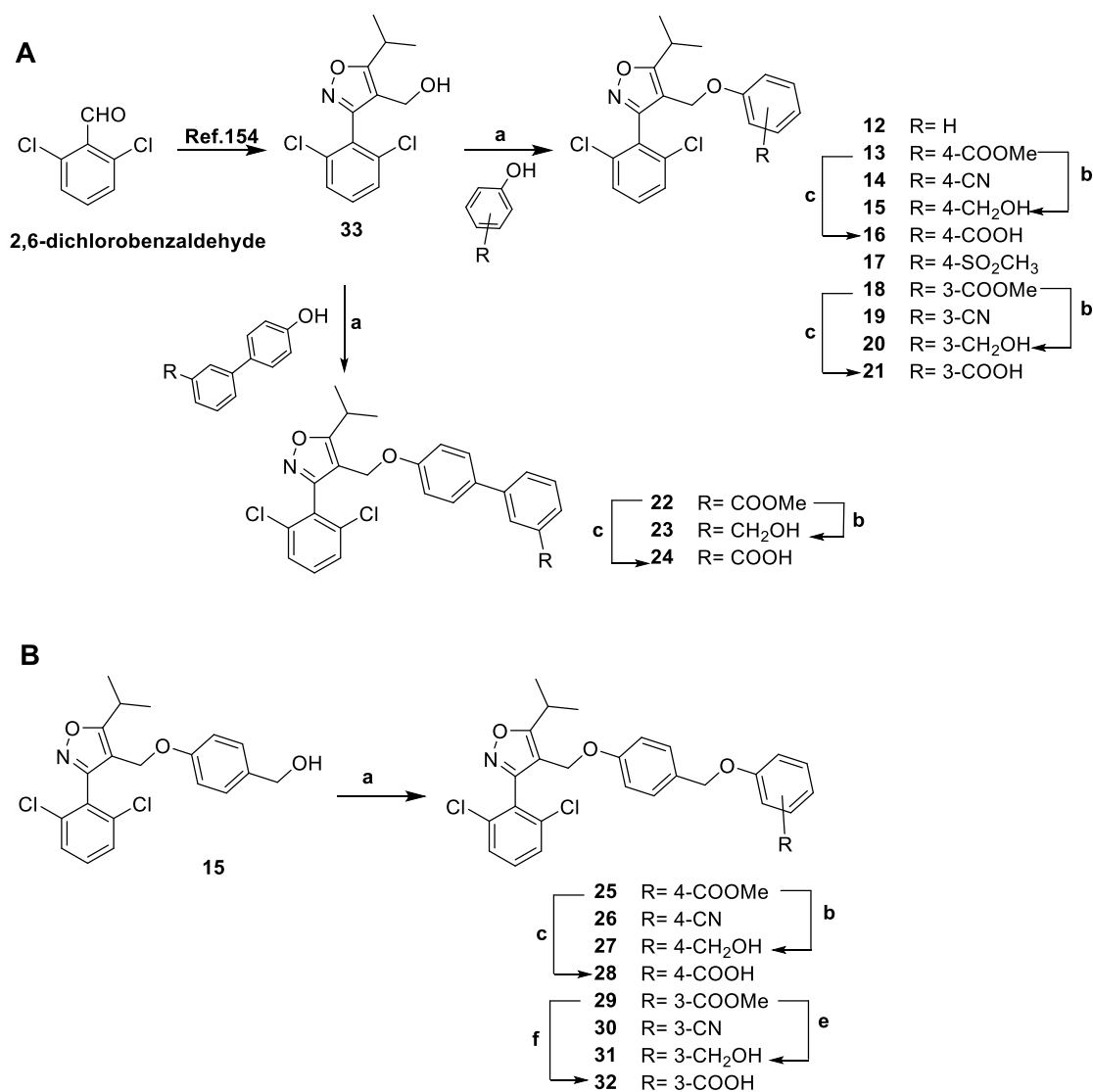

Figure 39. Library of new compounds

The synthesis of this library of derivatives has been designed by our laboratory and consists of a few reaction steps. It is extremely versatile and allows to obtain a vast library of coumpounds[153] using a several cheap and commercially available reagents.

Scheme 2: *Reagents and conditions:* **Ref. 154)**; a) P(Ph)$_3$, DIAD, phenol(R), THF dry, 0°C; **b**) LiBH$_4$, MeOH dry, THF dry; **c**) NaOH, MeOH/H$_2$O 1:1 v/v

We have synthetized compounds **12-21** starting from the same intermediate **33** which was obtained in a multi-step procedure described in a previously work. First, the 2,6-dichlorobenzaldehyde was treated with hydroxylamine hydrochloride which leads to the formation of oxime aldehyde.[154]
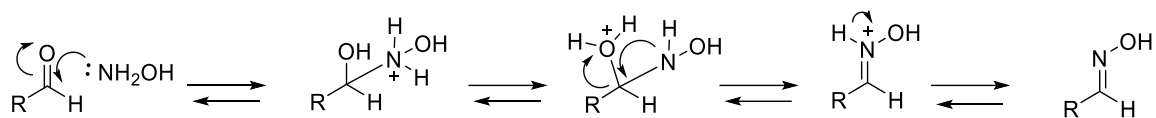
Figure 40. Mechanism of oxime formation

The next step involves the chlorination of the oxime with N-Cl-succinimide in dry DMF at 0 °C.[154]

To obtain cyclization and therefore the isoxazole nucleus, the chlorinated oxime reacts with ethyl isobutyl acetate, yielding 3-(2,6-dichlorophenyl)-5- isopropylisoxazole-4-carboxylate ethyl ester which was hydrolyzed in alkaline condition to the corresponding carboxylic acid (97% yield) which was reduced with diisobutyl aluminium hydride (DIBAL-H) to the key intermediate alcohol **33**. (69% yield)

Different Mitsunobu reactions on compound **33** using triphenylphosphine (PPh₃), di-isopropyl azodicarboxylate (DIAD) and different phenols lead to the formation of compounds **12**, **13**, **14**, **17**, **18**, **19** and **22**.

12 R= 4-H
13 R= 4-COOCH₃
14 R= 4-CN
17 R= 4-SO₂CH₃
18 R= 3-COOCH₃
19 R= 3-CN
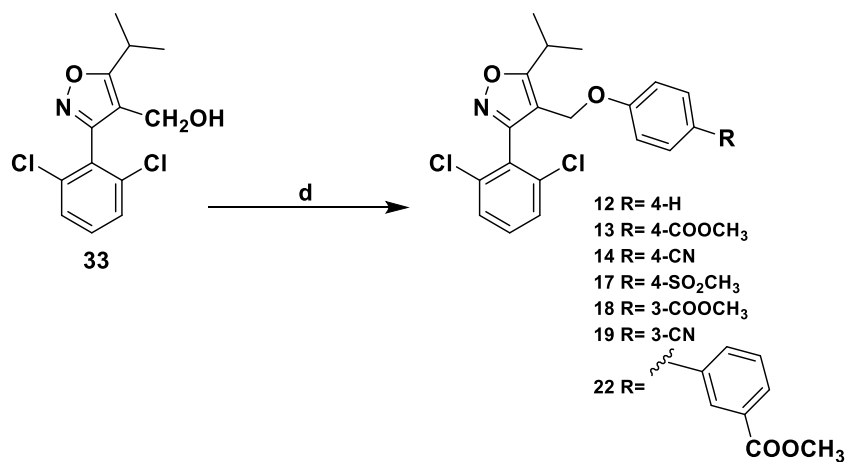
22 R=

Figure 41. *Reagents and conditions:* **d**) P(Ph)₃, DIAD, phenol(R), THF dry, 0°C

The Mitsunobu reaction, developed in 1967, is one of the most used reaction in organic synthesis, for its mild reaction conditions and its stereospecificity.[155] It is useful for the conversion of an alcohol into a variety of functional groups such as an ester using P(Ph₃) and an azodicarboxylate.

Specifically, the mechanism of the Mitsunobu reaction is quite complex and consists of several steps, as shown in Figure 33. Initially, triphenylphosphine acts as a nucleophile and attacks one of the two electrophilic nitrogen atoms of the DIAD with the formation of a betaine intermediate. Betaine deprotonates phenol via a Bronsted acid-base reaction. The phenate ion and the phosphonium salt are thus obtained as a saline intermediate. Phosphonium is an electrophilic centre and is attacked by the alcohol through a nucleophilic addition reaction which leads to the formation of adduct **1** with a positive charge on the oxygen atom.

This adduct undergoes an elimination reaction (adduct **2**) which involves the release of diisopropyl hydrazine-1,2-dicarboxylate as a dark insoluble by-product. This step gives rise to the formation of the key intermediate, the oxyphosphonium ion, necessary to activate the alcoholic hydroxyl as a good leaving group. The last reaction involves the attack of the phenate ion to the oxyphosphonium ion by means of an S_N2 with the formation of the ether product and triphenylphosphinoxide.[155]

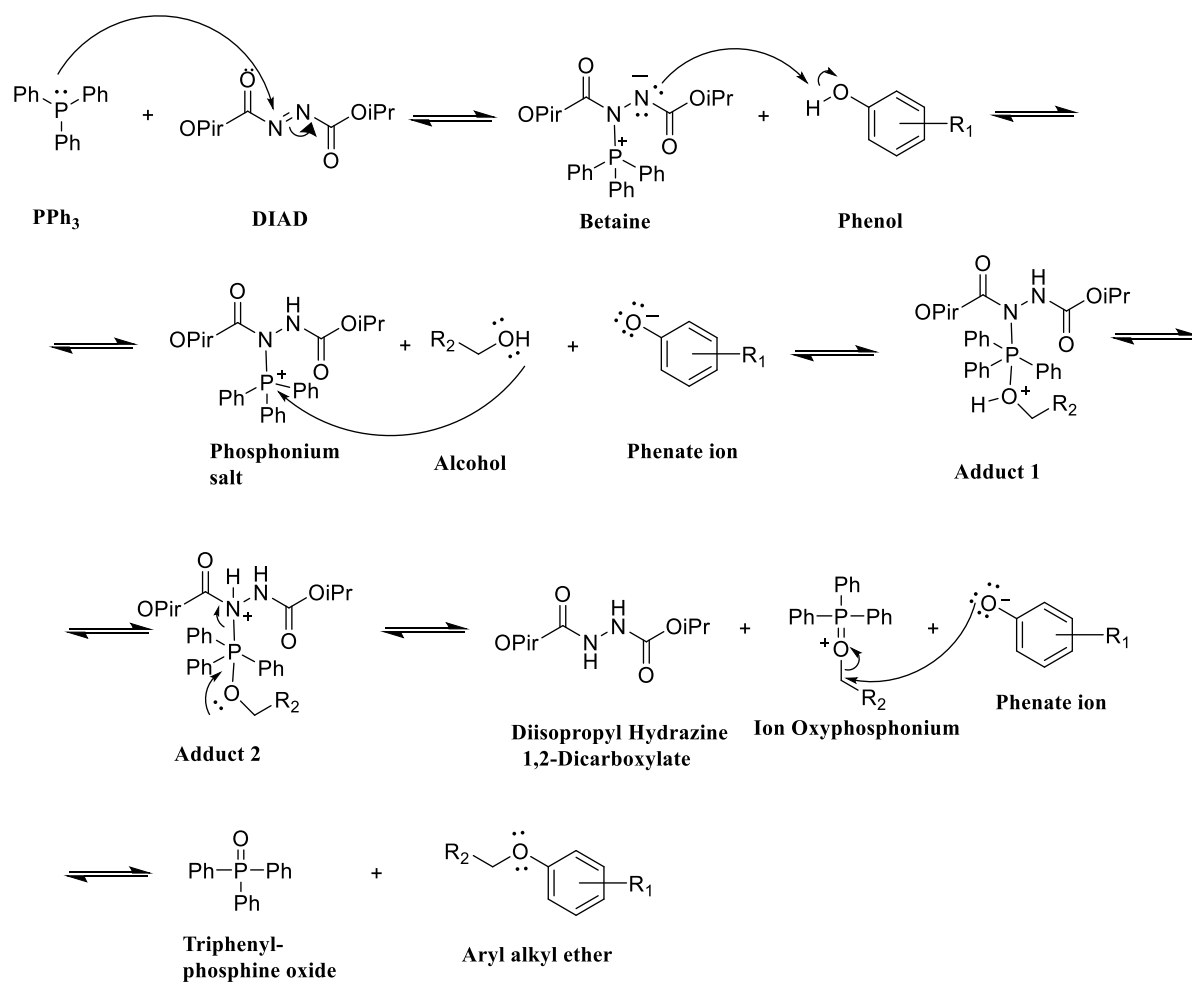**Figure 42**. Mitsunobu reaction mechanism.

Furthermore, a reduction was made on compounds **13**, **18** and **22** with lithium borohydride (LiBH$_4$) to obtain compounds **15**, **20** and **23**.

Compounds **16**, **21** and **24** were obtained by hydrolysis of esters **13**, **18** and **22** in an alkaline medium with sodium hydroxide (NaOH), methanol (CH$_3$OH) and H$_2$O in a 1: 1 v/v ratio.
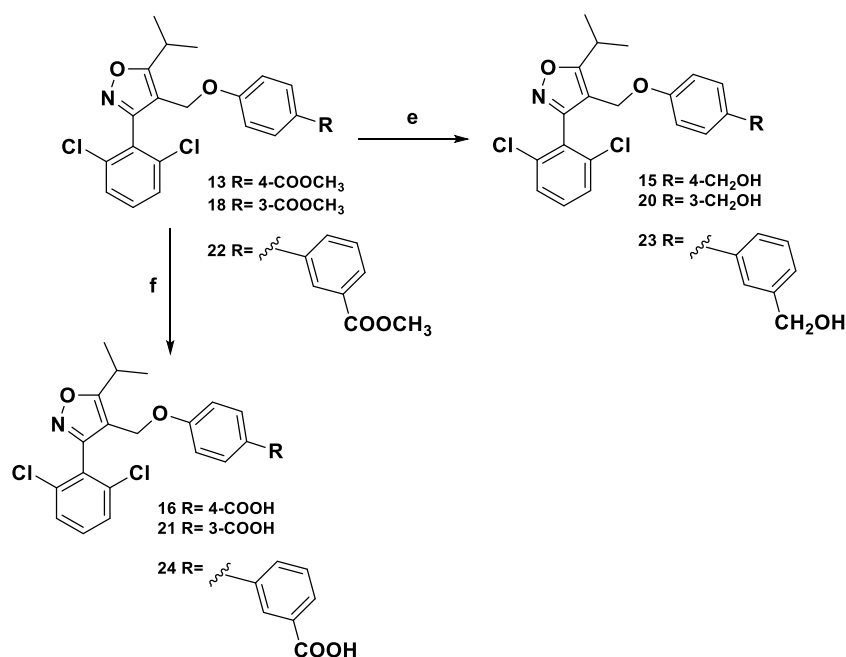
Figure 43. *Reagents and conditions:* **e**) LiBH$_4$, MeOH dry, THF dry; **f**) NaOH, MeOH/H$_2$O 1:1 v/v

Having developed a versatile and highly efficient synthetic strategy, the chemical space around the linker in position C-4 on the isoxazole core, was further explored and alcohol **15** was substrate for a second Mitsunobu reaction, to obtain compounds **25-32**.
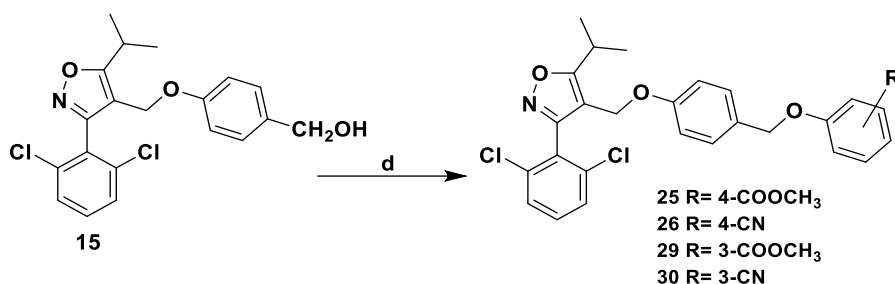
Figure 44. *Reagents and conditions:* **d**) P(Ph)$_3$, DIAD, phenol(R), THF dry, 0°C

At this point, as described for compounds **15**, **20** and **23**, a reduction with LiBH$_4$ was performed, on compounds **25** and **29**, to obtain compounds **27** and **31** and hydrolysis with NaOH to obtain compounds **28** and **32**, respectively.

Figure 45. *Reagents and conditions:* **e**) LiBH$_4$, MeOH dry, THF dry; **f**) NaOH, MeOH/H$_2$O 1:1 v/v

63

3.1.2. *In vitro* and *In vivo* assays

The efficacy on FXR was evaluated in cell-free by Alpha Screen assay compared with reference compounds CDCA (endogenous FXR ligand), 6-ECDCA (a potent semi-synthetic FXR agonist) and **GW4064** (non-steroidal FXR agonist).
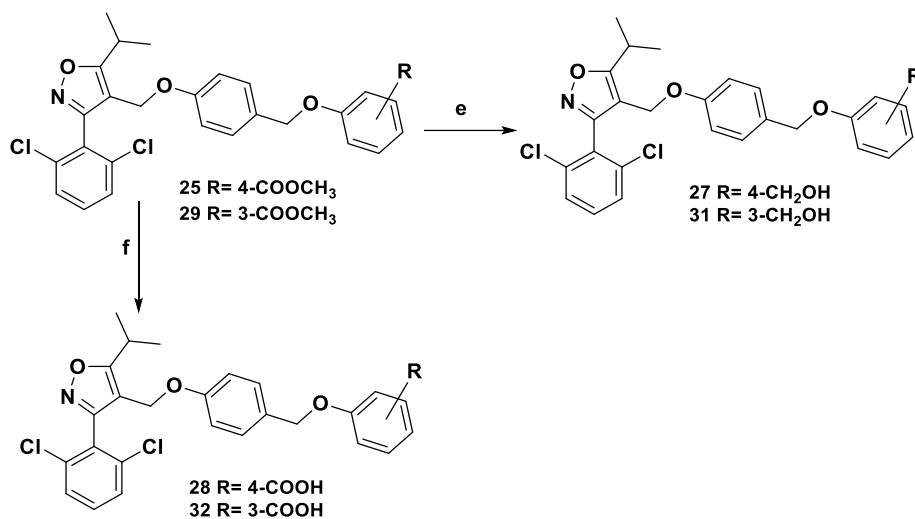
As reported in **Table 3**, the fragmentation of the **GW4064** structure has led to a drastic decrease in activity, particularly in compounds with a carboxyl group on the terminal aromatic ring such as compounds **16** and **21**. Compounds presenting a nitrile (**14**) or an alcohol (**15**) function in *para* of the aromatic ring showed similar activity to **GW4064** while the corresponding *m*-substituted derivatives (**19** and **20**) were less active indicating that the efficacy is influenced by the position of the nonacidic substituent.
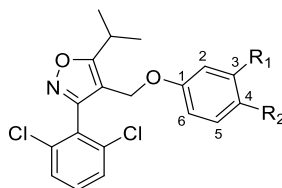
The substitution of the -COOH with the methyl sulfonate (**17**) led to an increase of efficacy and above all this compound could be the precursor of a class of drugs that can reduce in vivo phase II metabolism.

The addition of a second aromatic ring, however, showed, unlike the compounds previously described, that the terminal carboxyl group in this case is essential for the agonist activity on FXR. The position of the substituent was not of great importance, since compounds **28** and **32** have a comparable efficacy. Furthermore, the conformational freedom around the two aromatic rings does not influence the efficacy. Indeed, the constrained compound **24** exhibited a comparable efficacy than compound **32**.

Compounds **14**, **17**, **24**, **28** and **32** showed the best match in terms of efficacy and potency (Table 3) with compound **28** the most promising (EC$_{50}$ = 0.3±0.006 μM and an efficacy of 146%) of this library.[153]

Table 3. New FXR agonists

Compound	R₁	R₂	Eff (% Ref.)[a]		EC₅₀[b]
			vs CDCA	*vs* ECDCA	
CDCA	-	-	-	61±16	20
6-ECDCA	-	-	165±7	-	0.5
GW4064	-	-	166±15	101±15	0.02
12	H	H	114±7	69±7	1.59±0.35
13	H	COOMe	136±7	83±7	3.59±1.08
14	H	CN	151±6	92±6	0.81±0.20
15	H	CH₂OH	164±18	100±8	2.93±1.09
16	H	COOH	43±18	26±18	6.67±1.7
17	H	SO₂CH₃	167±7	102±7	1.09±0.1
18	COOMe	H	120±6	73±6	2.06±0.26
19	CN	H	93±17	56±17	10.17±0.84
20	CH₂OH	H	76±20	46±20	4.37±0.72
21	COOH	H	67±18	40±18	19.74±0.31
22	H	(COOMe benzyl)	125±3	64±3	2.8±0.36
23	H	(CH₂OH benzyl)	121±2	61±2	0.83±0.06
24	H	(COOH benzyl)	175±3	115±3	1.4±0.32
25	H	(O-phenyl COOMe)	92±1	56±1	0.73±0.07
26	H	(O-phenyl CN)	83±2	50±2	0.94±0.02
27	H	(O-phenyl CH₂OH)	103±4	63±4	0.74±0.02
28	H	(O-phenyl COOH)	149±12	91±13	0.30±0.006
29	H	(O-phenyl COOMe, meta)	97±3	36±3	1.15±0.37
30	H	(O-phenyl CN, meta)	117±5	56±5	5.4±0.51
31	H	(O-phenyl CH₂OH, meta)	124±14	63±14	0.67±0.038
32	H	(O-phenyl COOH, meta)	191±4	130±4	0.46±0.033

[a]Alpha Screen coactivator recruitment assay measure a immediate interaction of FXR with SRC-1; ligands were tested at 5 µM. Eff (%) is the maximum efficacy of the compounds in comparison to CDCA and/or 6-ECDCA set as 100%. Results are expressed as mean of three independent measurements ± standard error.

[b]Transactivation assays on HepG2 cells. EC50 values (µM) were calculated from a minimum of three experiments. Results are expressed as mean ± SEM.

However, although less effective than **GW4064** in transactivating FXR, these compounds showed a similar ability to recruit the SRC-1 coactivator.

To gain insight on its binding mode to the ligand binding domain (LDB), we have performed on compound **28** docking studies. The results showed that the ligand's 3-(2,6-dichlorophenyl)-5-isopropylisoxazole moiety occupies the hydrophobic cavity of the LBD defined by helices H3, H5, H6, H7, H11, and H12. The ligand forms favourable van der Waals interaction with the residues Phe284, Leu287, Phe329, Ile352, Trp454, and Leu465. Additionally, the isoxazole ring forms a hydrogen bond with the protonated His447 of H10 and π-stacking interactions with Trp469 of H12 (Figure 46A).[143,144,156]
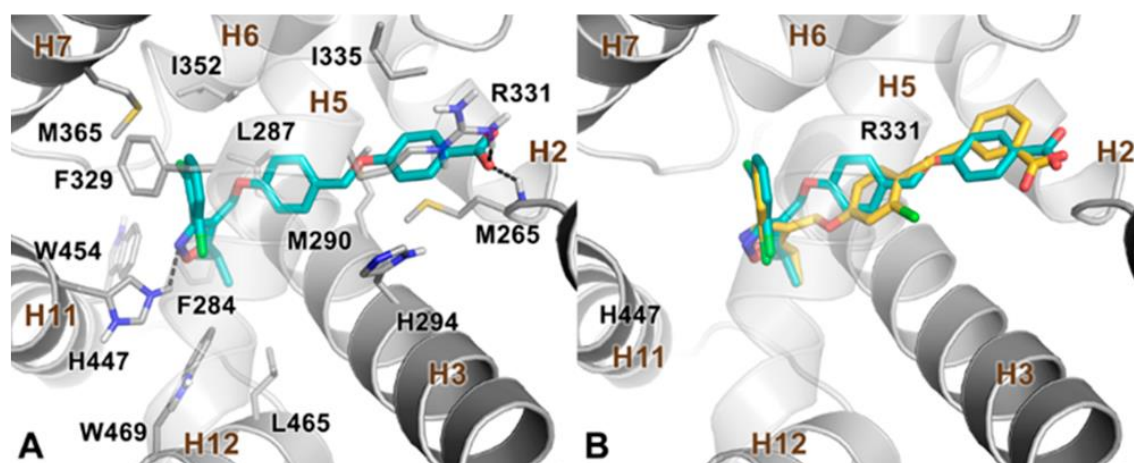

Figure 46. Docking study of compound **28** in FXR Ligand Bind Domain crystal structure. The receptor is in gray tapes, with the main amino acids for ligand binding highlighted as sticks. Non polar hydrogens are omitted for clarity. Hydrogen bonds are displayed as dotted black lines. (B) Overlap between the predicted binding mode of **28** and the crystallo-graphic pose of GW4064 (yellow sticks).

The ligand/protein interactions in the LDB of FXR stabilize the cation-π interaction which favour the receptor conformation responsible for the recruitment of the co-activator peptide. The carboxylic group of the compound **28** H-binds with a Met265 and forms a salt bridge with the side chain of Arg331 at H5. The latter is the strongest interaction and proves to be a ligand anchor point in the LBD. It has never been reported a similar interaction with Arg331 to stabilize the binding of bile acid derivatives to FXR.[144]

Finally, the *p*-(phenoxy-methyl)-phenoxy-methyl linker of the compound forms hydrophobic contacts with residues of Met265, Leu287, Met290, Ile335, and Ile352, which stabilize the ligand binding conformation. The elucidation of the binding mode of **28** allowed the rationalization of the various effectivity values of the opposite derivatives of the series reported in Table 1. From the structural point of view, the compounds differ for the distance of the isoxazole ring from the terminal functional group and the nature of the latter. Compounds endowed with the biphenyloxymethyl and the *p*-(phenoxy-methyl) phenoxy-methyl linker like compound **28** and presenting diverse terminal groups such as −COOH, −CH$_2$OH, −COOCH$_3$, and −CN, can similarly interact with Arg331. As a result, the derivatives with *para* and *meta* substituents show comparable efficacy. However, less polar groups like −COOCH$_3$ weaken the interaction with Arg331, so reduced the ligand-induced recruitment of the coactivator. The terminal group of the compounds is provided of the shorter phenoxymethyl linker that poorly interacts with Arg331, while it is placed close by hydrophobic residues like Ile335, Met265, and Met290 and the polar His294. Therefore, the presence of polar but not charged terminal groups leads to ligands with higher efficacy. Finally, considering the structural similarity between **28** and **GW4064**, we deemed important to compare the docking pose of **28** with the X-ray binding conformation of **GW4064**.[140] The overlap, in the LBD of FXR, of the two binding modes displayed a similar pattern of interaction with the receptor in which the two ligands similarly occupy the LBD, thus allowing the proper interaction with His447 and Arg331 (Figure 46B).

In conclusion, this study resulted in the identification of compound **28** as the most active FXR agonist.

Table 4. *In Vitro* Pharmacokinetics for Selected Derivatives

Compound	Solubility (µM)	Cl_{int}	$t_{1/2}(min)$	%
6-ECDCA	>200	109	21	27
GW4064	152	56	41	48
14	3	299	8	3
17	>200	112	21	26
24	75	53	44	56
28	44	32	72	67
32	>200	35	66	62

The physicochemical parameters of the most interesting compounds (**14**, **17**, **24**, **28** and **32**) were evaluated by LC-MS (**Table 4**). As expected, compound **14** showed a low aqueous solubility, while compound **17** was more polar in comparison with GW4064.

Comparing the compounds with a carboxylic acid in the chain (**24**, **28** and **32**), the compounds with this substituent in *meta* (compounds **24** and **32**) showed an improved aqueous solubility if we compared to the compound with the -COOH in *para*.(compound **28**) (Table 4) These results were further investigated by calculating the in *vitro* stability, incubating them with rat liver microsomes. Compounds **24**, **28** and **32** showed a moderate clearence, with a $t_{1/2}$ of more than 1h for compounds **28** and **32**. Lastly, compounds **14** and **17** displayed a low metabolic stability in *vitro* with a percentage of 3% and 26%, respectively, of unmodified molecule after 40min, thus, making them unsuitable as potential drugs.

The FXR activity of compounds **24**, **28** and **32** was further validated, evaluating the effect in modulating SHP (Shock head Protein) a target gene of FXR, by means of RT-PCR. Liver carcinoma cell line HepG2 and **GW4064** (10µM) were used as the reference compound. At a concentration of 5 µM, compounds **28** and **32** resulted more potent than **GW4064** in the induction of SHP mRNA expression. It is interesting to note that the position of the carboxylic group on the terminal aromatic ring is not essential for the agonistic activity. (Figure 47)
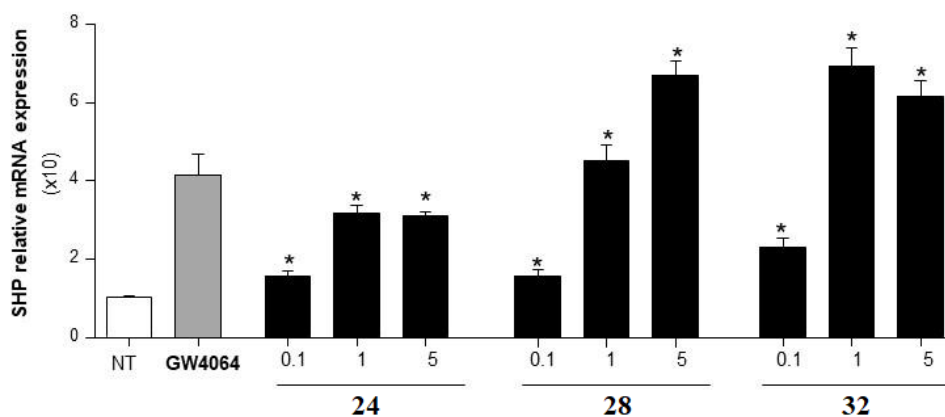
Figure 47. SHP mRNA expression in HepG2 cells started with increasing concentration of compounds **24**, **28** and **32** (0.1, 1 and 5 μM). GW4064 (10 μM) was used as positive control. Values are normalized to GAPDH and are expressed in comparison to those of not treated cells (NT) which are indiscriminately settled to 1. *$p < 0.05$ versus not treated cells (NT).

To confirm the selectivity of the compounds towards FXR, a transactivation assay was performed on HEK-293T cells and using TLCA (10μM) as a reference compound. As shown in figure 48, all compounds are inactive towards GPBAR1.
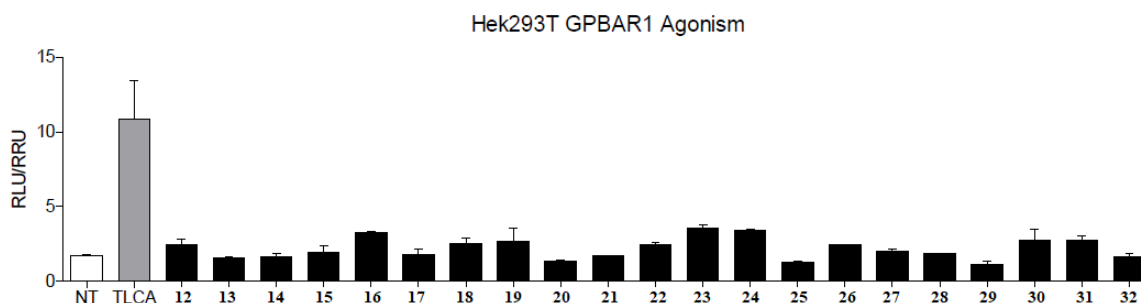

Figure 48. Agonism towards GPBAR1

It was also investigated the *in vitro* profile of compounds **24**, **28** and **32** considering the common off targets for bile acid receptor ligands. The results showed that these compounds were inactive in the transactivation of LXRα/LXRβ and PPARγ.
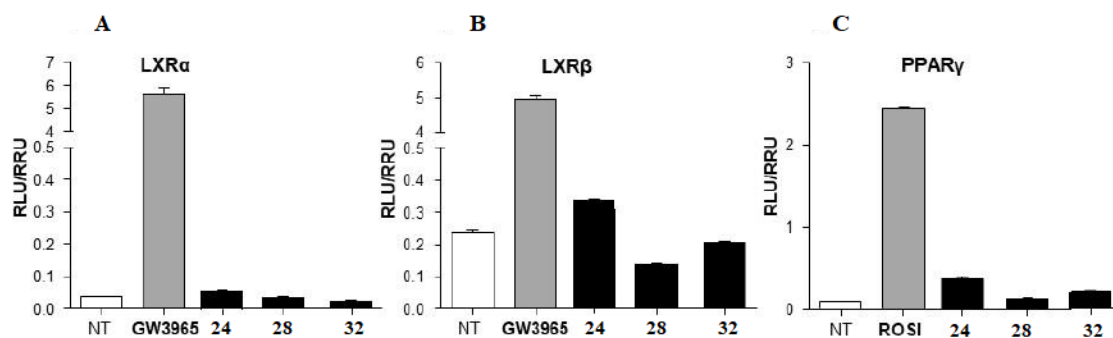
Figure 49. Evaluation of the activity on LXRα/β and PPARγ

To evaluate intestinal absorption, *in vivo*, only compound **28** were administered in mice for 3 days by o.s. or by i.p. and hepatic expression of target genes, like SHP and BSEP, measured by RT-PCR. The results shown in Figure 39 demonstrated that both genes were upregulated after the administration of **28**. (Figure 50)
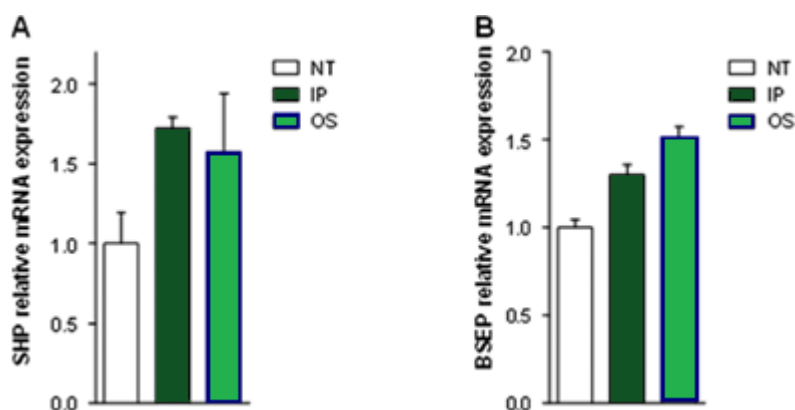

Figure 50. Mice were given with 10 mg/kg of **28**, daily by gavage (o.s.) or i.p. for 3 days. Total RNA extracted from liver was evaluate by quantitative real-time PCR the relative mRNA expression of (A) SHP and (B) BSEP. The kens are normalized to GADPH mRNA. Results are the mean ± SEM of 4 mice per group.

At this point, considering that FXR agonists show significant effects in reducing liver injury, we have decided to evaluate whether compound **28**, a potent FXR agonist, might rescue from acute liver failure caused in mice by APAP overdosing.[157] *In vivo* acetaminophen (APAP) is one among the foremost pre-scribed drugs worldwide. Although safe at therapeutic doses, APAP overdosing causes severe liver injury, which ends up in acute liver failure.[135] Presently, APAP o.d. is that the leading explanation for acute liver failure within the us and

most of Europe and represents a serious indication for liver transplantation. At therapeutic doses, APAP is metabolized within the liver by phase II clinical trial conjugation enzymes and remodelled within the corresponding sulphate and glucoronate derivatives, with solely a little quantity being born-again into the cytotoxic archangel acceptor N-acetyl-p quinoneimine (NAPQI), that successively is quickly detoxified by glutathione (GSH) conjugation. However, excessive NAPQI formation, ensuing from APAP o.d., saturates phase II clinical trial conjugation pathways, resulting in formation of enormous amounts of the cyanogenic NAPQI matter,[158] depletion of viscus GSH, and binding to cellular proteins with consequently hyperbolic aerophilous stress and mitochondrial injury. For this purpose, C57Bl6 mice were administered one dose of 500 mg/kg of APAP. After 24h, the mice survived were sacrificed and their blood and liver sections collected. The results showed a severe liver injury with increase of AST and ALT plasma level ($p < 0.01$ versus naiv̈ emice). This pattern was completely reversed by treating mice with compound **28** at the dose of 30 mg/kg kg ($p<0.01$ versus APAP alone). A similar result was shown in mice treated with **GW4064**. To gain insights on the molecular mechanism that supports protection afforded by compound **28**, we have then examined the effect of this agent on enzymes concerned in xenobiotic metabolism.[160] As shown in Figure 51D−F, exposure to APAP results in a dramatic downregulation of the expression of glucuronosyltransferases (Ugt1a1 and Ugt2b1) and sulfotransferase family 1A member 1 (Sult1a1) ($p < $ zero.01). These three genes cypher for phase II clinical trial enzymes concerned in xenobiotics detoxification and far-famed for being FXR regulated genes. The results showed that compound **28** restores the expression of these phase II genes. Consistent with these findings, compound **28** effectively re-established the liver levels of glutathione and SOD (superoxide dismutase) (Figure 51G and 51H, $p < 0.01$). Additionally, compound **28** reduced the level of lipoid peroxidation in

mice administered with APAP, as indicated by changes of malonyl-dialdehyde (MDA) levels within the liver of varied experimental teams (Figure 51I, $p < 0.01$).

APAP and its main Phase II conjugates (APAP-glucoronate and APAP-sulphate) in plasma were measured by LC−MS/MS and the relative concentrations square measure shown in Figure 51J. Plasma APAP concentration reached ∼1000 nM, in response to APAP treatment. Treatment with compound **28** decreased APAP plasma concentration (615 nM) but also increased the concentration of APAP metabolites, APAP-glucuronide and APAP-sulphate, thereby indicating that compound **28** will increase APAP metabolism by the liver.
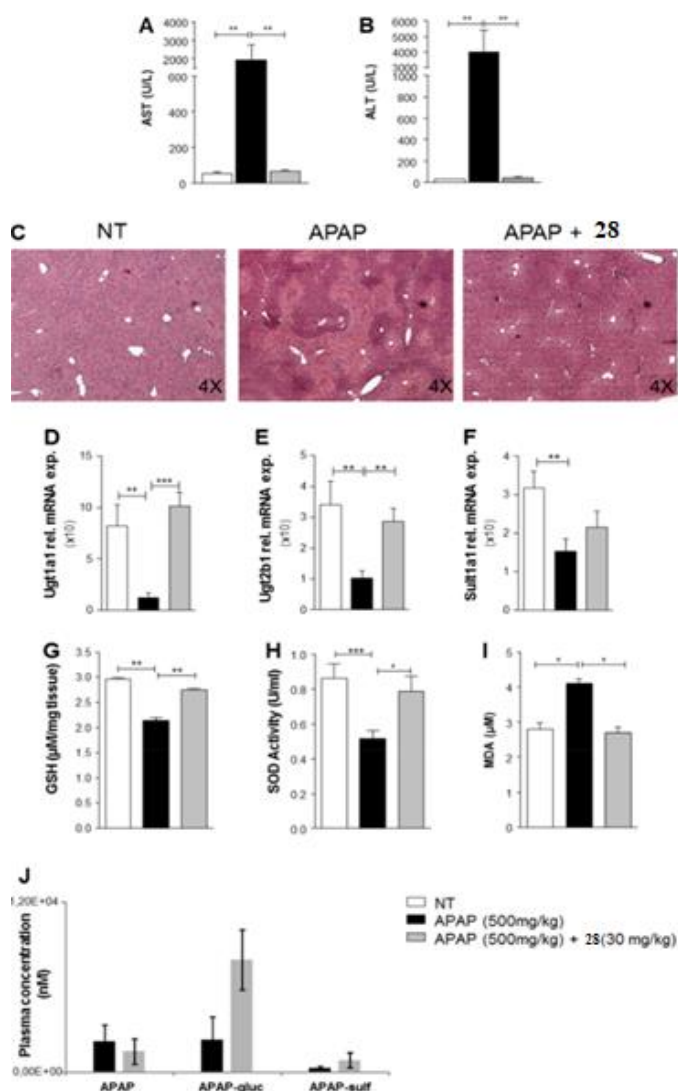

Figure 51. Compound **28** rescues mice form acute liver damage caused by APAP overdose. Serum levels of (**A**) AST and (**B**) ALT; (**C**) hematoxylin and eosin (H&E) dyeing on mice liver tissues; Relative mRNA levels of (**D**) Ugt1a1, (**E**) Ugt2b1, and (**F**) Sult1a1 in liver; (**G**) hepatic levels of GSH, (**H**) hepatic SOD activity, and (**I**) hepatic levels of MDA;(**J**) effects of **28** APAP metabolic disposal with mouse plasma contents (nM) of APAP, APAP-glucuronide, and APAP-sulfate. Each value represents the mean ± SEM of 5−8 animals per group. *$p < 0.01$.

In conclusion, the chemical manipulation on **GW4064** afforded the identification of several FXR agonists with nanomolar potency in transactivation and SRC-1 recruitment assays. This study resulted in the identification of compound **28**, an orally active FXR agonist that rescues mice from acute toxicity caused by APAP.

CHAPTER 4

PROJECT PRESENTATION

4.1. Dual Modulator of CysLT$_1$R and GPBAR1

In a recent study of the research group where I carried out my PhD a small group of antagonists of the CysLT$_1$ receptor has been tested on the two best known bile acid receptors, GPBAR1 and FXR, actually considered the promising targets for the treatment of metabolic dysregulation.[160] They decided to explore whether there existed a cross-talk between CysLT$_1$R antagonists and these two bile acid receptors (FXR and GPBAR1) in order to develop multitarget drugs for the treatment of various metabolic diseases such as type 2 diabetes, fatty liver disease, dyslipidemia and inflammatory states affecting the enterohepatic system.
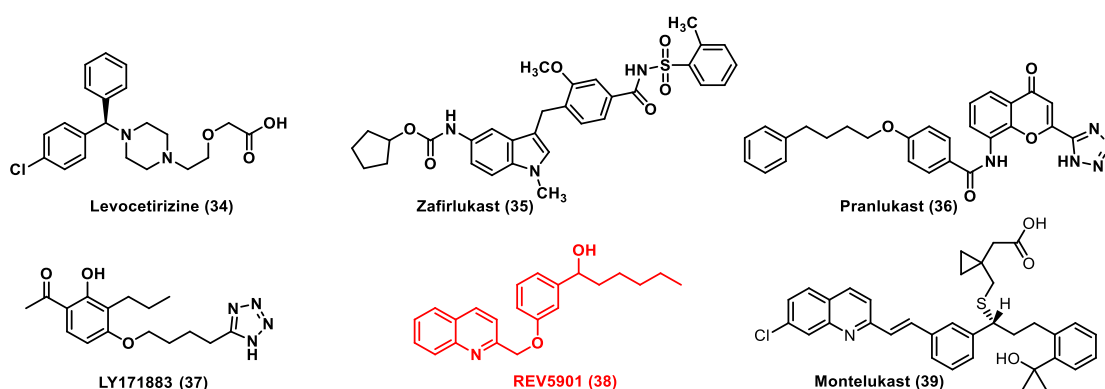

Figure 52. Chemical structures of tested CysLT1R antagonists

In this study six CysLT$_1$R antagonists were selected: Levocetirizine (**34**), Zafirlukast (**35**), Pranlukast (**36**) and Montelukast (**39**) (drugs used mainly for the treatment of asthma), LY171883 (**37**) and **REV5901**(**38**). The results showed that only the latter two were effective in transactivating GPBAR1 with **REV5901** the most active with an EC$_{50}$ of 2.5 µM. None of the tested compounds exhibited activity on FXR.(Figure 53)
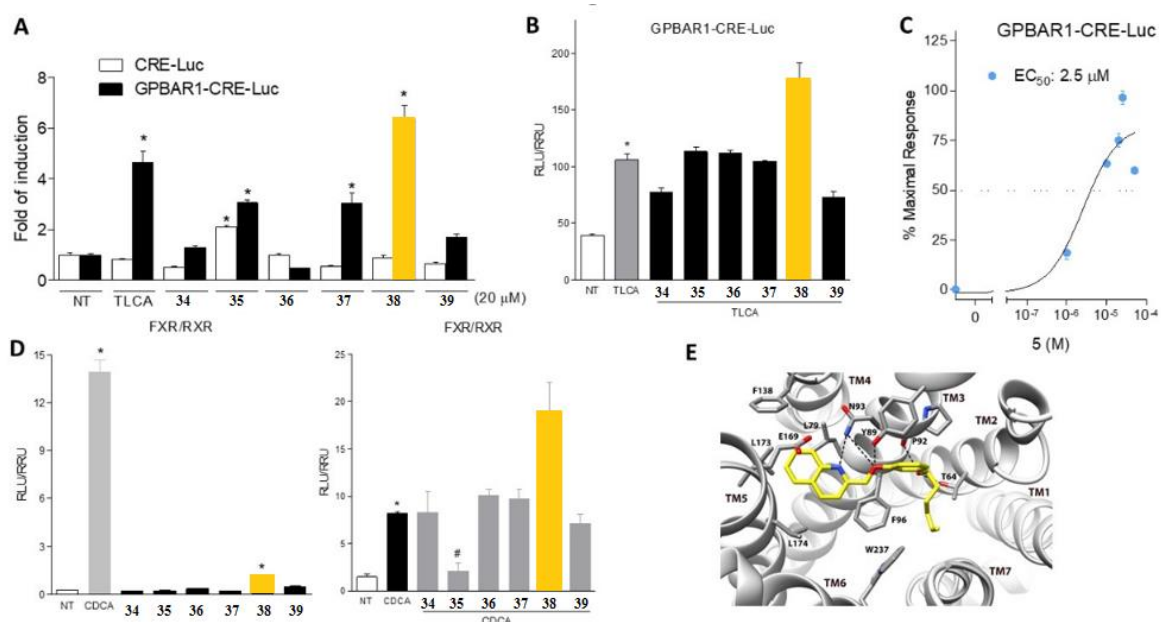
Figure 53. (A) Measure of induction of luciferase activity in cells transfected with CRE-Luc or GPBAR1-CRE-Luc and incubated with TLCA (10 µM) or compounds **34**-**39** (20 µM); (B) Antagonistic activity of compounds **34**-**39** towards GPBAR1 (TLCA = 10 µM, compounds 56-61 = 20 µM). Results are show as mean ± standard error. ∗$p < 0.05$ versus not treated cells (NT). (C) Dose-response curve of compound **38** (REV5901) to evaluate the activity on GPBAR1; cells were stimulated with different concentrations of **38** from 1 µM to 50 µM. (D). FXR transactivation on HepG2 cells transfected with pSG5-FXR, pSG5-RXR, PGL4.70-Renilla, and p(hsp27) TKLUC vectors, and with compounds **34**-**39** (20 µM) alone or with CDCA (10 µM). Results are show as mean ± standard error. ∗$p < 0.05$ versus not treated cells (NT). (E). Binding mode of REV5901. The ligand is in yellow, whereas the interacting leavings of the receptor are shown in grey. Oxygen atoms are in red and nitrogens in blue. GPBAR1 is represented as grey ribbons. Hydrogens are omitted and H-bonds are displayed as dashed lines.

In vivo studies on two different rodent models of colitis showed that **REV5901** acts as GPBAR1 agonist attenuating inflammation and immune dysfunction. (Figure 54)
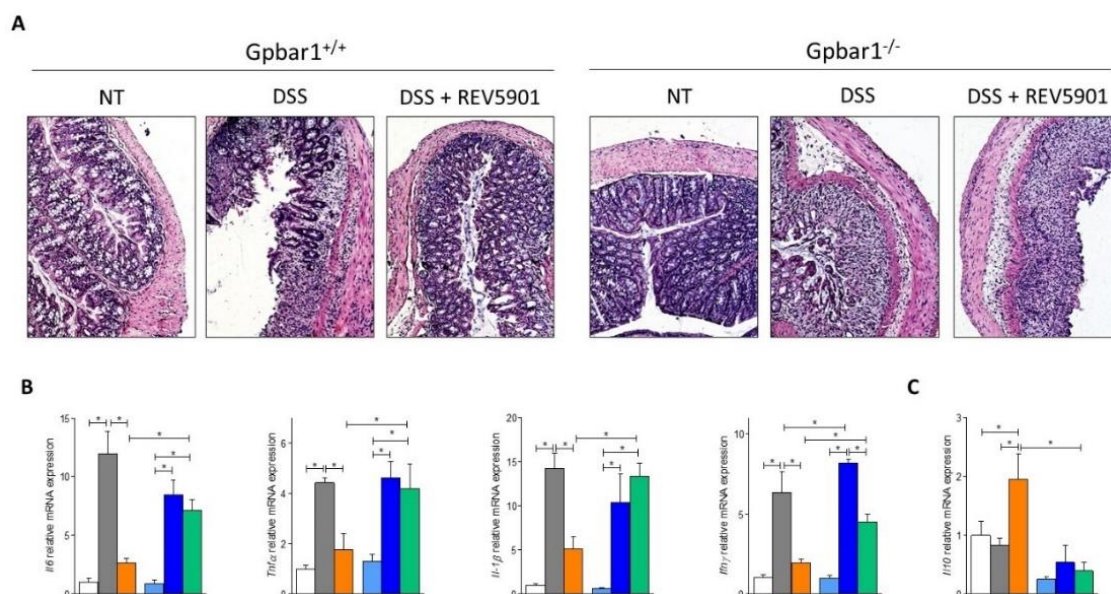
Figure 54. Gpbar1+/+ and Gpbar1−/− mice were treated with DSS and then administered with REV5901 (30 mg/kg/day) or Montelukast (10 mg/kg/day) by gavage for 8 days. (A) H&E staining of colon sections from control mice, mice treated with DSS, and mice treated with TNBS plus REV5901 or Montelukast (original magnification ×10). Relative mRNA expression of (B) pro-inflammatory cytokines (Il-6, Tnf-α, Il-1β, Ifn-γ), (C) anti-inflammatory cytokine (Il-10) in colon of Gpbar1+/+ and Gpbar1−/− mice was evaluated by real-time PCR. The data are normalized to Gapdh mRNA. Results are the mean ± SEM of 6−10 mice per group from two independent experiments. *$p < 0.05$.

The characterization of mRNA expression of pro-inflammatory and anti-inflammatory cytokines was carried out in the DSS (Dextran Sodium Sulphate) rodent model. The results showed that **REV5901** protects the gastrointestinal tissue from damage caused by colitis thanks to the activity on GPBAR1.[161] These results led to further explore the quinoline scaffold aiming to identify new multi-target ligands acting as CysLT$_1$R antagonist and GPBAR1 agonist.

4.1.1. Synthesis of REV5901 Derivatives

Therefore, I have synthetized a new library of compounds (figure 55) preserving the quinoline ring and modifying the substituents on the benzene ring of **REV5901**, introducing polar substituents or alkyl groups to mimic its side chain.[162]
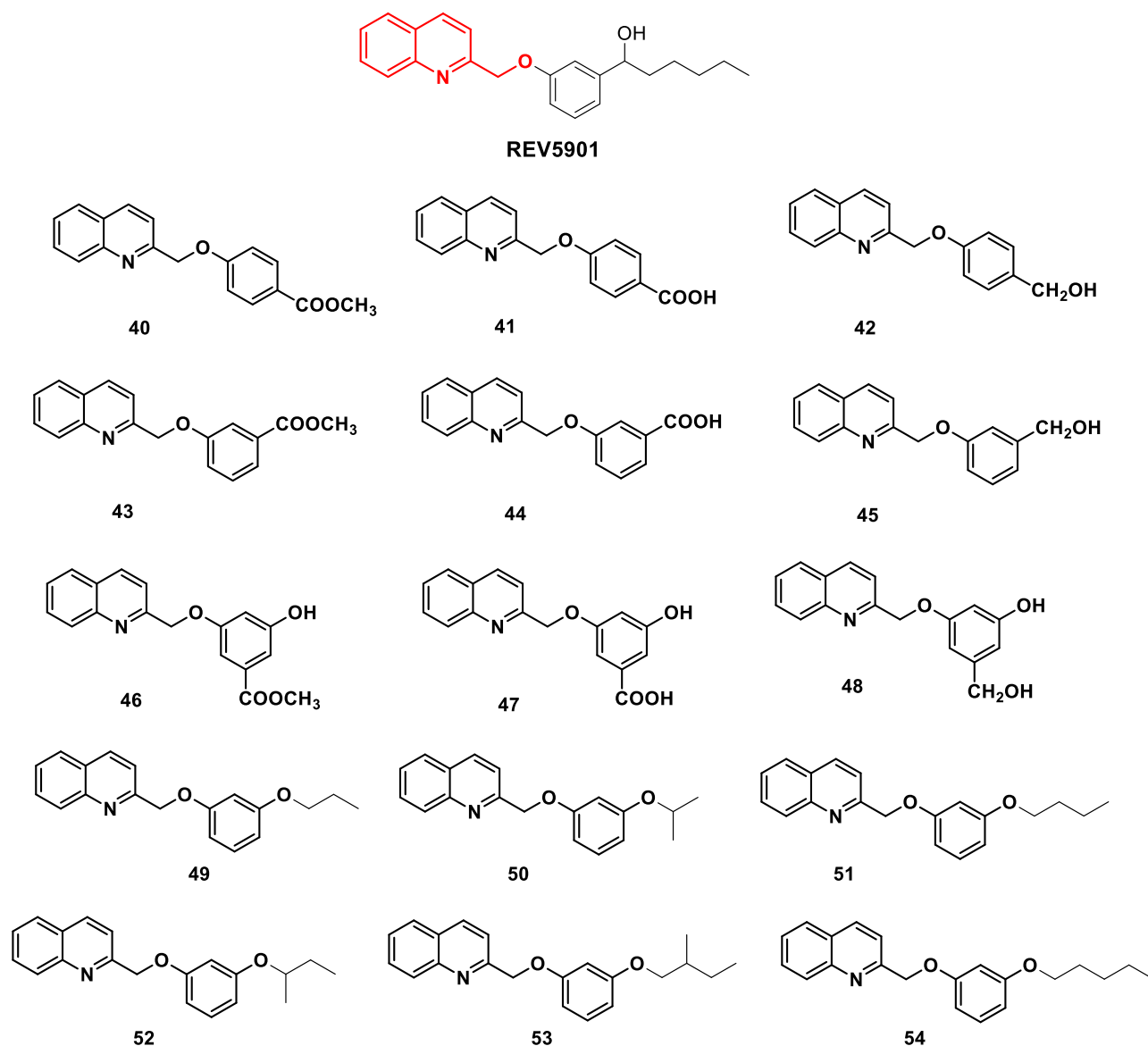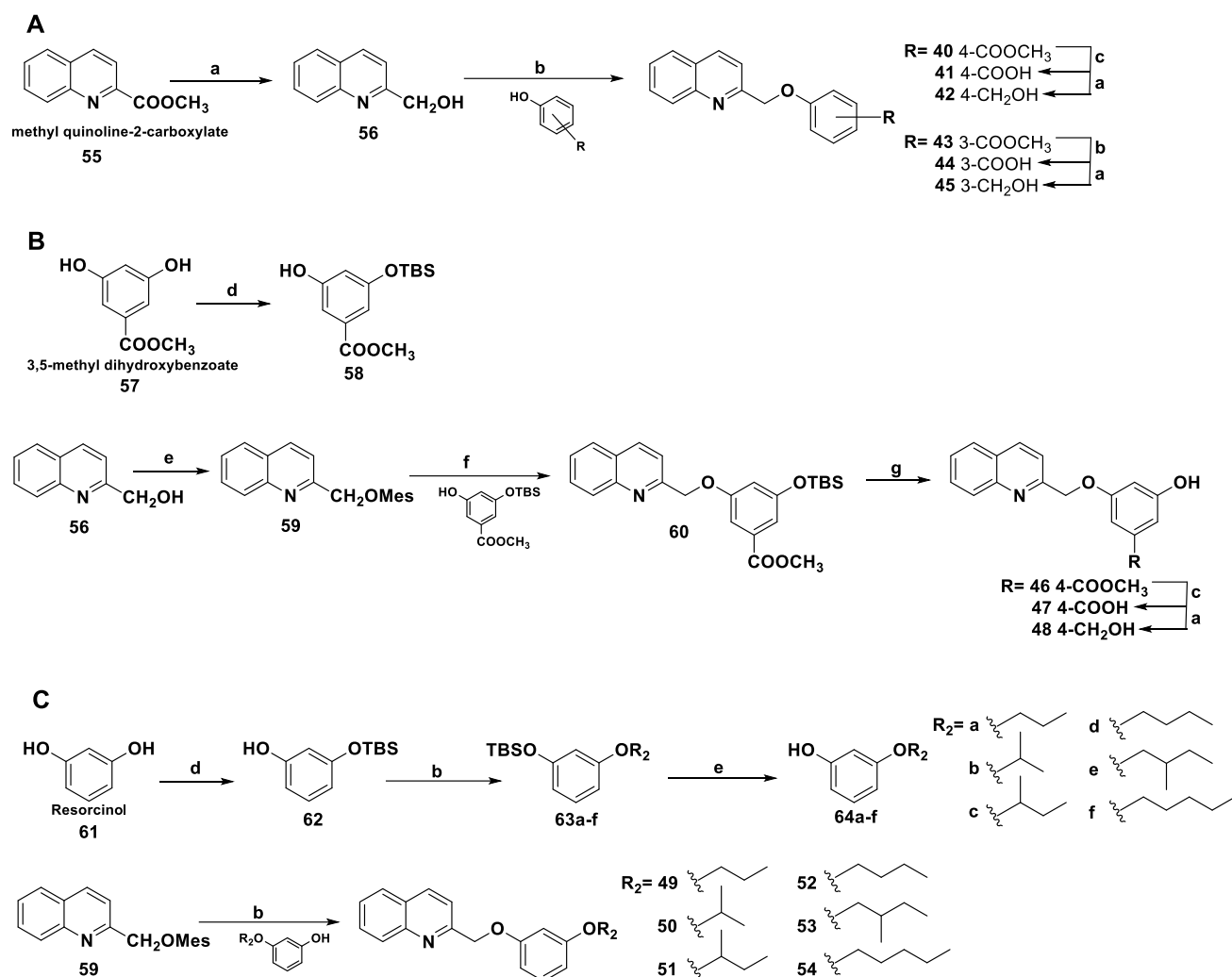

REV5901

Figure 55. Library of **REV5901** derivatives

The new library of compounds **40**-**54** was obtained by the following synthetic scheme 3. In particular:[162]

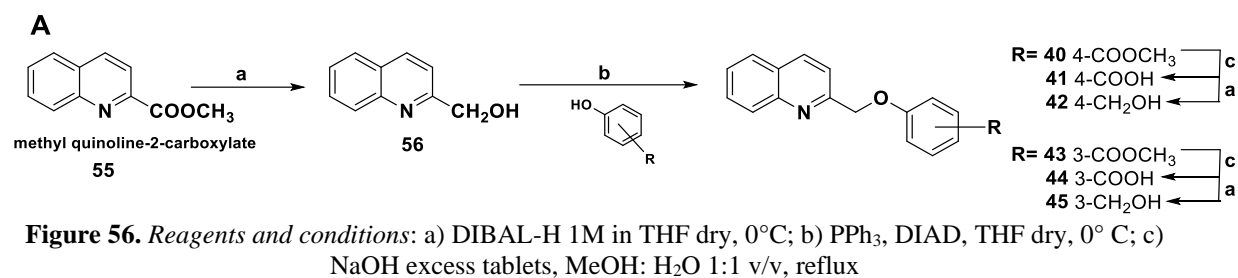❖ Panel A describes the steps to obtain compounds **40-45**

❖ Panel B describes the steps to obtain compounds **46-48**

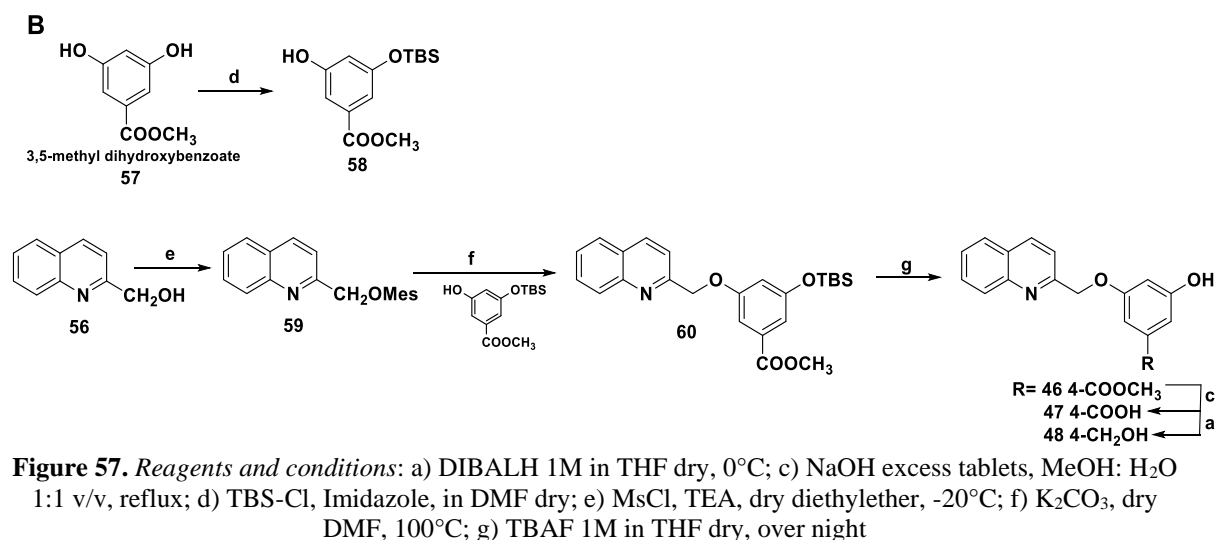❖ Panel C describes the synthesis of compounds **49-54**

Scheme 3. *Reagents and conditions*: a) DIBAL-H in THF, 0°C; b) PPh$_3$, DIAD,THF dry,0° C; c) NaOH excess tablets, MeOH: H$_2$O 1:1 v/v, reflux; d) TBS-Cl, Imidazole, in DMF dry; e) MesCl, TEA, dry diethylether, -20°C; f) K$_2$CO$_3$, dry DMF, 100°C; g) TBAF 1M in THF dry, over night

In panel A, the synthesis starts from methyl quinoline-2-carboxylate, available on the market at low cost, on which was performed a reduction with DIBAL-H to obtain compound **56** (72% to 31% yield). On compound **56** was performed a Mitsunobu reaction with DIAD and PPh$_3$ and different *meta/para* substituted phenols, as described in chapther 2.2.2., to obtain compounds **40** and **43** (76% and 78% yield respectively). A subsequent basic hydrolysis gives compounds **41** and **44** (43% and 68% yield). Finally, the reduction with DIBAL-H on compounds **40** and **43** furnished compounds **42** and **45**. (68% and 60% yield, respectively)[162]

A

Figure 56. *Reagents and conditions*: a) DIBAL-H 1M in THF dry, 0°C; b) PPh₃, DIAD, THF dry, 0° C; c) NaOH excess tablets, MeOH: H₂O 1:1 v/v, reflux

In panel B, to obtain intermediate **58,** the first reaction was the protection of the hydroxyl group of the 3,5-methyl dihydroxybenzoate using tert-butyldimethylsilyl chloride (TBS-Cl) and imidazole in DMF. After chromatographic purification, compound **58** was obtained with a yield of 50%. In order to obtain intermediate **59** (87% yield), we performed a mesylation of compound **56** followed by a Williamson reaction with compound **58**. The intermediate **60** was, then, deprotect with TBAF to give compound **46** (85% yield) which was subjected to hydrolysis and reduction giving compounds **47** and **48**. (quantitative and 92% yield respectively)[162]

B

Figure 57. *Reagents and conditions*: a) DIBALH 1M in THF dry, 0°C; c) NaOH excess tablets, MeOH: H₂O 1:1 v/v, reflux; d) TBS-Cl, Imidazole, in DMF dry; e) MsCl, TEA, dry diethylether, -20°C; f) K₂CO₃, dry DMF, 100°C; g) TBAF 1M in THF dry, over night

To increase the chemical space and to understand the structural requirements for the modulation on GPBAR1 and CysLT₁R receptors, I synthesized other derivatives introducing, on the aromatic ring, side chains whit different length.

In panel C the first step is the mono-protection of the resorcinol with TBS-Cl (47% yield), followed by a Mitsunobu reaction to introduce different alkyl chains and then deprotection with TBAF to obtain intermediates **64a**-**f** (47-84% yield over two steps). To obtain compounds **49**-**54** (61%-quantitative yield) was performed a Williamson reaction as described for compounds **46**-**48**.[162]
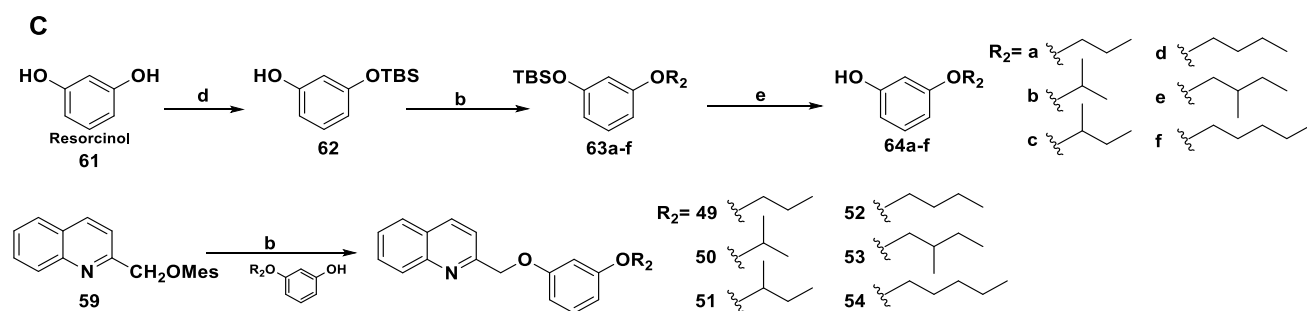

Figure 58. *Reagents and conditions*: a) DIBALH 1M in THF dry, 0°C; b) PPh$_3$, DIAD, THF dry, 0° C; d) TBS-Cl, Imidazole, in DMF dry; e) TBAF 1M in THF dry, over night

4.1.2. *In vitro* and *In vivo* assays

Compounds **40**-**54** were tested for GPBAR1 in a luciferase reports assay with HEK-293T cells. To evaluate the antagonist activity on CysLT$_1$R, CHO cells were transfected and the activity was determined by fluorometric method measuring the effect of compounds **40**-**54** on agonist-induced cytosolic Ca^{2+} ion mobilization.[160] As shown in **Table 5**, all derivatives do not show activity on FXR, but compounds **44** and **45** are GPBAR1 agonists and CysLT$_1$R antagonists, while compound **53** was found to be a selective agonist of GPBAR1.

The agonism on GPBAR1 was calculated by setting as 100% the activity of the control reference agonists TLCA. The antagonist effect on CysLT$_1$R was calculated as % of inhibition of control reference agonist LTD$_4$.[162]

Table 5. Efficacy and potency for compounds **40**-**54**.

Compounds	**GPBAR1^c**	**EC$_{50}$^{b}** (μM)	**CysLTR$_1$^{d}**	**IC$_{50}$^{b}** (μM)
REV5901		2.5	116.8	1.1
40	20.7	-	48	-
41	32.15	-	-11	-
42	12.63	-	85	2.1
43	23	-	85	3.9
44	74.8	3	71	2.8
45	92.69	7.4	97	1.2
46	17.58	-	59	>10
47	29.8	20	3	-
48	72.92	23	26	-
49	112.34	1	66	5.11
50	na	-	79	-
51	100.5	-	66	9.63
52	138.88	0.5	4	-
53	106.43	0.17	15	-
54	137	1.8	22	-

[a]Eff (%) is the maximum efficacy of the compound (10 μM) relative to CDCA (10 μM) set as 100% in transactivation of human FXR responsive element (FRE) on HepG2 cells; results are the mean of two experiments or more ±SD. [b]Results are mean of at least two experiments. [c]Eff (%) is the maximum efficacy of the compound (10 μM) relative to TLCA (10 μM) as 100 in transactivation of a cAMP responsive element (CRE) on HEK293T cells; results are the mean of two experiments or more ±SD. ND, not determined. [d]These assays were performed by Eurofins Cerep-Panlabs (France).

For compounds **44**, **45** and **53** was also evaluated whether they could carry out anti-inflammatory action *in vitro*, using mouse RAW264.7 macrophage cells line treated with lipopolysaccharides (LPS) and subsequently incubated with and without compounds at a concentration of 0.1, 1.5 and 10 μM.

As shown in figure 59 (A and B), the compounds under examination shown the ability to reduce the production of pro-inflammatory cytokines Tnfα and IL-1β, induced by the LPS. Furthermore, only compounds **45** and **53**, have the ability to increase the expression of the anti-inflammatory IL-10 gene (Figure 59C).[162]
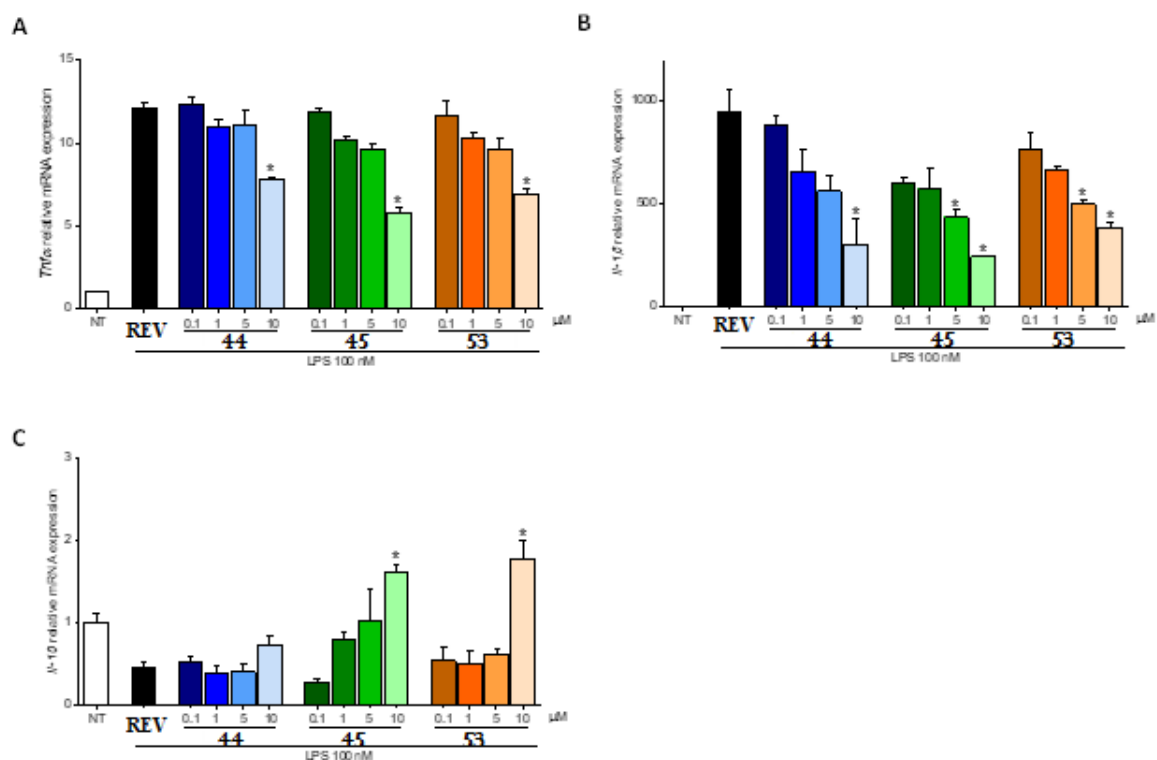

Figure 59. RAW264.7 cells were activated with LPS (100 nM) and then administrated with or without compound **44**, **45** or **53** at the concentration of 0.1, 1, 5 and 10 μM for 16 h. Quantitative real-time PCR analysis of expression of pro-inflammatory genes Tnf-α (**A**) and Il-1β (**B**), and anti-inflammatory genes Il-10 (**C**). These data are normalized to Gapdh/18s mRNA. Results represent the mean ± SEM. *$p < 0.05$ Vs LPS group. Anova-way analysis of variance was used for statistical comparisons.

Molecular docking studies were carried out on compounds **40**-**54** to examine the binding mode on CysLT$_1$R and GPBAR1.[150,152,163,164,165] As for the docking studies in CysLT$_1$R, it has been used the crystallographic structure with ID 6rz4[98], while was made use of both cryo-EM structure (PDB ID 7cfn and 7bw0)[166,167] and 3D model[144] for GPBAR1, already

used in many drug design studies.[121,168,169] the results showed that in GPBAR1 model, the quinoline core of compounds **40-54**, interacts with Tyr89, Asn93, Phe96 and Trp237 between TM3 and TM5, very important in the ligand/GPBAR1 bond.[119,121,144,160,170,171] In CysLT$_1$ Receptor the quinoline core is positioned in the pocket created by TM3, TM4 and TM5.[171] The results showed that the quinoline scaffold of the compounds is capable to interact with both GPBAR1 and CysLT$_1$R. It has been decided, so, to investigate the binding mode of compounds **44** and **45**, the most effective of the library, on the two receptors (GPBAR1 and CysLT$_1$R) and compound **53** on receptor GPBAR1.

Binding pose of 45 in GPBAR1

Compound **45** interacts with GPBAR1 through the quinoline core through H-bond with Asn93 in TM3 and TM5, and hydrophobic interactions with residue of Phe96, Leu97, Leu100, Leu173 and Leu174.(Figure 60A) Through a-polar interactions, the phenyl group, binds with a Leu71, Tyr89, Pro92, Glu169, Trp237 and Leu266, then, the methyl-hydroxyl group, forms H-bonds with Ser270 in TM1 and TM7. Through atomistic molecular dynamics calculations (MD) the binding mode of **45** has been confirmed. In the MD simulation, compound **45** takes a very similar pose to the docking one like showed in Figure 6C. This pose causes the location of the quinoline scaffold between TM3 and TM5, in which, bonds with residues of Tyr89, Leu97, Glu169, Leu173 and Leu244 and forms H-bond with Ans93 and π-π stacking interaction with Phe96. Lastly, through a t-shaped interaction, the phenyl group interacts with Leu68, Leu71, Thr74, Pro92 and Leu266. Thanks to H-bonds between the hydroxyl group of compound **45** and Ser270 and by the ethereal oxygen and Tyr240, the pose is stabilized.

Binding pose of 45 in CysLT$_1$R

In CysLT$_1$ Receptor, the quinoline scaffold of compound **45** is positioned orthogonal to TM3 and TM5 and fill the pocket created by Tyr108, Ser155, Phe158, Val186, Ser193 and Leu257. (Figure 60B) The pose is stabilized by cation-π bind with Arg253, by H-bond between the ethereal oxygen and Tyr104 and lastly, by T-shaped interaction between the phenyl group and Tyr249. The binding mode of compound **45** is very similar to the crystallographic binding pose of pranlukast, a well-known antagonist of CysLT$_1$R.[98] Pranlukast interacts with Arg79, thanks its tetrazole group, via water-mediated bond, and compound **45** mirrored this interaction, pointing its hydroxyl group towards Arg79, Val277 and Leu281 (Figure 60B and Figure 61). However, in these docking simulations, the water molecules involved in the bonds are not considered, so to fully understand the binding modality of compound **45** with CysLT$_1$R, studies of molecular dynamics and free-energy calculation were used, which include the water molecules present in the binding cavity and the flexibility of ligand and receptor is fully considered.
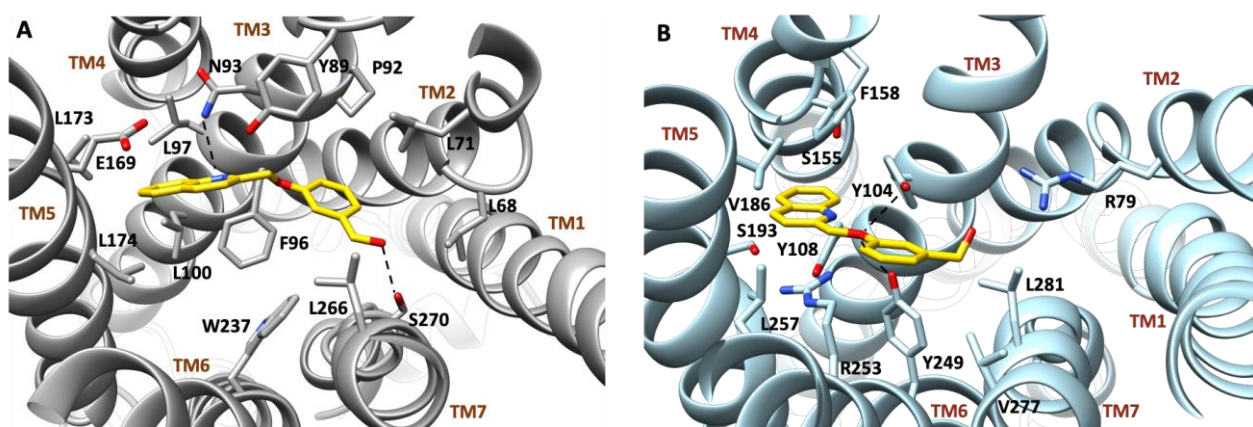

Figure 60. Compound 45 binding mode in (A) GPBAR1 and (B) CysLT$_1$R. The ligand is showed as gold sticks, while the aminoacidic residues are shown as grey (GPBAR1) or cyan (CysLT$_1$R) and labelled. Oxygen atoms are in red and nitrogen in blue. The receptors are showed as grey (GPBAR1) or cyan (CysLT$_1$R) ribbons. Hydrogens are omitted for clarity and H-bonds are as black dashed lines.
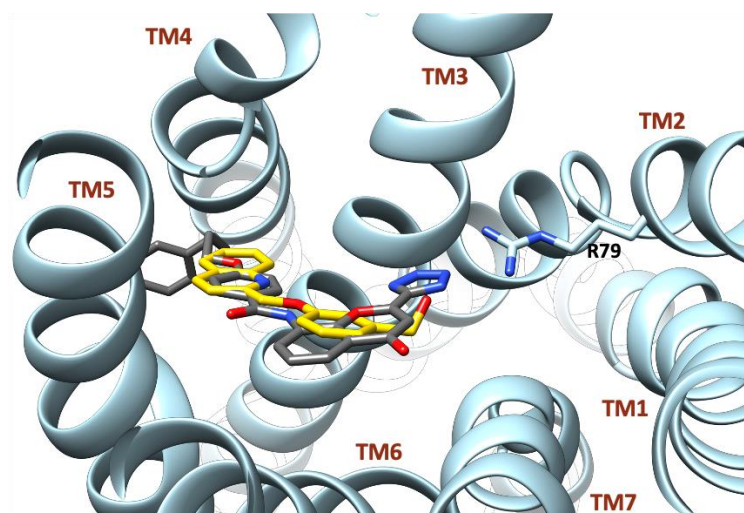
Figure 61. Compound 45 (gold sticks) and pranlukast (grey sticks) binding mode to CysLT$_1$R, in comparison. Oxygen atoms are represented in red and nitrogen in blue. The receptor is showed as cyan ribbons. Arg79 is represented in cyan sticks. Hydrogens are omitted for clarity.
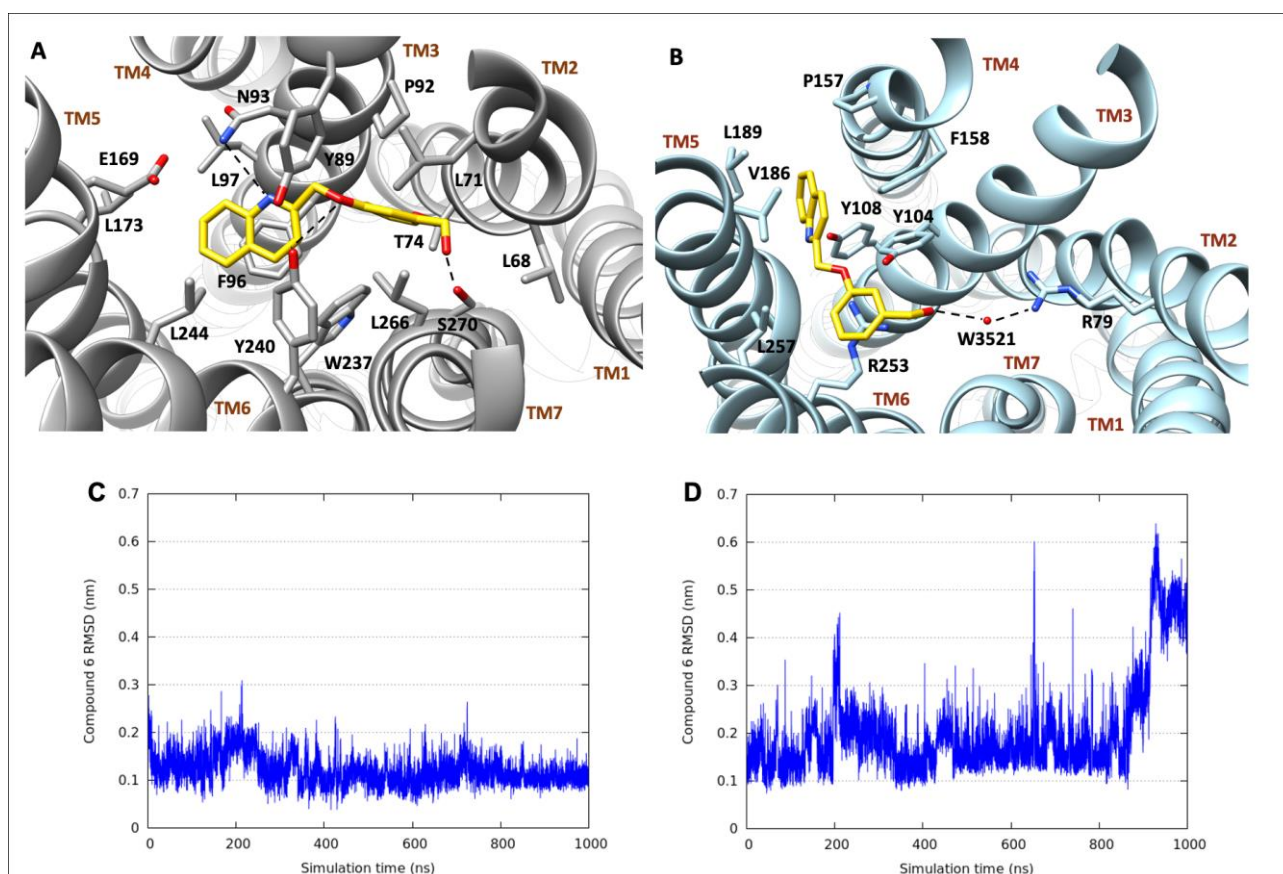

Figure 62. A-B. Compound 45 in (A) GPBAR1 and (B) CysLT$_1$R MD simulations. The ligand is showed as gold sticks, while the residues of the receptor are in grey (GPBAR1) or cyan (CysLT$_1$R). Oxygen atoms are in red and nitrogens in blue. The receptors are showed as grey (GPBAR1) or cyan (CysLT$_1$R) ribbons. Hydrogens are omitted for clarity and H-bonds and salt bridges are as black dotted lines. (**C-D).** RMSD of the heavy atoms of **compound 45** in GPBAR1 (C) and CysLT$_1$R (D) along the MD simulations. Prior to the RMSD calculations, trajectory frames were aligned on the same atoms.

MD and free-energy calculations

The 1 µs molecular docking simulation of compound **45** in CysLT$_1$R showed a slight difference in flexibility of the methyl-hydroxyl group in the last 100 ns (Figure 62D). This difference, allows the promotion of a H-bond between the hydroxyl group of **45** and Arg79 through a water molecule. (Figure 62B) In this model, the quinoline scaffold, unlike from the docking pose, is situated between TM4 and TM5 and forms interaction with Tyr108, Pro157, Val186, Leu189 and t-shaped contacts with Phe158. On the side chain, the phenyl ring binds with Tyr104, Leu257 and interacts through cation-π with Arg253. (Figure 60B/62B) The binding of **45** in CysLT$_1$R, given the differences found in the two studies (MD and Docking), was further investigated using a more precise method based on free-energy calculation, in particular metadynamics calculation (MetaD). This method is an advanced technique used by different research groups to discover ligand binding mode DNA and protein system including GPCRs.[172,173,174,175,176,177] The method consists in adding a Gaussian potential called Collective Variables (CV). In this way, the system probes the free energy scenario switching from one energy minimum to another, identifying the ligand binding mode as the lowest energy minimum. In our case, the distance between the ligand's quinoline ring and the C$_\beta$ of Arg79, was defined as CV. A lowest energy basin was found at 1.8.nm, as showed in Figure 63A. At this level the ligand binding mode is very similar to the pose in MD with a RMSD value of 0.08 nm. (Figure 63B) The results confirm the MD binding mode considering that during MetaD simulation, the ligand is free to move in the LBD.
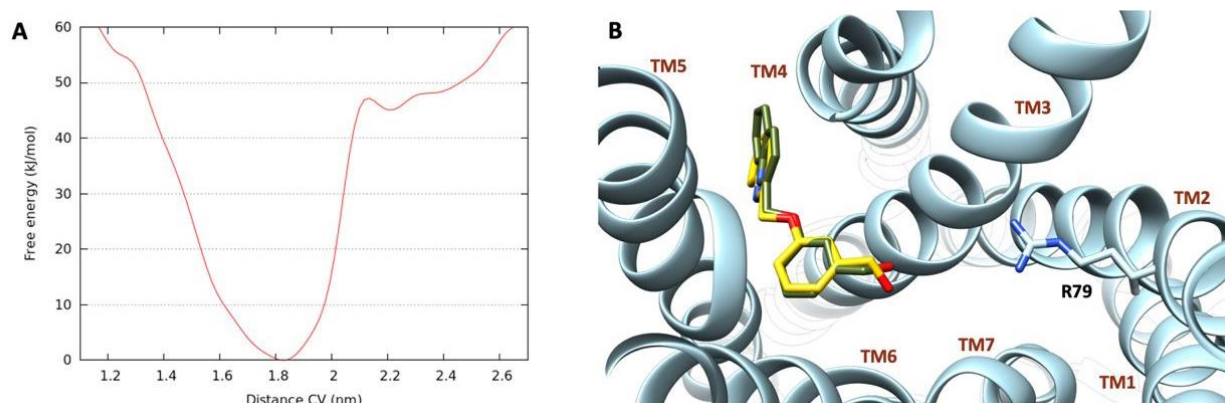
Figure 63. Results from **compound 45** MetaD calculations. **A.** Free energy profile of **compound 45** in CysLT$_1$R binding pocket. **B.** Differences between the energetically most stable pose obtained from MetaD (gold sticks), and the centroid of the MD most populated cluster (dark green sticks). Arg79 is represented as cyan sticks. Oxygen atoms are showed in red and nitrogens in blue. The receptor is showed as cyan ribbons. Hydrogens are omitted for clarity.

Binding mode of 44 in GPBAR1

Compound **44** is the second most effective dual ligand of the library studied. Thanks to the protein conformation in the MD simulation of compound **45** in GPBAR1, the accommodation in the ligand binding site structurally like the most potent of the library (compound **45**) it has been optimized. The best docking pose of **44** showed that, similarly to **45**, (Figure 60A) the quinoline core interacts in the amphipathic pocket formed by TM3, TM5 and TM6, with Tyr89, Leu97, Glu169, Leu173, Tyr240, Val241, Leu244.(Figure 60A) Then, it forms H-bonds with Asn93 and π–π stacking with Phe96. The phenyl ring, through a t-shaped interaction, binds with a Trp237 and towards TM2 and TM7 interacts with Leu68, Leu71, Thr74, Pro92, and Leu266, lastly, the carboxyl group forms a H-bond with a Ser270. (Figure 64A)
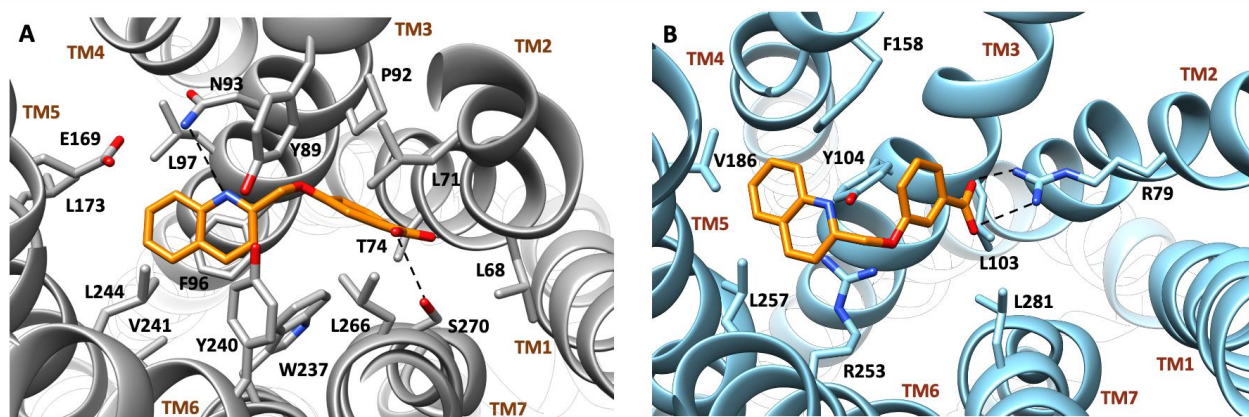
Figure 64. Binding mode of **compound 44** in (A) GPBAR1 and (B) CysLT$_1$R. The ligand is showed as orange sticks, while the residues of the receptor are represented in grey. Oxygen atoms are showed in red and nitrogens in blue. The receptors are showed as grey ribbons. Hydrogens are omitted for clarity and H-bonds and salt bridges are represented as black dotted lines.

Binding mode of 44 in CysLT1R

Following the same procedure used for GPBAR1, the docking of **44** in CysLT$_1$R was carried out using the MD simulation of compound **45**. In CysLT1R, similarly to compound **45**, the quinoline scaffold of compound **44**, fill the pocket created by TM4 and TM5. Here, forms hydrophobic interaction with Phe158, Val186 and Leu257 and a T-shaped π and cation-π interaction with Tyr104 and Arg253, respectively. The phenyl group of compound **44**, unlike compound **45**, points towards TM3 and TM2 and forms bonds with Leu103 and Leu281 and the carboxyl group interacts with Arg79, through a salt bridge. (Figure 64B)

Binding mode of 53 in GPBAR1

Finally, it was investigated the binding mode of compound **53**, the most potent selective agonist of GPBAR1. The quinoline core of compound **53**, as for **44** and **45**, positioned itself between TM3 and TM5 and interacts through H-bond with Asn93 and through hydrophobic interaction with Leu97, Leu100 and Leu174. The phenyl group binds with Pro92 and forms t-shaped π interaction with a Phe96. Lastly, the alkyl group reached TM1 and TM7 and here interacts with Leu68, Leu71 and Leu266 through hydrophobic interactions. (Figure 65)

The binding poses of the three compounds **44**, **45** and **53** is in agreement with the data previously described for REV5901.[160] In particular, the interactions that play a fundamental role in the binding of REV5901 and other GPBAR1 agonists with the receptor are also conserved in these compounds (such as: H-bond with Asn93 and hydrophobic interaction with Tyr89, Phe96 and Trp237)[119,121,160,170,171]
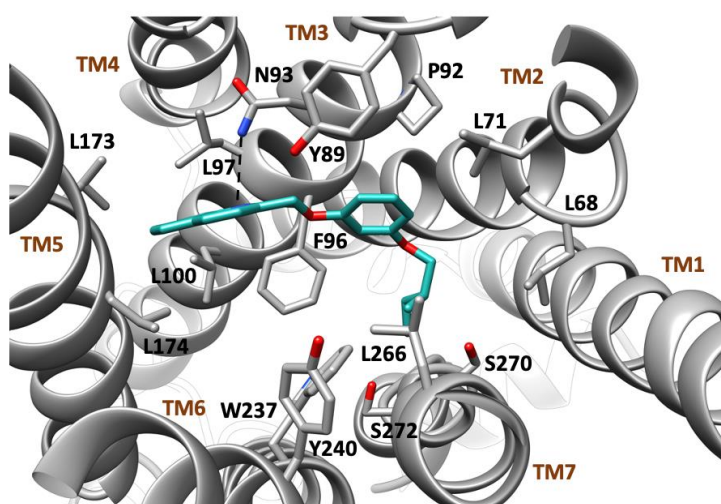

Figure 65. Compound 53 binding mode in GPBAR1. The ligand is showed as light sea green sticks, while the residues of the receptor are in grey. Oxygen atoms in red and nitrogens in blue. The receptor is showed as grey ribbons. Hydrogens are omitted for clarity and H-bonds are represented as black dotted lines.

The physicochemical parameters of the selected compounds were evaluated by LC-MS analysis. Compounds **44** and **45** shown interesting ADME properties. Compound **53**, however, is characterized by a poor aqueous solubility.

The proneness of these derivatives to be modified by human metabolizing enzymes contained in liver microsomal and S9 fractions resist microsomal enzymes and the S9 fractions was then evaluated by high-performance liquid chromatography-MS/MS analysis. As shown in table 6, compounds **44** and **45** are high stable to microsomal enzymes which are responsible for Phase I metabolization.[162]

Table 6. In *vitro* pharmacokinetics for selected derivatives

Compound	Solubility (μM)[a]	LogD	Microsomes		S9 fraction	
			$t_{1/2}$ (min)	C_{int}[b]	$t_{1/2}$ (min)	C_{int}
44	>200	0.12	210	11	247.5	9.3
45	141	2.8	48	48	119	19
53	3.5	1.01	22.3	103.3	-	-

Subsequently the metabolic stability of compounds **44** and **45** was investigated using the S9 fraction of the liver containing enzymes responsible for the Phase II metabolism. Compound **44** showed to be more stable with a **$t_{1/2}$** of 247.5min (CL_{int}= 9.3).

All these results show that compound **44** is the most effective dual modulator of GPBAR1 and $CyLT_1R$ in the library, both in terms of efficacy and potency and for its metabolic stability.[162]

The results obtained allow us to discuss the structure-activity relationship of this library of compounds. In compounds **40-45**, the carboxyl group is more effective (**41** and **44**) in activating the receptor GPBAR1 than the methoxycarbonyl group (**40–43**) whether is in *para* or *meta* position, the opposite is true for $CysLT_1R$. However, this difference is more marked in *meta* for GPBAR1 and in *para* for $CysLT_1R$.

As for compounds with the hydroxymethyl group (**42-45**), whether it is found in *para* or *meta* is indifferent to its efficacy on $CysLT_1R$, which is higher or similar to compounds with $COOCH_3$ or COOH, in the case of GPBAR1 an increase in efficacy is noted when the COOH group is in *meta* rather than *para*. Moreover, in compounds **46-48**, which have double substitution on the aromatic ring with a hydroxyl group in *meta*, they show a reduction in efficacy on $CysLT_1R$ compared with monosubstituted ones (**40-45**). Similarly, compounds **46** and **48** show a reduced efficacy against GPBAR1, while compound **47** has a good efficacy but with low potency, compared to compounds **44** and **45**.[162]

As regards the compounds **49**-**54**, which have an alkyl group in *meta* on the aromatic ring, they showed a reduction of the efficacy on $CysLT_1R$, while showed unchanged efficacy against GPBAR1, except for compound **50**.

In particular the composers having a butyl, a 2-methylbutyl and a pentyl on the ring (**52**,**53** and **54**), show a good efficacy and potency towards GPBAR1, with the compound **53** showing a low EC_{50} and which was therefore chosen for further in *vitro* tests. In conclusion, a polar or negatively charged group, suitably positioned on the aromatic ring, represents a structural requirement for the interaction with Arg79 of the $CysLT_1R$ and for obtaining the dual activity on $CysLT_1R$/GPBAR1. On the other hand, the presence of an alkyl group in *meta* on the aromatic ring allows to obtain selective agonist compounds of GPBAR1.[162]

CHAPTER 5

CONCLUSION

The research work carried out in the frame of my Ph.D. project has been devoted to the synthesis of a wide range of compounds, potential drugs for the treatment of various diseases of the liver and intestine. In particular, I focused my attention on editing three different scaffolds:

- Steroidal Scaffold: 6-ethylcholane derivatives

- Non-steroidal scaffold: isoxazole inspired by GW4064

- Non steroidal scaffold: quinoline derivatives

Steroidal Scaffold: 6-ethylcholane derivatives

Starting from 6-ECDCA, the most potent steroidal agonist of FXR, I have synthetized a new library of compounds. The main modifications concerned the introduction of non-acidic side chain to avoid the metabolization with taurine and glycine and consequently the accumulation in the body and the elimination of the 3-OH group on ring A to obtain selective FXR agonists.

Compounds **1** and **3**, featuring a non-acidic one carbon shortened side chain, resulted as dual modulators of FXR/GPBAR1 ($EC_{50}=1.8\pm0.5$ μM, $EC_{50}=0.14\pm0.032$ μM, respectively). Compound **6**, characterized by the absence of the 3-OH and featuring the same side chain of **1** and **3**, as a selective FXR agonist with improved metabolic stability, but reduced potency.

Non-steroidal scaffold: isoxazoles inspired by GW4064

My attention has been shifted to compounds with a non-steroidal nature. The compound of major interest was GW4064, a selective FXR agonist with a potency of 70 nM and an efficacy of 166% compared to CDCA, the FXR endogenous ligand. This compound has an isoxazole nucleus with a 2,6-dichloro-substituted phenyl at C3, an isopropyl at C5 and a stilbene group at C4 which causes the photosensitivity and the low aqueous solubility of this

compound. Therefore, I synthesized a large library of compounds focusing the modifications on the stilbene portion at C4. Among these, compound **28,** which presents at C4 two aromatic rings linked by an ethereal bridge and a carboxylic group in *para* on the second ring of the chain, showed improved pharmacokinetic and pharmacodynamic properties associated with a greater efficacy against FXR (EC_{50}=0.30±0.006 µM). Furthermore, it was decided to evaluate its ability to protect or reduce liver damage caused by paracetamol overdose (APAP), one of the most widespread causes of hepatic damage in murine models. Compound **28** was capable to reduce ALT and AST levels and tissue liver damage and restoring normal expression levels of several phase II genes (Ugt1a1, Ugt2b1, Sult1a1, GSH, and SOD).

Non-steroidal scaffold: quinoline derivatives

The last part of my PhD involved synthesis of REV5901 derivatives. REV5901 is a $CysLT_1$ receptor antagonist. A study conducted by the research group where I carried out my PhD has proved that this compound is capable of modulating both the $CysLT_1R$ receptor and the GPBAR1 bile acid receptor (EC_{50} of 2.5 µM). In *vivo* studies in mouse models of colitis have shown the ability of REV5901 to reduce intestinal damage, thanks to the activity on GPBAR1. Modifying the substituents on the aromatic ring in position C-2 on the quinoline scaffold introducing polar substituents or alkyl groups to mimic its side chain, I synthesized a library of 15 compounds. Compounds **44** and **45** (IC_{50} = 1.2 µM and EC_{50} = 7.4 µM, respectively). proved to be the most effective dual modulators in the series and with good metabolic stability. In *vitro* models demonstrated the ability to reduce the production of pro-inflammatory cytokines Tnfα and IL-1β, on macrophage cells line primed with lipopolysaccharides (LPS). Compound **53**, has been shown to be a good selective GPBAR1 agonist (EC_{50} of 0.17 µM), however it suffers from low aqueous solubility and instability.

CHAPTER 6

EXPERIMENTAL PROCEDURE: 6-ECDCA Derivatives

6.1. General Information

High-resolution electrospray ionization mass spectrometry (ESI-MS) was performed with a Micromass Q-TOF mass spectrometer (Q-TOF premier, Waters Co., Milford, MA, USA). High-performance liquid chromatography (HPLC, Phenomenex Inc, Torrance, CA, USA) was carried out utilizing a Waters Model 510 pump fitted out with Waters rheodyne injector and a differential refractometer, model 401 (Waters Co., Milford, MA, USA). Nuclear magnetic resonance (NMR) was executed on Varian Inova 400 NMR spectrometer (^{1}H at 400 MHz, ^{13}C at 100 MHz) equipped with a Sun hardware and recorded in CDCl$_3$ (^{1}H = 7.26 and ^{13}C = 77.0 ppm) and CD$_3$OD (^{1}H = 3.30 and ^{13}C = 49.0 ppm). J are in hertz (Hz) and chemical shifts (δ) are showed in ppm and referred to CHCl$_3$ and CHD$_2$OD as internal standards. the progress of the reaction was monitored by thin-layer chromatography (TLC) on Alugram® silica gel G/UV254 plates. All chemicals were obtained from Zentek S.r.l and Sigma Aldrich. Solvents and reagents were utilized as supplied from commercial sources. The exceptions are: Tetrahydrofuran, toluene, CH$_2$Cl$_2$, which were distilled from calcium hydride just before use. Magnesium turnings (1 g) and iodine (0.1 g) were refluxed in a small (5–10 mL) quantity of methanol until the magnesium has reacted. The mixture was diluted (up to 100 mL) with methanol and under reflux for 2–3 h was obtained Methanol dry. All reactions were carried out under argon atmosphere utilizing flame-dried glassware. Throught HPLC were evaluated the purity of the synthetized compounds. All compounds for biological testing were >95% pure.

6.2. Synthetic Procedure

Synthesis of 6α-Ethyl-3α-hydroxy-7-keto-24-nor-5β-chol-23-ene (9)

A portion of 6α-ethyl-3α-hydroxy-7-keto-5β-cholan-24-oic acid **7**, obtained as previously reported (2.0 g, 4.7 mmol)[144] was acetylated with acetic anhydride (2.2 mL, 23.5 mmol) in a solution of dry pyridine (30 mL). The mixture was stirred for 5 h, then, was evaporated under reduced pressure to remove the pyridine. The solution was extracted with ethyl acetate (3 × 50 mL) and the collected organic phases were dried over Na_2SO_4 anhydrous and evaporated under reduced pressure. The residue was subjected to the next reaction without further purification. The mixture (2.0 g, 4.34 mmol) was dissolved in dry toluene/dry pyridine (20 mL: 200 µL, 10:1 *v/v*) and $Cu(OAc)_2.H_2O$ (2.6 g, 13.0 mmol) was added in dark. After 30 min, $Pb(OAc)_4$ (9.6 g, 21.7 mmol) was added in dark. After 3 h the solution was heated to reflux for 1 h (no longer in the dark). The mixture was cooled, and aqueous ethylene glycol was added. The mixture was extracted with diethyl ether (3 × 50 mL). The organic phases were washed before with saturated solution of $NaHCO_3$ and then with water and brine. After drying over anhydrous Na_2SO_4, the residue was evaporated under vacuum to give 1.2 g of product as crude residue. This residue (1.2 g, 2.9 mmol) was treated with CH_3ONa (156 mg, 2.9 mmol) in dry MeOH (10 mL). After stirring for 12 h at room temperature, water was added and methanol was evaporated. The residue was extracted with EtOAc (3 × 50 mL). The organic layers were washed with brine, dried and evaporated to give a mixture that was purified on flash chromatography, using 95:5 hexane/ethyl acetate and 0.5% of TEA, as eluent, and affording 1.25 g of pure compound 8 (58% over three steps).

Selected ¹H-NMR (400 MHz, CDCl₃): δ 5.65 (1H, m), 4.87 (1H, d, *J* = 17.0 Hz), 4.80 (1H, d, *J* = 10.3 Hz), 3.50 (1H, m), 1.20 (3H, s), 1.01 (3H, d, *J* = 7.3 Hz), 0.78 (3H, t, *J* = 7.4 Hz), 0.67 (3H, s); **¹³C-NMR (100 MHz, CDCl₃):** δ 212.8, 114.9, 111.6, 71.1, 54.4, 51.9, 50.6,

49.9, 49.0, 43.7, 42.5, 41.0, 38.9, 35.6, 34.2, 31.7, 29.8, 28.5, 24.6, 23.5, 21.8, 20.1, 18.8, 12.2, 11.9. **HR ESIMS** m/z 373.3105 [M + H]+, $C_{25}H_{41}O_2$ requires 373.3101.

Synthesis of 6α-Ethyl-3α, 7α-dihydroxy-24-nor-5β-chol-23-ene (1)

Methanol dry (750 µL, 18.7 mmol) and $LiBH_4$ (9.3 mL, 2 M in THF, 18.7 mmol) were added at 0°C to a solution of **9** (1.0 g, 2.7 mmol) in dry THF (30 mL). The resulting mixture was stirred for 2 h at 0 °C, then was quenched by addition of 1M NaOH (5.4 mL) and then ethyl acetate. The organic phase was washed with water, dried (Na_2SO_4) and concentrated giving 980 mg of crude residue (98% yield). An analytic sample of compound **1** was obtained through purification with HPLC on a Luna Omega Polar C18 (5 µm; 4.6 mm i.d. × 250 mm), with $MeOH/H_2O$ (92:8) as eluent (flow rate 1 mL/min) (t_R = 14 min).

Selected ^{1}H-NMR (400 MHz, CDCl$_3$): δ 5.68 (1H, m), 4.91 (1H, dd, J = 16.8, 1.8 Hz), 4.83 (1H, dd, J = 10.2, 1.8 Hz), 3.71 (1H, br s), 3.41 (1H, m), 1.05 (3H, d, J = 6.3 Hz), 0.91 (3H, s), 0.91 (3H, t, J = 7.2 Hz), 0.70 (3H, s); ^{13}**C-NMR (100 MHz, CDCl$_3$):** δ 145.2, 111.6, 72.3, 70.9, 55.3, 50.5, 45.2, 42.6, 41.2, 41.1, 39.9, 39.5, 35.5 (2C), 33.9, 33.2, 30.6, 28.5, 23.7, 23.2, 22.2, 20.7, 20.1, 11.9, 11.6. **HR ESIMS** m/z 375.3255 [M + H]+, $C_{25}H_{43}O_2$ requires 375.3258.

Synthesis of 6α-Ethyl-3α, 7α -dihydroxy-24-nor-5β-cholane (2)

A solution of **1** (300 mg, 0.80 mmol) in dry THF/dry MeOH (30 mL, 1:1 v/v) was hydrogenated in presence of Pd(OH)$_2$/C 20 % wt on activated carbon (100 mg) degussa type. The mixture was flushed with nitrogen and then with hydrogen several times. The reaction was stirred at room temperature overnight. The catalyst was filtered through Celite under vacuum to give compound as crude product (320 mg, quantitative yield). HPLC on a Luna

Omega Polar C18 (5 µm; 4.6 mm i.d. × 250 mm), with MeOH/H_2O (92:8) as eluent (flow rate 1 mL/min) furnished pure compound **2** (t_R = 16 min).

Selected ^{1}H-NMR (400 MHz, CD₃OD): δ 3.66 (1H, br s), 3.31 (1H, m ovl), 0.94 (3H, d, J = 6.5 Hz), 0.92 (3H, s), 0.90 (3H, t, J = 7.1 Hz), 0.85 (3H, t, J = 7.6 Hz), 0.70 (3H, s); ^{13}C-NMR (100 MHz, CD₃OD): δ 73.2, 71.2, 57.2, 51.6, 46.9, 43.6, 43.2, 41.5, 41.0, 38.5, 36.8, 36.6, 34.5, 34.4, 31.2, 29.4, 29.3, 24.6, 23.7, 23.5, 22.0, 18.6, 12.3, 12.0, 10.7. **HR ESIMS** *m/z* 377.3416 [M + H]+, $C_{25}H_{45}O_2$ requires 377.3414.

Synthesis of 6α-Ethyl-3α, 7α -dihydroxy-23,24-dinor-5β-cholan-22-ol (3)

A stream of O_3 was bubbled into a solution of **1** (300 mg, 0.80 mmol) in dry CH_2Cl_2 (7 mL) kept at −78 ∘C until a blue-color solution resulted. Excess of O_3 was removed, after stirring for 1 min, upon bubbling N_2 and to the solution was added Methanol dry (5 mL) followed by an excess of $NaBH_4$. After stirring at −78 ∘C for 2 h, the reaction mixture was left to room temperature and treated with dry MeOH (1 mL). The solution was concentrated and the resulting mixture was partitioned between EtOAc and H_2O (3 × 50 mL). The organic layer was evaporated to give the corresponding alcohol (298 mg, quantitative yield). Purification by HPLC on a Luna Omega Polar C18 (5 µm; 4.6 mm i.d. × 250 mm), with MeOH/H_2O (86:14) as eluent (flow rate 1 mL/min), furnished a pure aliquot of compound **3** (t_R = 12 min).

Selected ^{1}H-NMR (400 MHz, CDCl₃): δ 3.70 (1H, br s), 3.65 (1H, m), 3.49 (1H, br s), 3.37 (1H, m), 1.05 (3H, d, J = 6.7 Hz), 0.90 (3H, t, J = 7.1 Hz), 0.89 (3H, s), 0.68 (3H, s); ^{13}C-NMR (100 MHz, CDCl₃): δ 72.2, 70.8, 68.0, 52.5, 50.3, 45.1, 42.8, 41.2, 40.1, 39.5, 38.8, 35.5 (2C), 34.0, 33.2, 30.7, 27.8, 23.8, 23.1, 22.2, 20.7, 16.7, 11.8, 11.6. **HR ESIMS** *m/z* 379.3205 [M + H]+, $C_{24}H_{43}O_3$ requires 379.3207.

Synthesis of 6α-Ethyl-7-keto-5β-cholan-24-oic acid (10)

On a methyl 6α-ethyl-7-keto-5β-cholan-24-oate, obtained previously (500 mg, 1.2 mmol)[115], was carried out a Hydrolysis with NaOH in MeOH: H_2O 1:1 *v/v* (20mL). The mixture was stirred for 4 h at reflux. The solution was acidified with HCl 6N and extracted with ethyl acetate (3 × 50 mL). The organic phases were washed with brine, dried over Na_2SO_4 anhydrous and evaporated under reduced pressure to give the carboxylic acid intermediate **10** (480 mg, quantitative yield).

Selected ¹H-NMR (400 MHz, CD₃OD): δ 1.25 (3H, s), 0.96 (3H, d, *J* = 6.4 Hz), 0.79 (3H, t, *J* = 7.2 Hz), 0.70 (3H, s). **¹³C-NMR (100 MHz, CDCl₃):** δ 215.1, 178.0, 54.7, 51.4, 50.7, 50.5, 48.7, 45.6, 43.2, 42.4, 37.5, 36.3, 35.1, 31.0 (2C), 30.3, 28.1, 26.7, 26.3, 24.9, 23.0, 21.3 (2C), 20.4, 18.8, 12.0. **HR ESIMS** *m/z* 403.3205 [M + H]+, $C_{26}H_{43}O_3$ requires 403.3207.

Synthesis of 6α-Ethyl-7α-hydroxy-24-nor-5β-chol-23-ene (4)

Compound **10** (250 mg, 0.62 mmol) was dissolved in dry toluene/dry pyridine (20 mL: 200 µL, 10:1 *v/v*) and in dark was added Cu(OAc)₂.H₂O (372 mg, 1.8 mmol). After 30 min Pb(OAc)₄ (1.3 g, 3.1 mmol) in the same condition. After 3 h the solution was heated to reflux for 1 h (no longer in the dark). The mixture was then cooled, and aqueous ethylene glycol was added. The resulting mixture was extracted with diethyl ether (3 × 50 mL). The organic layers were washed with saturated solution of NaHCO₃, and then with water and brine. After drying over anhydrous Na₂SO₄, the residue was evaporated under vacuum to give 100 mg of product as crude residue. On a solution of the residue (100 mg, 0.28 mmol) in dry THF (10 mL) was added at 0 ∘C, dry methanol (76 µL, 1.9 mmol) and LiBH₄ (980 µL, 4 M in THF, 1.9 mmol). The resulting mixture was stirred for 2 h at 0°C. The mixture was quenched by addition of 1M NaOH (1.24 mL) and then ethyl acetate. The organic layer was washed

with water, dried (Na_2SO_4), and concentrated giving 91 mg of crude residue (91% yield). An analytic sample of compound **4** was obtained through purification with HPLC on a Synergi Fusion-RP C18 (4 µm; 4.6 mm i.d. × 250 mm), with MeOH/H_2O (99:1) as eluent (flow rate 1 mL/min) (t_R = 8 min).

Selected ^{1}H-NMR (400 MHz, CDCl$_3$): δ 5.67 (1H, m), 4.91 (1H, d, J = 17.3 Hz), 4.82 (1H, d, J = 10.1 Hz), 3.70 (1H, br s), 1.04 (3H, d, J = 6.4 Hz), 0.90 (3H, s), 0.90 (3H, t ovl), 0.69 (3H, s). ^{13}C-NMR (100 MHz, CDCl$_3$): δ 145.2, 111.5, 71.2, 55.4, 50.6, 46.9, 42.7, 41.4, 41.3, 40.1, 39.6, 38.0, 36.3, 33.4, 28.5, 27.6, 24.3, 24.0, 23.8, 22.2, 21.3, 20.8, 20.1, 11.9, 11.7. **HR ESIMS** m/z 359.3305 [M + H]+, $C_{25}H_{41}O$ requires 359.3308.

Synthesis of 6α-Ethyl-7α-hydroxy-23,24-dinor-5β-cholane (5)

Starting from compound **4** (35 mg, 0.1 mmol) and using the same experimental conditions previously described for compound **2** we obtained compound **5** (35 mg, quantitative yield). An analytic sample of compound **5** was obtained through purification with HPLC on a Synergy fusion-RP C18 (4 µm; 4.6 mm i.d. × 250 mm), with MeOH/H_2O (99:1) as eluent (flow rate 1.5 mL/min) (t_R = 9.1 min).

Selected ^{1}H-NMR (400 MHz, CDCl$_3$): δ 3.71 (1H, br s), 0.92 (3H, d, J = 6.8 Hz), 0.90 (3H, s), 0.90 (3H, t ovl), 0.83 (3H, t, J = 7.3 Hz), 0.67 (3H, s). ^{13}C-NMR (100 MHz, CDCl$_3$): δ 71.2, 55.5, 50.6, 46.9, 42.6, 41.4, 40.1, 39.6, 37.9, 36.9, 36.4, 33.4, 28.2, 28.1, 27.6, 24.3, 24.0, 23.7, 22.2, 21.4, 20.8, 18.0, 11.8, 11.7, 10.3. **HR ESIMS** m/z 361.3461 [M + H]+, $C_{25}H_{45}O$ requires 361.3465.

Synthesis of 6α-Ethyl-7α-hydroxy-23,24-dinor-5β-cholan-22-ol (6)

Using as starting material compound **4** (35 mg, 0.1 mmol), was obtained the compound **6** (34 mg, 95%) in the same experimental conditions previously described for compound **3**.

An analytic sample of compound **6** was obtained through purification with HPLC on a Luna Omega Polar C18 (5 µm; 4.6 mm i.d. $\times$ 250 mm), with MeOH/H$_2$O (92:8) as eluent (flow rate 1.5 mL/min) (t_R = 19.3 min).

Selected ^{1}H-NMR (400 MHz, CDCl$_3$): δ 3.70 (1H, br s), 3.65 (1H, dd, J = 10.3, 3.0 Hz), 3.36 (1H, dd, J = 10.3, 7.0 Hz), 1.05 (3H, d, J = 6.7 Hz), 0.90 (3H, s), 0.90 (3H, t, J = 7.0 Hz), 0.69 (3H, s). **^{13}C-NMR (100 MHz, CDCl$_3$):** δ 71.2, 68.0, 52.5, 50.3, 46.9, 42.8, 41.3, 40.5, 39.5, 38.7, 37.9, 36.3, 33.3, 27.7, 27.6, 24.3, 23.9, 23.8, 22.2, 21.3, 20.7, 16.7, 11.8, 11.7. **HR ESIMS** m/z 363.3255 [M + H]+, C$_{24}$H$_{43}$O$_2$ requires 363.3258.

6.3. NMR Spectra

¹H NMR (400 MHz, CDCl₃) of compound 1
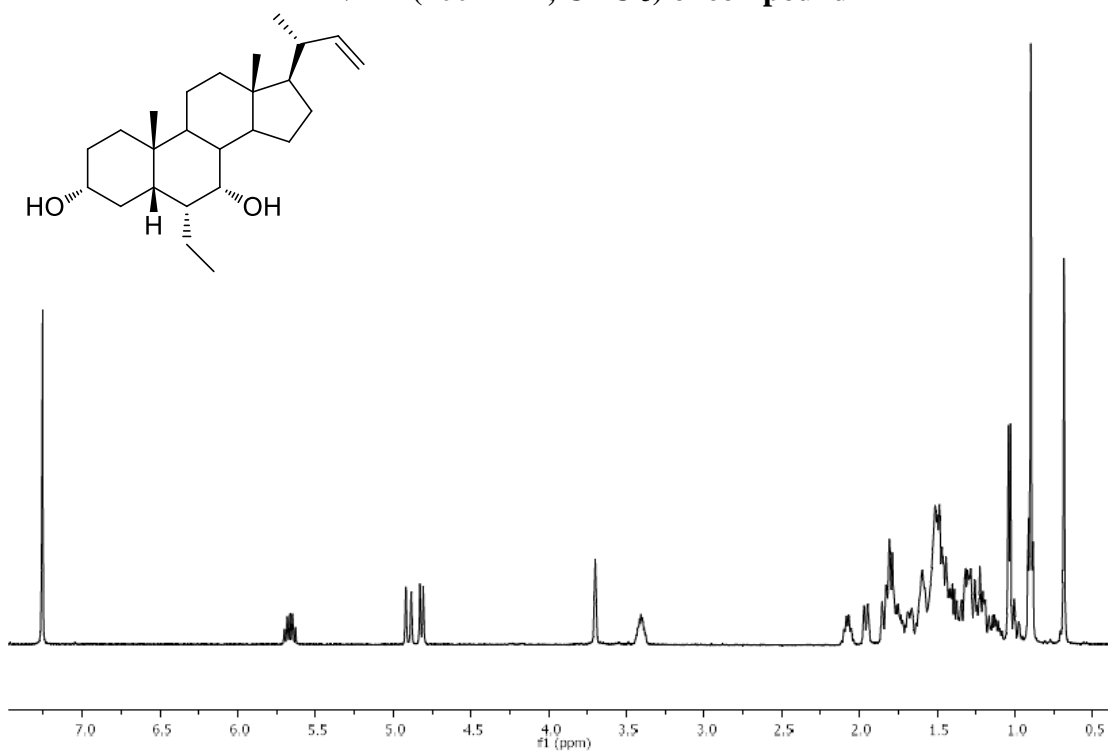
¹³C NMR (100 MHz, CDCl₃) of compound 1
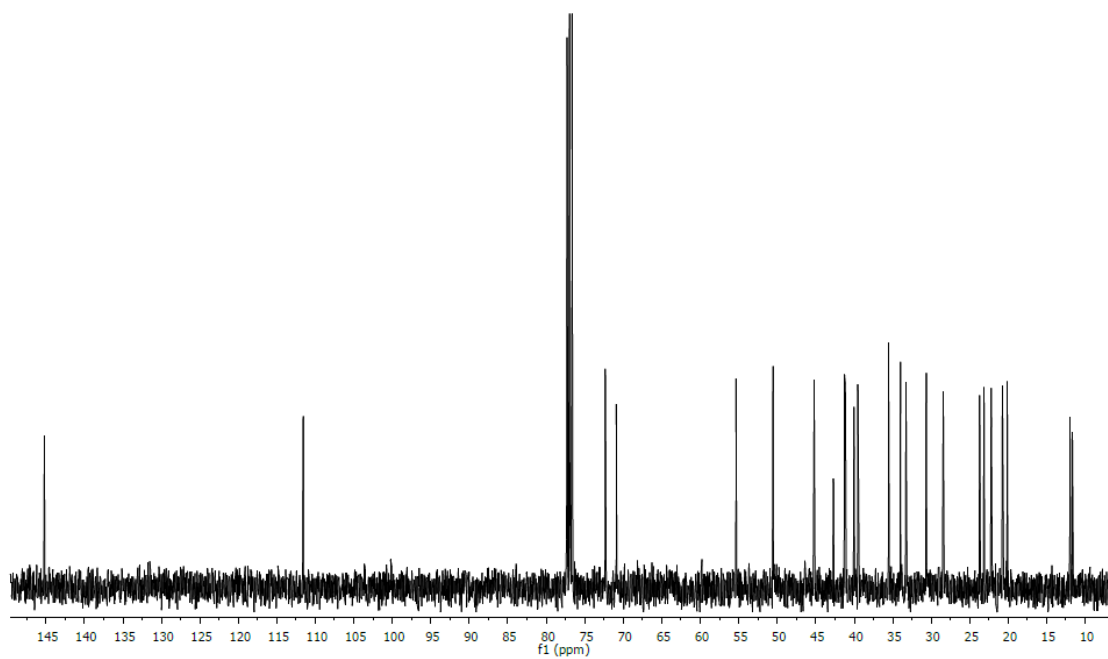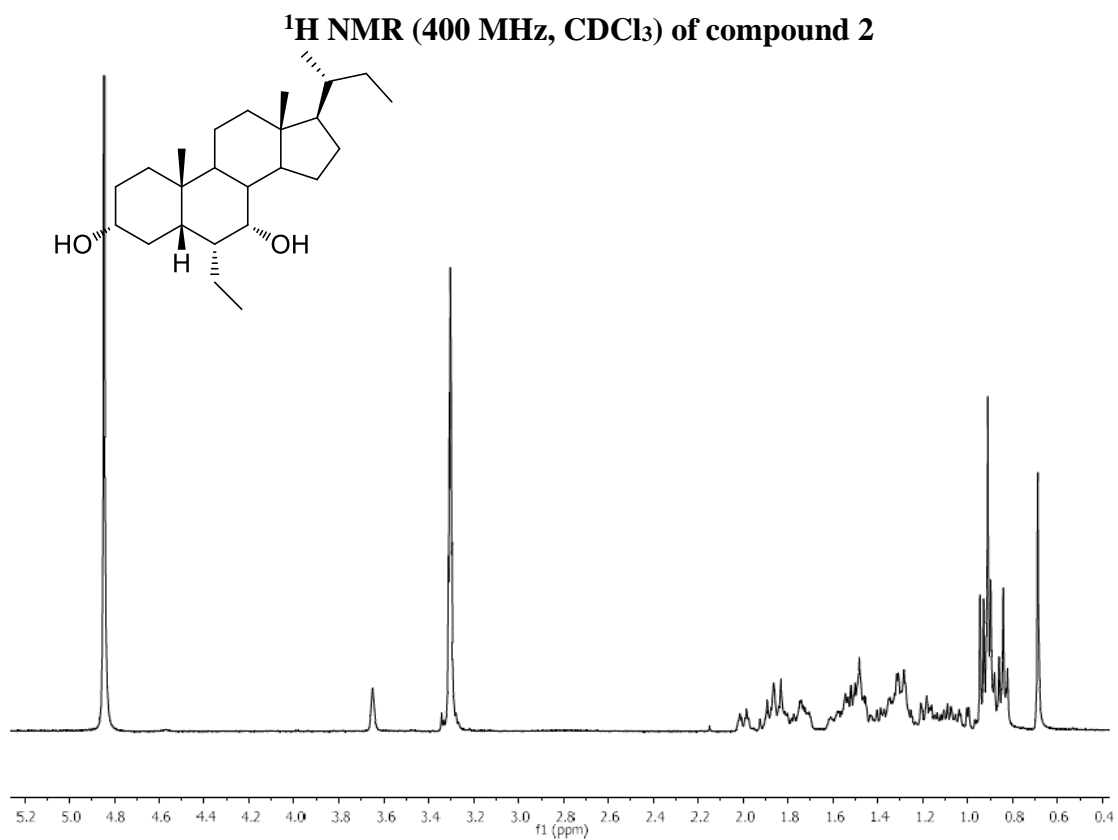
^{1}H NMR (400 MHz, CDCl$_3$) of compound 2

^{13}C NMR (100 MHz, CDCl$_3$) of compound 2
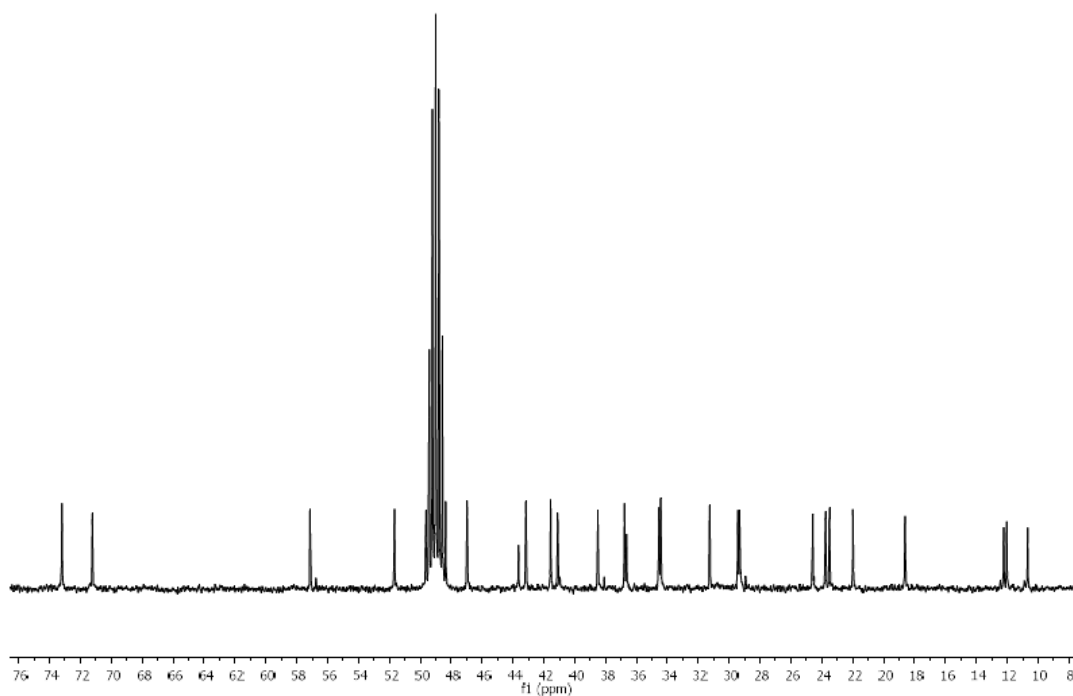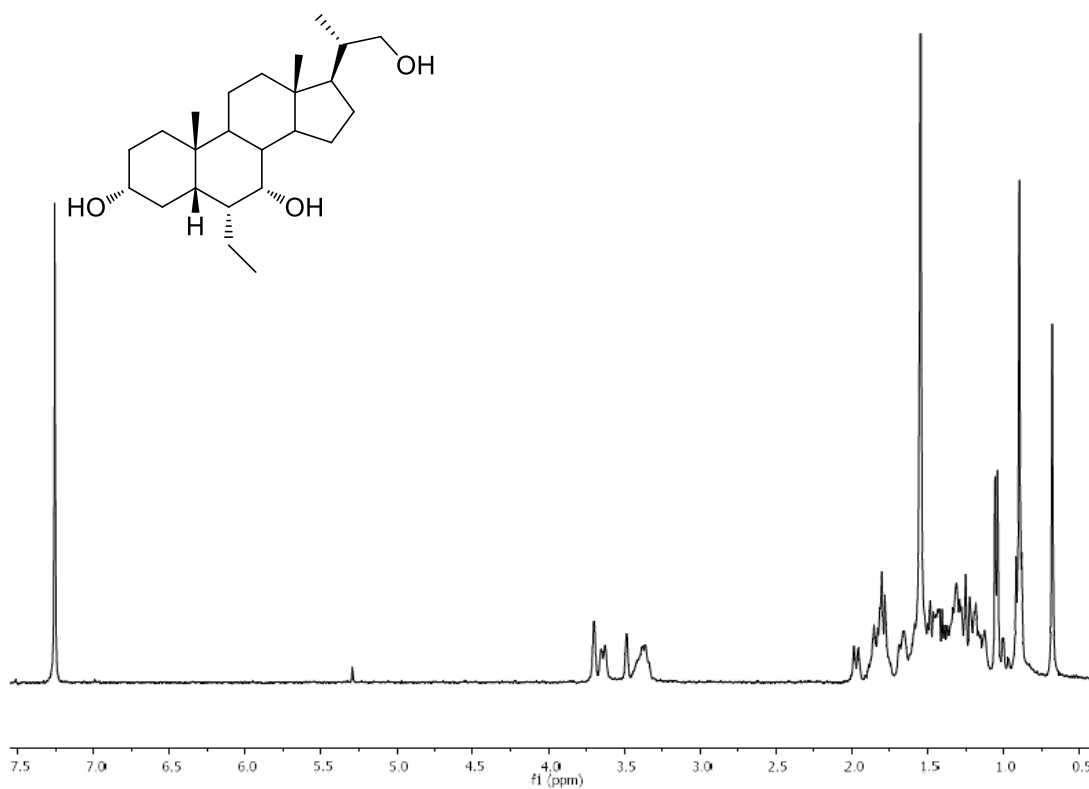
¹H NMR (400 MHz, CDCl₃) of compound 3

₁₃C NMR (100 MHz, CDCl₃) of compound 3
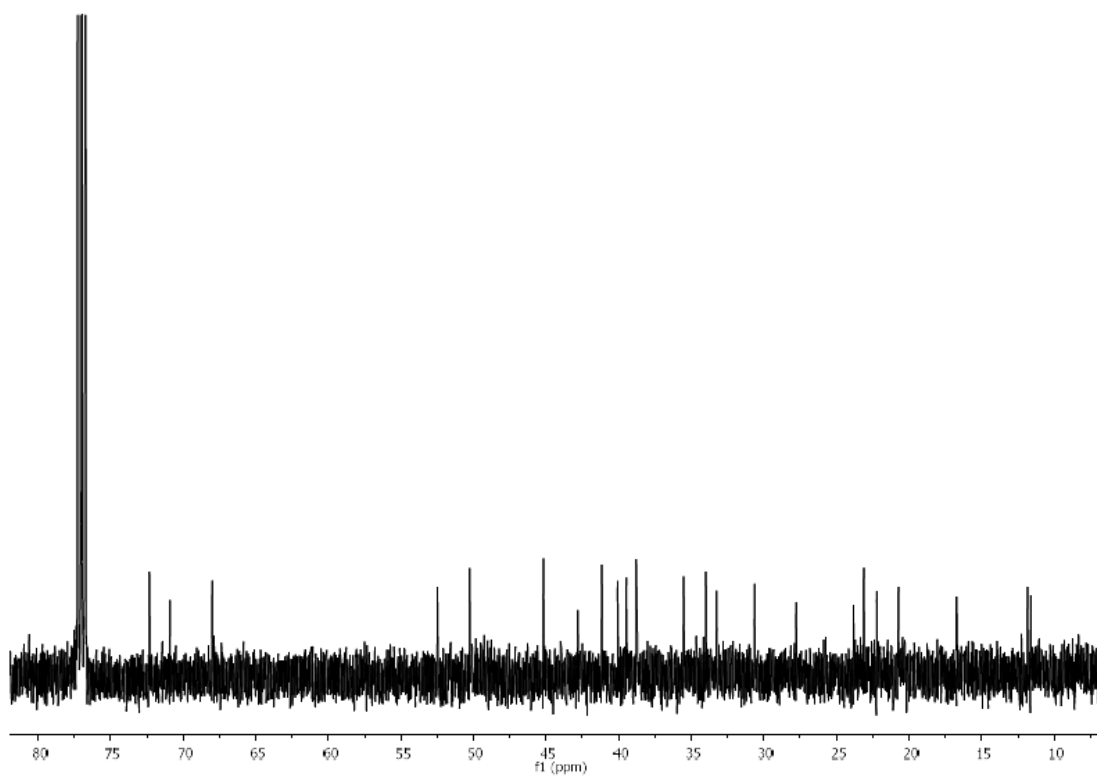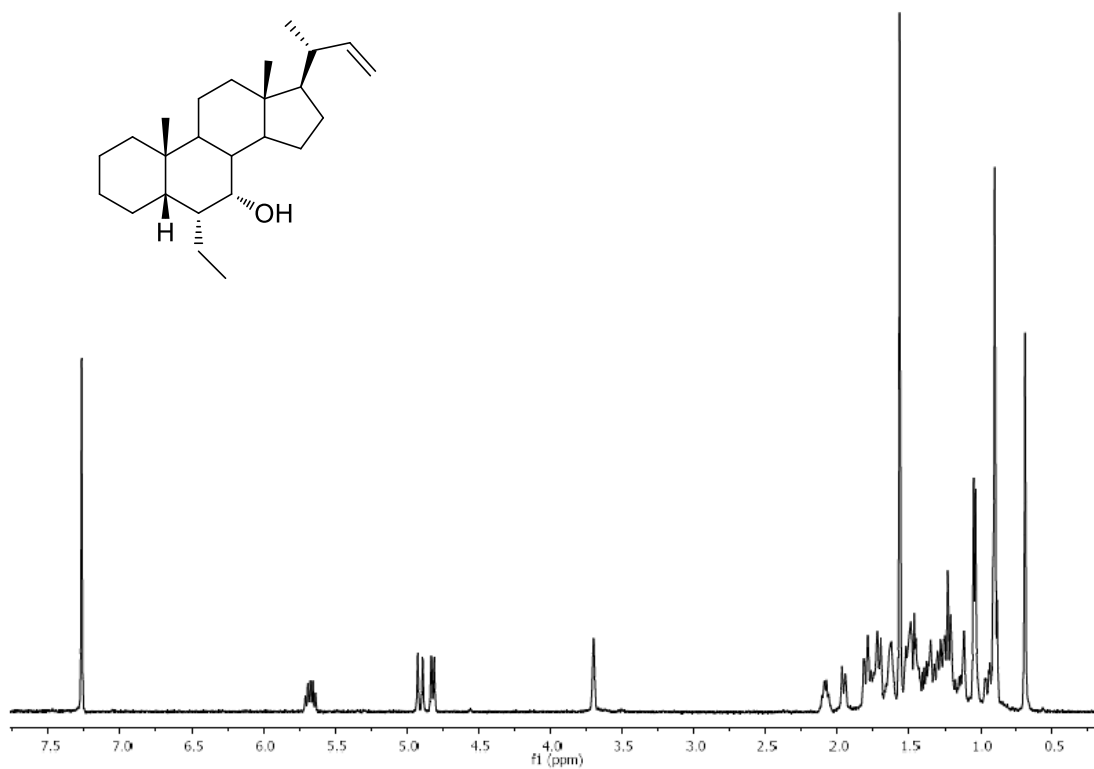
¹H NMR (400 MHz, CDCl₃) of compound 4

¹³C NMR (100 MHz, CDCl₃) of compound 4
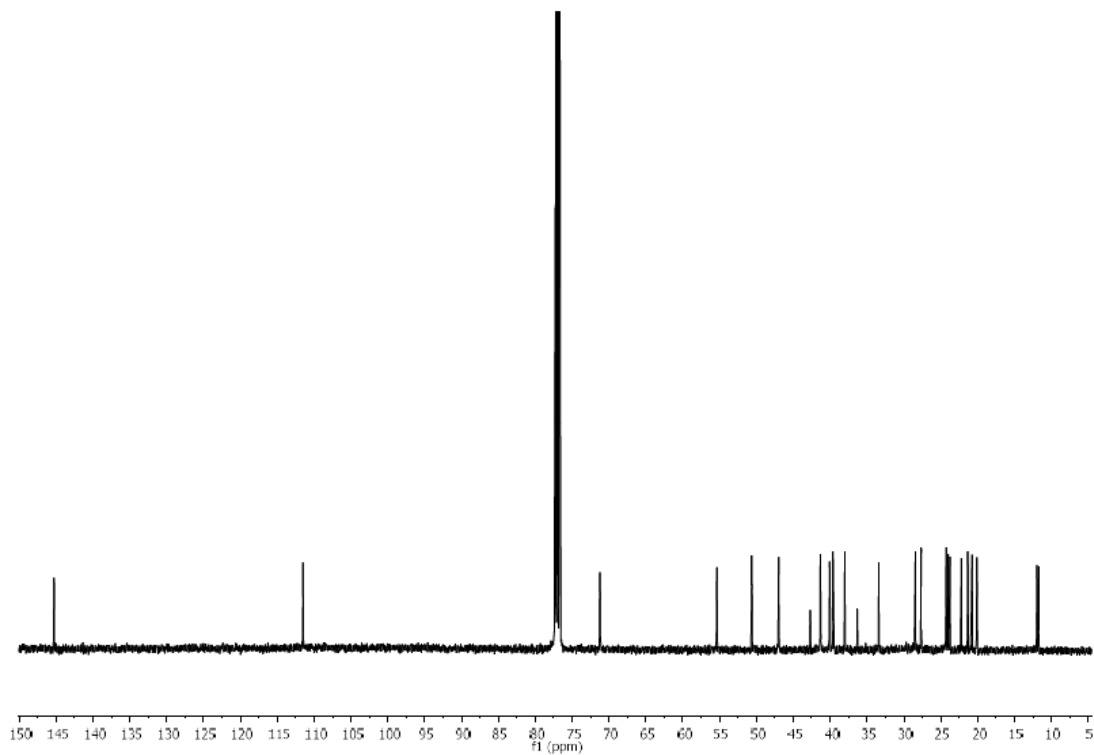
^{1}H NMR (400 MHz, CDCl$_3$) of compound 5
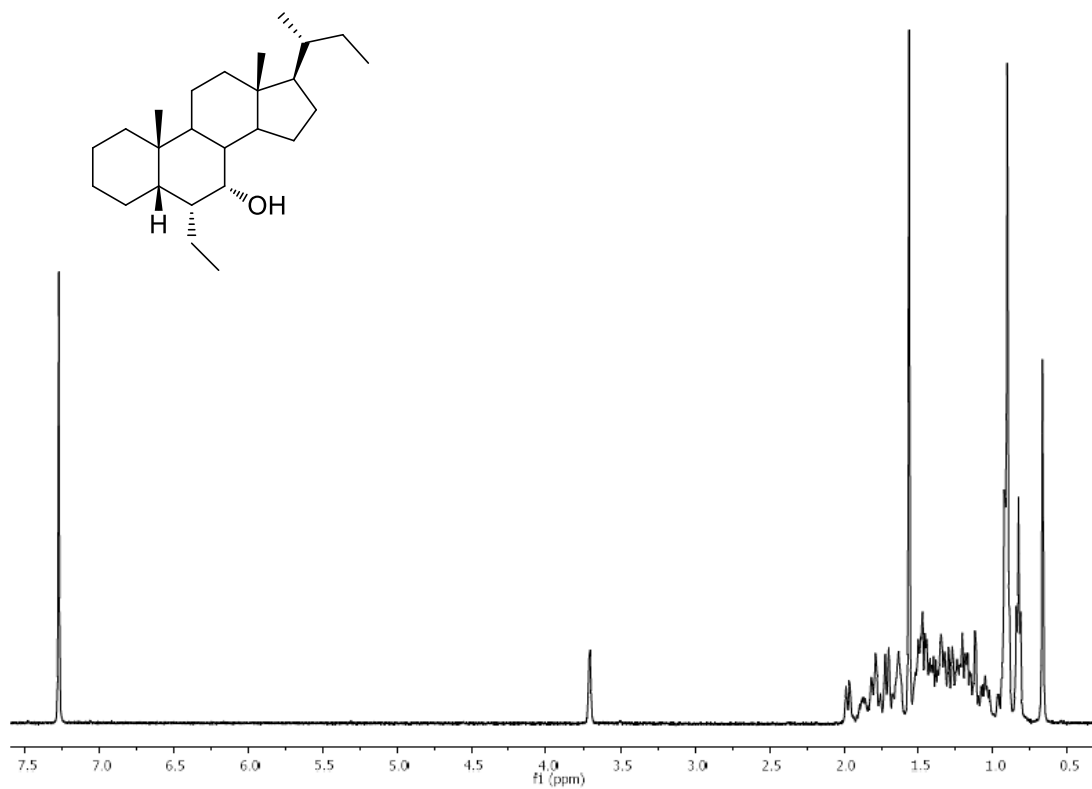
^{13}C NMR (100 MHz, CDCl$_3$) of compound 5
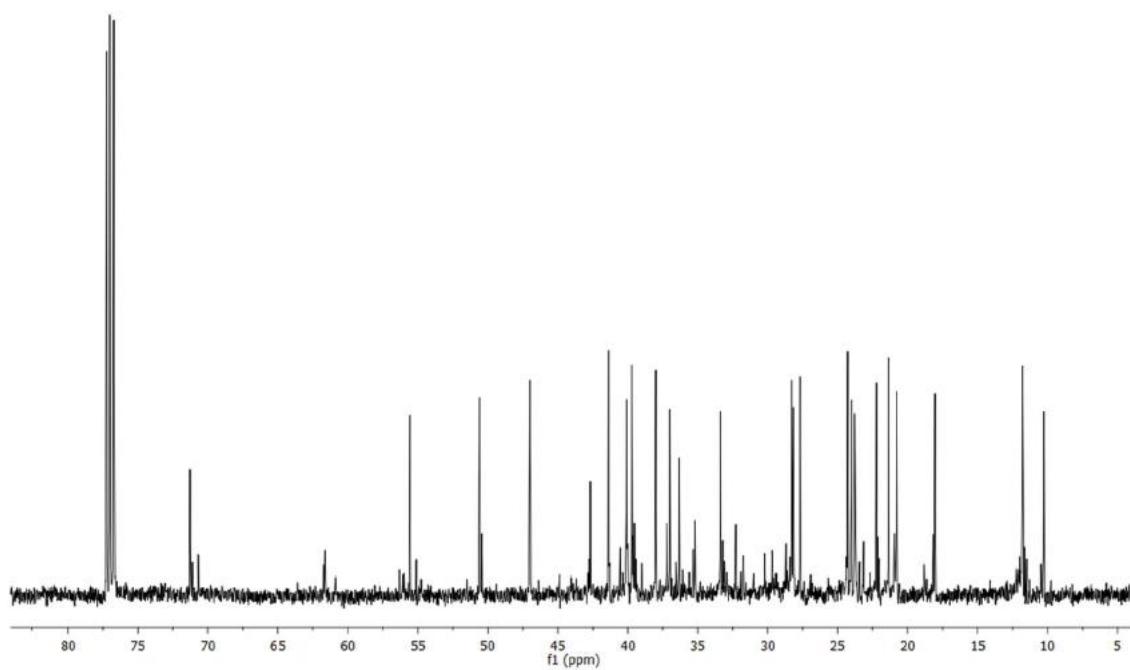
Experimental Information

^{1}H NMR (400 MHz, CDCl$_3$) of compound 6
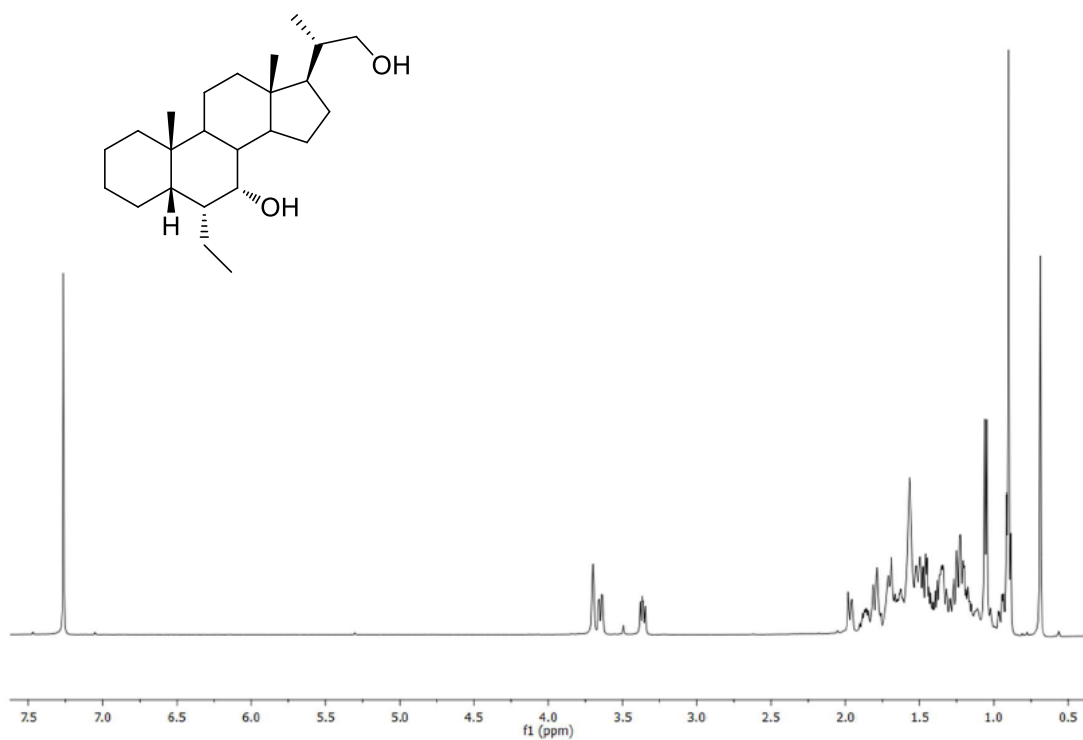
^{13}C NMR (100 MHz, CDCl$_3$) of compound 6
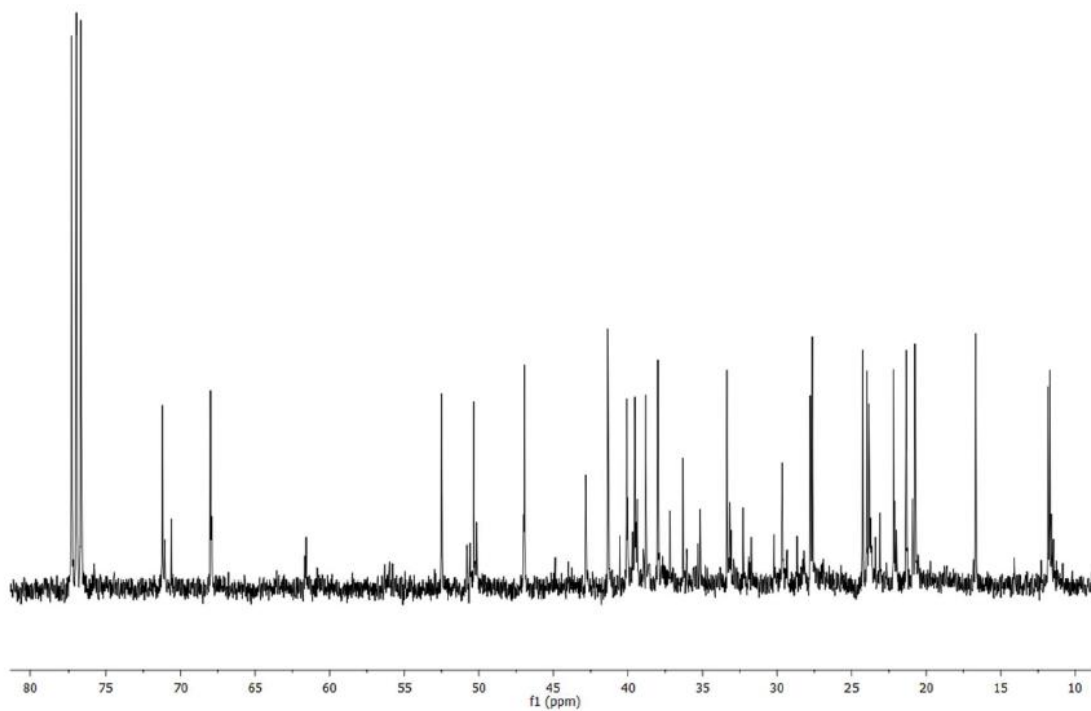
6.4. Biological Assays

Cell Culture

HepG2, a human immortalized hepatocarcinoma cell line, was cultured and maintained at 37 ^{13}C and 5% CO2 in E-MEM additioned with 10% FBS, 1% glutamine and 1% penicillin/streptomycin. HEK293T and GLUTag cells, a murine intestinal endocrine cell line, were cultured and maintained at 37 ^{13}C and 5% CO_2 in D-MEM and was additioned with 10% FBS, 1% glutamine and 1% penicillin/streptomycin.

Transactivation Assay

HepG2 cells were transfected with 100 ng of human pSG5-FXR 100 ng of human pSG5-RXR, 200 ng of the reporter vector p(hsp27)-TK-LUC containing the FXR response element IR1 cloned from the promoter of heat shock protein 27 (hsp27) and with 100 ng of pGL4.70 (Promega), a vector encoding the human Renilla gene to evaluate FXR mediated transactivation. HEK293T cells were transfected with 200 ng of human pGL4.29 (Promega), a reporter vector containing a cAMP response element (CRE) that drives the transcription of the luciferase reporter gene luc2P, with 100 ng of pCMVSPORT6-human GPBAR1, and with 100 ng of pGL4.70. At 24 h post-transfection to evaluate transactivation mediated by GPBAR1, cells were stimulated 18 h with CDCA, TLCA and compounds **1**–**6** (10 µM). In another assay, at 24h post-transfection, cells were stimulated with 50 µM of compounds in combination with CDCA or TLCA (10 µM). After treatments, 10 µL of cellular lysates were read utilizing a Dual-Luciferase Reporter Assay System (Promega Italia srl, Milan, Italy) according manufacturer specifications using the Glomax20/20 luminometer (Promega Italia srl, Milan, Italy). Luciferase activities were assayed and normalized with Renilla activities.

Dose–Response Curve on FXR and GPBAR1

Dose response curves were carried out in HepG2 and HEK293T cells transfected as described before and then treated with increasing concentrations of compounds **1**, **2**, **3**, and **6** (from 0.5 to 50 µM) to calculate the EC_{50} of FXR and GPBAR1. At 18 h post stimulations, cellular lysates were tested for luciferase and Renilla activities utilizing the Dual-Luciferase Reporter Assay System (E1980, Promega Italia srl, Milan, Italy). Luminescence was measured using Glomax 20/20 luminometer (Promega Iralia srl, Milan, Italy). Luciferase activities were normalized with Renilla activities.

RNA Isolation and RT-PCR

HepG2 and GLUTag cells were plated at 1×106 cells/well in a six well plate. After an overnight incubation, cells were starved and then stimulated for 18 h with compounds **1**, **2**, **3**, and **6**, 1 and 10 µM, or with CDCA or TLCA 10 µM. Total RNA was isolated from cells using the TRIzol reagent according to the manufacturer's specifications (Invitrogen, Carlsbad, CA, USA). One microgram of purified RNA was treated with DNase-I and reverse transcribed with Superscript II (Invitrogen, Carlsbad, CA, USA). For Real Time PCR, 10 ng template was dissolved in 25 µL containing 200 nmol/L of each primer and 12.5 µL of $2\times$ SYBR FAST Universal ready mix (Invitrogen, Carlsbad, CA, USA). All reactions were carried out in triplicate, and the thermal cycling conditions were as follows: 2 min at 95 ◦C, followed by 40 cycles of 95 ◦C for 20 s and 60 ◦C for 30 s in StepOnePlus (Applied Biosystems, Foster City, CA, USA). The relative mRNA expression was calculated accordingly to the Ct method. Primers were planned utilizing the software PRIMER31 using published data obtained from the NCBI database. Forward and reverse primer sequences were the following:

human GAPDH, gaaggtgaaggtcggagt and catgggtggaatcatattggaa;

human SHP, tctcttcttccgccctatca and aagggcttgctggacagtta;

mouse GAPDH, ctgagtatgtcgtggagtctac and gttggtggtgcaggatgcattg;

mouse pro-glucagon, tgaagacaaacgccactcac and caatgttgttccggttcctc.

6.5. Physiochemical Properties and Pharmacokinetic Characterization

LC-MS/MS ADME Methods

Utilizing an Alliance pump system coupled to a Q-ToF Premiere (Waters Co., Milford, MA, USA) was performed Chromatography assay. The mixture was separated on a Luna 5 µm C8(2) 100◦ A 150 × 2 mm from Phenomenex. The mobile phase consisted of 0.2% formic acid (FA) in water as solvent A and 0.2% FA in acetonitrile as solvent B at a flow rate of 200 µL/min. The gradient was as follows: 0–2 min (70% A and 30% B), 2–20 min (5% A and 95% B), 20–30 min (70% A and 30% B). The detection of analytes was achieved by electrospray ionization (ESI) in the positive mode with the appropriate MS/MS transitions, if necessary.

Solubility Measurements

Ten microliters of a 10 mM solution in DMSO of each compound was diluted either in 490 µL of PBS pH 7.4 or in organic solvent MeOH (in triplicate). The tubes were gently shaken 24 h at room temperature, then centrifuged for 5 min at 4000 rpm. 10 microliters of sample were diluted in 490 µL of MeOH. The solubility is determined by the ratio of mass signal area PBS/organic solvent.

Microsomal Stability

To evaluate microsomal stability were utilized male mouse (CD-1) liver microsomes (Sigma-Aldrich, St. Louis, MO, USA. All incubations were carried out in duplicate in a shaking water bath at 37 °C. The incubation mixtures contained 1 µM compound with 1% DMSO utilized as a vehicle, mouse liver microsomes (0.3 mg of microsomal protein per mL), 5 mM MgCl$_2$, 1 mM NADP, 5 mM glucose 6-phosphate, 0.4 U·mL$-$1 glucose 6-phosphate dehydrogenase, and 50 mM potassium phosphate buffer (pH 7.4) in a final

volume of 0.5 mL. Aliquots were removed at 0, 5, 10, 20, 30, and 40 min after microsome addition and the reaction was stopped by adding 200 μL of ice-cold acetonitrile [119]. After two hours, the samples were centrifuged for 10 min at 10,000 rpm, and the supernatants were transferred in matrix tubes for LC-MS/MS analysis. LC-MS/MS analysis were carried out setting the m/z window around the value of the MH+ of the unmodified compounds.

Propranolol, known as a high hepatic clearance drug in rodents, was utilizeed as a quality-control compound for the microsomal incubations. The slope of the linear regression of the curve obtained reporting the natural logarithm of compound area versus incubation time ($-k$) was utilized in the conversion to in vitro $t_{1/2}$ values by $t_{1/2} = -\ln(2)/k$. In vitro intrinsic clearance (Cl_{int} expressed as μL/min/mg) was measured according to the following formula: $Cl_{int} = $ volume of reaction (μL)/$t_{1/2}$(min)/protein of liver microsomes (mg). The percentage of unmodified compound has been measured assuming the area of the compound peak at time 0 min as 100%.

6.6. Computational studies

Molecular docking

The Glide [178] software was utilized to conduct molecular docking calculations in the crystal structure of the *Rattus Norvegicus* FXR-LDB (PDB code 1osv)[145] and in the homology model of human GPBAR1, previously developed by us [144]. It was seen that the *Rattus Norvegicus* FXR-LBD shares the 95% of homology with the human FXR-LBD, and the residues in the ligand binding site are the same among the two species. Therefore, the *Rattus Norvegicus* FXR-LDB X-ray structure can be utilized to study the binding mode of ligands of human FXR. Protein and ligand were got ready as described in previous papers [122,156]. For each receptor, a box of 30 Å × 30 Å × 30 Å centered on the ligand binding pocket was created to calculate the interaction grids. Upon docking calculations, ligands macrocyclic rings were treated as rigid; otherwise, default parameters were applied. The standard precision (SP) mode of the GlideScore function was utilized to score and rank the predicted binding poses [165, 166]. For each ligand, the best 10 docking poses were considered for visual inspection. For FXR, all the residue numbers were taken from the wild-type sequence of FXR.

CHAPTER 7

EXPERIMENTAL PROCEDURES: GW4064 Derivatives

7.1. General Information

High-resolution electrospray ionization mass spectrometry (ESI-MS) was performed with a Micromass Q-TOF mass spectrometer (Q-TOF premier, Waters Co., Milford, MA, USA). High-performance liquid chromatography (HPLC, Phenomenex Inc, Torrance, CA, USA) was carried out utilizing a Waters Model 510 pump fitted out with Waters rheodyne injector and a differential refractometer, model 401 (Waters Co., Milford, MA, USA). Nuclear magnetic resonance (NMR) was executed on Varian Inova 400 NMR spectrometer (^1H at 400 MHz, ^{13}C at 100 MHz) equipped with a Sun hardware and recorded in $CDCl_3$ ($^1H = 7.26$ and $^{13}C = 77.0$ ppm) and CD_3OD ($^1H = 3.30$ and $^{13}C = 49.0$ ppm). J are in hertz (Hz) and chemical shifts (δ) are showed in ppm and referred to $CHCl_3$ and CHD_2OD as internal standards. the progress of the reaction was monitored by thin-layer chromatography (TLC) on Alugram® silica gel G/UV254 plates. All chemicals were obtained from Zentek S.r.l and Sigma Aldrich. Solvents and reagents were utilized as supplied from commercial sources. The exceptions are: Tetrahydrofuran, toluene, CH_2Cl_2, which were distilled from calcium hydride just before use. Magnesium turnings (1 g) and iodine (0.1 g) were refluxed in a small (5–10 mL) quantity of methanol until the precipitate turns from black to white. The mixture was diluted (up to 100 mL) with methanol and under reflux for 2–3 h to obtaine Methanol dry. All reactions were carried out under argon atmosphere utilizing flame-dried glassware. Throught HPLC were evaluated the purity of the synthetized compounds. All compounds for biological testing were >95% pure.

7.2. Synthetic Procedure

Mitsunobu reaction.

After dissolving PPh$_3$ (3.5 eq) in dry THF at 0 °C, was added dropwise DIAD (3.5 eq). The suspension was stirred for 10 min, then compound **33** (or **15**) dissolved in dry THF was added. After 10 min, was added the corresponding phenol in dry THF. After 3h/overnight, was added water (10 mL) and the reaction was evaporated at rotavapor. The residue was than extracted with EtOAc (3 x 50 mL). The organic layers were washed with a solution of KOH 2.5 M and water, dried and evaporated to give a yellow oil. Purification by flash chromatography on silica gel gave compounds **12-14**, **17-19**, **22**, **25-26** and **29-30**.

LiBH$_4$ reduction. To esters **13**, or **18**, **22**, **25** and **29** dissolved in dry THF (25 mL), at 0 °C, was added dry methanol (3.0 eq) and LiBH$_4$ (3.0 eq). The resulting mixture was stirred for 4 h-8h at 0 °C. The reaction, then, was quenched by addition of 1M NaOH (2.0 eq) and extracted with ethyl acetate. The organic phase was washed with water, dried (Na$_2$SO$_4$) and concentrated giving crude residue, which was purified with HPLC or silica gel column chromatography.

Basic hydrolysis. Another portion of esters **13**, or **18**, **22**, **25** and **29** was hydrolyzed with NaOH (5.0 eq) in a solution of MeOH: H$_2$O 1:1 v/v (30 mL). The mixture was stirred for 8 h under reflux. The resulting solution was then acidified with HCl 6N and extracted with ethyl acetate (3 x 50 mL). The organic layers were washed with brine, dried over Na$_2$SO$_4$ anhydrous and evaporated under reduced pressure to give compound crude residue that was subjected to the purification through HPLC or flash chromatography.

Synthesis of 3-(2,6-dichlorophenyl)-5-isopropyl-4-(phenoxymethyl)isoxazole (12).

Purification by silica gel (hexane and 0.5% TEA) gave compound **12** (40%). An analytic sample of **12** was obtained through purification with HPLC on a Nucleodur 100-5 C18 (5 μm; 4.6 mm i.d. x 250 mm), with MeOH/H_2O (82:18) as eluent (flow rate 1 mL/min) (t_R = 10 min). **^{1}H NMR (CDCl$_3$, 400 MHz):** δ 7.39 (2H, d, J = 7.7 Hz), 7.31 (1H, t, J = 7.7 Hz), 7.22 (2H, t, J = 7.8 Hz), 6.93 (1H, t, J = 7.8 Hz), 6.78 (2H, d, J = 7.8 Hz), 4.72 (2H, s), 3.33 (1H, septet, J = 6.9 Hz), 1.41 (6H, d, J = 6.9 Hz); **^{13}C NMR (CDCl$_3$, 100 MHz)** δ 176.3, 159.1, 158.9, 135.8 (2C), 131.2, 129.4 (2C), 128.0 (3C), 121.2, 114.7 (2C), 109.4, 59.2, 27.0, 20.8 (2C); **HR ESIMS** m/z 362.0707 [M+H]$^+$, $C_{19}H_{18}Cl_2NO_2$ requires 362.0709.

Synthesis of Methyl 4-((3-(2,6-dichlorophenyl)-5-isopropylisoxazol-4-yl)methoxy)benzoate (13).

Purification by silica gel (9:1 hexane/AcOEt and 0.5% TEA) gave compound **13** (82%). An analytic sample of **13** was obtained through purification with HPLC on a Nucleodur 100-5 C18 (5 μm; 4.6 mm i.d. x 250 mm), with MeOH/H_2O (82:18) as eluent (flow rate 1 mL/min) (t_R = 12 min). **^{1}H NMR (CDCl$_3$, 400 MHz):** δ 7.91 (2H, d, J = 8.2 Hz), 7.39 (2H, d, J = 7.6 Hz), 7.31 (1H, t, J = 7.6 Hz), 6.78 (2H, d, J = 8.2 Hz), 4.77 (2H, s), 3.86 (3H, s), 3.32 (1H, septet, J = 6.7 Hz), 1.42 (6H, d, J = 6.7 Hz). **^{13}C NMR (CDCl$_3$, 100 MHz):** δ 176.5, 166.7, 161.8, 159.0, 135.7 (2C), 131.5, 131.3 (2C), 128.1 (2C), 127.7, 123.0, 114.1 (2C), 108.8, 59.5, 51.9, 27.1, 20.8 (2C). **HR ESIMS** m/z 420.0763 [M+H]$^+$, $C_{21}H_{20}Cl_2NO_4$ requires 420.0764.

Synthesis of 4-((3-(2,6-dichlorophenyl)-5-isopropylisoxazol-4-yl)methoxy)benzonitrile (14).

Purification by silica gel (9:1 hexane/AcOEt and 0.5% TEA) gave compound **14** (89%). An analytic sample of **6** was obtained through purification with HPLC on a Nucleodur 100-5 C18 (5 μm; 4.6 mm i.d. x 250 mm), with MeOH/H$_2$O (82:18) as eluent (flow rate 1 mL/min) (t$_R$ = 7.4 min). **^{1}H NMR (CDCl$_3$, 400 MHz):** δ 7.52 (2H, d, J = 8.5 Hz), 7.40 (2H, d, J = 7.0 Hz), 7.33 (1H, t, J = 7.0 Hz), 6.81 (2H, d, J = 8.5 Hz), 4.77 (2H, s), 3.31 (1H, septet, J = 6.8 Hz), 1.42 (6H, d, J = 6.8 Hz). **^{13}C NMR (CDCl$_3$, 100 MHz):** δ 176.61, 161.3, 158.9, 135.7 (2C), 133.9 (2C), 131.4, 128.1 (2C), 127.5, 118.9, 115.2 (2C), 108.5, 104.5, 59.5, 27.1, 20.8 (2C). **HR ESIMS** m/z 387.0665 [M+H]+, C$_{20}$H$_{17}$Cl$_2$N$_2$O$_2$ requires 387.0662.

Synthesis of (4-((3-(2,6-dichlorophenyl)-5-isopropylisoxazol-4-yl)methoxy)phenyl)methanol (15).

Purification by silica gel (100% CH$_2$Cl$_2$) gave compound **7** (95%). An analytic sample of **7** was obtained through purification with HPLC on a Nucleodur 100-5 C18 (5 μm; 4.6 mm i.d. x 250 mm), with MeOH/H$_2$O (70:30) as eluent (flow rate 1 mL/min) (t$_R$ = 13 min). **^{1}H NMR (CDCl$_3$, 400 MHz):** δ 7.39 (2H, d, J = 7.2 Hz), 7.32 (1H, t, J = 7.2 Hz), 7.22 (2H, d, J = 7.3 Hz), 6.76 (2H, d, J = 7.3 Hz), 4.71 (2H, s), 4.58 (2H, s), 3.32 (1H, septet, J = 6.6 Hz), 1.41 (6H, d, J = 6.6 Hz). **^{13}C NMR (CDCl$_3$, 100 MHz):** δ 176.3, S7 159.1, 157.8, 135.8 (2C), 133.7, 131.2, 128.5 (2C), 128.1 (2C), 127.8, 114.8 (2C), 109.4, 64.9, 59.4, 27.1, 20.7 (2C). **HR ESIMS** m/z 392.0817 [M+H]+, C$_{20}$H$_{20}$Cl$_2$NO$_3$ requires 392.0815.

Synthesis of 4-((3-(2,6-dichlorophenyl)-5-isopropylisoxazol-4-yl)methoxy)benzoic acid (**16**). Purification by silica gel (100% CH_2Cl_2) gave compound **16** (quantitative yield). An analytic sample of **16** was obtained through purification with HPLC on a Nucleodur 100-5 C18 (5 μm; 4.6 mm i.d. x 250 mm), with MeOH/H2O (75:25) as eluent (flow rate 1 mL/min) (t_R = 9.2 min). **^{1}H NMR (CDCl$_3$, 400 MHz):** δ 7.94 (2H, d, J = 6.5 Hz), 7.37 (2H, d, J = 7.0 Hz), 7.29 (1H, t, J = 7.0 Hz), 6.77 (2H, d, J = 6.5 Hz), 4.77 (2H, s), 3.31 (1H, septet, J = 6.4 Hz), 1.41 (6H, d, J = 6.4 Hz). **^{13}C NMR (CDCl$_3$, 100 MHz):** δ 177.4, 162.4, 162.3, 158.9, 135.7 (2C), 132.2 (2C), 131.3, 128.0 (2C), 127.7, 123.0, 114.2 (2C), 108.8, 59.4, 27.1, 20.8 (2C). **HR ESIMS** m/z 404.0460 [M-H]-, $C_{20}H_{16}Cl_2NO_4$ requires 404.0462.

Synthesis of 3-(2,6-dichlorophenyl)-5-isopropyl-4-((4-(methylsulfonyl)phenoxy)methyl)isoxazole (**17**).

Purification by silica gel (100% CH_2Cl_2) gave compound **17** (67%). An analytic sample of **17** was obtained through purification with HPLC on a Nucleodur 100-5 C18 (5 μm; 4.6 mm i.d. x 250 mm), with MeOH/H$_2$O (75:25) as eluent (flow rate 1 mL/min) (t_R = 13.5 min). **^{1}H NMR (CDCl$_3$, 400 MHz):** δ 7.79 (2H, d, J = 8.5 Hz), 7.40 (2H, d, J = 7.8 Hz), 7.32 (1H, t, J = 7.8 Hz), 6.88 (2H, d, J = 8.5 Hz), 4.80 (2H, s), 3.32 (1H, septet, J = 6.9 Hz), 3.0 (3H, s), 1.43 (6H, d, J = 6.9 Hz). **^{13}C NMR (CDCl$_3$, 100 MHz):** δ 176.6, 162.1, 158.9, 135.7 (2C), 132.8, 131.48, 129.5 (2C), 128.1 (2C), 127.5, 114.9 (2C), 108.5, 59.7, 44.2, 27.1, 20.8 (2C). **HR ESIMS** m/z 440.0487 [M+H]+, $C_{20}H_{20}Cl_2NO_4S$ requires 440.0485.

Synthesis of Methyl 3-((3-(2,6-dichlorophenyl)-5-isopropylisoxazol-4-yl)methoxy)benzoate (18).

Purification by silica gel (8:2 hexane/AcOEt and 0.5% TEA) gave compound **18** (57%). An analytic sample of **18** was obtained through purification with HPLC on a Nucleodur 100-5 C18 (5 μm; 4.6 mm i.d. x 250 mm), with MeOH/H_2O (82:18) as eluent (flow rate 1 mL/min) (t_R = 16.5 min). **^{1}H NMR (CDCl$_3$, 400 MHz):** δ 7.60 (1H, d, J = 7.8 Hz), 7.43 (1H, s), 7.38 (2H, d, J = 7.7 Hz), 7.32-7.25 (2H, m, ovl), 6.94 (1H, d, J = 8.3 Hz), 4.77 (2H, s), 3.89 (3H, s), 3.33 (1H, septet, J = 6.9 Hz), 1.42 (6H, d, J = 6.9 Hz). **^{13}C NMR (CDCl$_3$, 100 MHz):** δ 176.4, 166.7, 159.1, 158.1, 135.7 (2C), 131.4, 131.2, 129.4, 128.1 (2C), 127.8, 122.5, 120.3, 114.6, 109.1, 59.5, 52.1, 27.1, 20.8 (2C). **HR ESIMS** *m/z* 420.0766 [M+H]+, $C_{21}H_{20}Cl_2NO_4$ requires 420.0764.

Synthesis of 3-((3-(2,6-dichlorophenyl)-5-isopropylisoxazol-4-yl)methoxy)benzonitrile (19). Purification by silica gel (9:1 hexane/AcOEt and 0.5% TEA) gave compound **19** (73%). An analytic sample of **19** was obtained through purification with HPLC on a Nucleodur 100-5 C18 (5 μm; 4.6 mm i.d. x 250 mm), with MeOH/H2O (82:18) as eluent (flow rate 1 mL/min) (t_R = 11.4 min). **^{1}H NMR (CDCl$_3$, 400 MHz):** δ 7.40 (1H, s), 7.39 (2H, d, J = 7.8 Hz), 7.33 (1H, dd, ovl), 7.31 (1H, t, ovl), 7.21 (1H, d, J = 7.7 Hz), 6.99 (1H, d, J = 8.0 Hz), 4.75 (2H, s), 3.31 (1H, septet, J = 6.8 Hz), 1.41 (6H, d, J = 6.8 Hz). **^{13}C NMR (CDCl$_3$, 100 MHz):** δ 176.6, 158.9, 158.1, 135.7 (2C), 131.4, 130.4, 128.1 (2C), 127.6, 125.0, 120.0, 118.4, 117.5, 113.2, 108.6, 59.6, 27.1, 20.8 (2C). **HR ESIMS** *m/z* 387.0666 [M+H]+, $C_{20}H_{17}Cl_2N_2O_2$ requires 387.0662.

Synthesis of (3-((3-(2,6-dichlorophenyl)-5-isopropylisoxazol-4-yl)methoxy)phenyl)methanol (20).

Purification, obtained through purification with HPLC on a Nucleodur 100-5 C18 (5 μm; 4.6 mm i.d. x 250 mm), with MeOH/H_2O (75:25) as eluent (flow rate 1 mL/min) (t_R = 18 min) gave compound **20** (quantitative yield). **^{1}H NMR (CDCl$_3$, 400 MHz):** δ 7.39 (2H, d, J = 7.5 Hz), 7.30 (1H, t, J = 7.5 Hz), 7.19 (1H, t, J = 7.8 Hz), 6.9 (1H, d, J = 7.8 Hz), 6.80 (1H, s), 6.70 (1H, d, J = 7.8 Hz), 4.73 (2H, s), 4.61 (2H, d, J = 4.1 Hz), 3.33 (1H, septet, J = 6.9 Hz), 1.41 (6H, d, J = 6.9 Hz). **^{13}C NMR (CDCl$_3$, 100 MHz):** δ 176.5, 159.0, 158.5, 142.5, 135.8 (2C), 131.2, 129.5, 128.1 (2C), 127.8, 119.6, 114.1, 112.8, 109.4, 65.0, 59.2, 27.1, 20.8 (2C). **HR ESIMS** m/z 392.0818 [M+H]+, $C_{20}H_{20}Cl_2NO_3$ requires 392.0815.

Synthesis of 3-((3-(2,6-dichlorophenyl)-5-isopropylisoxazol-4-yl)methoxy)benzoic acid (**21**). Purification, obtained through purification with HPLC on a Nucleodur 100-5 C18 (5 μm; 4.6 mm i.d. x 250 mm), with MeOH/H_2O (75:25) as eluent (flow rate 1 mL/min) (t_R = 22.5 min) gave compound **21** (89%). **^{1}H NMR (CDCl$_3$, 400 MHz):** δ 7.65 (1H, d, J = 7.0 Hz), 7.47 (1H, s), 7.37 (2H, d, J = 7.5 Hz), 7.31-S9 7.25 (2H, m, ovl), 6.97 (1H, d, J = 7.8 Hz), 4.77 (2H, s), 3.32 (1H, septet, J = 7.1 Hz), 1.41 (6H, d, J = 7.1 Hz). **^{13}C NMR (CDCl$_3$, 100 MHz):** δ 176.41, 159.7, 159.1, 158.2, 135.7 (2C), 131.3, 129.5 (2C), 128.0 (2C), 127.6, 123.2, 121.0, 115.2, 109.1, 59.5, 27.1, 20.8 (2C). **HR ESIMS** m/z 404.0465 [M-H]-, $C_{20}H_{16}Cl_2NO_4$ requires 404.0462.

Experimental Information

Synthesis of Methyl 4'-((3-(2,6-dichlorophenyl)-5-isopropylisoxazol-4-yl)methoxy)-[1,1'-biphenyl]-3-carboxylate (22).

Purification by silica gel (100% CH_2Cl_2) gave compound **22** (68%). An analytic sample of **22** was obtained through purification with HPLC on a Nucleodur 100-5 C18 (5 μm; 4.6 mm i.d. x 250 mm), with MeOH/H_2O (90:10) as eluent (flow rate 1 mL/min) (t_R = 9.9 min). **^{1}H NMR (CDCl$_3$, 400 MHz):** δ 8.2 (1H, s), 7.98 (1H, d, J = 7.7 Hz), 7.71 (1H, d, J = 7.7 Hz), 7.49 (2H, d, J = 8.5 Hz), 7.48 (1H, t, J = 7.7 Hz), 7.42 (2H, d, J = 8.0 Hz), 7.33 (1H, dd, J = 7.1, 8.0 Hz), 6.87 (2H, d, J = 8.5 Hz), 4.78 (2H, s), 3.95 (3H, s), 3.36 (1H, septet, J = 7.1 Hz), 1.44 (6H, d, J = 7.1 Hz). **^{13}C NMR (CDCl$_3$, 100 MHz):** δ 176.4, 167.1, 159.1, 158.1, 140.8, 135.8 (2C), 133.2, 131.2, 131.0, 130.6, 128.8, 127.8, 127.7, 128.1 (4C), 126.8, 115.1 (2C), 109.3, 59.4, 52.1, 27.1, 20.8 (2C). **HR ESIMS** m/z 496.1073 [M+H]+, $C_{27}H_{24}Cl_2NO_4$ requires 496.1077.

Synthesis of (4'-((3-(2,6-dichlorophenyl)-5-isopropylisoxazol-4-yl)methoxy)-[1,1'-biphenyl]-3-yl)methanol (23).

Purification by silica gel (9:1 hexane/AcOEt and 0.5% TEA) gave compound **23** (83%). An analytic sample of **23** was obtained through purification with HPLC on a Nucleodur 100-5 C18 (5 μm; 4.6 mm i.d. x 250 mm), with MeOH/H_2O (83:17) as eluent (flow rate 1 mL/min) (t_R = 8.5 min). **^{1}H NMR (CD$_3$OD, 400 MHz):** δ 7.53 (1H, s), 7.52 (2H, d, J = 7.5 Hz), 7.47 (1H, t ovl), 7.46 (2H, d, J = 8.8 Hz), 7.43 (1H, d, J = 7.8 Hz), 7.36 (1H, t, J = 7.8 Hz), 7.27 (1H, d, J = 7.8 Hz), 6.84 (2H, d, J = 8.8 Hz), 4.84 (2H, s), 4.64 (2H, s), 3.43 (1H, septet, J = 6.7 Hz), 1.42 (6H, d, J = 6.7 Hz). **^{13}C NMR (CDCl$_3$, 100 MHz):** δ 176.4, 157.8, 154.1, 141.4, 137.4, 135.8 (2C), 134.0, 131.2, 129.0, 128.1 (4C), 126.0, 125.4, 125.3, 122.8, 115.1 (2C), 109.3, 65.4, 59.4, 27.0, 20.8 (2C). **HR ESIMS** m/z 468.1125 [M+H]+, $C_{26}H_{24}Cl_2NO_3$ requires 468.1128.

Synthesis of 4'-((3-(2,6-dichlorophenyl)-5-isopropylisoxazol-4-yl)methoxy)-[1,1'-biphenyl]-3-carboxylic acid (24).

Purification by silica gel (99:1 CH_2Cl_2/MeOH) gave compound **24** (64%). An analytic sample of **24** was obtained through purification with HPLC on a Nucleodur 100-5 C18 (5 μm; 4.6 mm i.d. x 250 mm), with MeOH/H_2O (83:17) as eluent (flow rate 1 mL/min) (t_R = 12.5 min). **^{1}H NMR (CDCl$_3$, 400 MHz):** δ 8.27 (1H, s), 8.04 (1H, d, J = 8.0 Hz), 7.76 (1H, d, J = 7.7 Hz), 7.51 (2H, d, J = 8.2 Hz), 7.50 (1H, t, J = 8.0 Hz), 7.42 (2H, d, J = 7.6 Hz), 7.33 (1H, t, J = 7.6 Hz), 6.87 (2H, d, J = 8.2 Hz), 4.78 (2H, s), 3.36 (1H, septet, J = 7.1 Hz), 1.44 (6H, d, J = 7.1 Hz). **^{13}C NMR (CDCl$_3$, 100 MHz):** δ 176.4, 164.9, 160.6, 158.1, 140.8, 135.8 (2C), 133.1, 132.1, 131.5, 131.2, 128.8, 128.3, 128.1 (4C), 127.8, 127.7, 115.1 (2C), 109.3, 59.4, 27.1, 20.8 (2C). **HR ESIMS** *m/z* 480.0773 [M-H]-, $C_{26}H_{20}Cl_2NO_4$ requires 480.0775.

Synthesis of Methyl 4-((4-((3-(2,6-dichlorophenyl)-5-isopropylisoxazol-4-yl)methoxy)benzyl)oxy)benzoate (25). Purification by silica gel (100% CH_2Cl_2) gave compound **25** (63%). An analytic sample of **25** was obtained through purification with HPLC on a Phenomenex C18 5 μm (5 μm; 4.6 mm i.d. x 250 mm), with MeOH/H2O (85:15) as eluent (flow rate 1 mL/min) (t_R = 10.4 min). **^{1}H NMR (CDCl$_3$, 400 MHz):** δ 7.98 (2H, d, J = 8.0 Hz), 7.40 (2H, d, J = 7.7 Hz), 7.33-7.26 (3H, m, ovl), 6.96 (2H, d, J = 8.0 Hz), 6.79 (2H, d, J = 7.7 Hz), 5.00 (2H, s), 4.72 (2H, s), 3.88 (3H, s), 3.32 (1H, septet, J = 6.9 Hz), 1.41 (6H, d, J = 6.9 Hz). **^{13}C NMR (CDCl$_3$, 100 MHz):** δ 176.4, 166.8, 162.4, 159.1, 158.2, 135.7 (2C), 131.5, 131.2 (2C), 129.2 (2C), 128.8, 128.1 (2C), 127.3, 122.7, 114.9 (2C), 114.4 (2C), 109.3, 69.7, 59.4, 51.85, 27.1, 20.7 (2C). **HR ESIMS** *m/z* 526.1180 [M+H]+, $C_{28}H_{26}Cl_2NO_5$ requires 526.1183.

Synthesis of 4-((4-((3-(2,6-dichlorophenyl)-5-isopropylisoxazol-4-yl)methoxy)benzyl)oxy)benzonitrile (26). Purification by silica gel (7:3 hexane/AcOEt and 0.5% TEA) gave compound **26** (quantitative yield). An analytic sample of **26** was obtained through purification with HPLC on a Phenomenex C18 5 μm (4.6 mm i.d. x 250 mm), with MeOH/H$_2$O (87:13) as eluent (flow rate 1 mL/min) (t_R = 8 min). **^{1}H NMR (CDCl$_3$, 400 MHz):** δ 7.58 (2H, d, *J* = 8.5 Hz), 7.40 (2H, d, *J* = 8.0 Hz), 7.32 (1H, t, *J* = 8.4 Hz), 7.27 (2H, d, *J* = 8.4 Hz), 6.98 (2H, d, *J* = 8.5 Hz), 6.80 (2H, d, *J* = 8.0 Hz), 5.00 (2H, s), 4.73 S11 (2H, s), 3.32 (1H, septet, *J* = 6.9 Hz), 1.42 (6H, d, *J* = 6.9 Hz). **^{13}C NMR (CDCl$_3$, 100 MHz):** δ 176.1, 161.7, 158.8, 158.1, 135.5 (2C), 133.7 (2C), 131.1, 129.0 (2C), 128.1, 127.8 (2C), 127.5, 118.9, 115.3 (2C), 114.7 (2C), 109.1, 103.8, 69.7, 59.2, 26.8, 20.5 (2C). **HR ESIMS** *m/z* 493.1083 [M+H]+, C$_{27}$H$_{23}$Cl$_2$N$_2$O$_3$ requires 493.1080.

**(4-((4-((3-(2,6-dichlorophenyl)-5-isopropylisoxazol-4-yl)methoxy)benzyl)oxy)phenyl)methanol (27).** Purification, obtained through purification with HPLC on a Phenomenex C18 5 μm (4.6 mm i.d. x 250 mm), with MeOH/H$_2$O (75:25) as eluent (flow rate 1 mL/min) (t_R = 24 min) gave compound **27** (quantitative yield). **^{1}H NMR (CDCl$_3$, 400 MHz):** δ 7.39 (2H, d, *J* = 7.9 Hz), 7.31 (1H, ovl), 7.28 (4H, d, ovl), 6.94 (2H, d, *J* = 8.3 Hz), 6.80 (2H, d, *J* = 8.3 Hz), 4.96 (2H, s), 4.72 (2H, s), 4.62 (2H, d, *J* = 5.1 Hz), 3.33 (1H, septet, *J* = 6.9 Hz), 1.41 (6H, d, *J* = 6.9 Hz). **^{13}C NMR (CDCl$_3$, 100 MHz):** δ 176.5, 159.3, 158.4, 158.2, 135.7 (2C), 133.7, 131.4, 129.8 (2C), 129.2 (2C), 128.8, 128.2 (2C), 128.0, 115.0 (4C), 109.5, 69.8, 64.9, 59.6, 27.3, 20.9 (2C). **HR ESIMS** *m/z* 498.1230 [M+H]+, C$_{27}$H$_{26}$Cl$_2$NO$_4$ requires 498.1233.

Synthesis of 4-((4-((3-(2,6-dichlorophenyl)-5-isopropylisoxazol-4-yl)methoxy)benzyl)oxy)benzoic acid (28

). Purification by silica gel (7:3 hexane:AcOEt) gave compound **28** (93%). An analytic sample of **28** was obtained through purification with HPLC on a Nucleodur 100-5 (5 μm; 10 mm i.d. x 250 mm), with hexane/AcOEt (50:50) as eluent (flow rate 3 mL/min) (t_R = 15 min). **^{1}H NMR (CDCl$_3$, 400 MHz):** δ 8.05 (2H, d, J = 8.6 Hz), 7.40 (2H, d, J = 7.89 Hz), 7.33-7.29 (3H, m, ovl), 6.99 (2H, d, J = 8.6 Hz), 6.81 (2H, d, J = 8.4 Hz), 5.03 (2H, s), 4.73 (2H, s), 3.32 (1H, septet, J = 6.9 Hz), 1.42 (6H, d, J = 6.9 Hz). **^{13}C NMR (CDCl$_3$, 100 MHz):** δ 176.4, 163.2, 162.4, 158.9, 158.3, 135.8 (2C), 132.3, 131.2 (2C), 129.2 (2C), 128.7, 128.1 (2C), 127.8, 121.7, 114.9 (2C), 114.5 (2C), 109.3, 69.8, 59.4, 27.1, 20.8 (2C). **HR ESIMS** m/z 510.0885 [M-H]-, $C_{27}H_{22}Cl_2NO_5$ requires 510.0881.

Synthesis of Methyl 3-((4-((3-(2,6-dichlorophenyl)-5-isopropylisoxazol-4-yl)methoxy)benzyl)oxy)benzoate (29).

Purification by silica gel (100% CH$_2$Cl$_2$) gave compound **29** (61%). An analytic sample of **29** was obtained through purification with HPLC on a Nucleodur 100-5 C18 (5 μm; 4.6 mm i.d. x 250 mm), with MeOH/H$_2$O (85:15) as eluent (flow rate 1 mL/min) (t_R = 18 min). **^{1}H NMR (CDCl$_3$, 400 MHz):** δ 7.63 (2H, d, J = 7.6 Hz), 7.40 (2H, d, J = 8.1 Hz), 7.33 (1H, t, J = 8.1 Hz), 7.30-7.29 (3H, m, ovl), 7.13 (1H, d, J = 7.9 Hz), 6.79 (2H, d, J = 8.3 Hz), 5.00 (2H, s), 4.72 (2H, s), 3.91 (3H, s), 3.32 (1H, septet, J = 6.9 Hz), 1.41 (6H, d, J = 6.9 Hz). **^{13}C NMR (CDCl$_3$, 100 MHz):** δ 176.4, 171.1, 169.3, 157.0, 152.9, 135.8 (2C), 131.2, 129.4, 129.2 (4C), 128.1 (2C), 122.2, 120.8, 120.2, 115.0, 114.8 (2C), 109.3, 69.8, 59.4, 52.2, 27.1, 20.7 (2C). **HR ESIMS** m/z 526.1185 [M+H]+, $C_{28}H_{26}Cl_2NO_5$ requires 526.1183.

Synthesis of 3-((4-((3-(2,6-dichlorophenyl)-5-isopropylisoxazol-4-yl)methoxy)benzyl)oxy)benzonitrile (30). Purification by silica gel (100% CH_2Cl_2) gave compound **30** (93%). An analytic sample of **30** was obtained through purification with HPLC on a Nucleodur 100-5 C18 (5 μm; 4.6 mm i.d. x 250 mm), with MeOH/H_2O (82:18) as eluent (flow rate 1 mL/min) (t_R = 16 min). **^{1}H NMR (CDCl$_3$, 400 MHz):** δ 7.40 (2H, d, J = 7.8 Hz), 7.33 (1H, t, J = 7.8 Hz), 7.29-7.23 (4H, m, ovl), 7.16 (2H, ovl), 6.79 (2H, d, J = 8.5 Hz), 4.97 (2H, s), 4.72 (2H, s), 3.32 (1H, septet, J = 7.0 Hz), 1.41 (6H, d, J = 7.0 Hz). **^{13}C NMR (CDCl$_3$, 100 MHz):** δ 176.4, 163.2, 159.1, 158.3, 135.7 (2C), 131.2, 130.4, 129.7, 129.1 (2C), 128.1 (2C), 124.7, 123.9, 120.5, 118.9, 118.7, 114.9, 114.8, 114.6, 109.3, 69.9, 59.4, 27.1, 20.8 (2C). **HR ESIMS** *m/z* 493.1078 [M+H]+, $C_{27}H_{23}Cl_2N_2O_3$ requires 493.1080.

Synthesis of (3-((4-((3-(2,6-dichlorophenyl)-5-isopropylisoxazol-4-yl)methoxy)benzyl)oxy)phenyl)methanol (31). Purification obtained through HPLC on a Phenomenex C18 5 μm (4.6 mm i.d. x 250 mm), with MeOH/H_2O (80:20) as eluent (flow rate 1 mL/min) (t_R = 10 min) gave compound **31** (84%). **^{1}H NMR (CDCl$_3$, 400 MHz):** δ 7.40 (2H, d, J = 7.70 Hz), 7.33 (1H, t, J = 7.70 Hz), 7.28 (2H, d, J = 8.4 Hz), 7.27 (1H, dd, ovl), 6.98 (1H, s), 6.94 (1H, d, J = 7.5 Hz), 6.87 (1H, d, J = 8.0 Hz), 6.78 (2H, d, J = 8.4 Hz), 4.96 (2H, s), 4.72 (2H, s), 4.66 (2H, br s), 3.32 (1H, septet, J = 6.9 Hz), 1.41 (6H, d, J = 6.9 Hz). **^{13}C NMR (CDCl$_3$, 100 MHz):** δ 176.3, 159.1, 158.9, 158.1, 142.5, 135.7 (2C), 131.2, 129.6, 129.0 (3C), 128.0 (2C), 123.2, 119.3, 114.8 (2C), 114.1, 113.2, 109.3, 69.6, 65.2, 59.3, 27.1, 20.8 (2C). **HR ESIMS** *m/z* 498.1231 [M+H]+, $C_{27}H_{26}Cl_2NO_4$ requires 498.1233.

Synthesis of 3-((4-((3-(2,6-dichlorophenyl)-5-isopropylisoxazol-4-yl)methoxy)benzyl)oxy)benzoic acid (32).

Purification by silica gel (8:2 hexane/AcOEt) gave compound **32** (72%). An analytic sample of **32** was obtained through purification with HPLC on a Phenomenex C18 5 μm (4.6 mm i.d. x 250 mm), with MeOH/H$_2$O (80:20) as eluent (flow rate 1 mL/min) (t_R = 12 min). **^{1}H NMR (CD$_3$OD, 400 MHz):** δ 7.58 (1H, s), 7.57 (1H, d, J = 8.0 Hz), 7.49 (2H, d, J = 7.7 Hz), 7.43 (1H, dd, J = 8.0, 8.4 Hz), 7.30 (1H, t, J = 7.7 Hz), 7.28 (2H, d, J = 8.6 Hz), 7.10 (1H, d, J = 8.4 Hz), 6.77 (2H, d, J = 8.6 Hz), 5.00 (2H, s), 4.81 (2H, s), 3.41 (1H, septet, J = 7.1 Hz), 1.40 (6H, d, J = 7.1 Hz). **^{13}C NMR (CDCl$_3$, 100 MHz):** δ 176.3, 169.7, 159.1, 158.6, 158.1, 135.7 (2C), 132.0 (2C), 131.2, 129.5, 129.2, 128.4, 128.0 (2C), 122.7, 120.8, 116.1, 115.3, 114.8 (2C), 109.3, 69.7, 59.3, 27.1, 20.7 (2C). **HR ESIMS** m/z 510.0878 [M-H]-, C$_{27}$H$_{22}$Cl$_2$NO$_5$ requires 510.0881.

7.3. NMR Spectra

¹H NMR (400 MHz, CDCl₃) of compound **12**
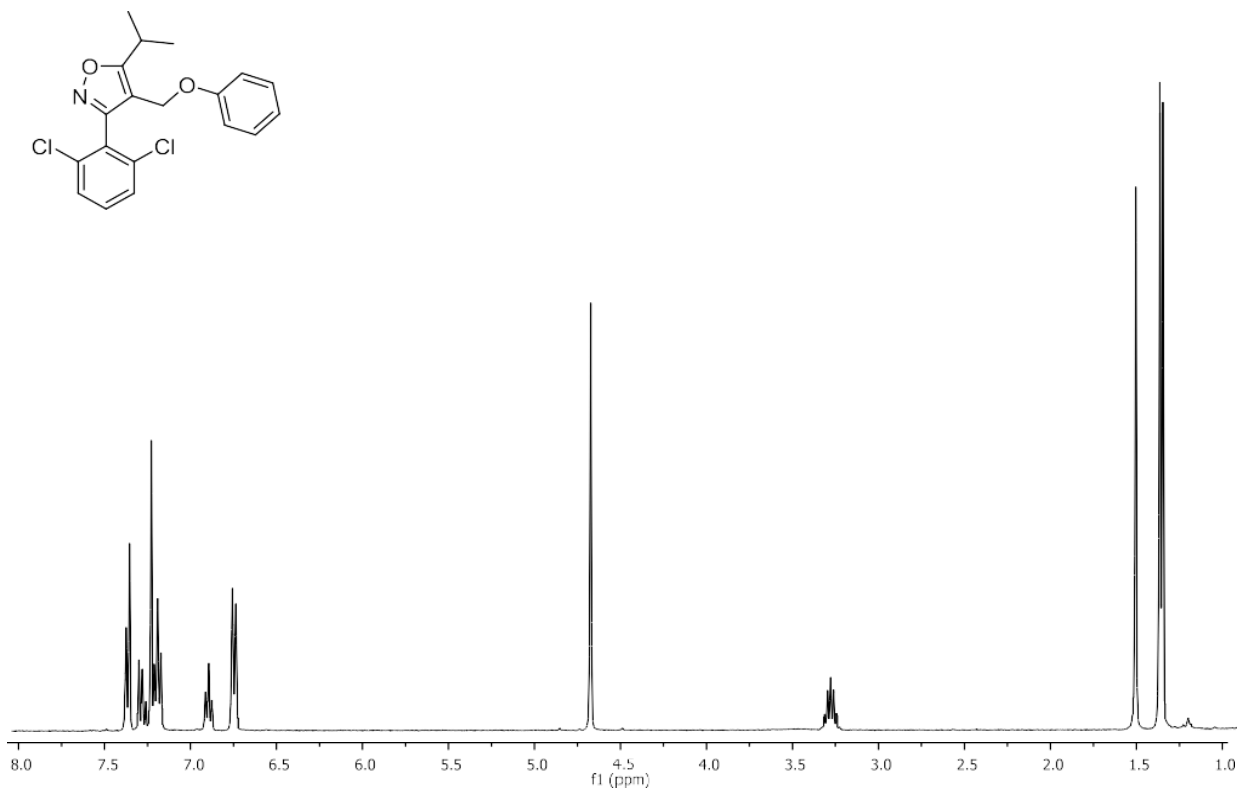
¹³C NMR (100 MHz, CDCl₃) of compound **12**
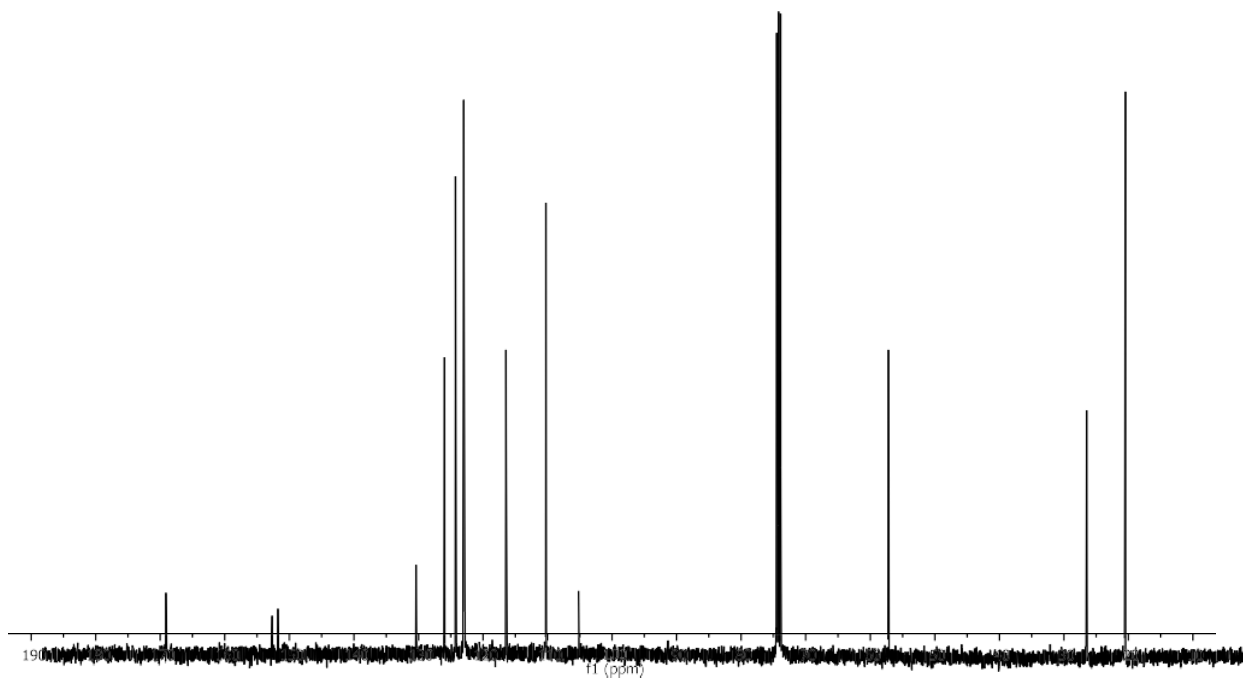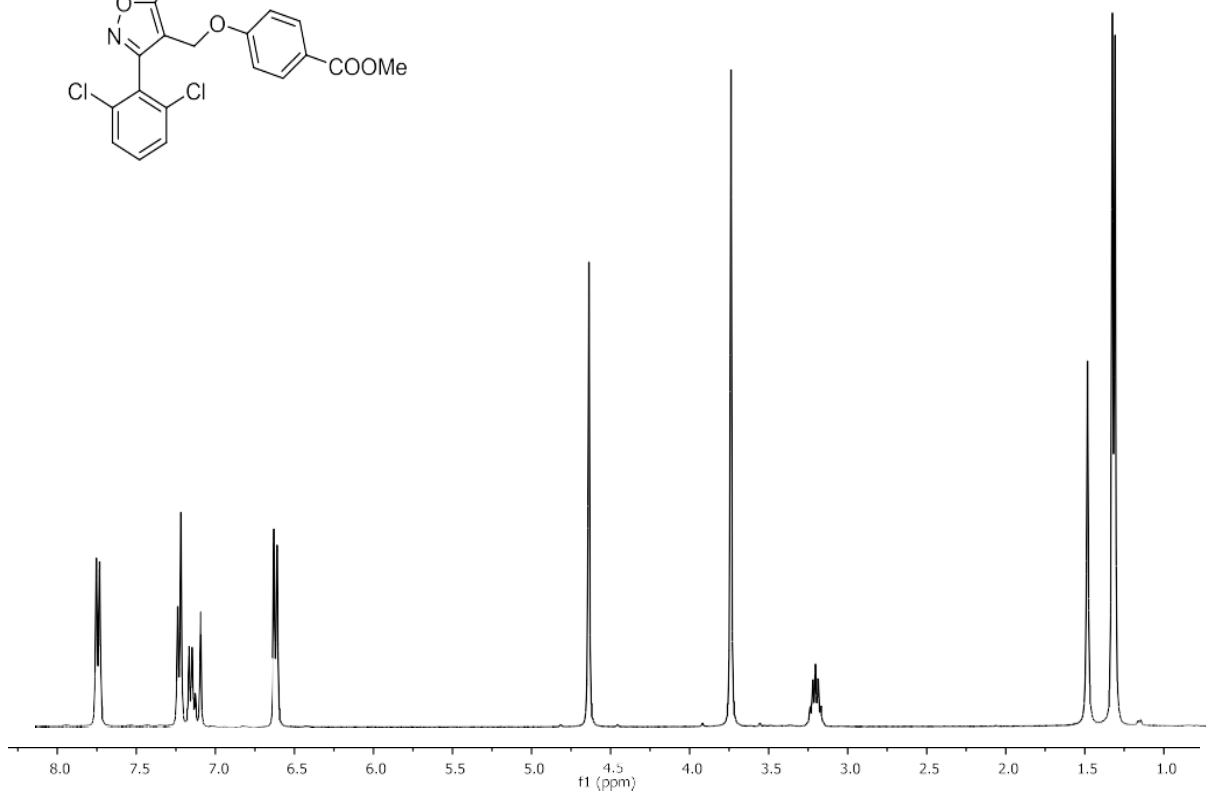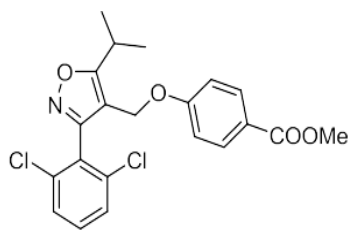
^{1}H NMR (400 MHz, CDCl$_3$) of compound **13**

^{13}C NMR (100 MHz, CDCl$_3$) of compound **13**
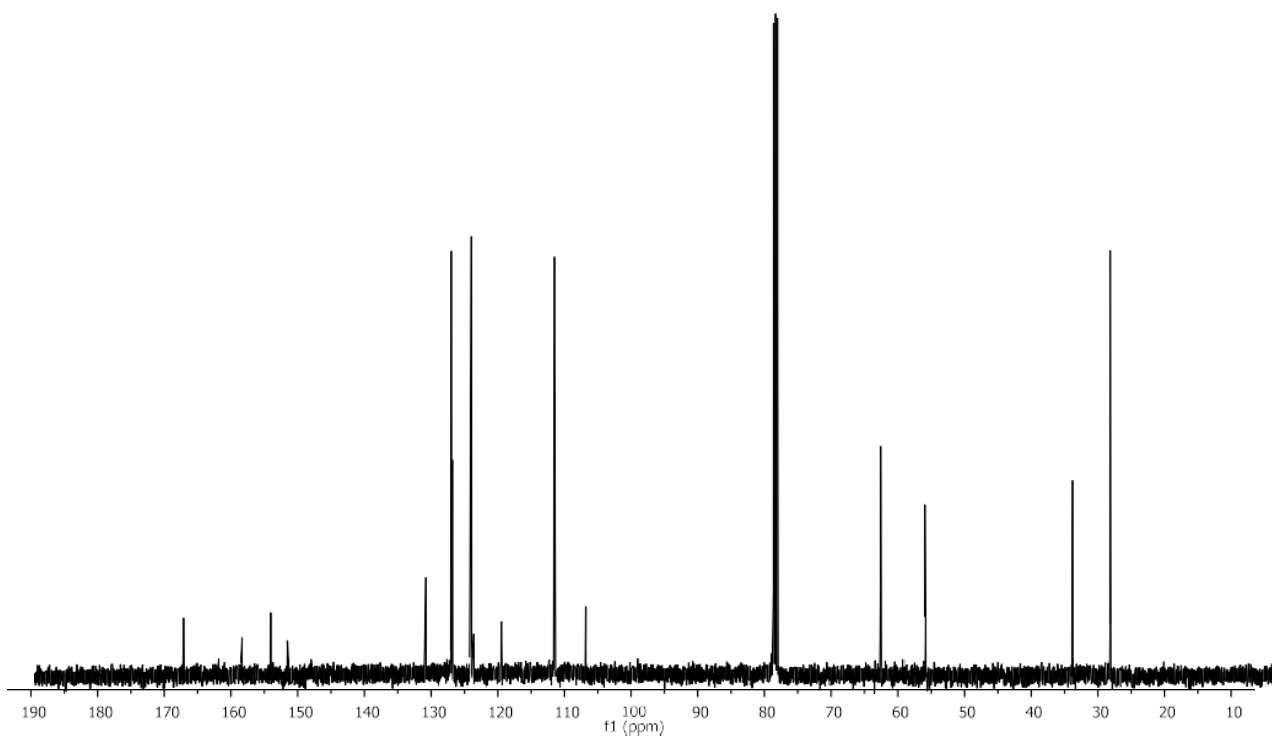
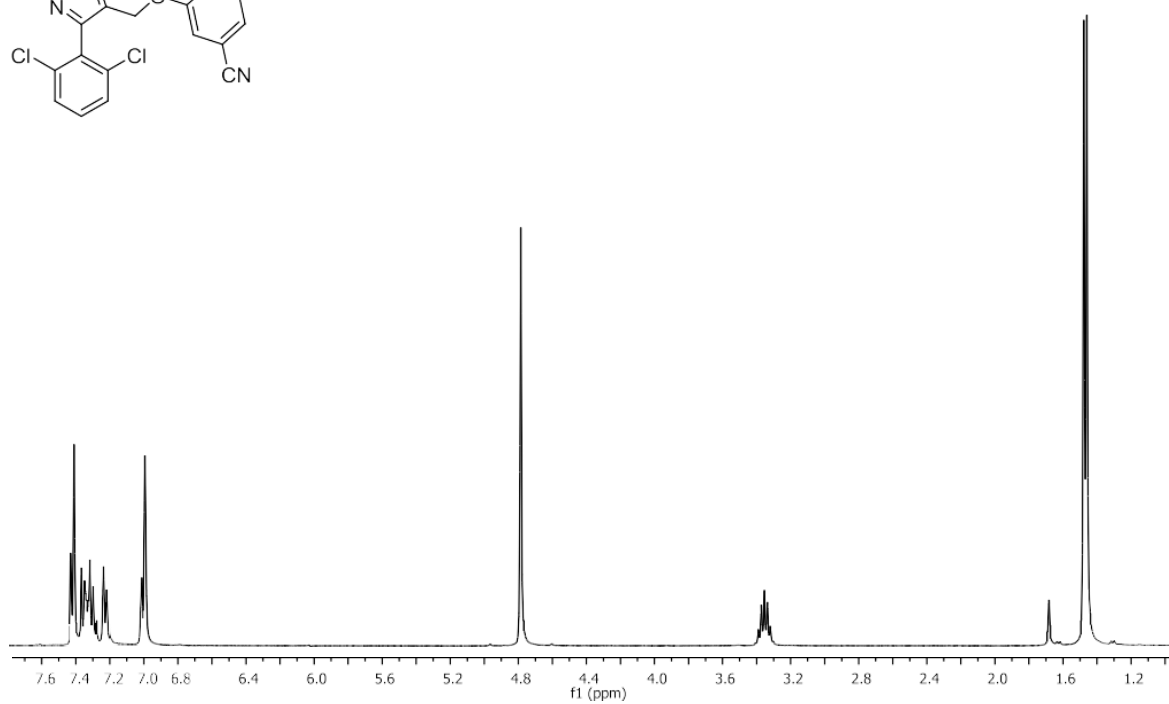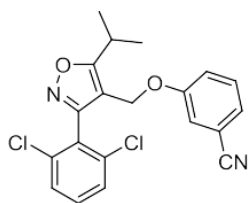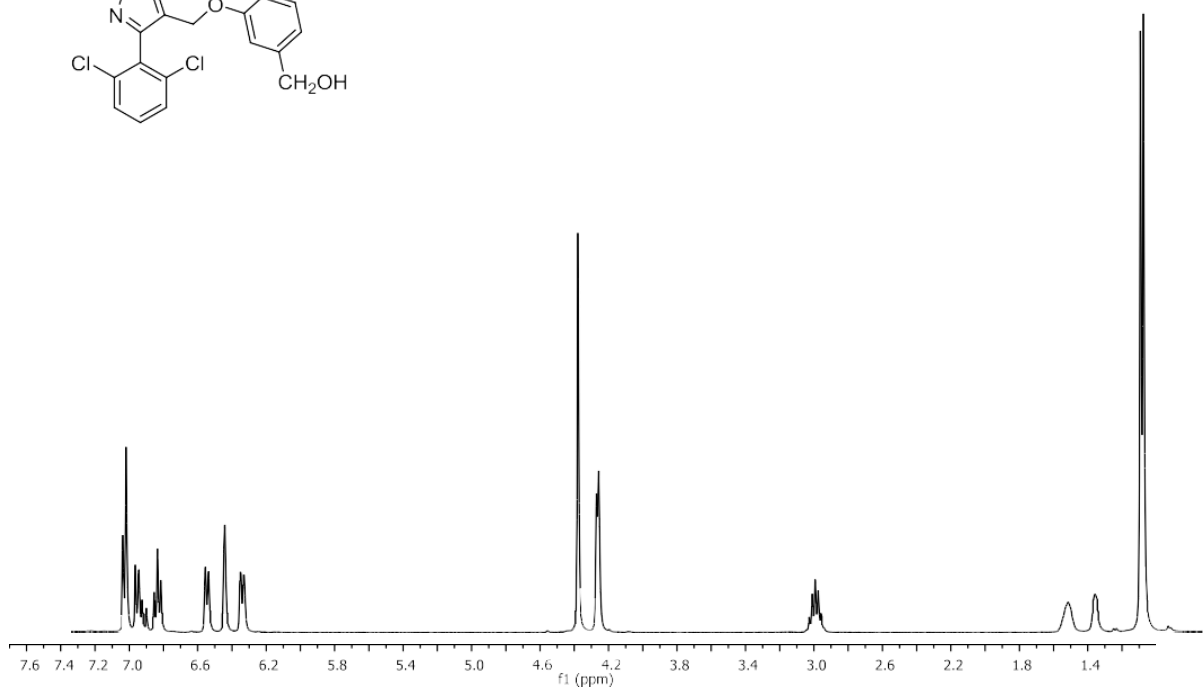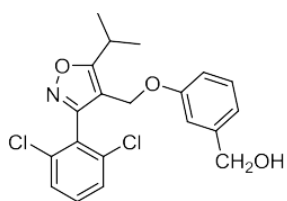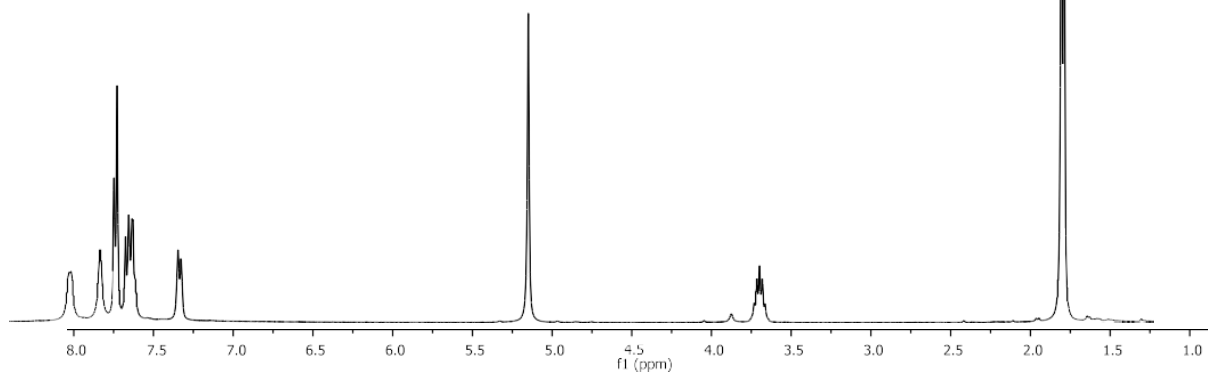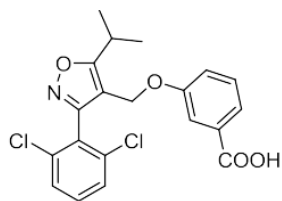## ^{1}H NMR (400 MHz, CDCl$_3$) of compound **14**
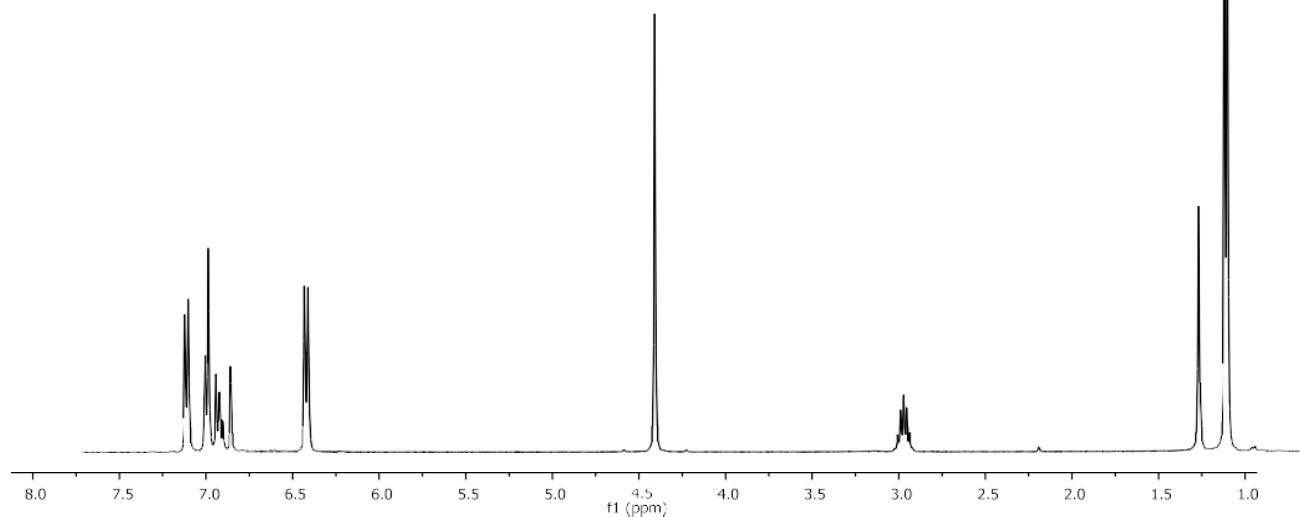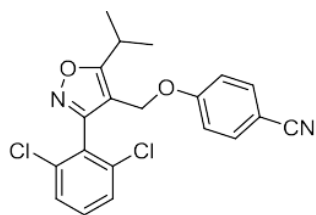
^{13}C NMR (100 MHz, CDCl$_3$) of compound **14**
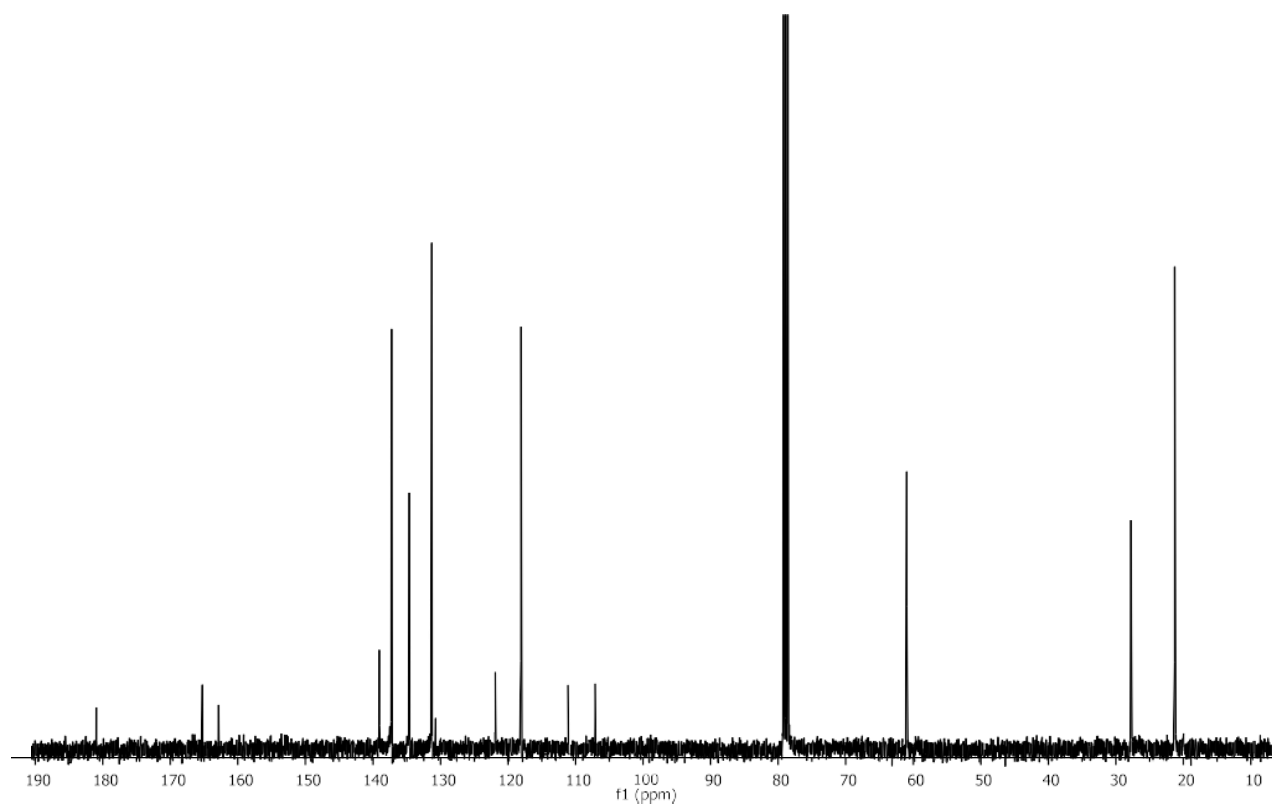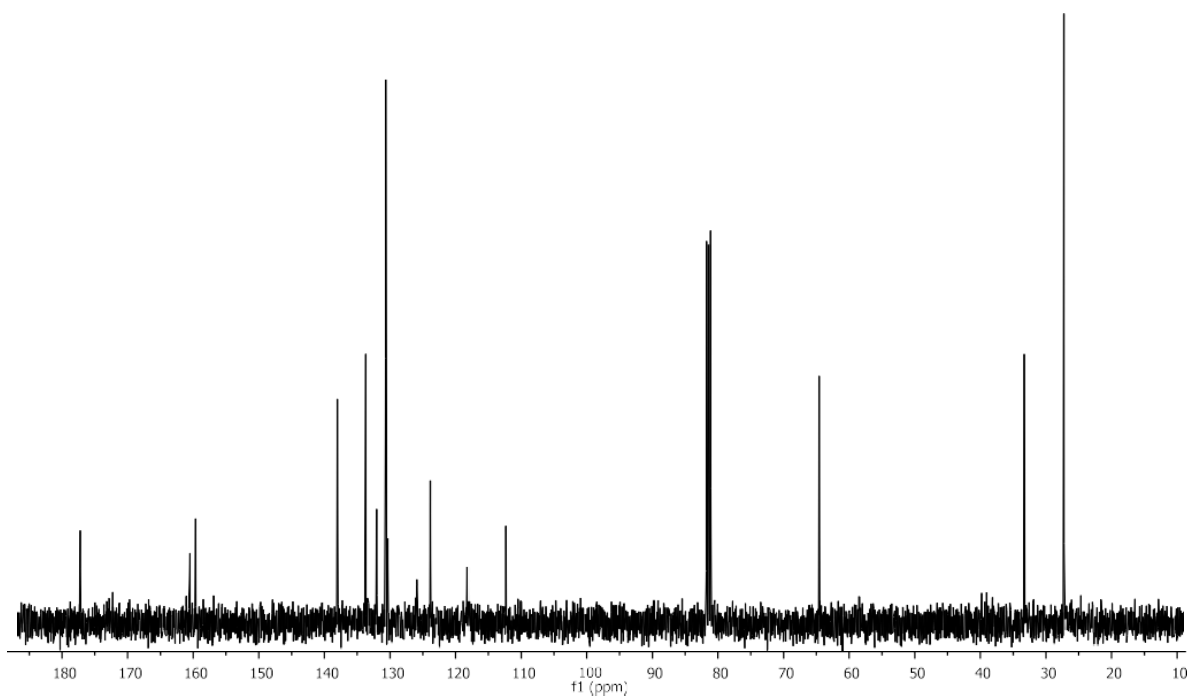
Experimental Information
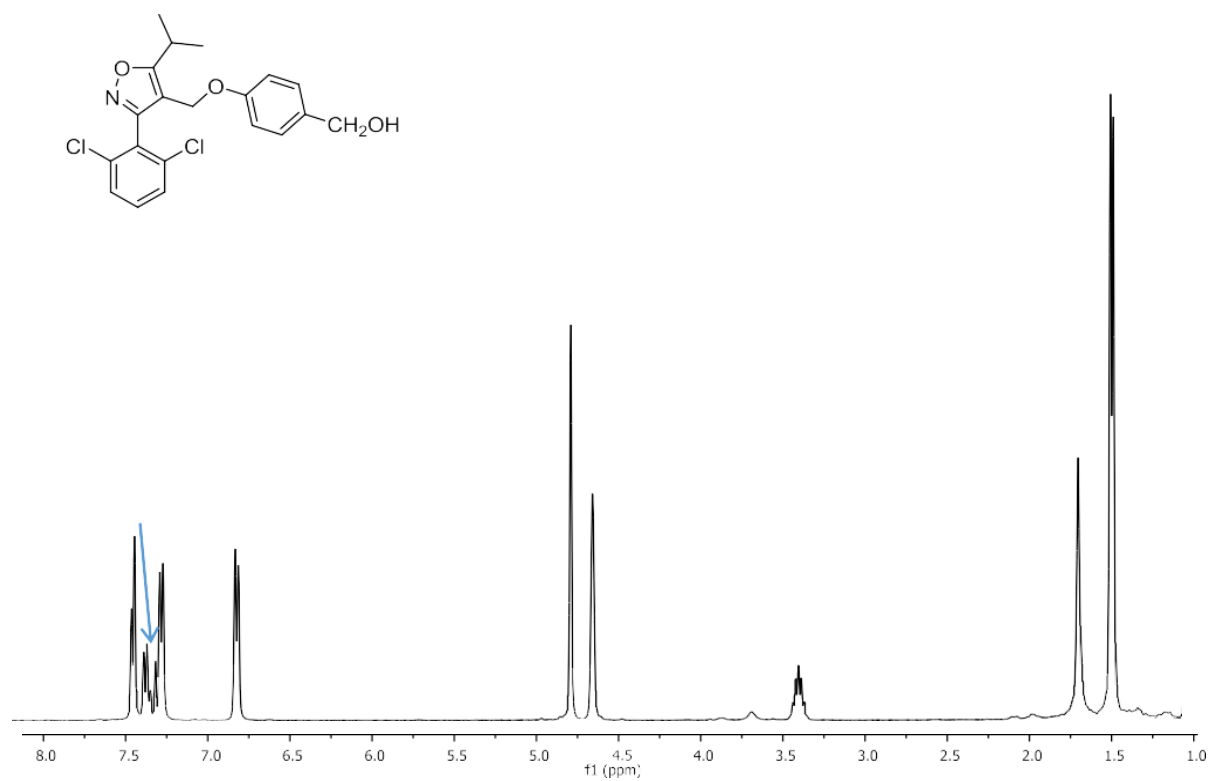
¹H NMR (400 MHz, CDCl₃) of compound **15**

¹³C NMR (100 MHz, CDCl₃) of compound **15**
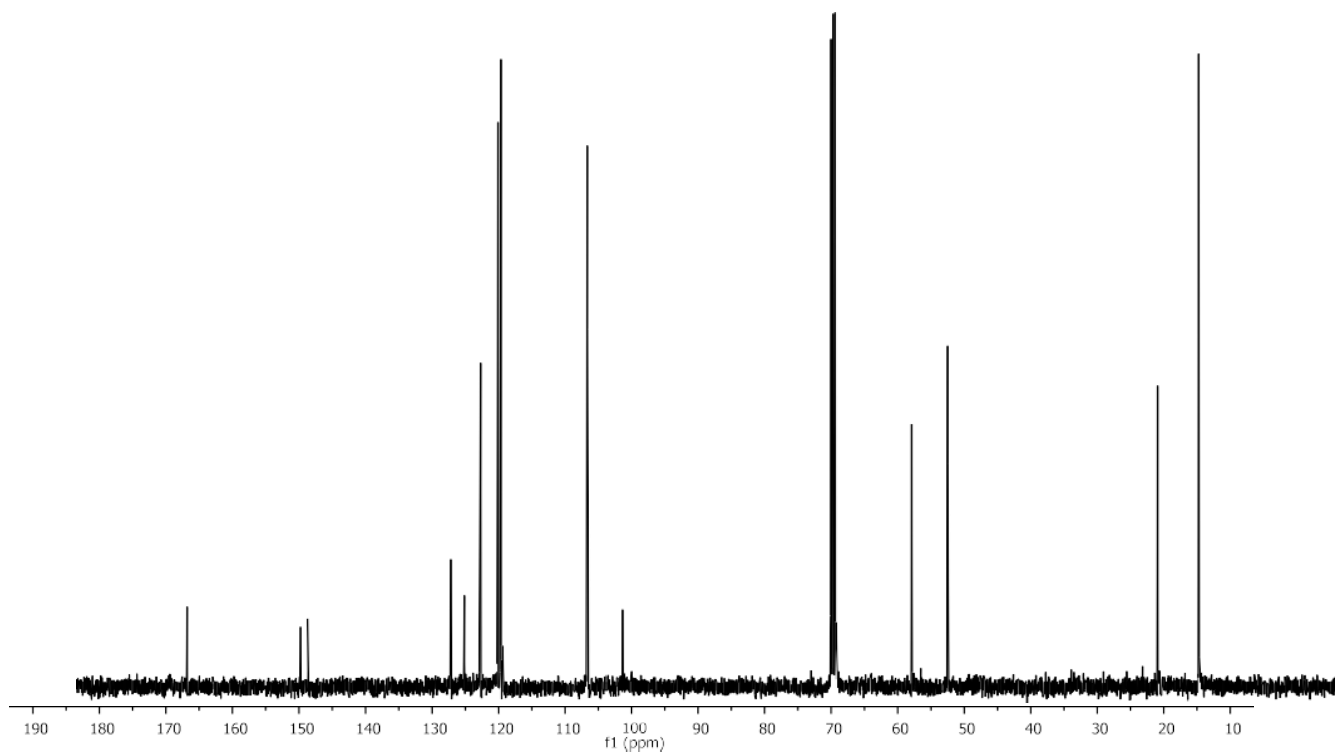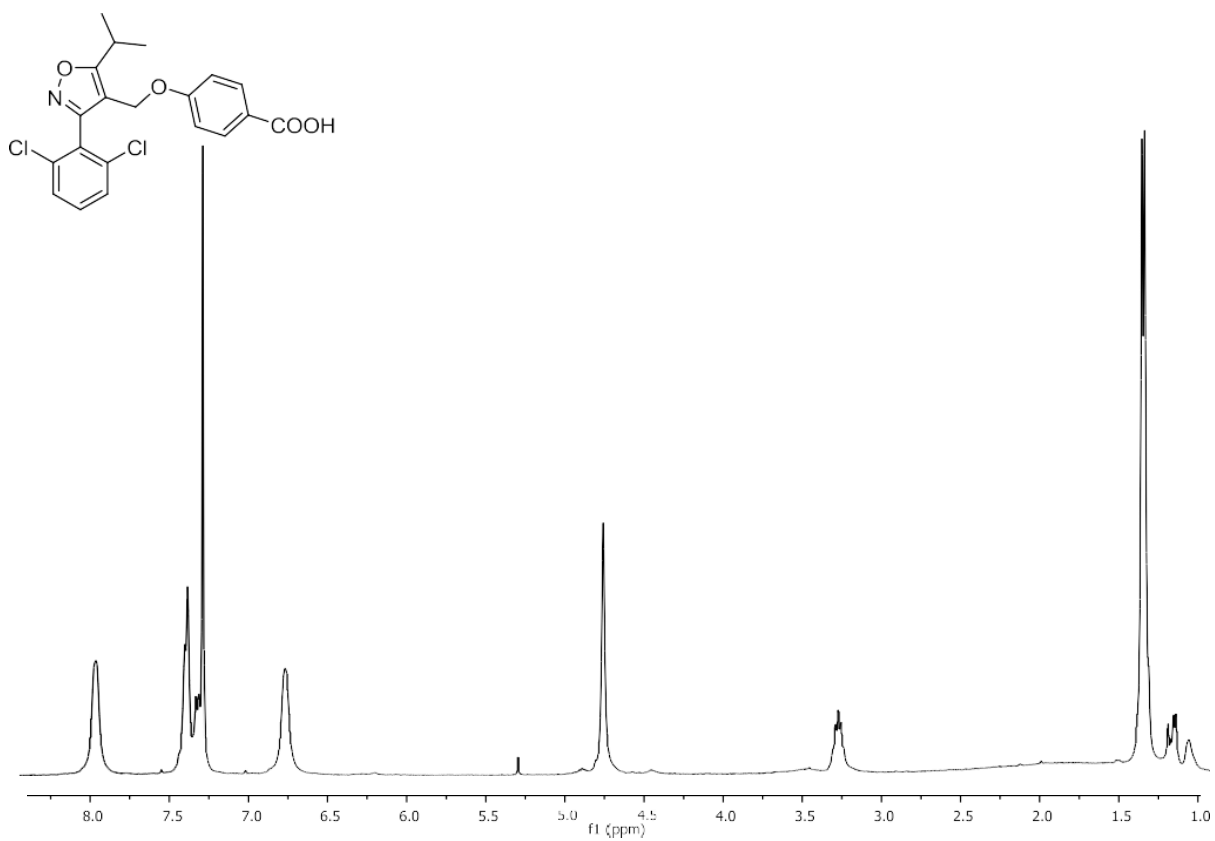
^{1}H NMR (400 MHz, CDCl$_3$) of compound 16

^{13}C NMR (100 MHz, CDCl$_3$) of compound 16
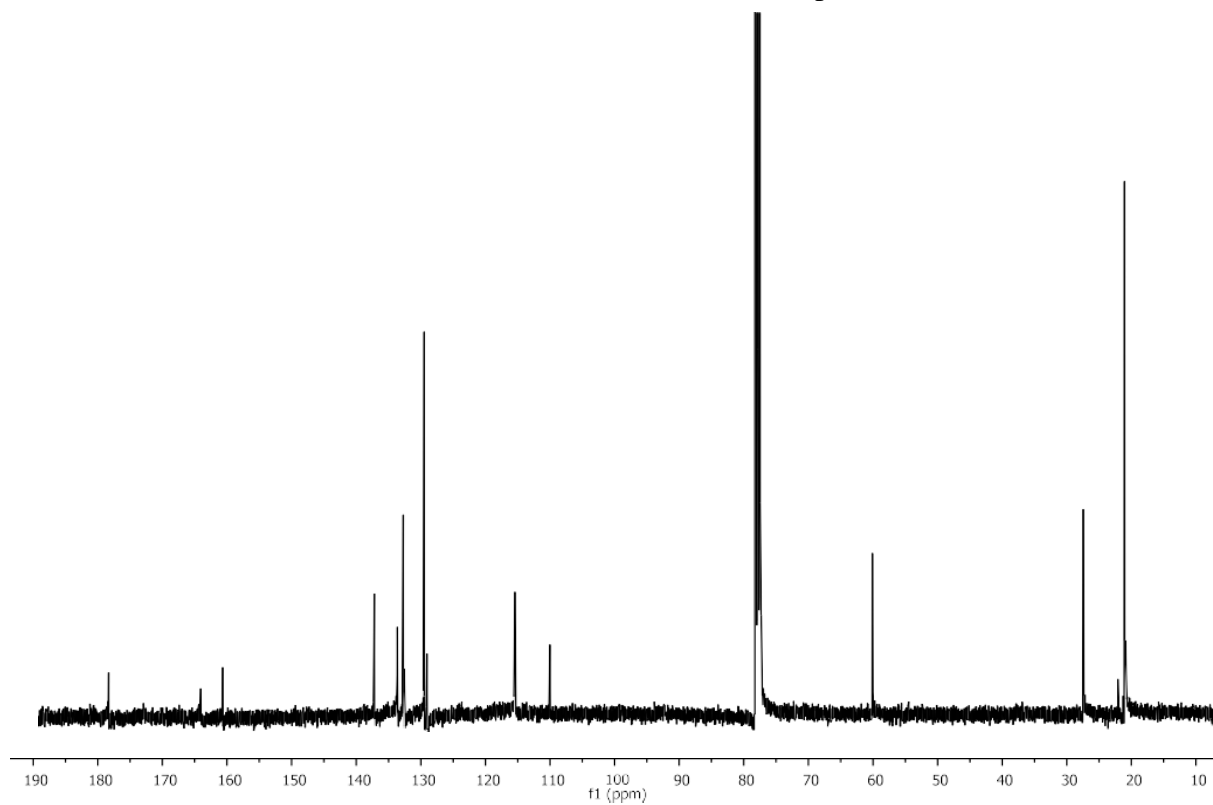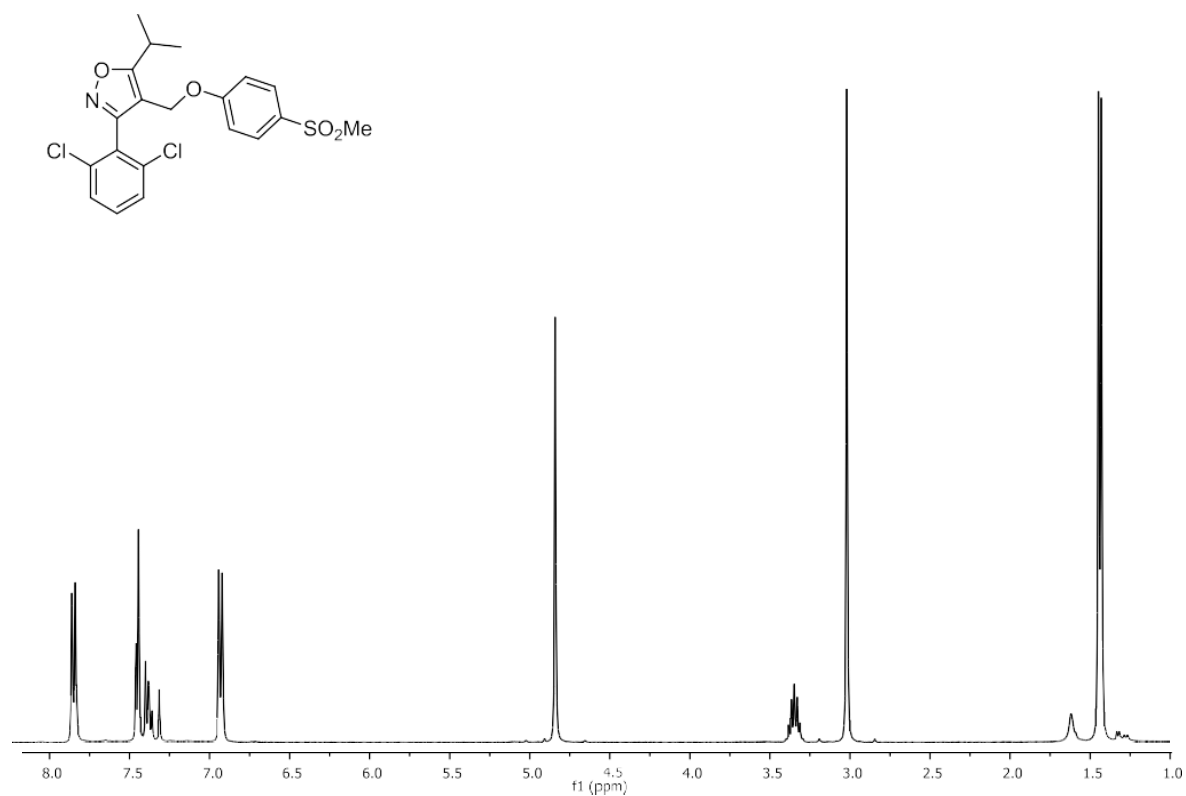
^{1}H NMR (400 MHz, CDCl$_3$) of compound **17**

^{13}C NMR (100 MHz, CDCl$_3$) of compound **17**
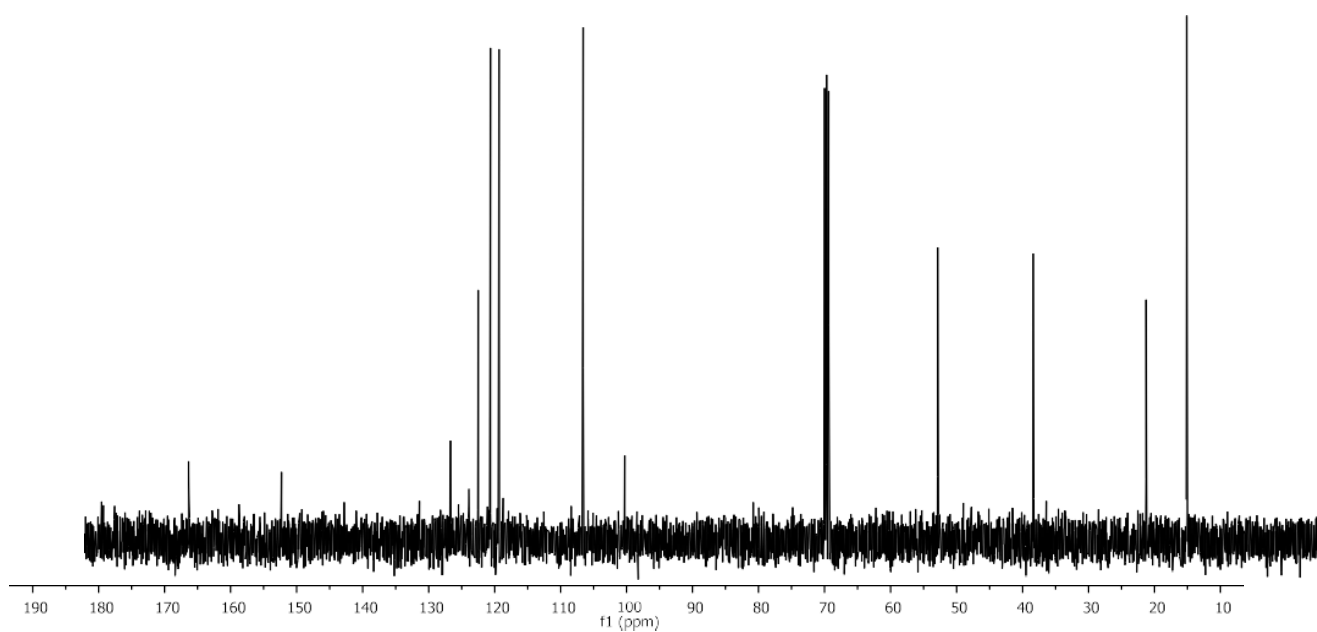
^{1}H NMR (400 MHz, CDCl$_3$) of compound **18**
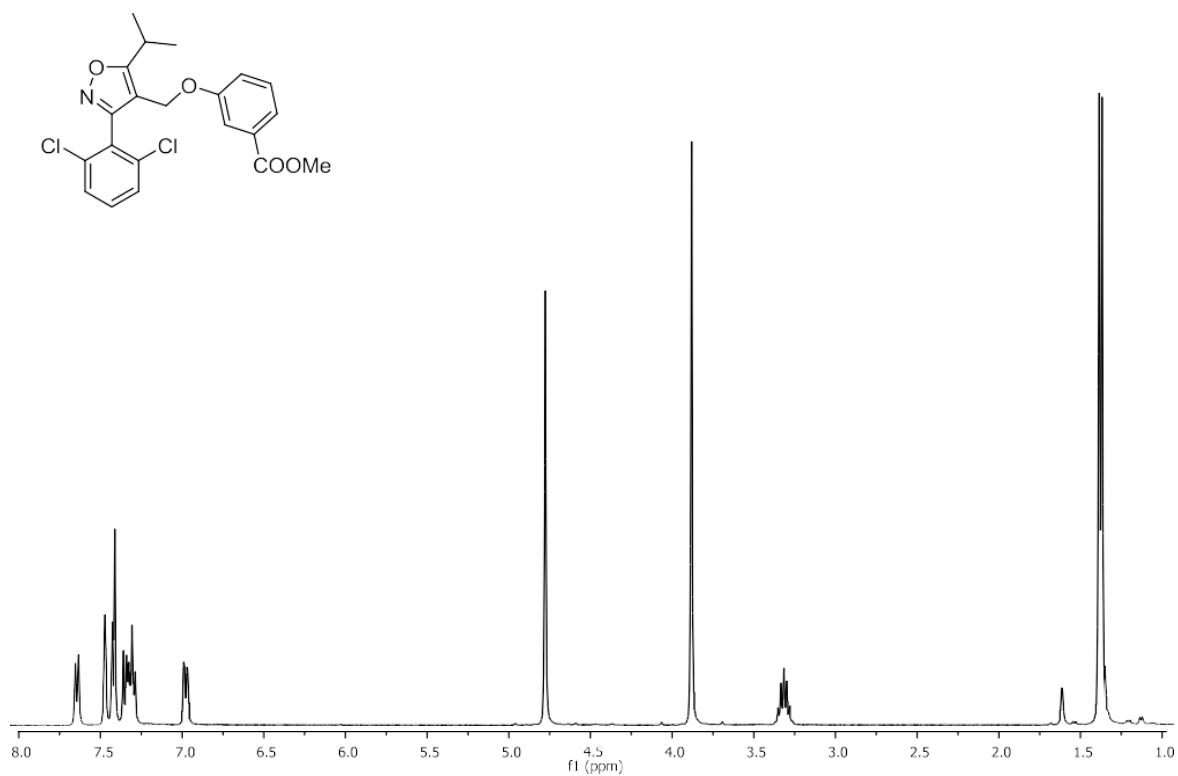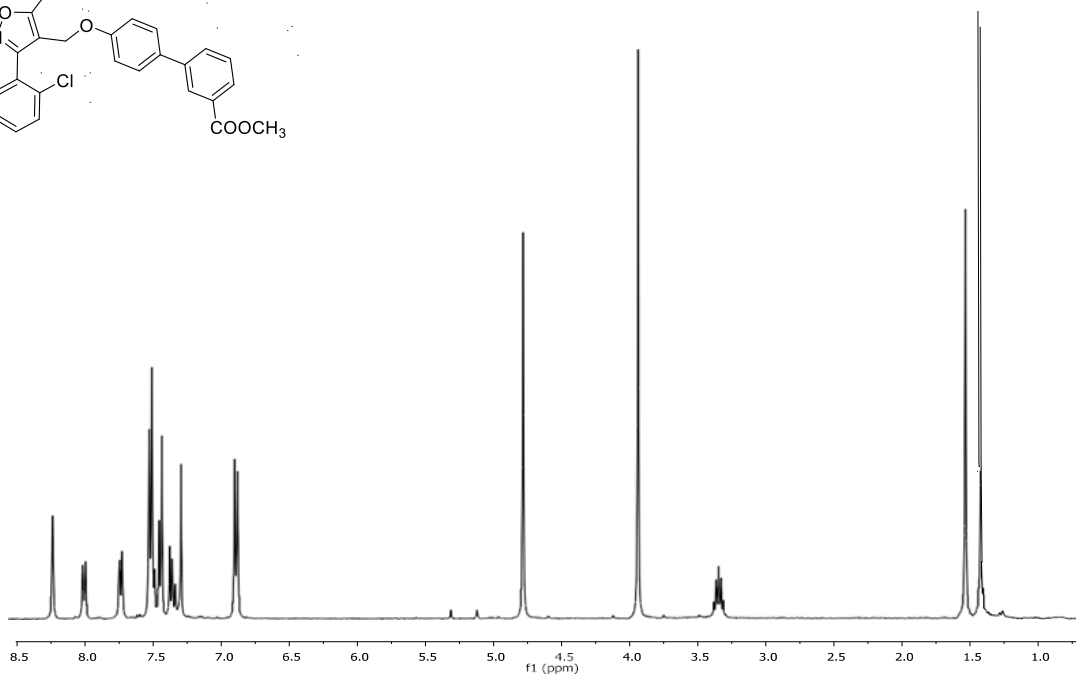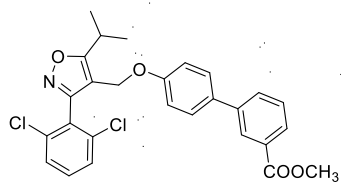

^{13}C NMR (100 MHz, CDCl$_3$) of compound **18**
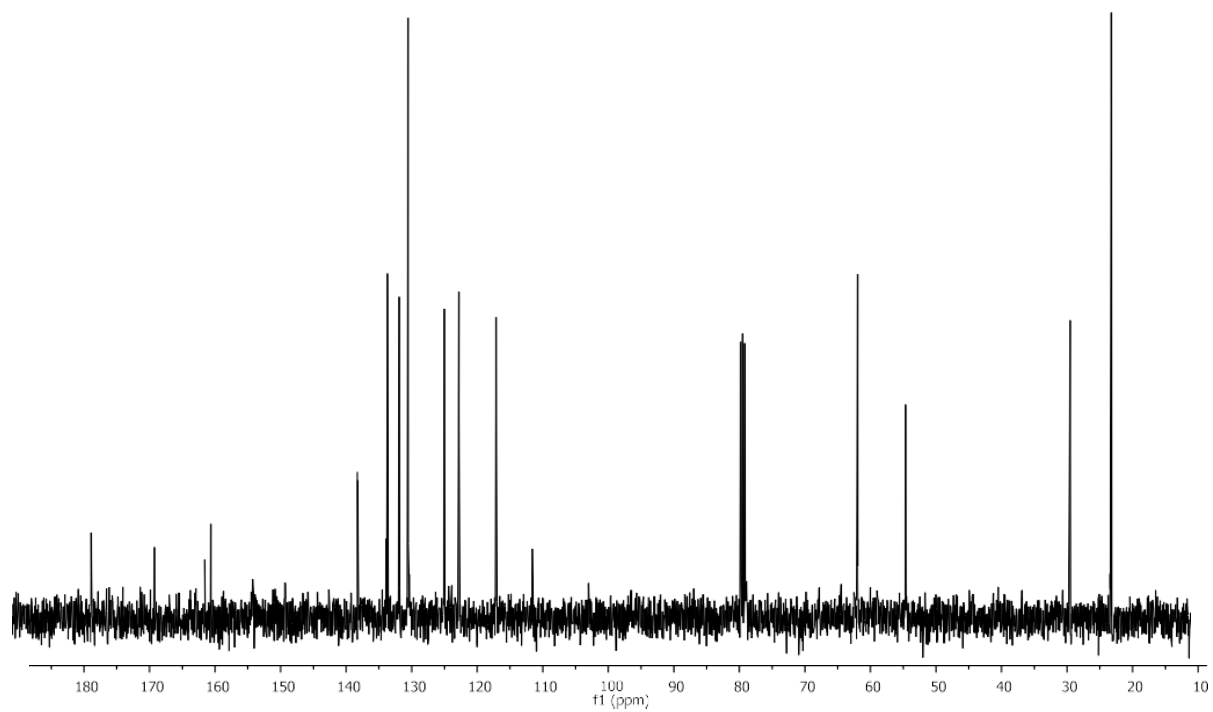
Experimental Information

¹H NMR (400 MHz, CDCl₃) of compound **19**

¹³C NMR (100 MHz, CDCl₃) of compound **19**
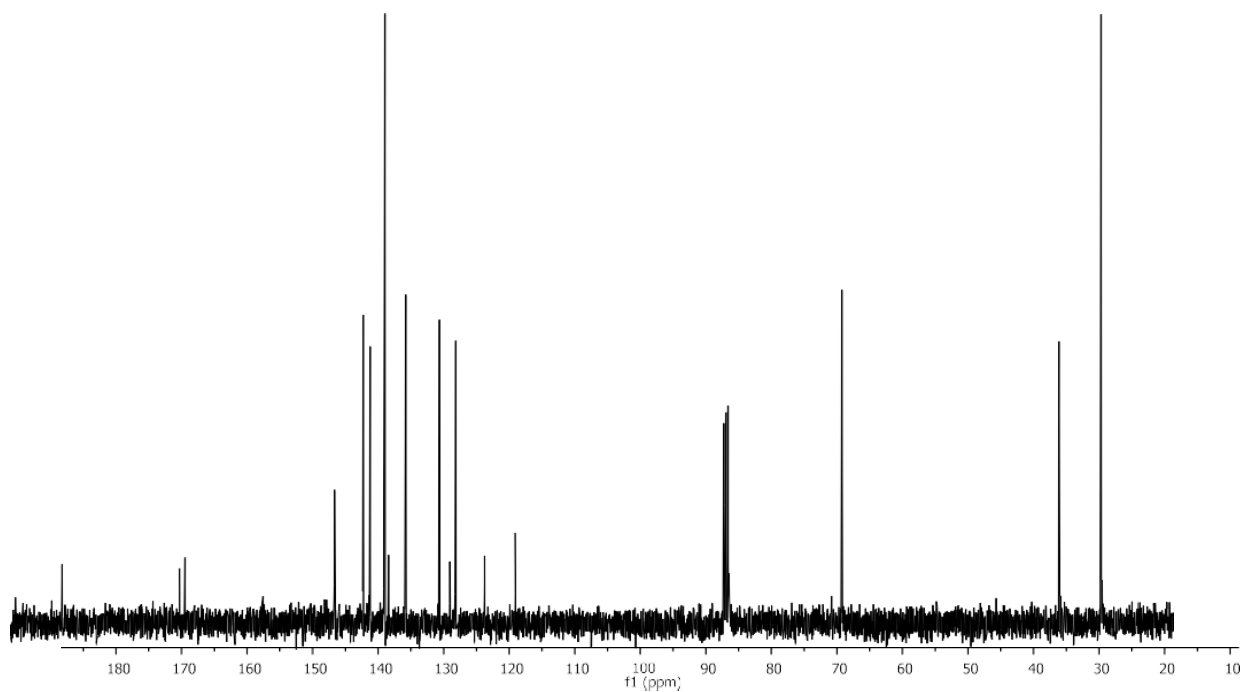
^{1}H NMR (400 MHz, CDCl$_3$) of compound **20**

^{13}C NMR (100 MHz, CDCl$_3$) of compound **20**
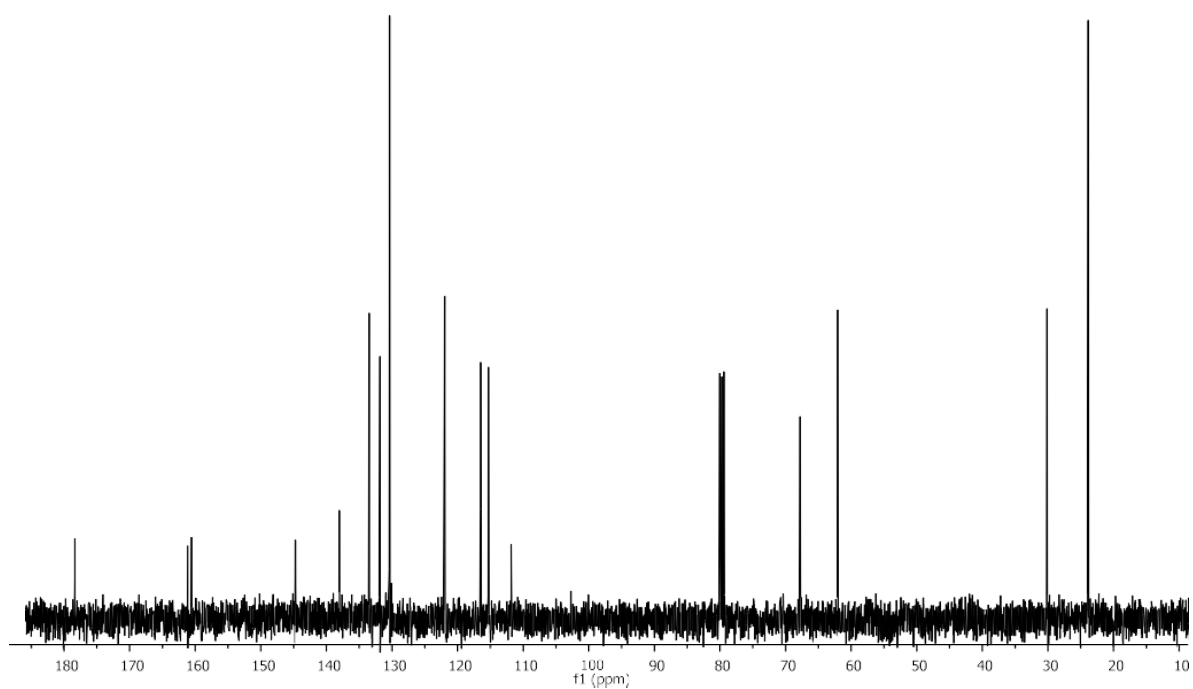
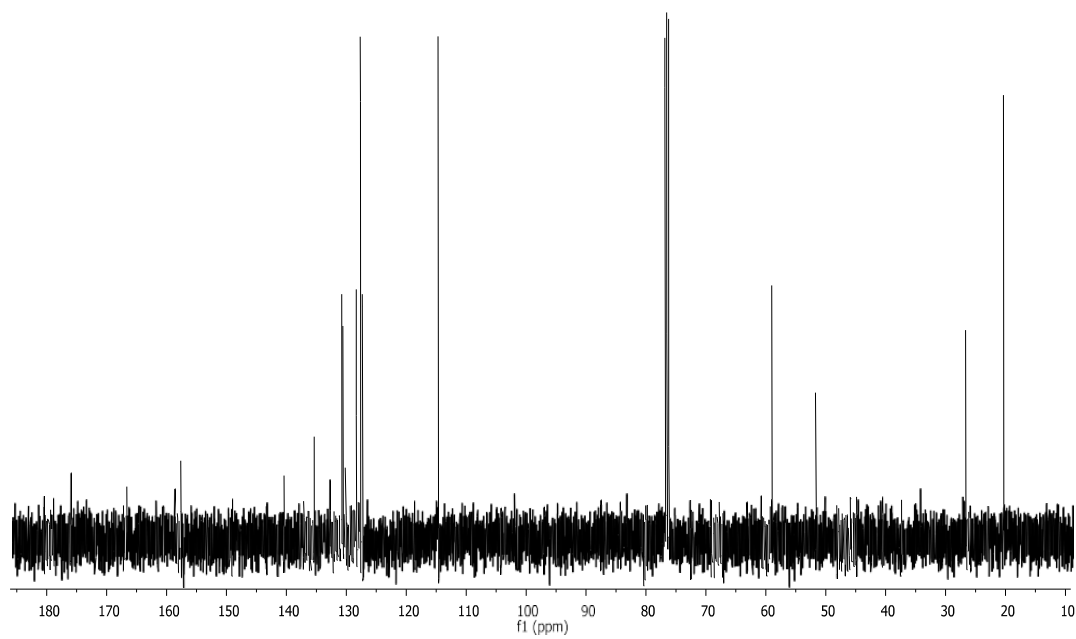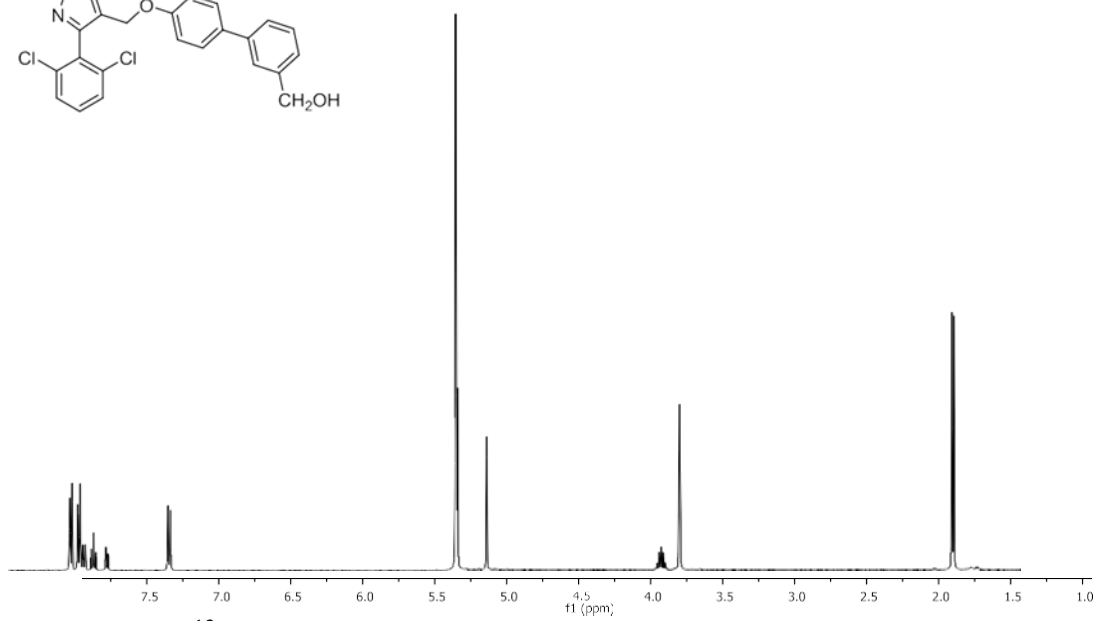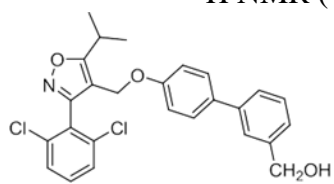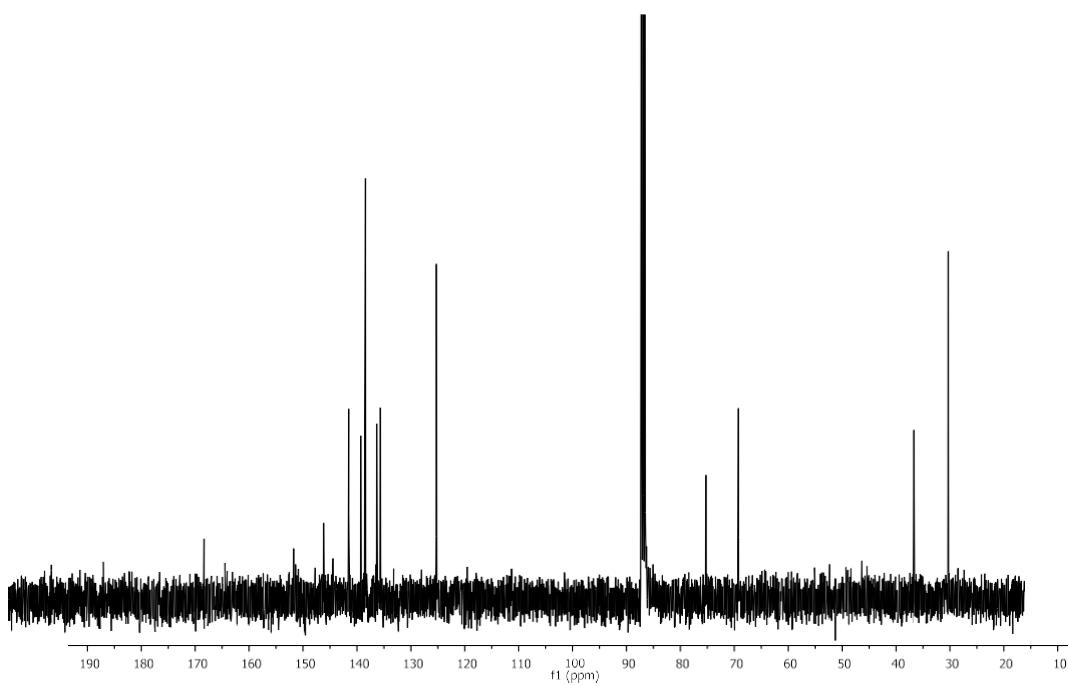Experimental Information

¹H NMR (400 MHz, CDCl₃) of compound **21**

¹³C NMR (100 MHz, CDCl₃) of compound **21**

^{1}H NMR (400 MHz, CDCl$_3$) of compound **22**

^{13}C NMR (100 MHz, CDCl$_3$) of compound **22**

^{1}H NMR (400 MHz, CD$_3$OD) of compound **23**

^{13}C NMR (100 MHz, CDCl$_3$) of compound **23**

¹H NMR (400 MHz, CDCl₃) of compound **24**

^{1}H NMR (400 MHz, CDCl$_3$) of compound **24**

^{13}C NMR (100 MHz, CDCl$_3$) of compound **24**

^{1}H NMR (400 MHz, CDCl$_3$) del composto **25**
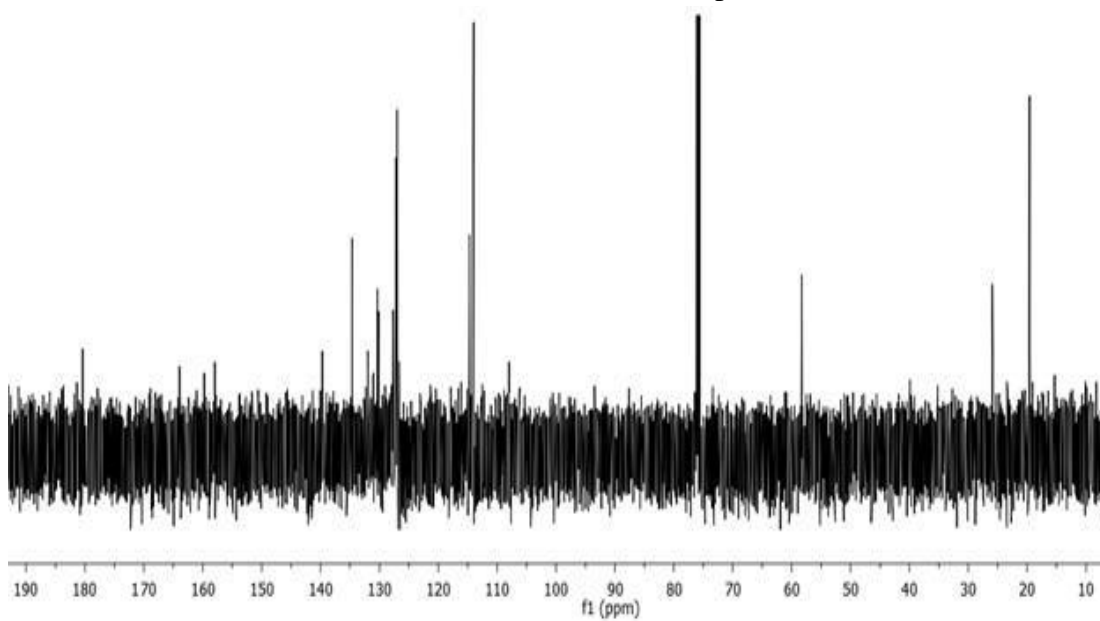
^{13}C NMR (100 MHz, CDCl$_3$) del compost **25**

¹H NMR (400 MHz, CDCl₃) del composto **26**

¹³C NMR (100 MHz, CDCl₃) del composto **26**

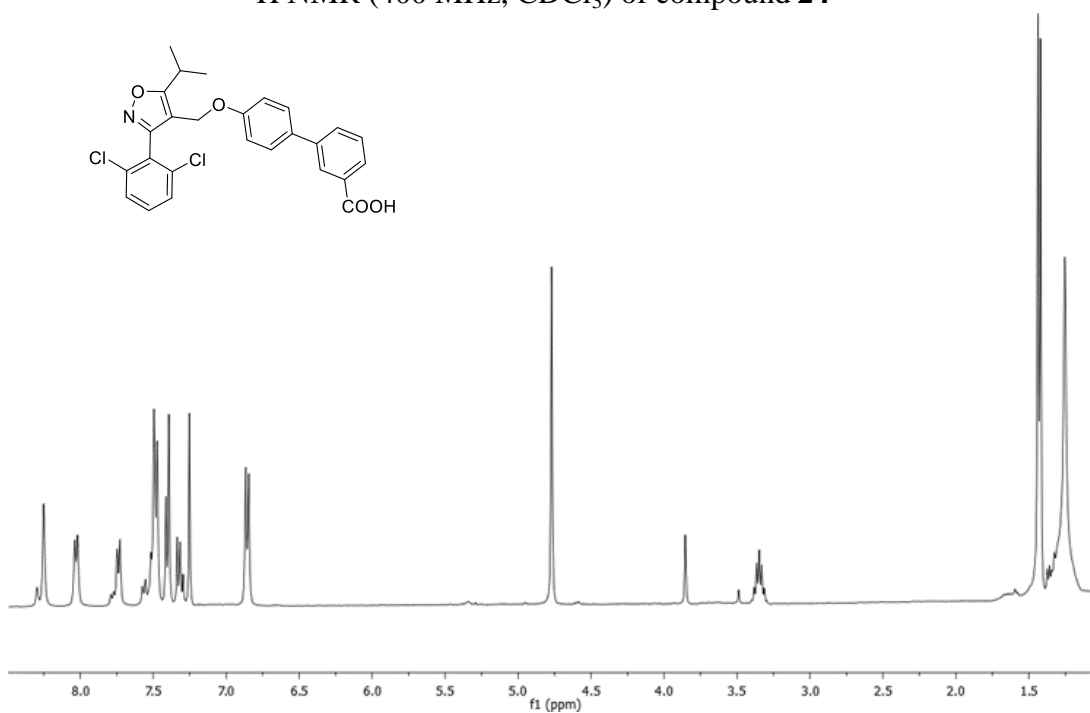¹H NMR (400 MHz, CDCl₃) of compound **27**
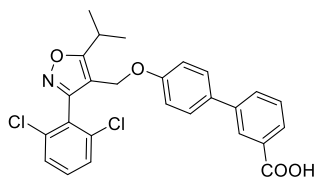

¹³C NMR (100 MHz, CDCl₃) of compound **27**

Experimental Information

^{1}H NMR (400 MHz, CDCl$_3$) del composto **28**

^{13}C NMR (100 MHz, CDCl$_3$) of compound **28**
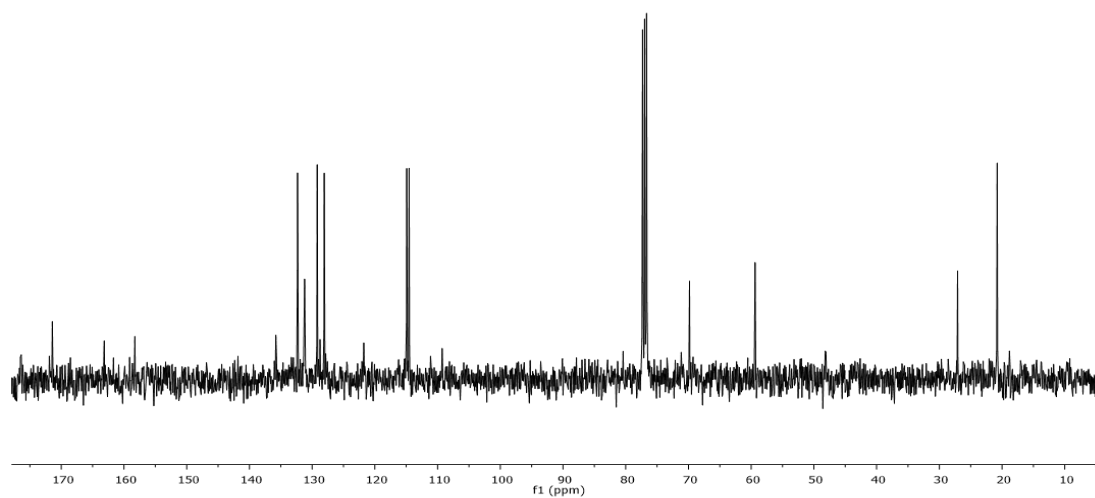
^{1}H NMR (400 MHz, CDCl$_3$) del composto **29**

^{13}C NMR (100 MHz, CDCl$_3$) of compound **29**

¹H NMR (400 MHz, CDCl₃) del composto **30**

¹³C NMR (100 MHz, CDCl₃) of compound **30**
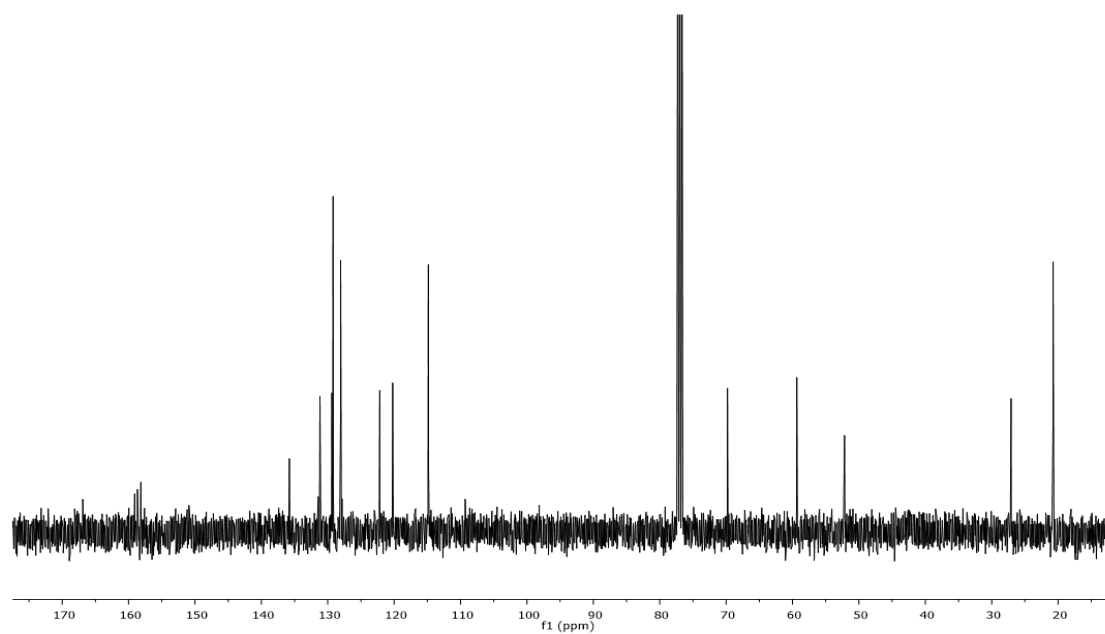
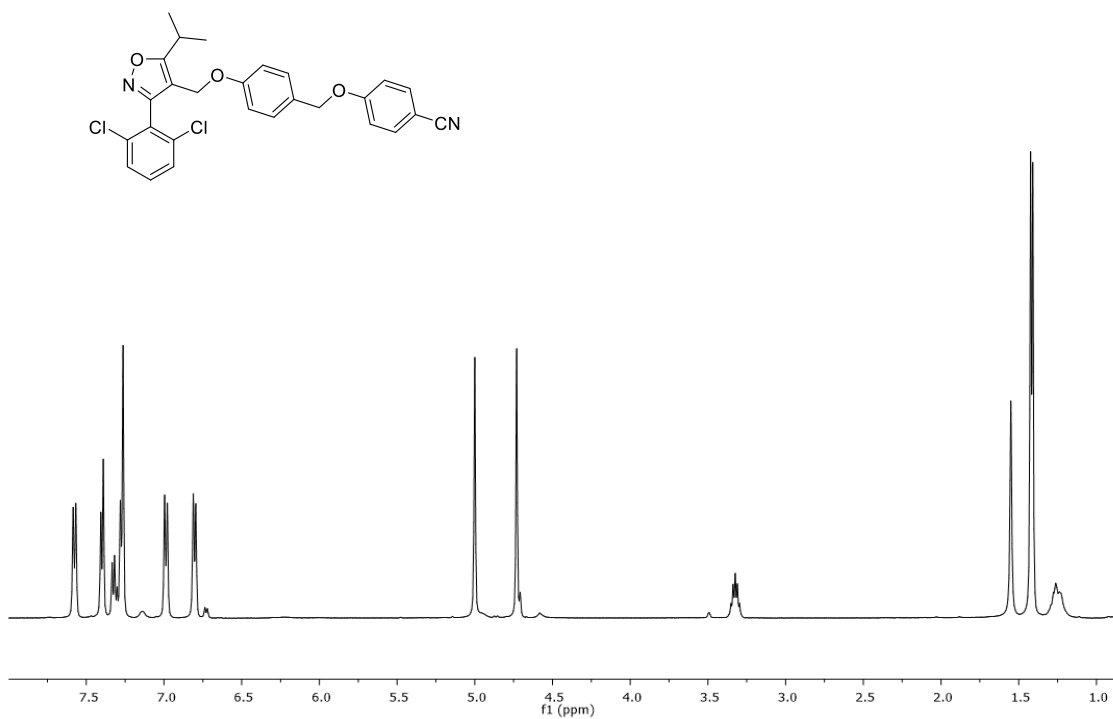## ^{1}H NMR (400 MHz, CDCl$_3$) del composto **31**
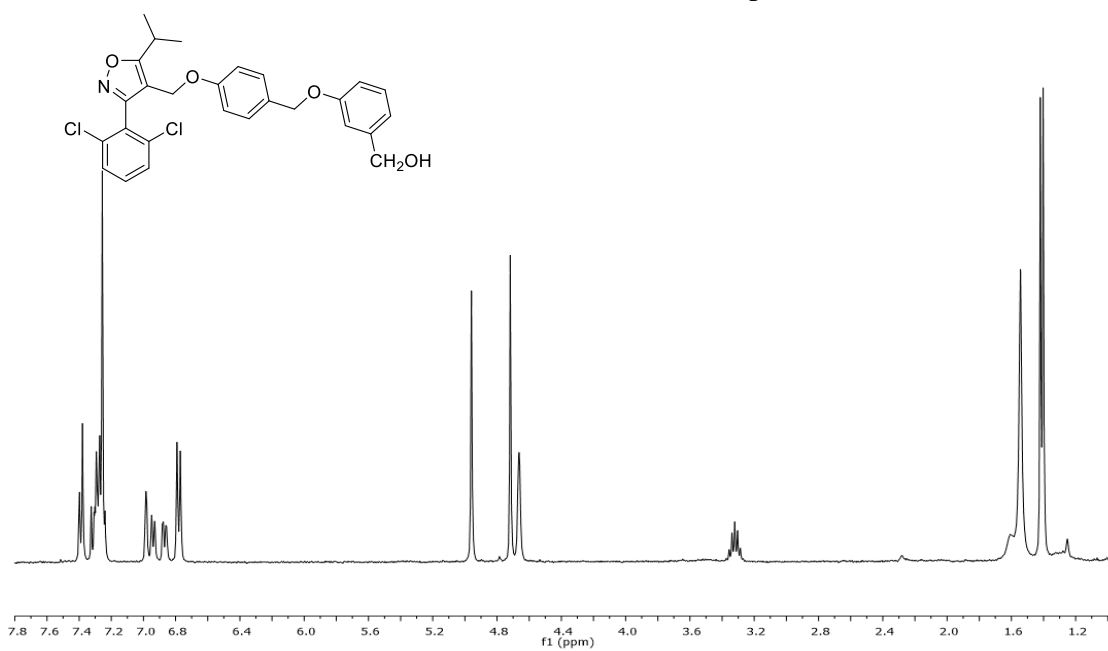
^{13}C NMR (100 MHz, CDCl$_3$) of compound **31**
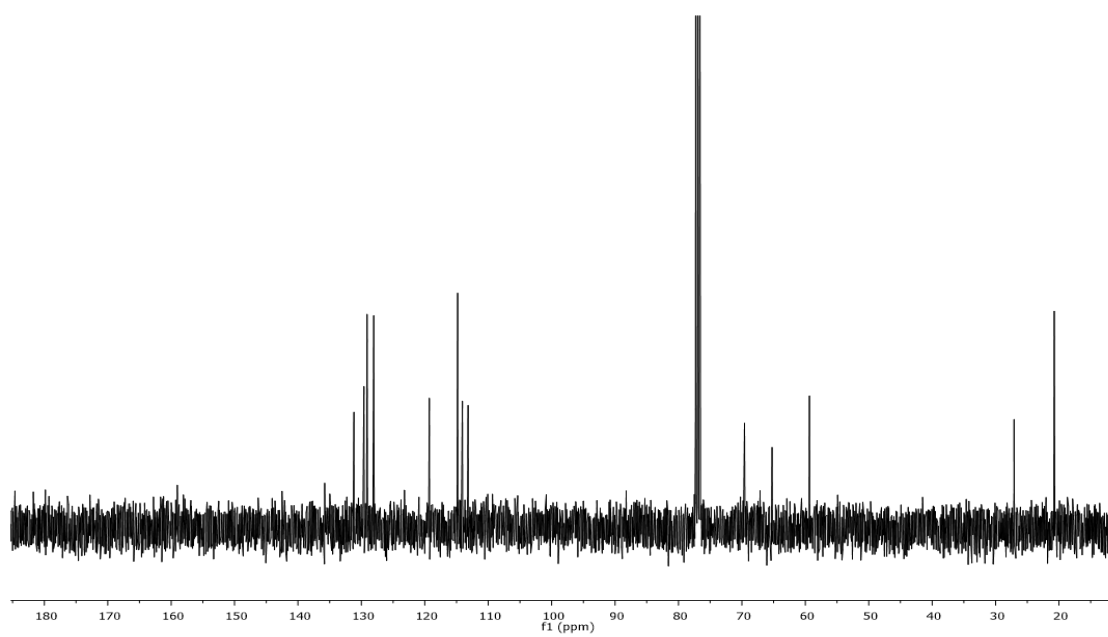
Experimental Information

^{1}H NMR (400 MHz, CDCl$_3$) del composto **32**
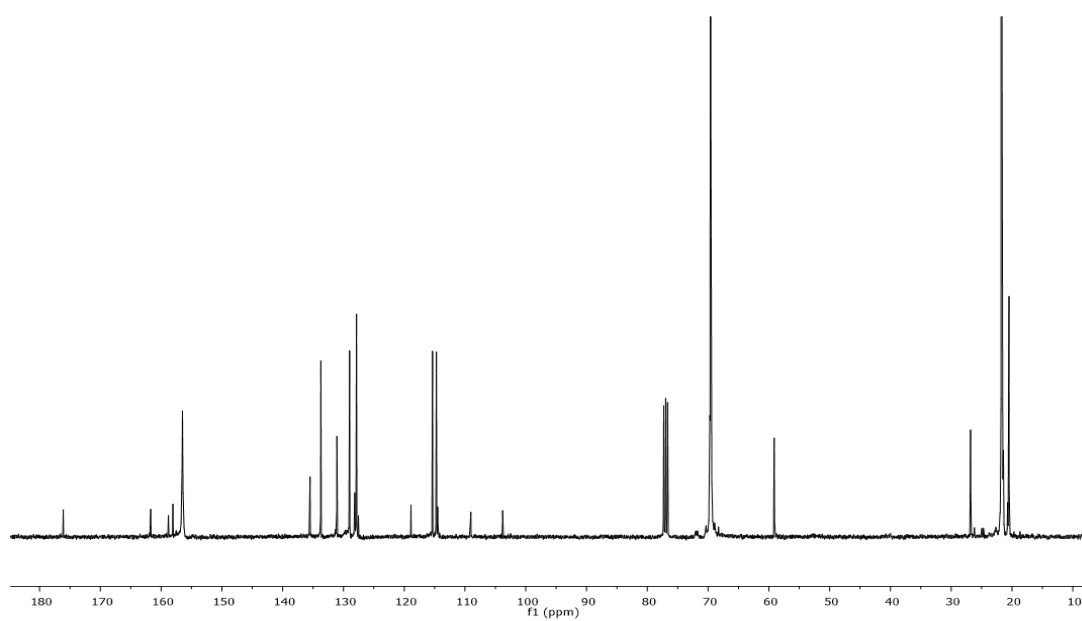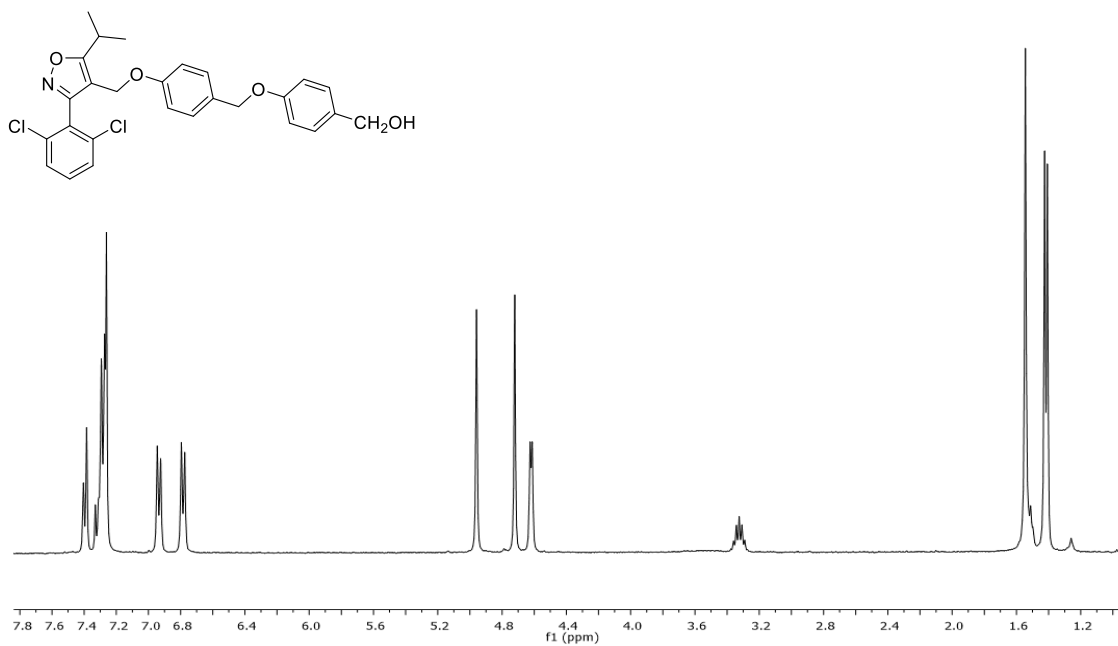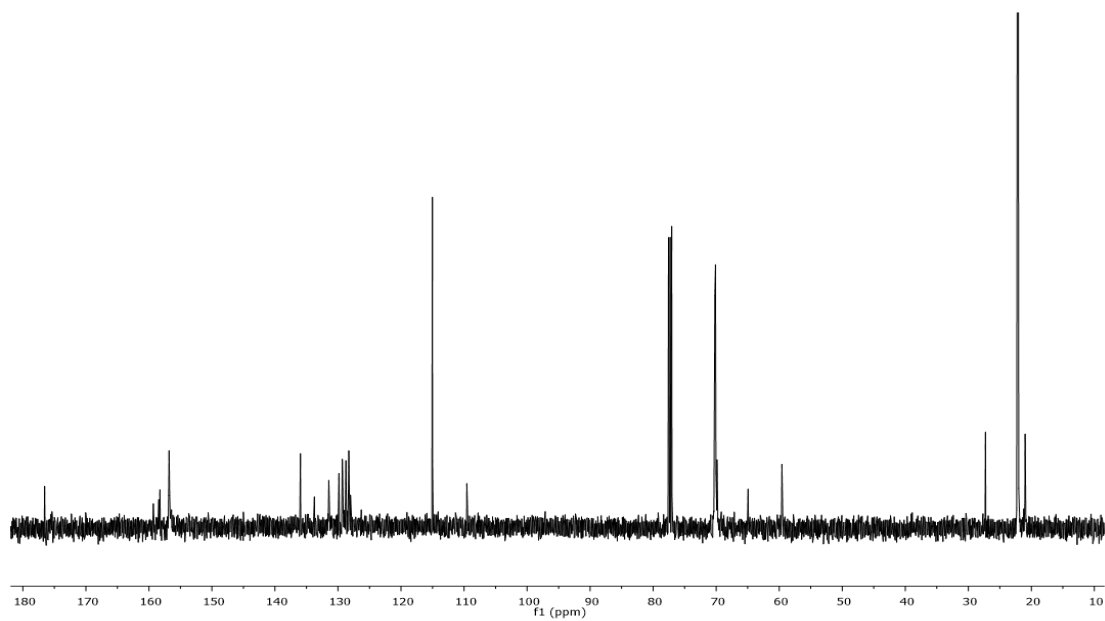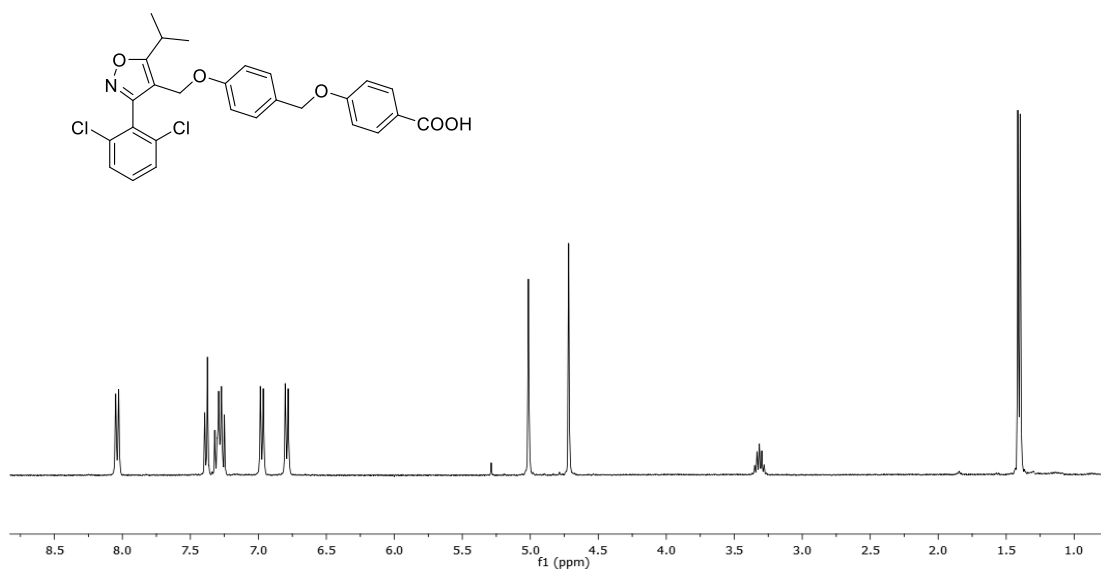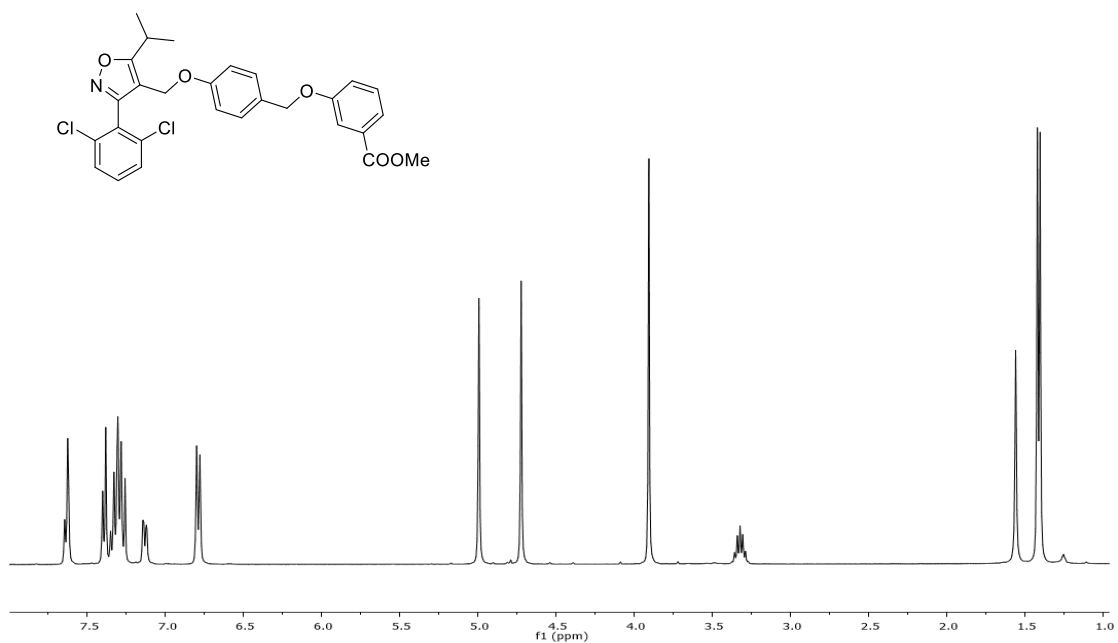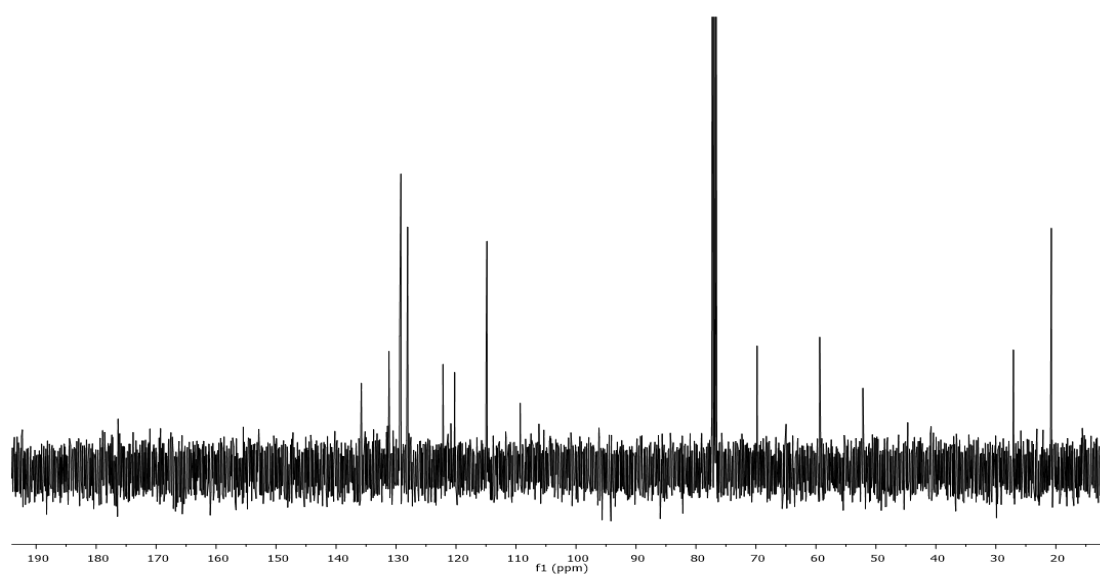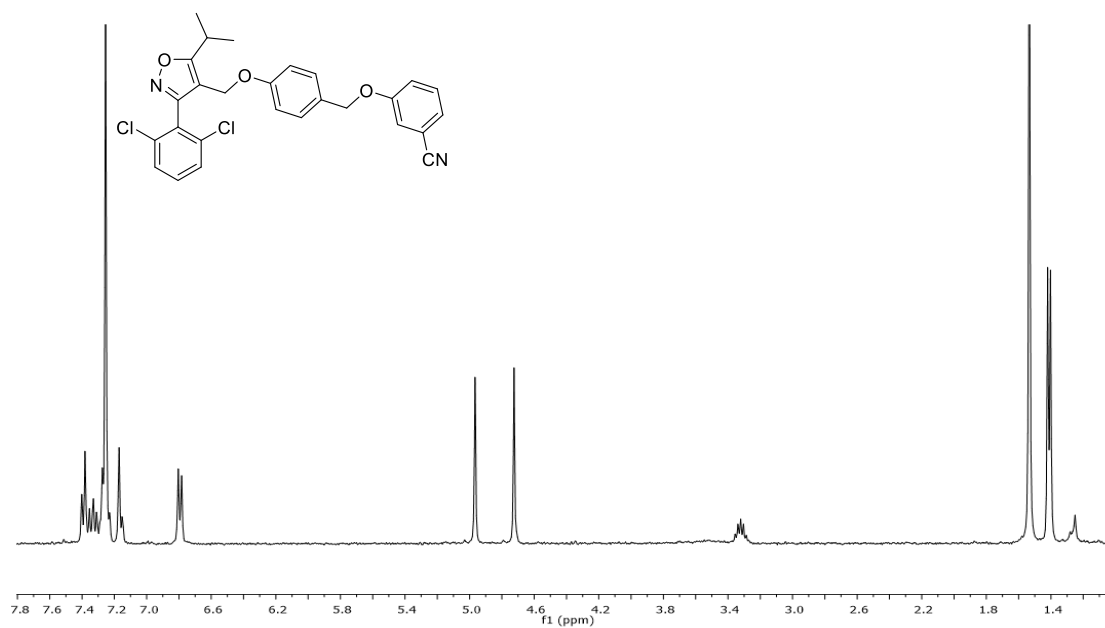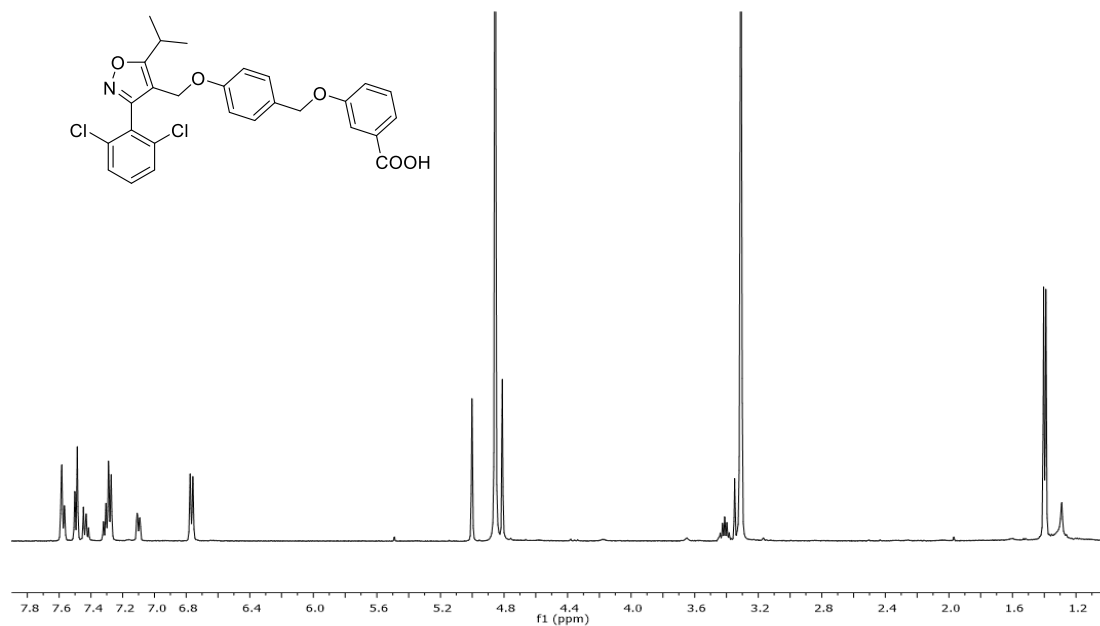

^{13}C NMR (100 MHz, CDCl$_3$) of compound **32**
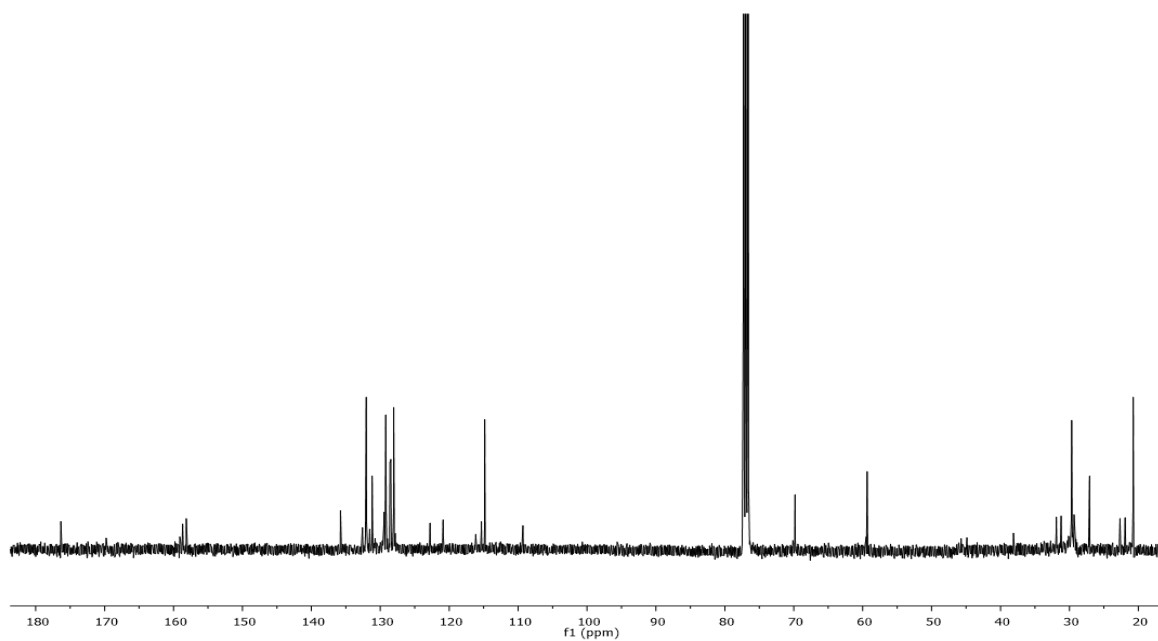
7.4. Biological Assays

In vitro coactivator recruitment assay by Alpha Screening.

Activation of FXR has been measured by Alpha Screen Technology in a Coactivator Recruitment Assay. Anti-GST-coated acceptor beads were utilized to capture the GST-fusion FXR-LBD, while the biotinylated-SRC-1 peptide was captured by the streptavidin donor beads. Upon illumination at 680 nm, chemical energy is transferred from donor to acceptor beads across the complex streptavidin-donor/SRC-1-biotin/GSTFXR-LBD/anti-GST-acceptor and a signal is produced. The assay has been performed in white, low-volume, 384-well Optiplates (Perkin Elmer) using a final volume of 25 μL containing final concentrations of 10 nM of purified GST-tagged FXR-LBD protein, 30 nM biotinylated SRC-1 peptide, 20 mg/mL anti-GST acceptor beads, and 10 mg/mL of streptavidin donor bead (PerkinElmer). The assay buffer contained 50 mM Tris (pH 7.4), 50 mM KCl and 1 mM DTT. The stimulation times with 1 μL of tested compound (each at a final concentration of 5 μM) were fixed to 30 min at room temperature. The concentration of DMSO in each well was maintained at a final concentration of 2%. After the addition of the detection mix (acceptor and donor beads), the plates were incubated in the dark for 3 h at room temperature and then were read in an Envision microplate analyzer (Perkin Elmer).

Cell culture.

HepG2, an immortalized human epatocarcinoma cell line, was cultured and maintained at 37 °C and 5% CO_2 in E-MEM additioned with 10% FBS, 1% glutamine and 1% penicillin/streptomycin. HEK-293T were cultured and maintained at 37 °C and 5% CO_2 in D-MEM additioned with 10% FBS, 1% glutamine and 1% penicillin/streptomycin.

Luciferase reporter gene assay and Dose-response curves.

HepG2 cells were transfected with 200 ng of the reporter vector p(hsp27)-TK-LUC containing the FXR response element IR1 cloned from the promoter of heat shock protein 27 (hsp27), 100 ng of pSG5-FXR, 100 ng of pSG5-RXR, and 100 of pGL4.70 (Promega), a vector encoding the human Renilla gene to investigate the FXR activation. At 24 h post transfection, cells were stimulated with compounds **12**-**32** (10 μM) and CDCA, 6-ECDCA and GW4064 were used as positive controls. To evaluate the EC_{50} of compounds, dose-response curves were performed in HepG2 cells transfected as described and treated with increasing concentrations of compounds **12**-**32** (0.1, 0.5, 1, 2.5, 5, 7.5, 10, 12.5, 25 and 50 μM).

To evaluate the specificity of compounds **24**, **28** and **32** versus LXRα and LXRβ mediated transactivation, HepG2 cells were transfected with 200 ng of the reporter vector p(UAS)5XTKLuc, 100 ng of a vector containing the ligand binding domain of LXRα or LXRβ cloned upstream of the GAL4-DNA binding domain (i.e. pSG5-LXRαLBD-GAL4DBD or pSG5-LXRβLBD-GAL4DBD) and 100 of pGL4.70 (Promega), a vector encoding the human Renilla gene.

To evaluate the specificity of compounds **24**, **28** and **32** versus PPARγ, HepG2 cells were transfected with 200 ng reporter vector p(UAS)5XTKLuc, 100 ng pGL4.70 and with a vector containing the ligand binding domain of nuclear receptors PPARγ cloned upstream of the GAL4-DNA binding domain (pSG5-PPARγLBD-GAL4DBD).

To evaluate the specificity of compounds **12**- **32** versus GPBAR1 activation, HEK-293T cells were transiently transfected with Fugene HD reagent (Promega) using the following vectors: pCMVSPORT6-human GPBAR1, pGL4.29 (Promega), a reporter vector containing a cAMP response element (CRE) cloned upstream to the luciferase reporter gene luc2P and pGL4.70. At 24 h post transfection, cells were stimulated with specific

receptor agonists GW3965 (10 µM), Rosiglitazon (500 nM) and TLCA (10 µM) respectively, or with compounds **24**, **28** and **32** (10 µM).

At 18 h post stimulations, cellular lysate was tested for luciferase and Renilla activities using the Dual-Luciferase Reporter assay system (E1980, Promega). Luminescence was measured using Glomax 20/20 luminometer (Promega). Luciferase activities were normalized with Renilla activities.

RNA isolation and RT-PCR.

HepG2 cells were covered at the density of 1x106 cells/flask in T25 flask. After an overnight incubation, cells were starved and then stimulated for 18 hours with 10 µM GW3965 or compounds **24**, **28** and **32** (0.1, 1 and 5 µM). Total RNA was isolated from HepG2 cells or liver tissue using the TRIzol reagent according to the manufacturer's specifications (Invitrogen). One microgram of purified RNA was treated with DNase-I and reverse transcribed with QuantiTect Reverse Transcription Kit (Qiagen). For Real Time PCR, 10 ng template was dissolved in 25 µL containing 200 nmol/L of each primer and 12.5 µL of 2× SYBR FAST Universal ready mix (Invitrogen). All reactions were performed in triplicate, and the thermal cycling conditions were as follows: 2 min at 95 °C, followed by 40 cycles of 95 °C for 20 s and 60 °C for 30 s in StepOnePlus (Applied Biosystems). The relative mRNA expression was calculated in accord to the Ct method. Forward and reverse primer sequences were the following:

human GAPDH: gaaggtgaaggtcggagt and catgggtggaatcatattggaa;

human SHP: gctgtctggagtccttctgg and ccaatgatagggcgaaagaag;

mouse GAPDH, ctgagtatgtcgtggagtctac and gttggtggtgcaggatgcattg;

mouse Shp acgatcctcttcaacccaga and agggctccaagacttcacac;

mouse Fxr: agcttccagggtttcagaca and cttccaacaggtctgcatga;

mouse Bsep: gatgcttcccaagttcaagg and taaagaggaaggcgatgagc;

mouse Ugt1a1: tgggatccatggtctcagag and tggtctagttccggtgtagc;

mouse Ugt2b1: gagaacatggtgtggtggtg and accttctgtggaatctgggc;

mouse Sult1a1: ccccaggtcttgaaactctg and ggcaacgtagatcaccttga

Animals and Protocols.

C57BL/6N male mice were from The Jackson's Laboratory. Mice were housed under controlled temperatures (22°C) and photoperiods (12:12-hour light/dark cycle), allowed unrestricted access to standard mouse chow and tap water and allowed to acclimate to these conditions for at least 5 days before inclusion in an experiment. The experimental protocol was approved by the Animal Care and Use Committee of the University of Perugia and by the Italian Minister of Health and Istituto Superiore di Sanità (Italy) and were in agreement with the European guidelines for use of experimental animals (permission n. 214/2017-PR). The general health of the animals was monitored daily by the Veterinarian in the animal facility. To evaluate the in vivo intestinal absorption and the successful transport to the liver, mice were administered with 10 mg/kg of compound **28** dissolved in methylcellulose, daily by gavage (o.s.) or i.p. for 3 days. At the end of the treatment the animals were sacrificed and blood and liver collected for further analysis. For the induction of hepatitis, mice received acetaminophen (APAP) at the concentration of 500 mg/kg by oral administration (o.s.). In APAP model of hepatitis compound **28** (30 mg/kg) was administered per o.s. 45 min after dosing APAP starts. At the end of the experiment surviving mice were weighed and sacrificed, blood samples collected by cardiac puncture, and the liver was excised and weighed.

Histological analysis.

For histological examination, portions of the right and left liver lobes were fixed in 10% formalin, embedded in paraffin, sectioned and stained with Hematoxylin/Eosin (H&E).

Hepatic GSH, SOD and MDA determinations.

Frozen liver tissues were thawed rinsed with PBS. The tissues were then homogenized in ice-cold MES buffer for GSH determination, in ice-cold PBS for SOD determination and in ice-cold RIPA buffer containing protease inhibitors for MDA determination. The homogenate was centrifuged at 1600xg, 4°C for 10 min and the supernatants were assayed for GSH, superoxide dismutase (SOD) and malonildialdehyde (MDA) levels using the commercially available assay kits according the manufacturer's instructions (Cayman Chemical Glutathione Assay Kit #703002, Superoxide Dismutase Assay Kit #706002, TBARS Assay Kit #10009055).

LC-MS/MS analysis of APAP and its metabolites.

Plasma samples of 25 μL were mixed with internal standard (IS= d4-APAP at 4 ng/μL), and diluted with 400 μL of methanol. Samples were then incubated for 20 min on ice and centrifuged for 10 min at 11000 rpm, and the supernatants were evaporated to dryness and dissolved in 100 μL of water and transferred for LC/MS-MS analysis. RP-S17 UPLC analysis of d4-APAP, APAP, APAP-glucuronide (APAP-gluc), APAP-sulfate (APAP-sulf) were performed by a Luna Polar PS C18, 1.6 μm, 100 °A from Phenomenex (50X2.10 mm) at 40 °C at a flow rate 0.4 mL/min. Mobile phase A was water with 0.2% formic acid, while mobile phase B was methanol with 0.1% formic acid. The best chromatographic results were achieved using the following gradient: 2% B from 0 to 1 min, 2% to 80% B from 1 to 7.0 min, 80% to 95% B from 7.0 to 7.1 min, held at 95% B

for 3 min and then to 2% B. The retention times of d4-APAP and APAP, APAP-gluc and APAP-sulf were at 2.11 min for APAP and its deuterated form, 1.56 min for APAP-gluc and 3.09 min for APAP-sulf.

Q-TRAP 6500 LC-MS/MS System from AB Sciex equipped with Shimadzu LC-20A LC and AutoSampler system and with electrospray ionization (ESI) source has been used for LC-MS/MS analyses in MRM (multiple reaction monitoring) mode. In positive ionization mode, d4-APAP and APAP were protonated, whereas APAP-gluc and APAP-sulf were deprotonated in negative ionization mode. The MRM transitions used for d4-APAP, APAP, APAP-gluc and APAP-sulf were *m/z* 156.1/114.1, 152.1/110.1, *m/z* 326.0/149.8 and *m/z* 230.0/150.0, respectively. For positive ion, the following parameters were set: DP 70 eV, EP 10 psi, CE 20 eV, CXP 13 V, CUR 20 psi, CAD Medium, IS 5500 V, TEM 350 °C, GS1 and GS2 50 psi. For negative ions, the following parameters were set: DP -65 eV, EP -10 psi, CE -30 eV, CXP -13 V, CUR 20 psi, CAD Medium, IS -4500 V, TEM 350 °C, GS1 and GS2 50 psi. Each standard curve was plotted by the peak area ratio of each analyte to d4-APAP against the corresponding concentration of APAP, APAP-gluc or APAP-sulf standard.

7.5. Physiochemical properties and pharmacokinetic characterization

LC-MS/MS ADME Methods.

Chromatography was performed using an Alliance pump system coupled to a Q-ToF Premiere (Waters Co.). The mixture was separated on a Luna 5 μm C8(2) 100 °A 150X2 mm from Phenomenex. The mobile phase consisted of 0.2% formic acid (FA) in water as solvent A and 0.2% FA in acetonitrile as solvent B at a flow rate of 200 μL/min. The gradient was as follows: 0-2 min (75% A and 25% B), 2-20 min (5% A and 95% B), 20-30 min (75% A and 25% B). The detection of analytes was achieved by electrospray ionization (ESI) in the positive mode with the appropriate MS/MS transitions, if necessary.

Solubility Measurements.

Ten microliters of a 10 mM solution in DMSO of the compound was diluted either in 490 μL of PBS pH 7.4 or in organic solvent MeOH (in triplicate). The tubes were gently shaken 24 h at room temperature, then centrifuged for 5 min at 4000 rpm. Ten microliters of sample was diluted in 490 μL of MeOH. The solubility is determined by the ratio of mass signal area PBS/organic solvent.

Microsomal Stability.

Male mouse (CD-1) liver microsomes (Sigma-Aldrich) were used. All incubations were performed in duplicate in a shaking water bath at 37 °C. The incubation mixtures contained 1 μM compound with 1% DMSO used as a vehicle, mouse liver microsomes (0.3 mg of microsomal protein per mL), 5 mM $MgCl_2$, 1 mM NADP, 5 mM glucose 6-phosphate, 0.4 U·mL−1 S19 glucose 6-phosphate dehydrogenase, and 50 mM potassium phosphate buffer (pH 7.4) in a final volume of 0.5 mL. Aliquots were removed at 0, 5,

10, 20, 30, and 40 min after microsome addition and the reaction was stopped by adding 200 μL of ice-cold acetonitrile. After 2 h, the samples were centrifuged for 10 min at 10000 rpm, and the supernatants were transferred in matrix tubes for LC-MS/MS analysis. Propranolol, known as a high hepatic clearance drug in rodents, was used as a quality-control compound for the microsomal incubations. The slope of the linear regression of the curve obtained reporting the natural logarithm of compound area versus incubation time (-k) was used in the conversion to in vitro $t_{1/2}$ values by $t_{1/2}=-\ln(2)/k$. In vitro intrinsic clearance (Cl_{int} expressed as μL/min/mg) was calculated according to the following formula: Cl_{int} = volume of reaction (uL)/ $t_{1/2}$(min)/protein of liver microsomes (mg). The percentage of unmodified compound has been calculated assuming the area of the compound peak at time 0 min as 100%.

7.6. Computational studies

Molecular Docking.

The crystal structure of FXR in complex with GW4064 and the steroid receptor coactivator peptide SRC-1 (PDB code: 3DCT) was selected for docking calculations. Prior to docking, the receptor was prepared using the "Protein Preparation Wizard" panel of the Schrödinger molecular modeling package.2 First, bond orders were assigned and all the hydrogen atoms were added. A prediction of ionization and tautomeric states of the amino acids side chains was then carried out using Epik.3 An optimization of the hydrogen-bonding network was then performed and the positions of the hydrogen atoms were optimized. Finally, all the water molecules were deleted.

The ligands tridimensional structures were generated with Maestro4 and prepared for docking using Ligprep.5 Protonation states were predicted using Epik.

Docking studies were carried out with the grid-based program Glide 7.2.6 For the grid generation, a box of 23 Å × 23 Å × 23 Å, surrounding the ligand binding cavity site, was considered. The standard precision (SP) mode of the GlideScore function was used to score and rank the predicted binding poses. The OPLS3 force field7 was employed for docking. All of the pictures were rendered with PyMOL.

CHAPTER 8

EXPERIMENTAL PROCEDURE: REV5901 Derivatives

8.1. General information

High-resolution ESI-MS spectra were carried out with a LTQ-XL equipped with an Ultimate 3000 HPLC system (Thermo Fisher scientific) mass spectrometer. NMR spectra were obtained on Bruker 400 spectrometer (^{1}H at 400, ^{13}C at 100 MHz), recorded in CDCl$_3$ (δ_H =7.26 and δ_C =77.0 ppm) and CD$_3$OD (δ_H=3.30 and δ_C=49.0 ppm). *J* are in hertz and chemical shifts (δ) are reported in ppm and referred to CHCl$_3$ and CHD$_2$OD as internal standards. HPLC was carried out using a Waters Model 510 pump equipped with Waters Rheodine injector and a differential refractometer, model 401. Reaction progress was monitored throught thin-layer chromatography (TLC) on Alugram® silica gel G/UV254 plates. Silica gel MN Kieselgel 60 (70-230 mesh) from Macherey-Nagel Company was utilized for column chromatography. The chemicals were procured by Zentek or Sigma Aldrich. Solvents and reagents were utilized as supplied from commercial sources. The exceptions are: Tetrahydrofuran, toluene, CH$_2$Cl$_2$, which were distilled from calcium hydride just before use. Magnesium turnings (1 g) and iodine (0.1 g) were refluxed in a small (5–10 mL) quantity of methanol until the precipitate turns from black to white. The mixture was diluted (up to 100 mL) with methanol and under reflux for 2–3 h was obtained Methanol dry. All reactions were carried out under argon atmosphere using flame-dried glassware. The purity of all of the intermediates, monitored by ^{1}H NMR, was greater than 95%. The purity of compounds was showed to be always greater than 95% by analytical HPLC analysis as reported for each compound**.**

8.2. Synthetic Procedures

DIBAL-H reduction.

At a solution of methyl quinoline-2-carboxylate in dry THF (25 mL) at 0 °C, a solution of DIBAL-H (2.0 eq, 1.0 M in THF) was added dropwise. The resulting mixture was stirred at room temperature for 8h at 0 °C. When the TLC shows the end of the substrate, the reaction was quenched by slow addition of a solution of saturated sodium potassium tartrate and, after dilution with CH_2Cl_2 stirred for 2h. The mixture was partitioned three times with CH_2Cl_2, and the combined organic extracts dried over Na_2SO_4. The solution was concentrated in vacuum, to obtain a residue, which is further purified on silica column using 6:4 v/v hexane/ethil acetate and 0.1% TFA, to give quinoline-2-ylmethanol (**56**) in quantitative yield.

Mitsunobu reaction.

At a solution of PPh_3 (3.5 eq) in dry THF a 0 °C, 3.5 eq of diisopropyl azodicarboxylate (DIAD) were added dropwise. After 10 minutes, a solution of alcohol **56** in dry THF was added and the mixture was stirred for further 10 minutes. After this time a solution of methyl 4-hydroxybenzoate or methyl 3-hydroxybenzoate in dry THF was added. The mixture was stirred vigorously for 12 hours, then partitioned between water and EtOAc (3 x 50 mL). The organic layer was collected and washed twice with aqueous KOH 2.5 M L solution, then with brine, dried over Na_2SO_4, filtered and concentrated under reduced pressure. The resulted residue was purified on silica column to give compounds **40** and **43**, respectively.

Synthesis of Methyl 4-(quinolin-2-ylmethoxy)benzoate (40).

Purification by flash column chromatography (silica gel, hexane: ethyl acetate 8:2 and 0.1% of TEA) furnished compound **40** (76% yield). An analytic sample was further purified by HPLC on a Nucleodur 100-5 C18 (5 μm; 10 mm i.d. x 250 mm) with MeOH/H_2O 82:18 v/v as eluent (flow rate 3 mL/min, t_R = 13 min); **^{1}H NMR (CDCl$_3$, 400 MHz):** δ 8.21 (1H, d, J = 8.5 Hz), 8.09 (1H, d, J = 8.3 Hz), 8.00 (2H, d, J = 9.0 Hz), 7.84 (1H, d, J = 8.3 Hz), 7.76 (1H, t, J = 8.3 Hz), 7.65 (1H, d, J = 8.5 Hz), 7.57 (1H, t, J = 8.3 Hz), 7.06 (2H, d, J = 9.0 Hz), 5.43 (2H, s), 3.88 (3H, s). **^{13}C NMR (CDCl$_3$, 100 MHz)**: δ 166.7, 162.0, 157.1, 147.4, 137.1, 131.5 (2C), 129.9, 128.9, 127.7, 127.6, 126.6, 123.0, 118.9, 114.6 (2C), 71.3, 51.7. **HRMS-ESI** *m/z* 294.1128 [M+H$^+$], C$_{18}$H$_{16}$NO$_3$ requires 294.1125.

Synthesis of Methyl 3-(quinolin-2-ylmethoxy)benzoate (43).

Chromatographic purification of the residue (silica gel, hexane: EtOAc 9:1 v/v and 0.1% of TEA) gave compound **43** (78% yield). An analytic sample was further purified by HPLC on a Nucleodur 100-5 C18 (5 μm; 10 mm i.d. x 250 mm) with MeOH/H_2O 82:18 v/v as eluent (flow rate 3 mL/min, tR = 14.8 min); **^{1}H NMR (CDCl$_3$, 400 MHz):** δ 8.22 (1H, d, J = 8.4 Hz), 8.10 (1H, d, J = 8.0 Hz), 7.85 (1H, d, J = 8.0 Hz), 7.74 (2H, ovl), 7.68 (2H, ovl), 7.57 (1H, t, J = 8.0 Hz), 7.37 (1H, t, J = 7.7 Hz), 7.24 (1H, d, J = 7.7 Hz), 5.44 (2H, s), 3.91 (3H, s). **^{13}C NMR (CDCl$_3$, 100 MHz)**: δ 169.6, 158.4, 157.3, 147.5, 137.1, 131.6, 129.8, 129.5, 128.9, 127.7, 127.6, 126.6, 122.4, 119.7, 119.0, 115.6, 71.4, 52.1. **HRMS-ESI** *m/z* 294.1127 [M+H$^+$], C$_{18}$H$_{16}$NO$_3$ requires 294.1125.

Basic hydrolysis. An aliquot of esters **40** and **43** was dissolved in MeOH/H_2O (1:1 v/v) and treated with NaOH (5 mol eq.) at 0 °C. The resulting mixture was stirred under reflux

for 8 h. The mixture was treated with 6 N HCl, until pH reached 7-8, then was partitioned three times with EtOAc and the combined organic extracts were dried over Na_2SO_4. The solution was concentrated in vacuum. The residue was purified on silica column to give carboxylic acids **41** and **44**, respectively.

Synthesis of 4-(quinolin-2-ylmethoxy)benzoic acid (41).

Purification by flash column chromatography (silica gel, DCM: MeOH 99:1) furnished compound **41** (43% yield). An analytic sample was further purified by HPLC on a Phenomenex Luna C18 (5 μm; 4.6 mm i.d. x 250 mm), with MeOH/H_2O 60:40 v/v and 0.1% of TFA as eluent (flow rate 1 mL/min, t_R = 7.2 min); **^{1}H NMR (CD₃OD, 400 MHz):** δ 8.62 (1H, d, J = 8.5 Hz), 8.15 (1H, d, J = 8.0 Hz), 8.07 (1H, d, J = 8.0 Hz), 8.02 (2H, d, J = 8.6 Hz), 7.92 (1H, t, J = 8.0 Hz), 7.86 (1H, d, J = 8.5), 7.73 (1H, t, J = 8.0), 7.17 (2H, d, J = 8.6 Hz), 5.53 (2H, s). **^{13}C NMR (CD₃OD, 100 MHz):** δ 169.4, 163.4, 158.1, 147.0, 140.6, 132.8 (2C), 132.3, 129.3 (2C), 128.6, 127.9, 124.9, 120.8, 115.6 (2C), 71.1. **HRMS-ESI** *m/z* 278.0825 [M-H⁻], $C_{17}H_{12}NO_3$ requires 278.0823.

Synthesis of 3-(quinolin-2-ylmethoxy)benzoic acid (44).

Purification of compound **44** (68% yield) was carried out on column chromatography by silica gel, using DCM: MeOH 99:1 v/v as eluent. An analytic sample was purified by HPLC on a Nucleodur 100-5 (5 μm; 10 mm i.d. x 250 mm), with hexane/ EtOAc 40:60 v/v (flow rate 3 mL/min, t_R = 6.9 min).

^{1}H NMR (CD₃OD, 400 MHz): δ 8.40 (1H, d, J = 8.5 Hz), 8.06 (1H, d, J = 8.3 Hz), 7.95 (1H, d, J = 8.3 Hz), 7.80 (1H, t, J = 8.3 Hz), 7.74 (1H, d, J = 8.5 Hz), 7.70 (1H, s), 7.64 (1H, t, J = 8.3 Hz), 7.62 (1H, d ovl), 7.41 (1H, t), 7.30 (1H, dd, J = 1.5, 8.0 Hz), 5.42 (2H, s); **^{13}C NMR (CD₃OD, 100 MHz):** δ 169.4, 159.9, 158.8, 148.4, 139.1, 133.5, 131.3,

130.7, 129.2, 129.1, 129.0, 128.0, 123.7, 120.8, 120.7, 116.6, 71.9. **HRMS-ESI** *m/z* 278.0827 [M-H$^-$], C$_{17}$H$_{12}$NO$_3$ requires 278.0823.

Synthesis of (4-(quinolin-2-ylmethoxy)phenyl)methanol (42) and (3-(quinolin-2-ylmethoxy)phenyl)methanol (45). Starting from esters **40** and **43**, we performed the DIBAL-H reduction in the same experimental conditions previously reported for methyl quinoline-2-carboxylate, in order to obtain compounds **42** and **45**, respectively.

(4-(quinolin-2-ylmethoxy)phenyl)methanol (42). Chromatographic purification of the residue (silica gel, DCM: MeOH 99:1 v/v) gave compound **42** (68% yield). An analytic sample was further purified by HPLC on a Nucleodur 100-5 C18 (5 μm; 10 mm i.d. x 250 mm) with MeOH/H$_2$O 40:60 v/v as eluent (flow rate 3 mL/min, t$_R$ = 15.8 min); **^{1}H NMR (CDCl$_3$, 400 MHz):** δ 8.21 (1H, d, *J* = 8.0 Hz), 8.12 (1H, d, *J* = 7.3 Hz), 7.84 (1H, d, *J* = 7.3 Hz), 7.76 (1H, t, *J* = 7.3 Hz), 7.68 (1H, d, *J* = 8.0 Hz), 7.57 (1H, t, *J* = 7.3 Hz), 7.30 (2H, d, *J* = 8.0 Hz), 7.02 (2H, d, *J* = 8.0 Hz), 5.41 (2H, s), 4.62 (2H, s). **^{13}C NMR (CDCl$_3$, 100 MHz):** δ 157.9, 157.8, 147.4, 137.1, 133.8, 129.8, 128.8, 128.7 (2C), 127.6, 127.5, 126.5, 119.0, 114.9 (2C), 71.1, 64.7. **HRMS-ESI** *m/z* 266.1178 [M+H$^+$], C$_{17}$H$_{16}$NO$_2$ requires 266.1176.

(3-(quinolin-2-ylmethoxy)phenyl)methanol (45). Purification by flash column chromatography (silica gel, DCM: MeOH 99:1 v/v) furnished compound **45** (60% yield). An analytic sample was further purified by HPLC on a Nucleodur 100-5 C18 (5 μm; 10 mm i.d. x 250 mm) with MeOH/H$_2$O 75:15 v/v as eluent (flow rate 3 mL/min, t$_R$ = 9.3 min); **^{1}H NMR (CDCl$_3$, 400 MHz):** δ 8.20 (1H, d, *J* = 8.4 Hz), 8.10 (1H, d, *J* = 7.4 Hz), 7.84 (1H, d, *J* = 7.4 Hz), 7.75 (1H, t, *J* = 7.4 Hz), 7.68 (1H, d, *J* = 8.4 Hz), 7.56 (1H, t, *J* = 7.4 Hz), 7.28 (1H, dd, *J* = 7.3, 8.0 Hz), 7.08 (1H, s), 7.0 (1H, d, *J* = 8.4 Hz), 6.95 (1H,

d, J = 7.3 Hz), 5.40 (2H, s), 4.68 (2H, s). **^{13}C NMR (CDCl$_3$, 100 MHz)**: δ 158.6, 157.8,

147.4, 142.8, 137.1, 129.8, 129.6, 128.7, 127.7, 127.6, 126.5, 119.6, 119.1, 113.9, 113.4,

71.1, 64.9. **HRMS-ESI** *m/z* 266.1179 [M+H$^+$], C$_{17}$H$_{16}$NO$_2$ requires 266.1176.

Synthetic procedures to prepare compounds 46-48.

TBS protection.

Synthesis of intermediate **58.** To a solution of the methyl 3,5-dihydroxybenzoate (2.0 g,

12 mmol), imidazole (1.5 eq), and DMF (10 mL) was added portionwise TBSCl (1.2 eq).

The reaction mixture was stirred at RT for 1 h. The mixture was concentrated *in vacuo*,

diluted with NH$_4$Cl saturated solution, and extracted with diethylether (3x50 mL). The

combined organics were washed with brine, dried, and concentrated to provide the

product as an oil which was purified on silica gel, using DCM: MeOH 95:5 as eluent (50

% yield).

Mesylation

Synthesis of intermediate **59.** To a solution of the quinoline-2-ylmethanol (1.6 g, 10

mmol) in diethylether (10 mL) at -20°C was added TEA (6.0 eq) followed by MeSO$_2$Cl

(5.0 eq). The reaction mixture was stirred at -20° C for 30 min, then was allowed to warm

to RT over 2 h. The mixture was quenched with aqueous saturated solution of NaHCO$_3$

(10 mL) and extracted with diethylether (3 x 30 mL). The combined organics were

washed with H$_2$O (20 mL), brine (20 mL), dried (Na$_2$SO$_4$), and concentrated under

vacuum. The resulting material was used without further purification (quantitative yield).

Williamson reaction.

The crude mesylate **59** (1.2 eq) was added to a stirred mixture of the phenol **58** (1.0 eq), K_2CO_3 (2.5 eq), and dry DMF. The reaction mixture was stirred at 100° C for 12h. The mixture was diluted with H_2O and extracted with EtOAc (3 x 30 mL). The combined organics were washed with brine, dried (Na_2SO_4), concentrated, and purified by flash chromatography (hexane/ EtOAc 95:5 v/v) to provide compound **46** (87% yield).

TBS cleavage.

A mixture of the compound **60** and TBAF (5.0 eq) in THF (3 mL) was stirred at RT overnight. Upon completion, the resulting solution was concentrated in vacuo to provide crude residue which was purified by silica gel flash chromatography to provide pure compound **46**.

Synthesis of Methyl 3-hydroxy-5-(quinolin-2-ylmethoxy)benzoate (46).

Purification by flash column chromatography (silica gel, DCM: MeOH 998:2 v/v) furnished compound **46** (85% yield). An analytic sample was further purified by HPLC on a Nucleodur 100-5 (5 μm; 10 mm i.d. x 250 mm) with hexane/EtOAc 7:3 v/v as eluent (flow rate 3 mL/min, t_R = 23.7 min); **^{1}H NMR (400 MHz, CDCl$_3$):** δ 8.17 (1H, d, J = 8.5 Hz), 8.00 (1H, d, J = 8.0 Hz), 7.79 (1H, d, J = 8.0 Hz), 7.68 (1H, t, J = 8.0 Hz), 7.62 (1H, t, J = 8.5 Hz), 7.54 (1H, t, J = 8.0 Hz), 7.28 (1H, s), 7.21 (1H, s), 6.76 (1H, s), 5.38 (2H, s), 3.89 (3H, s). **^{13}C NMR (100 MHz, CDCl$_3$):** δ 167.2, 159.1, 157.9, 157.3, 146.7, 137.8, 131.8, 130.2, 127.8, 127.7, 127.6, 126.8, 119.2, 109.8, 107.8, 106.8, 70.4, 52.1. **HRMS-ESI** *m/z* 310.1077 [M+H$^+$], $C_{18}H_{16}NO_4$ requires 310.1074.

Synthesis of 3-hydroxy-5-(quinolin-2-ylmethoxy)benzoic acid (47) and 3-(hydroxymethyl)-5-(quinolin-2-ylmethoxy)phenol (48).

Starting from ester **46**, we performed NaOH hydrolysis and DIBAL-H reduction in the same experimental conditions previously reported for methyl quinoline-2-carboxylate, in order to obtain compounds **47** and **48**, respectively.

3-hydroxy-5-(quinolin-2-ylmethoxy)benzoic acid (47). Purification of compound **47** (quantitative yield) was carried out in column chromatography by silica gel, using DCM: MeOH 95:5 v/v as eluent. An analytic sample was purified by HPLC on a PFP C18 (5 μm; 4.6 mm i.d. x 250 mm), with MeOH/H_2O 55:45 v/v and 0.1% TFA (flow rate 1 mL/min, t_R = 9.2 min). **^{1}H NMR (400 MHz, CD₃OD):** δ 8.39 (1H, d, J = 8.4 Hz), 8.05 (1H, d, J = 8.0 Hz), 7.96 (1H, d, J = 8.0 Hz), 7.79 (1H, t, J = 8.0 Hz), 7.72 (1H, d, J = 8.4 Hz), 7.62 (1H, t, J = 8.0 Hz), 7.18 (1H, s), 7.08 (1H, s), 6.66 (1H, s), 5.37 (2H, s). **^{13}C NMR (100 MHz, CD₃OD):** δ 160.7, 159.7, 158.2, 148.2, 139.1, 131.4, 131.3, 129.2, 129.1, 129.0, 128.9, 128.0, 120.6, 110.8, 107.8, 107.0, 71.8. **HRMS-ESI** m/z 294.0775 [M-H⁻], $C_{17}H_{12}NO_4$ requires 294.0772.

3-(hydroxymethyl)-5-(quinolin-2-ylmethoxy)phenol (48). Purification of compound **48** (92% yield) was carried out in column chromatography by silica gel, using DCM: MeOH 95:5 v/v as eluent. An analytic sample was purified by HPLC on a PFP C18 (5 μm; 4.6 mm i.d. x 250 mm), with MeOH/H_2O 60:40 v/v and 0.1% TFA (flow rate 1 mL/min, t_R = 12.2 min). **^{1}H NMR (400 MHz, CDCl₃):** δ 8.20 (1H, d, J = 8.5 Hz), 8.10 (1H, d, J = 8.0 Hz), 7.84 (1H, d, J = 8.0 Hz), 7.75 (1H, t, J = 8.0 Hz), 7.67 (1H, d, J = 8.5 Hz), 7.57 (1H, t, J = 8.0 Hz), 6.65 (1H, s), 6.49 (1H, s), 6.46 (1H, s), 5.40 (2H, s), 4.62 (2H, s). **^{13}C NMR (100 MHz, CDCl₃):** δ 161.1, 159.8, 159.6, 148.3, 145.5, 139.0, 131.3,

129.1, 129.0, 128.9, 127.9, 120.6, 107.8, 105.5, 102.1, 71.6, 65.1. **HRMS-ESI** *m/z* 282.1127 [M+H$^+$], C$_{17}$H$_{16}$NO$_3$ requires 282.1125.

Synthetic procedures to prepare alkylarilethers 49-54.

Starting from resorcinol (**61**), we performed TBS protection (47%), Mitsunobu reaction with several different alcohols (propan-1-ol, propan-2-ol, butan-2-ol, butan-1-ol, 2-methylbutan-1-ol, and pentan-1-ol) and TBS cleavage in the same experimental conditions previously described in order to obtain compounds **46-48** (47-84% yields).

Finally, Williamson ether synthesis between **64a-f** and quinolin-2-ylmethyl methanesulfonate (**59**) with the same experimental procedures previously defined, gave us compounds **49-54**.

2-((3-propoxyphenoxy)methyl)quinoline (49). Purification of compound **49** (quantitative yield) was carried out in HPLC using a Nucleodur 100-5 (5 μm; 10 mm i.d. x 250 mm), with hexane/EtOAc 9:1 v/v (flow rate 3 mL/min, t_R = 16.5 min). **^{1}H NMR (400 MHz, CDCl$_3$):** δ 8.20 (1H, d, *J* = 8.6 Hz), 8.09 (1H, d, *J* = 7.5 Hz), 7.84 (1H, d, *J* = 7.5 Hz), 7.74 (1H, t, *J* = 7.5 Hz), 7.68 (1H, d, *J* = 8.6 Hz), 7.56 (1H, t, *J* = 7.5 Hz), 7.17 (1H, t, *J* = 8.0 Hz), 6.63 (1H, s), 6.61 (1H, ovl), 6.54 (1H, dd, *J* = 8.0, 2.0 Hz), 5.38 (2H, s), 3.90 (2H, t, *J* = 7.0 Hz), 1.80 (2H, sextet, *J* = 7.0 Hz), 1.03 (3H, t, *J* = 7.0 Hz). **^{13}C NMR (100 MHz, CDCl$_3$):** δ 160.4, 159.7, 157.9, 147.6, 137.0, 130.0, 129.7, 129.0, 127.7, 127.6, 126.5, 119.2, 107.6, 106.8, 101.8, 71.1, 69.7, 22.5, 10.5. **HRMS-ESI** *m/z* 294.1492 [M+H$^+$], C$_{19}$H$_{20}$NO$_2$ requires 294.1489.

2-((3-isopropoxyphenoxy)methyl)quinoline (50). Compound **50** (61% yield) was purified by HPLC using a Nucleodur 100-5 (5 μm; 10 mm i.d. x 250 mm), with hexane/EtOAc 95:5 v/v (flow rate 3 mL/min, t_R = 38 min). **^{1}H NMR (400 MHz, CDCl$_3$):**

δ 8.19 (1H, d, *J* = 8.6 Hz), 8.09 (1H, d, *J* = 7.5 Hz), 7.84 (1H, d, *J* = 7.5 Hz), 7.74 (1H, t, *J* = 7.5 Hz), 7.68 (1H, d, *J* = 8.6 Hz), 7.56 (1H, t, *J* = 7.5 Hz), 7.17 (1H, t, *J* = 8.0 Hz), 6.61 (1H, s), 6.60 (1H, ovl), 6.52 (1H, dd, *J* = 8.0, 2.0 Hz),5.38 (2H, s), 4.52 (1H, septet, *J* = 6.0 Hz), 1.32 (6H, d, *J* = 6.0 Hz). **¹³C NMR (100 MHz, CDCl₃):** δ 159.6, 159.2, 157.9, 147.5, 136.9, 129.9, 129.7, 128.9, 127.7, 127.6, 126.4, 119.1, 108.8, 106.8, 103.0, 71.3, 69.9, 22.0 (2C). **HRMS-ESI** *m/z* 294.1493 [M+H⁺], C₁₉H₂₀NO₂ requires 294.1489.

2-((3-(sec-butoxy)phenoxy)methyl)quinoline (51). Compound **51** (quantitative yield) was purified by HPLC using a Nucleodur 100-5 (5 μm; 10 mm i.d. x 250 mm), with hexane/EtOAc 9:1 v/v (flow rate 3 mL/min, t_R = 15 min). **¹H NMR (400 MHz, CDCl₃):** δ 8.19 (1H, d, *J* = 8.6 Hz), 8.09 (1H, d, *J* = 7.5 Hz), 7.84 (1H, d, *J* = 7.5 Hz), 7.74 (1H, t, *J* = 7.5 Hz), 7.68 (1H, d, *J* = 8.6 Hz), 7.56 (1H, t, *J* = 7.5 Hz), 7.17 (1H, t, *J* = 8.0 Hz), 6.61 (1H, s), 6.60 (1H, ovl), 6.52 (1H, dd, *J* = 8.0, 2.0 Hz), 5.37 (2H, s), 4.27 (2H, sextet, *J* = 6.1 Hz), 1.73 (1H, m), 1.60 (1H, m), 1.27 (2H, d, *J* = 6.1 Hz), 0.96 (3H, t, *J* = 7.4 Hz). **¹³C NMR (100 MHz, CDCl₃):** δ 159.7, 159.6, 158.0, 147.5, 136.9, 129.9, 129.7, 128.9, 127.7, 127.6, 126.4, 119.2, 108.9, 106.7, 103.1, 75.2, 71.1, 29.2, 19.2, 9.9. **HRMS-ESI** *m/z* 308.1647 [M+H⁺], C₂₀H₂₂NO₂ requires 308.1645.

2-((3-butoxyphenoxy)methyl)quinoline (52). Purification of compound **52** (quantitative yield) was carried out in HPLC using a Nucleodur 100-5 (5 μm; 10 mm i.d. x 250 mm), with hexane/EtOAc 9:1 v/v (flow rate 3 mL/min, t_R = 17.3 min). **¹H NMR (400 MHz, CDCl₃):** δ 8.19 (1H, d, *J* = 8.6 Hz), 8.09 (1H, d, *J* = 7.5 Hz), 7.84 (1H, d, *J* = 7.5 Hz), 7.74 (1H, t, *J* = 7.5 Hz), 7.68 (1H, d, *J* = 8.6 Hz), 7.56 (1H, t, *J* = 7.5 Hz), 7.17 (1H, t, *J* = 8.0 Hz), 6.61 (1H, s), 6.60 (1H, ovl), 6.52 (1H, dd, *J* = 8.0, 2.0 Hz), 5.38 (2H, s), 3.95 (2H, t, *J* = 7.0 Hz), 1.75 (2H, pentet, *J* = 7.0 Hz), 1.48 (2H, sextet, *J* = 7.4 Hz), 0.97 (3H,

t, J = 7.4 Hz). **^{13}C NMR (100 MHz, CDCl$_3$):** δ 160.5, 159.6, 158.0, 147.6, 137.0, 129.9, 129.7, 128.9, 127.7, 127.6, 126.5, 119.1, 107.6, 106.8, 101.7, 71.2, 67.7, 31.3, 19.2, 13.8. **HRMS-ESI** *m/z* 308.1648 [M+H$^+$], C$_{20}$H$_{22}$NO$_2$ requires 308.1645.

2-((3-(2-methylbutoxy)phenoxy)methyl)quinoline (53). HPLC purification of the residue on a Nucleodur 100-5 (5 μm; 10 mm i.d. x 250 mm) with hexane/EtOAc 9:1 v/v as eluent (flow rate 3 mL/min, t$_R$ = 14.0 min) gave compound **53**, as pure compound (90% yield). **^{1}H NMR (400 MHz, CDCl$_3$):** δ 8.19 (1H, d, J = 8.6 Hz), 8.09 (1H, d, J = 7.5 Hz), 7.84 (1H, d, J = 7.5 Hz), 7.74 (1H, t, J = 7.5 Hz), 7.68 (1H, d, J = 8.6 Hz), 7.56 (1H, t, J = 7.5 Hz), 7.17 (1H, t, J = 8.0 Hz), 6.61 (1H, s), 6.60 (1H, ovl), 6.52 (1H, dd, J = 8.0, 2.0 Hz), 5.38 (2H, s), 3.80 (1H, dd, J = 9.0, 6.0 Hz), 3.71 (1H, dd, J = 9.0, 6.6 Hz), 1.85 (1H, septet, J = 6.6 Hz), 1.56 (1H, m), 1.25 (1H, m), 1.00 (3H, d, J = 6.6 Hz), 0.94 (3H, t, J = 7.3 Hz). **^{13}C NMR (100 MHz, CDCl$_3$):** δ 160.6, 159.6, 158.0, 147.5, 136.9, 129.9, 129.8, 128.9, 127.8, 127.6, 126.5, 119.1, 107.7, 106.8, 101.8, 73.0, 71.2, 34.6, 26.1, 16.5, 11.3. **HRMS-ESI** *m/z* 322.1805 [M+H$^+$], C$_{21}$H$_{24}$NO$_2$ requires 322.1802.

2-((3-(pentyloxy)phenoxy)methyl)quinoline (54). Compound **54** (95% yield) was purified by HPLC using a Nucleodur 100-5 (5 μm; 10 mm i.d. x 250 mm), with hexane/EtOAc 9:1 v/v (flow rate 3 mL/min, t$_R$ = 13.8 min). **^{1}H NMR (400 MHz, CDCl$_3$):** δ 8.19 (1H, d, J = 8.6 Hz), 8.09 (1H, d, J = 7.5 Hz), 7.84 (1H, d, J = 7.5 Hz), 7.74 (1H, t, J = 7.5 Hz), 7.68 (1H, d, J = 8.6 Hz), 7.56 (1H, t, J = 7.5 Hz), 7.17 (1H, t, J = 8.0 Hz), 6.61 (1H, s), 6.60 (1H, ovl), 6.52 (1H, dd, J = 8.0, 2.0 Hz), 5.38 (2H, s), 3.93 (2H, t, J = 7.0 Hz), 1.77 (2H, m), 1.40 (4H, m), 0.93 (3H, t, J = 7.0 Hz). **^{13}C NMR (100 MHz, CDCl$_3$):** δ 160.4, 159.6, 157.9, 147.5, 136.9, 129.9, 129.7, 128.9, 127.7, 127.6, 126.4,
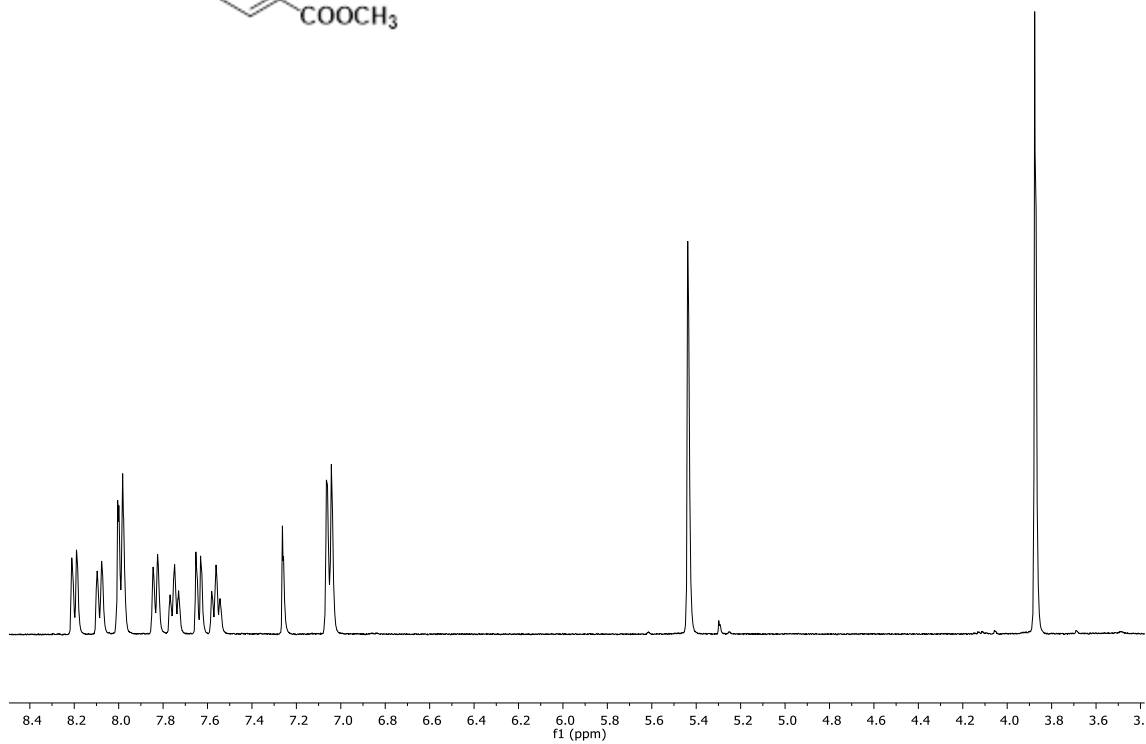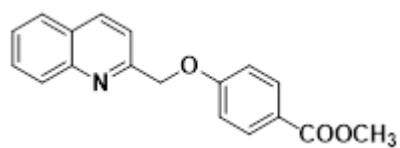
119.1, 107.6, 106.8, 101.8, 71.2, 68.0, 28.9, 28.2, 22.4, 13.9. **HRMS-ESI** *m/z* 322.1807
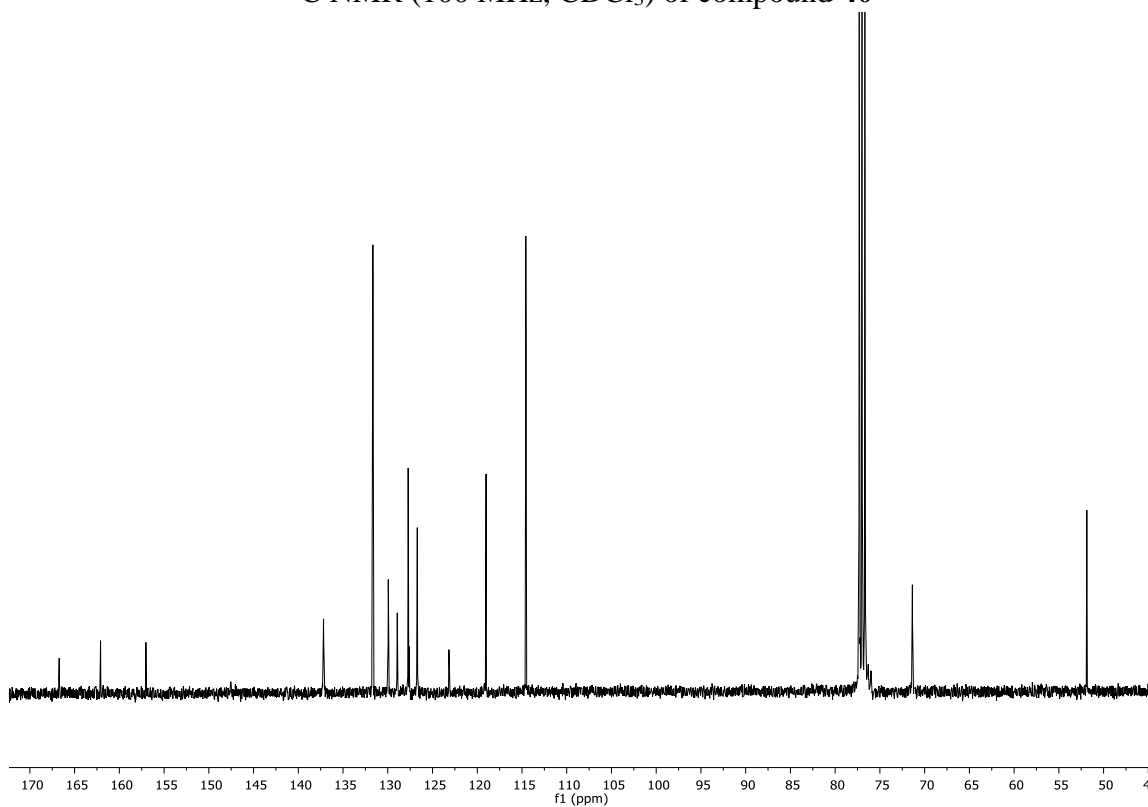
[M+H$^+$], C$_{21}$H$_{24}$NO$_2$ requires 322.1802.

8.3. NMR Spectra

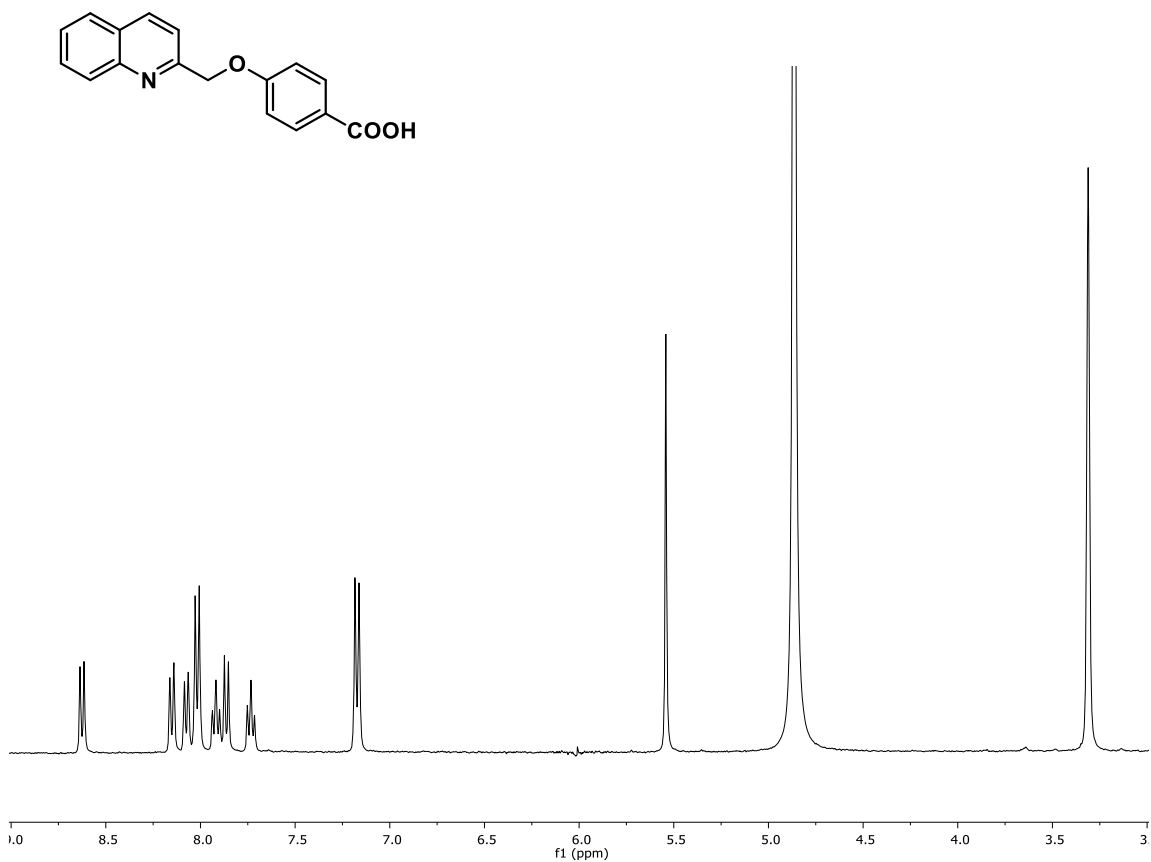¹H NMR (400 MHz, CDCl₃) of compound **40**

¹³C NMR (100 MHz, CDCl₃) of compound **40**

^{1}H NMR (400 MHz, CD$_3$OD) of compound **41**

^{13}C NMR (100 MHz, CD$_3$OD) of compound **41**

^{1}H NMR (400 MHz, CDCl$_3$) of compound **42**

^{13}C NMR (100 MHz, CDCl$_3$) of compound **42**

^{1}H NMR (400 MHz, CDCl$_3$) of compound **43**

^{13}C NMR (100 MHz, CDCl$_3$) of compound **43**

^{1}H NMR (400 MHz, CD$_3$OD) of compound **44**

^{13}C NMR (100 MHz, CD$_3$OD) of compound **44**

¹H NMR (400 MHz, CDCl₃) of compound **45**

¹³C NMR (100 MHz, CDCl₃) of compound **45**
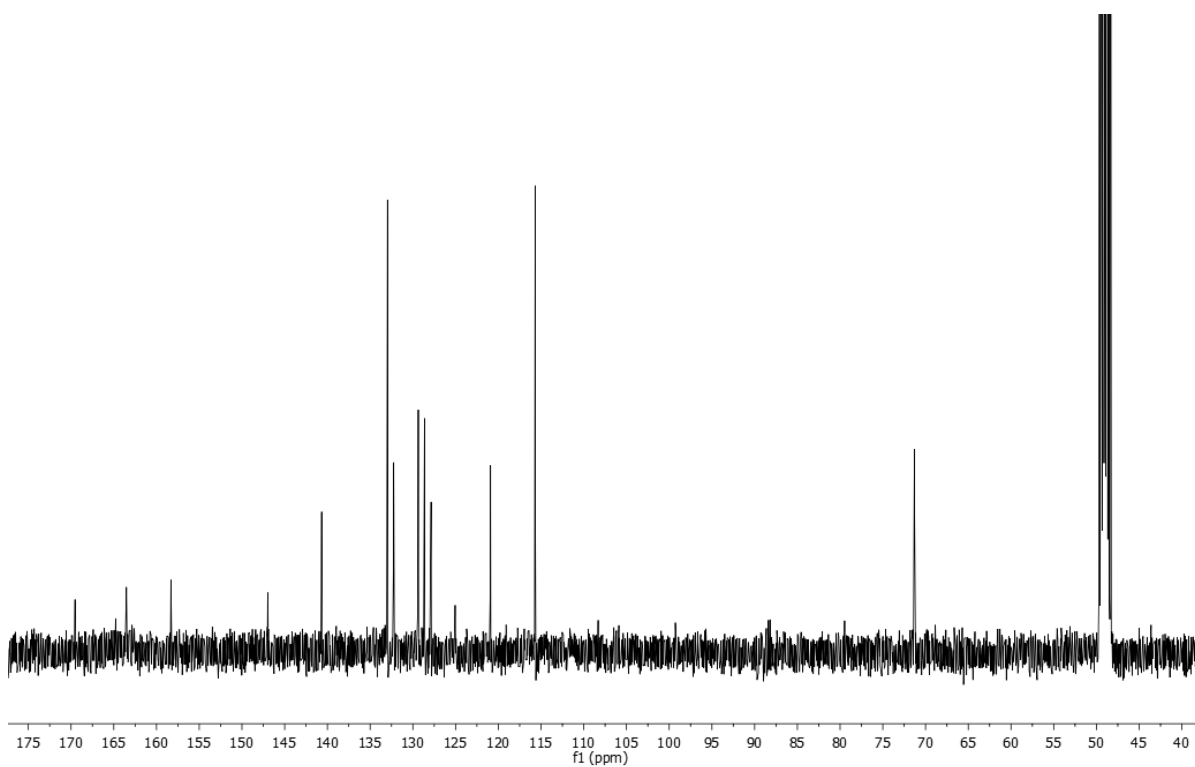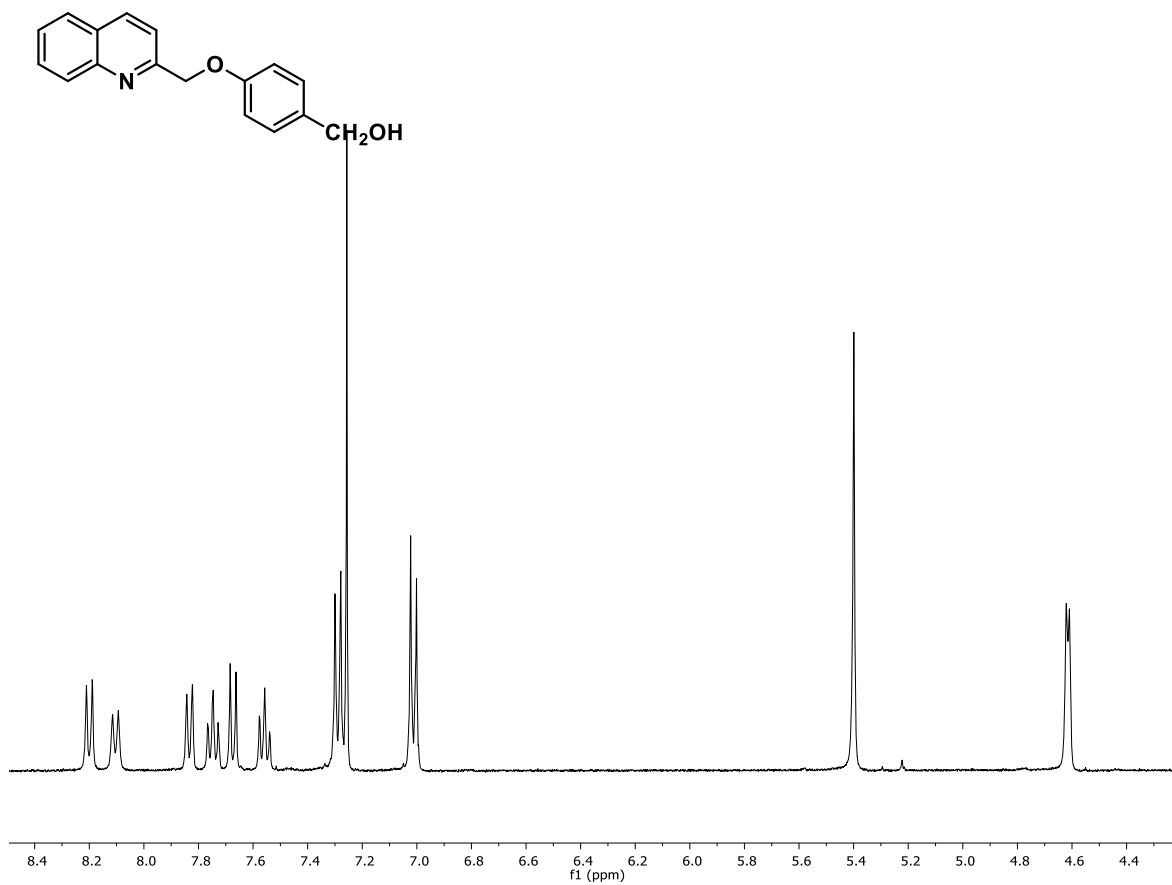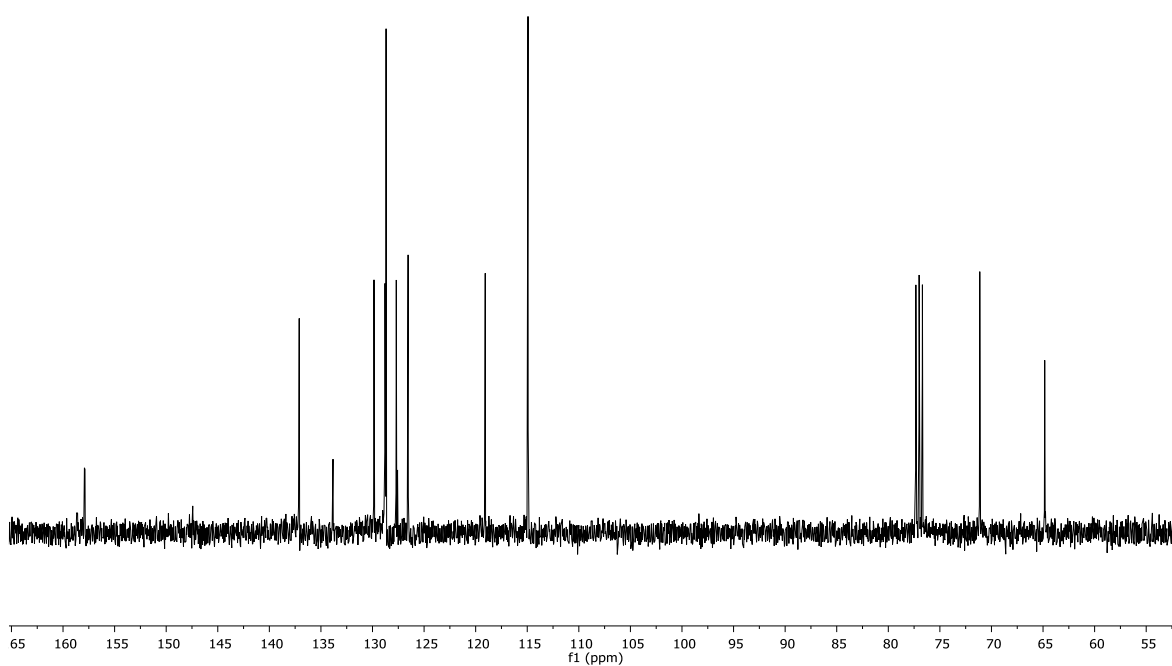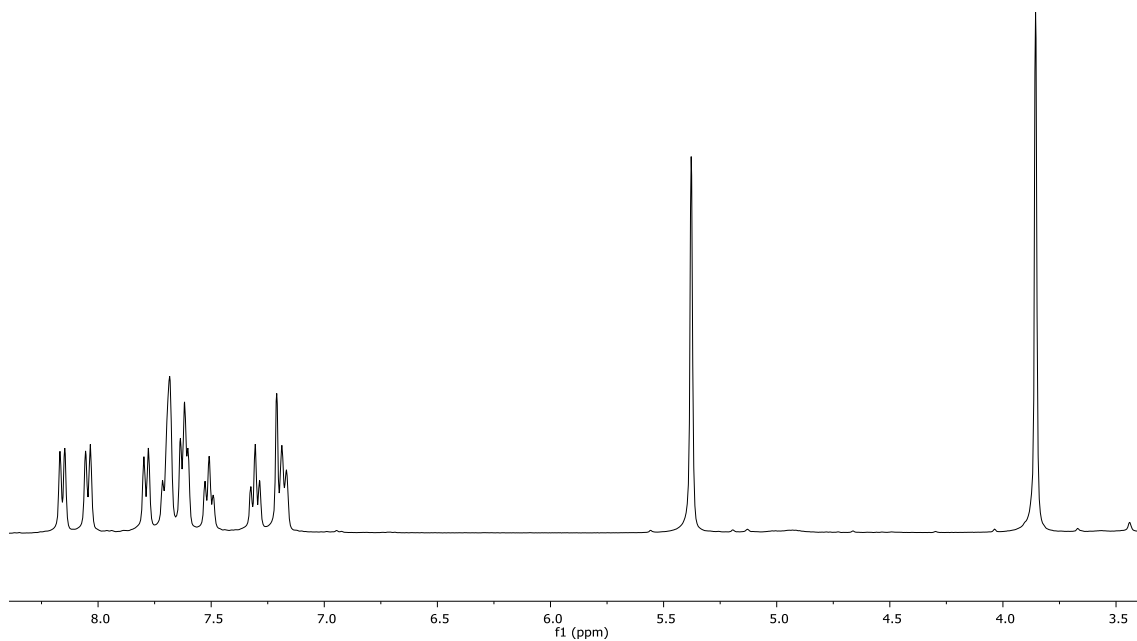
Experimental Information

^{1}H NMR (400 MHz, CDCl$_3$) of compound **46**
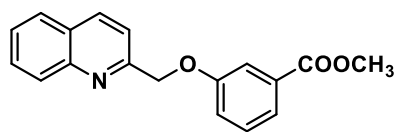

^{13}C NMR (100 MHz, CDCl$_3$) of compound **46**

174

Experimental Information

^{1}H NMR (400 MHz, CD$_3$OD) of compound **47**

^{13}C NMR (100 MHz, CD$_3$OD) of compound **47**

¹H NMR (400 MHz, CD₃OD) of compound **48**
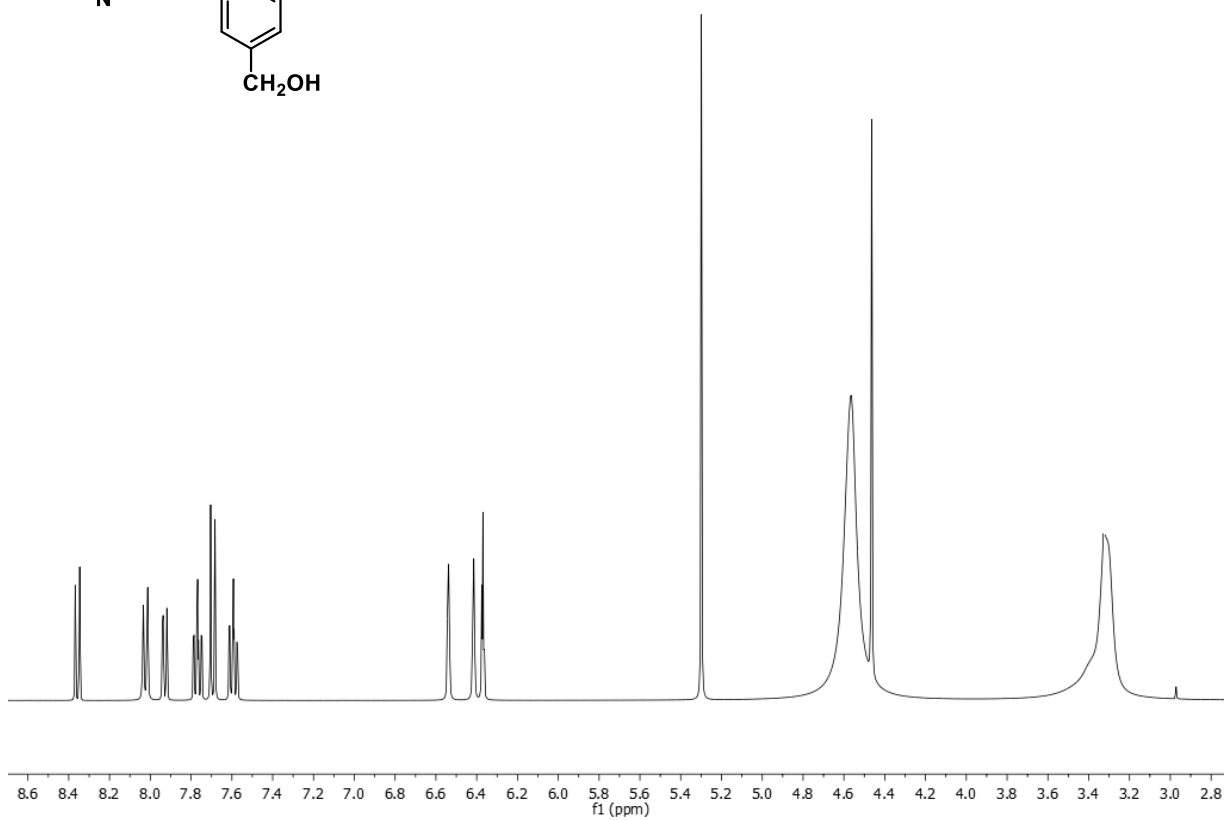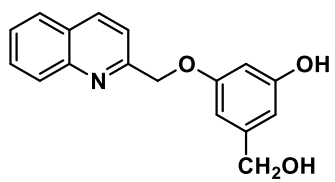
¹³C NMR (100 MHz, CD₃OD) of compound **48**
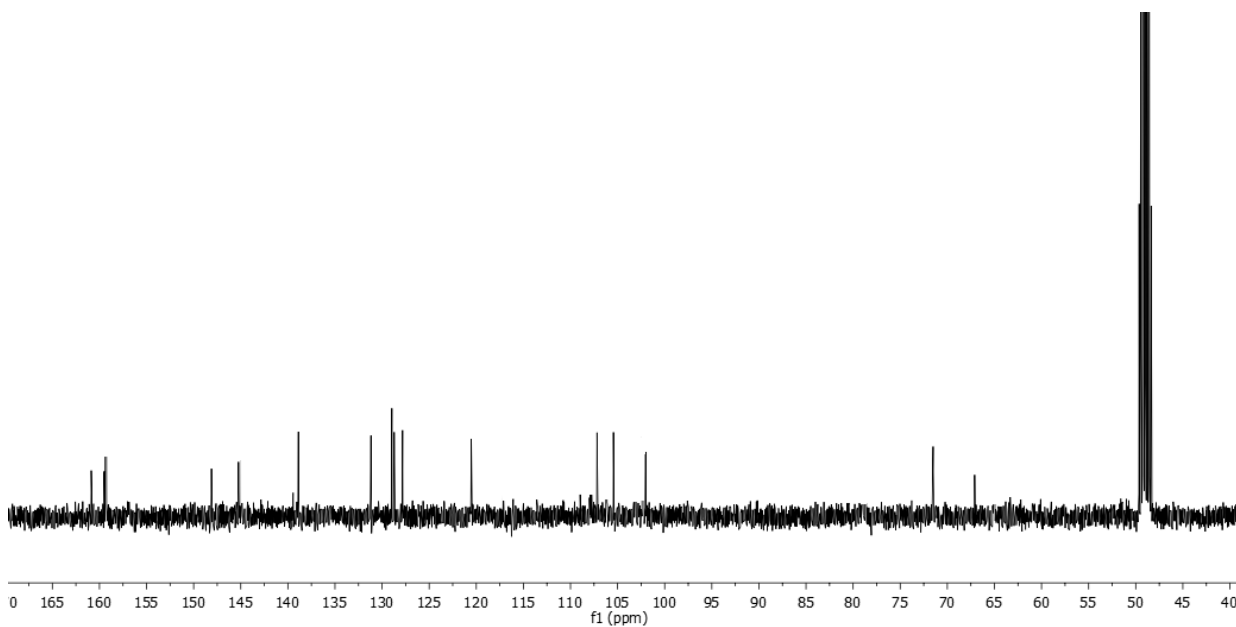
¹H NMR (400 MHz, CDCl₃) of compound **49**
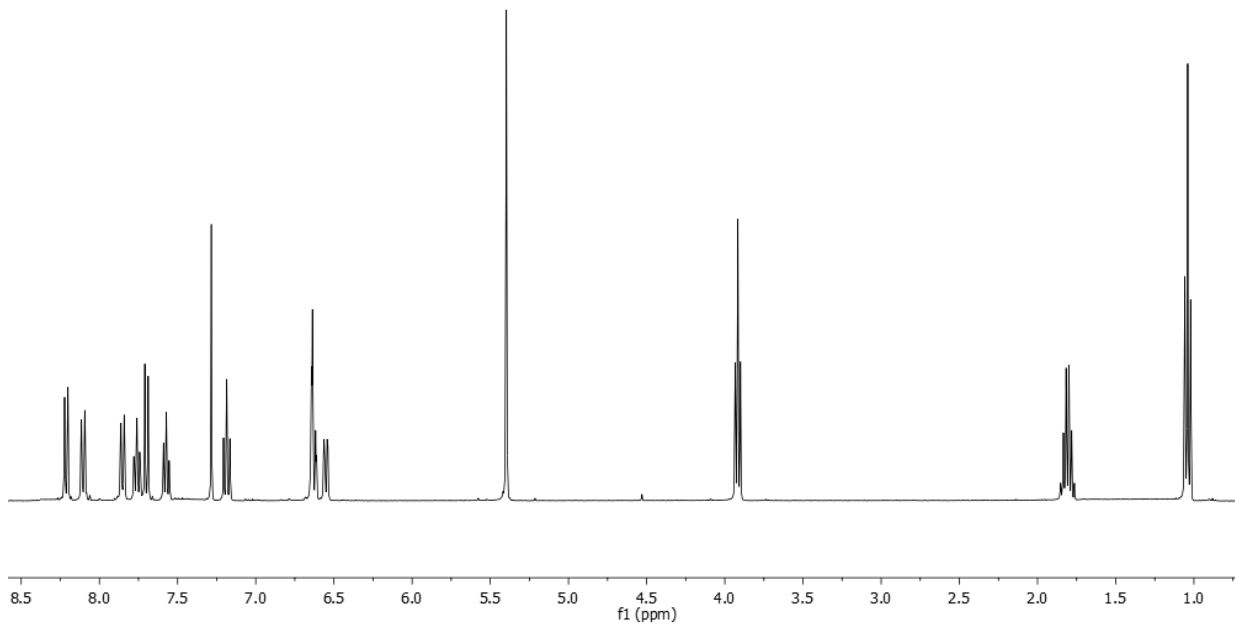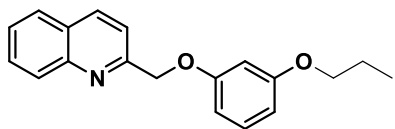
^{1}H NMR (400 MHz, CDCl$_3$) of compound **49**

^{13}C NMR (100 MHz, CDCl$_3$) of compound **49**
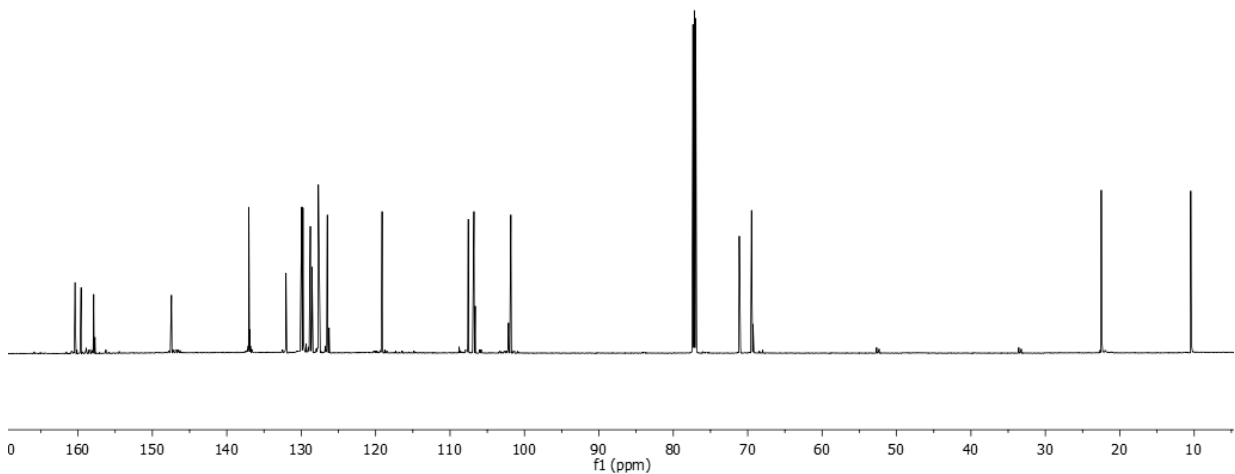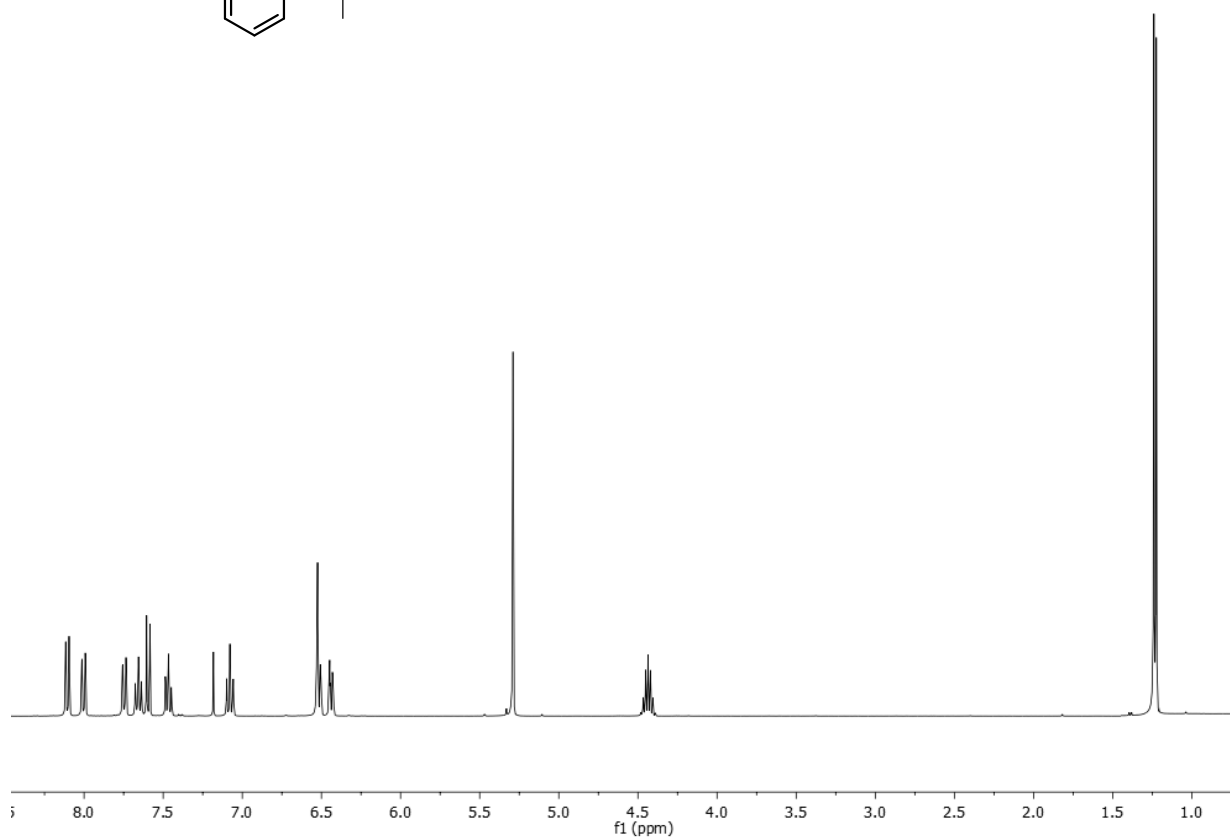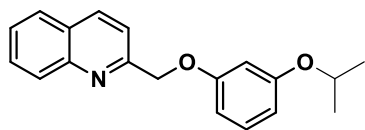
^{1}H NMR (400 MHz, CDCl$_3$) of compound **50**

^{13}C NMR (100 MHz, CDCl$_3$) of compound **50**
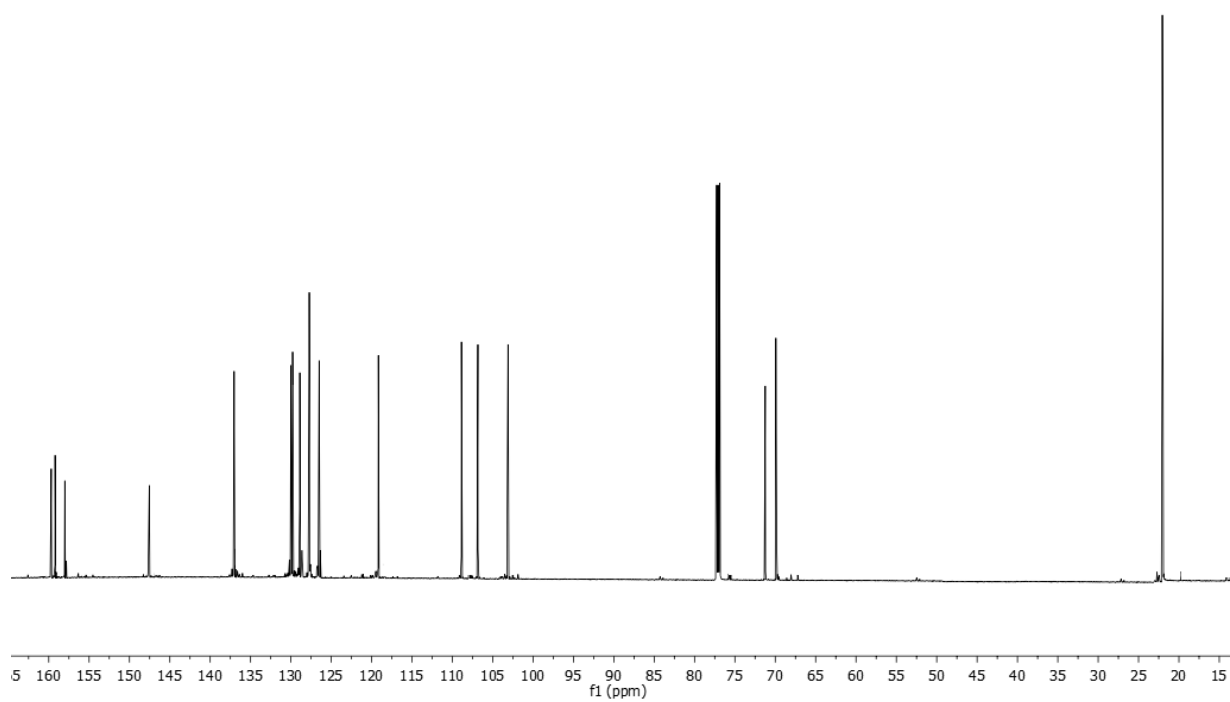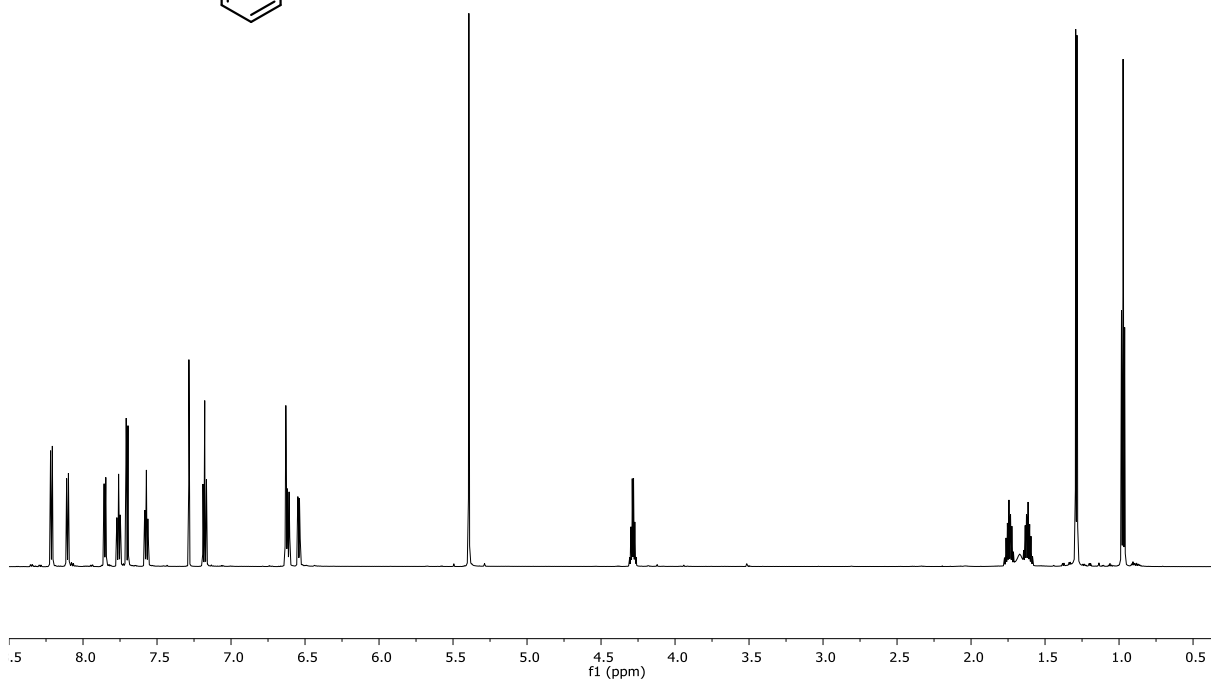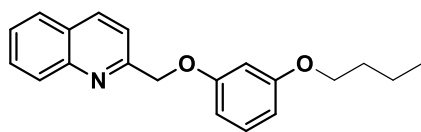
^{1}H NMR (400 MHz, CDCl$_3$) of compound **51**

^{13}C NMR (100 MHz, CDCl$_3$) of compound **51**
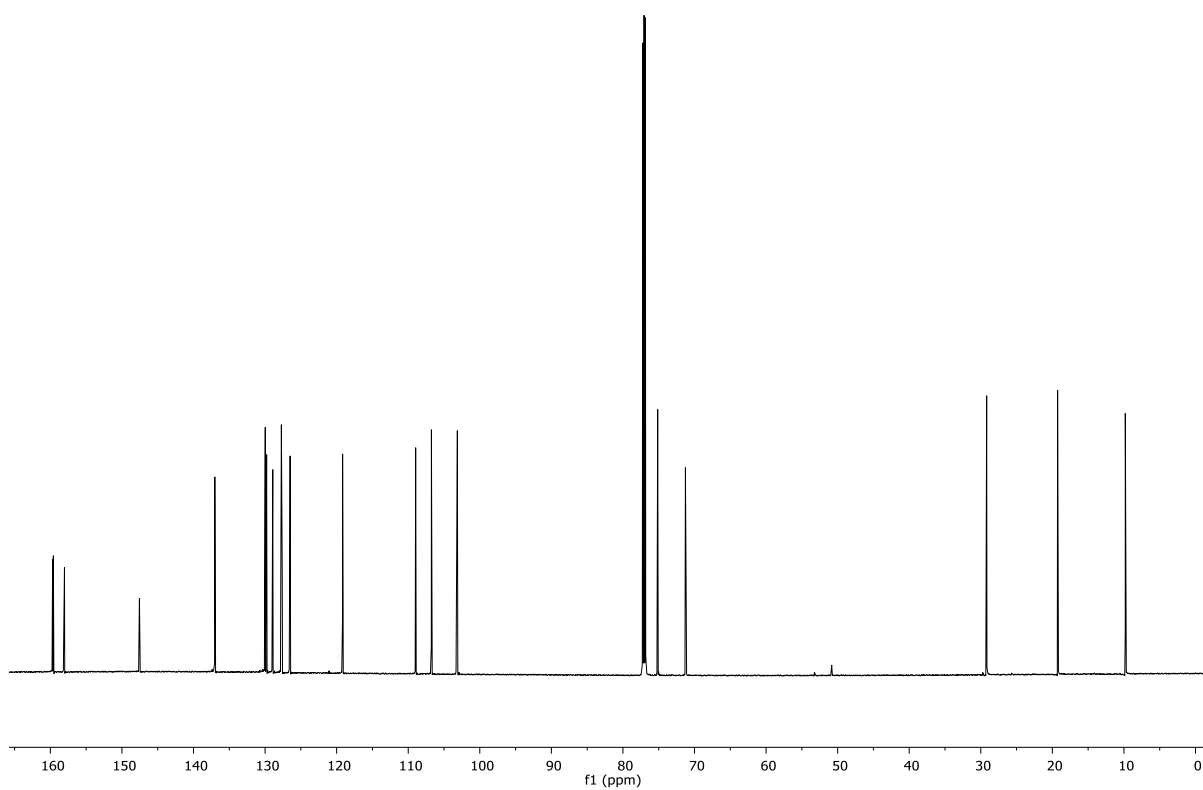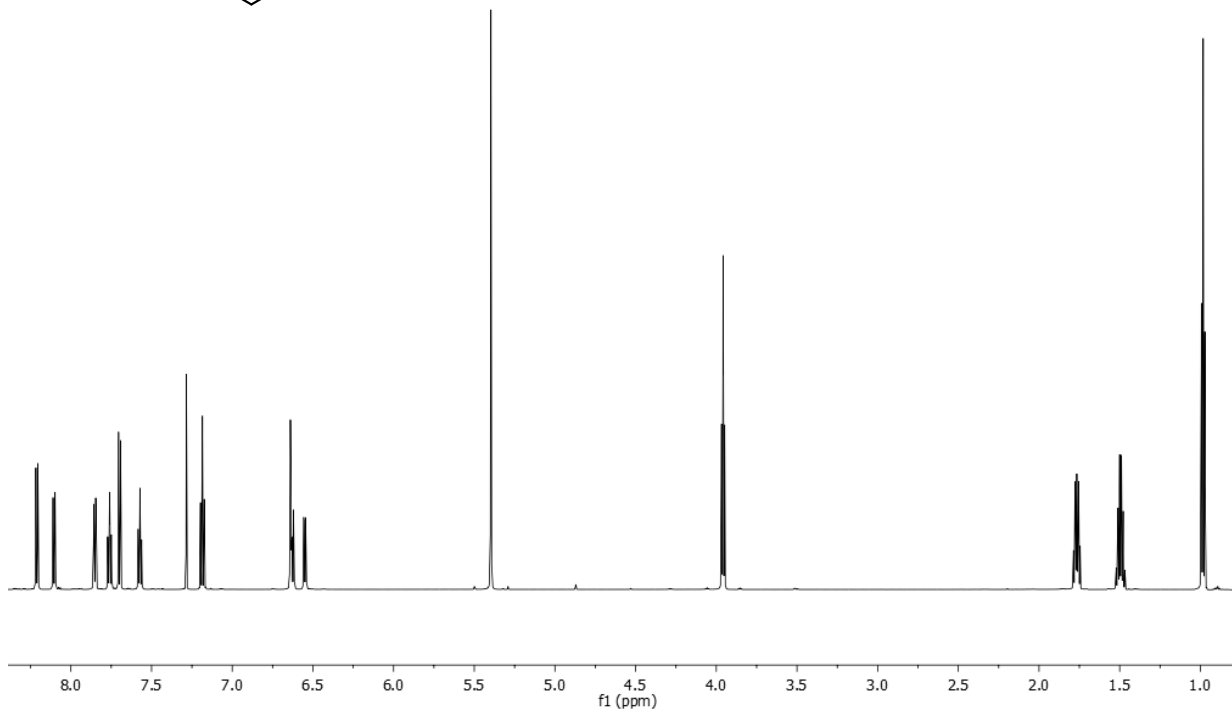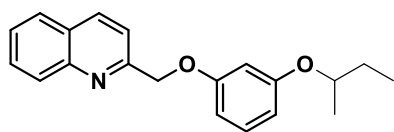
^{1}H NMR (400 MHz, CDCl$_3$) of compound **52**

^{13}C NMR (100 MHz, CDCl$_3$) of compound **52**
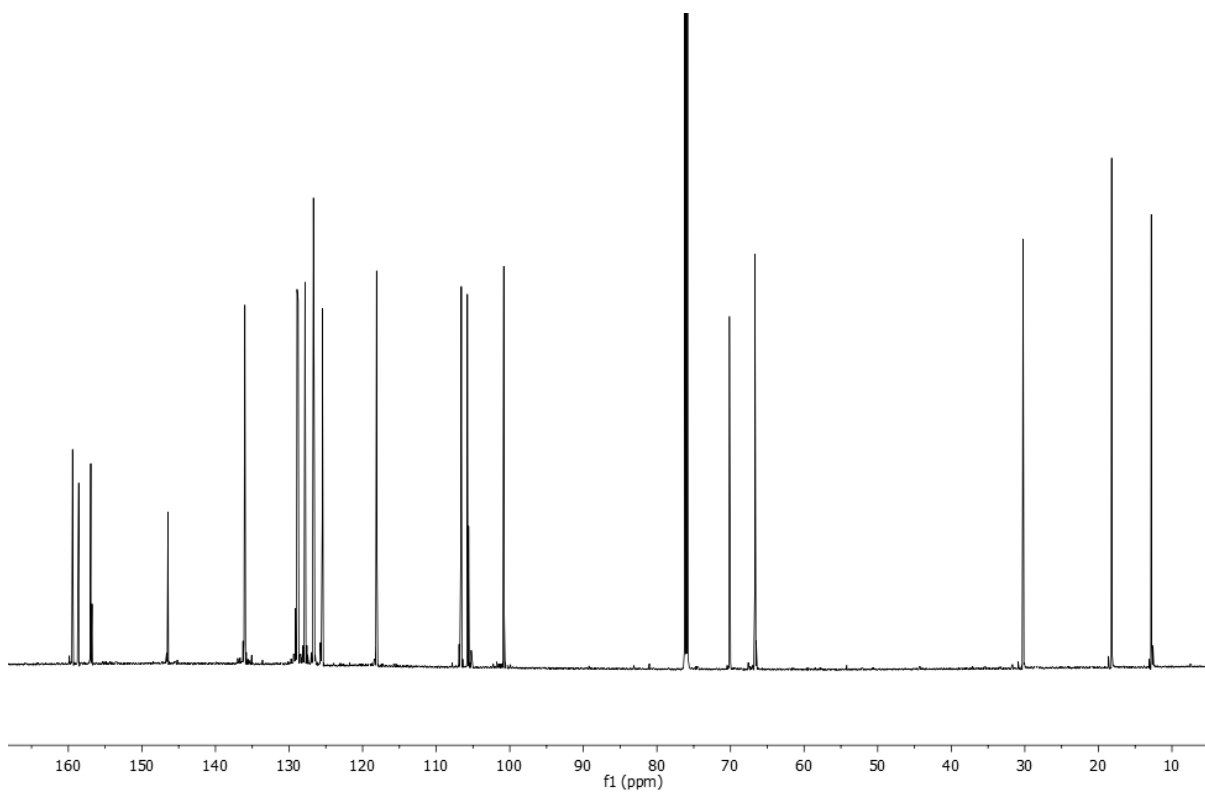
^{1}H NMR (400 MHz, CDCl$_3$) of compound **53**
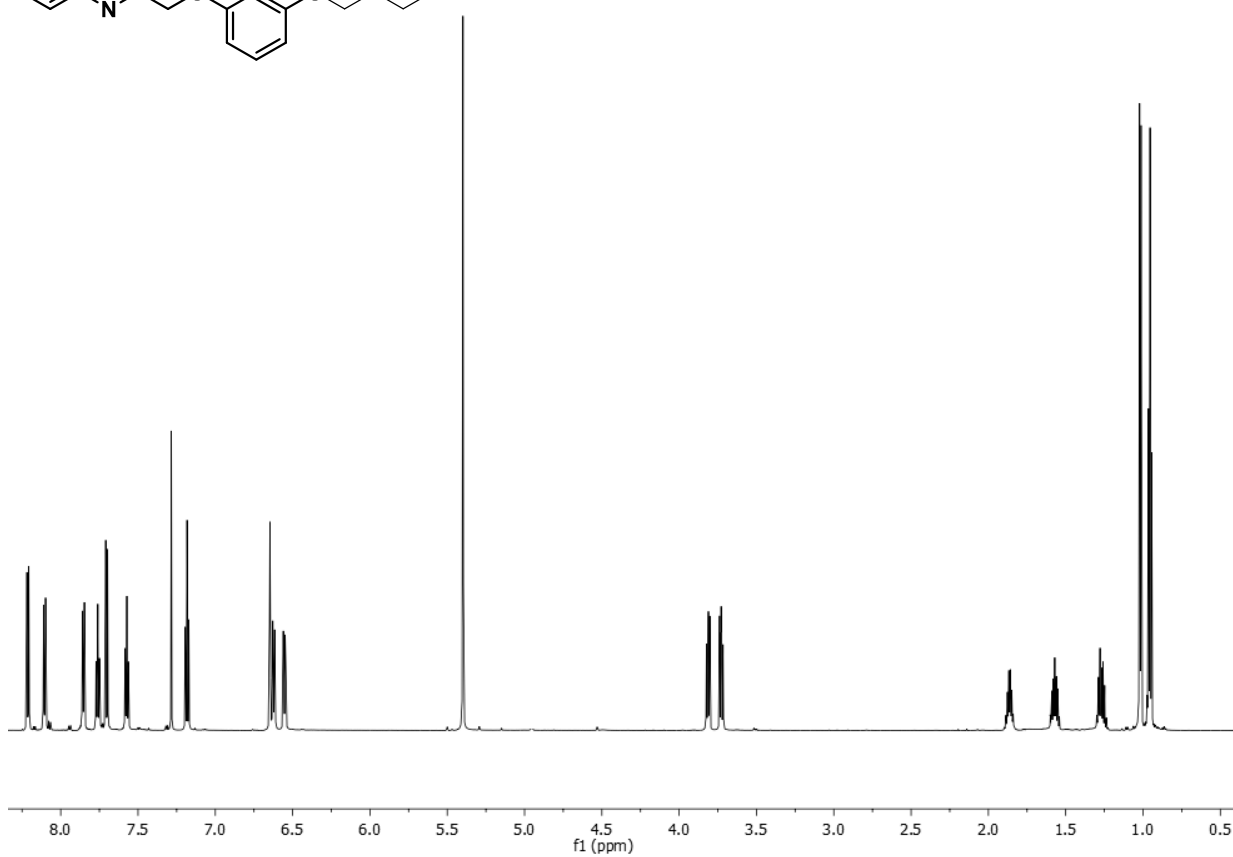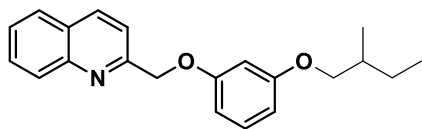
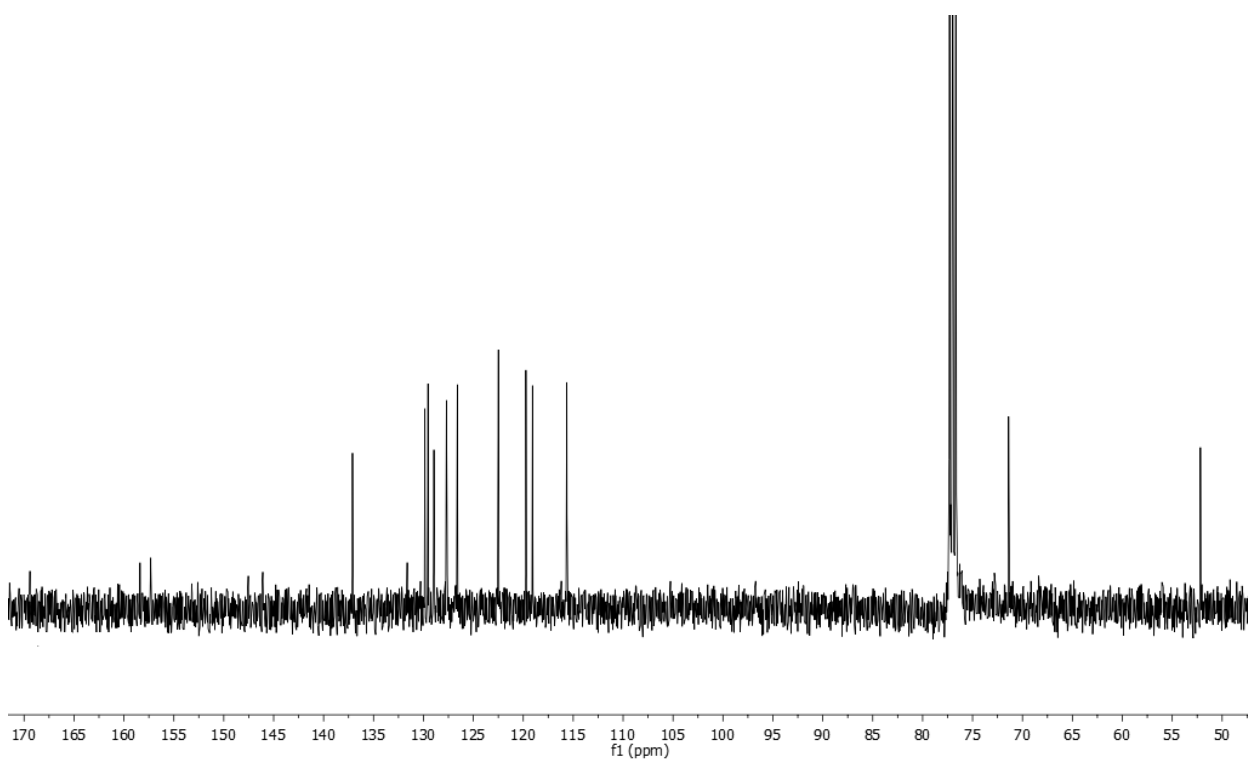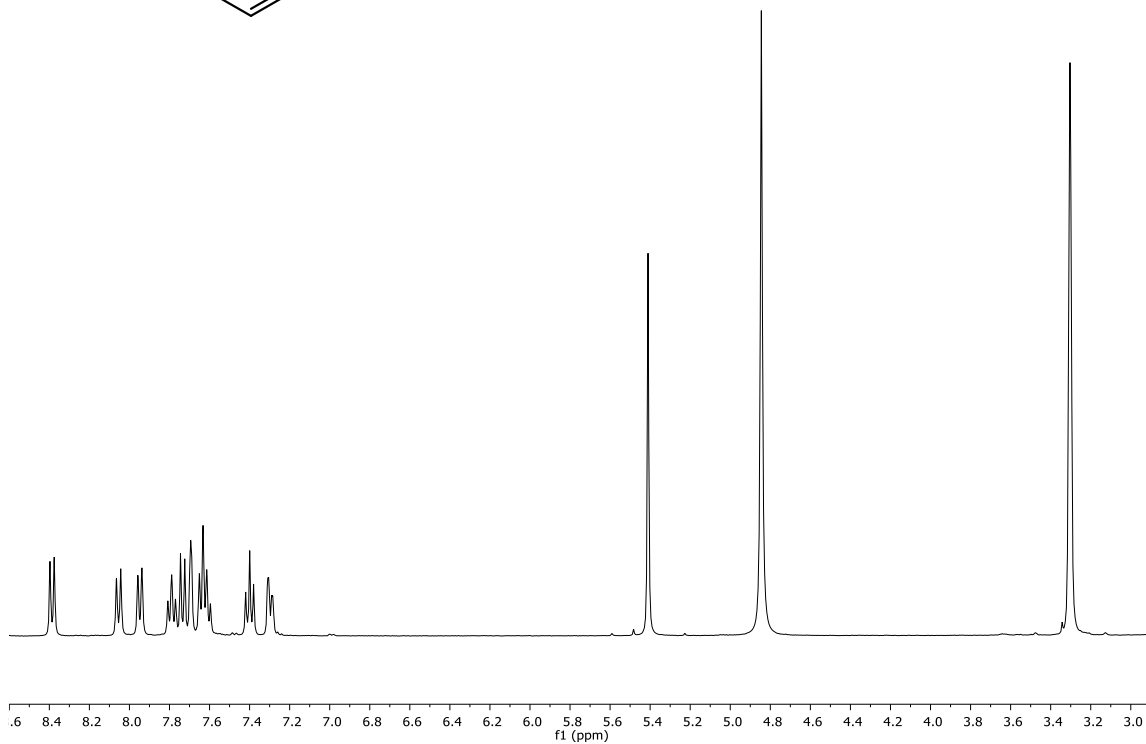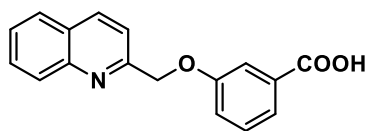^{13}C NMR (100 MHz, CDCl$_3$) of compound **53**
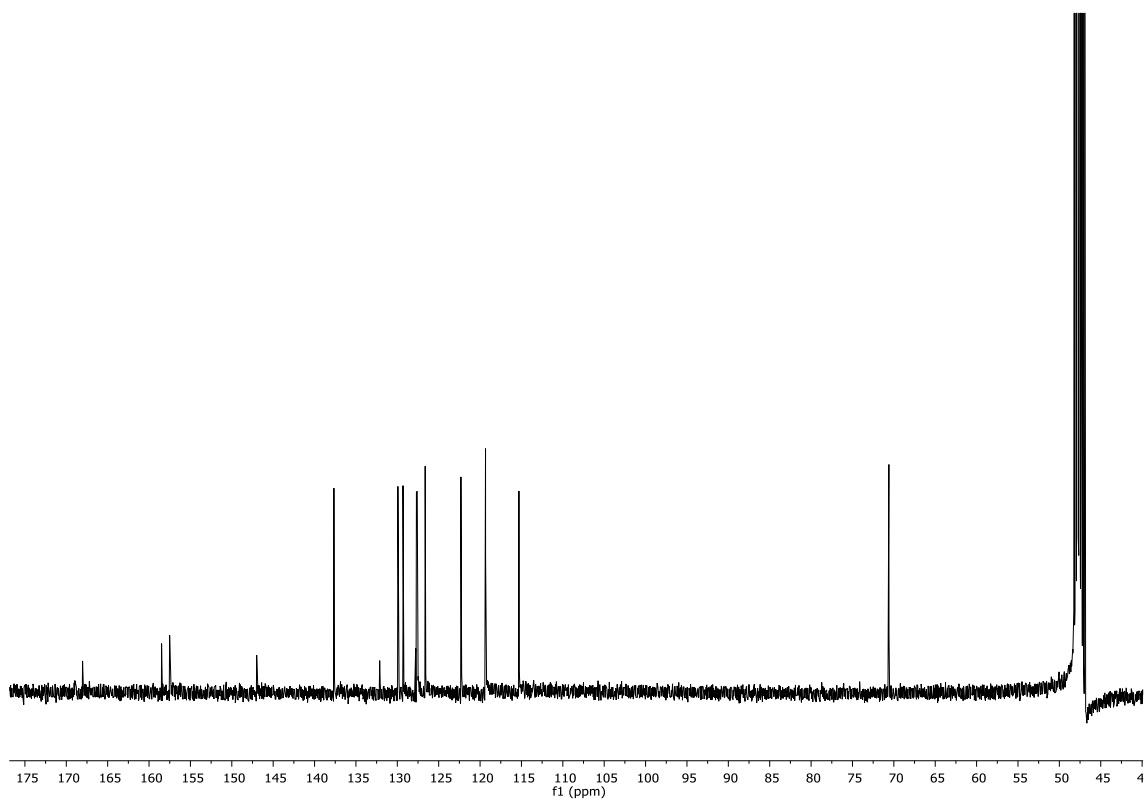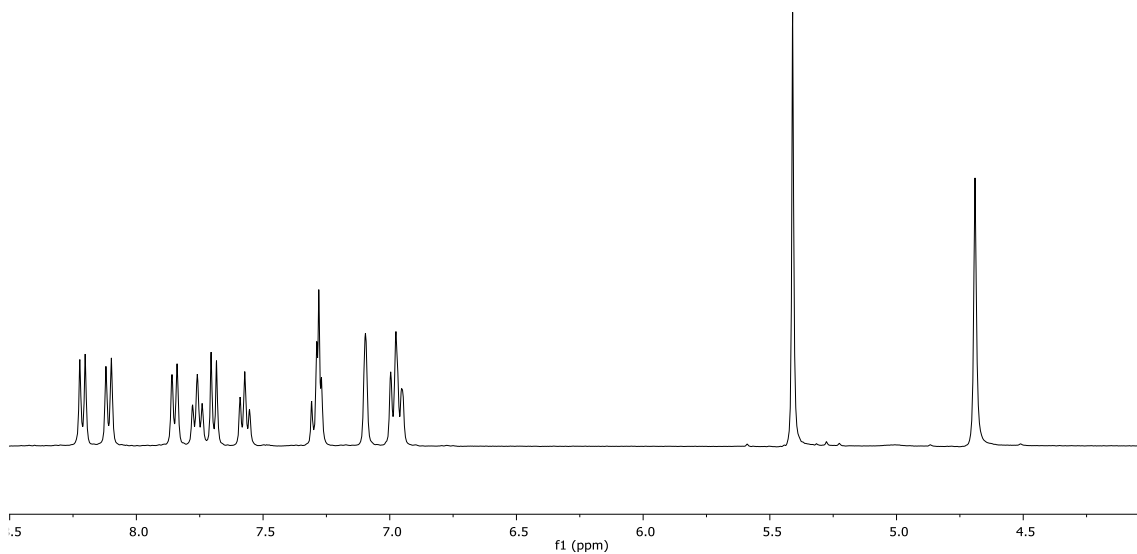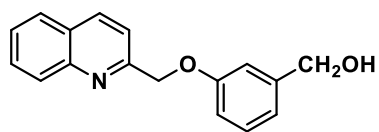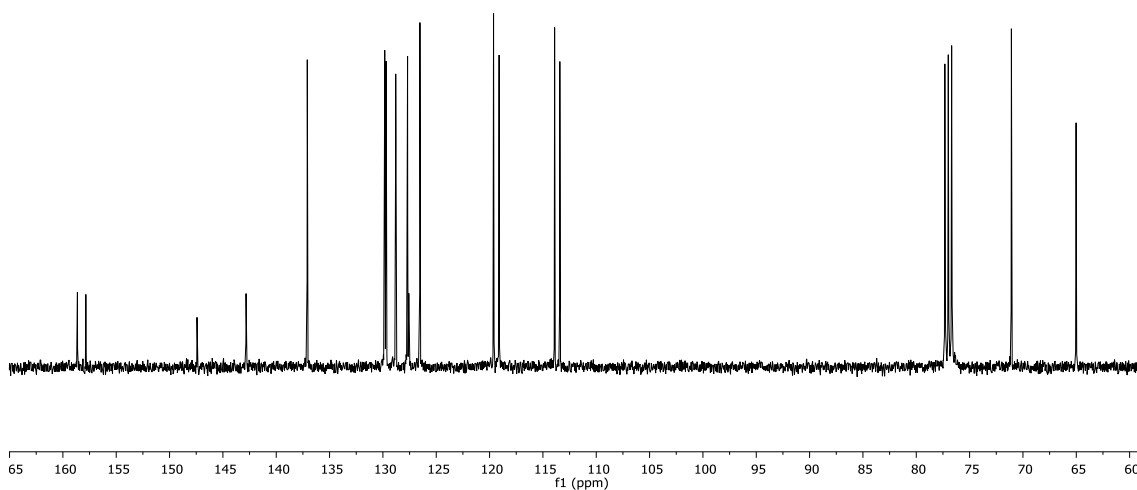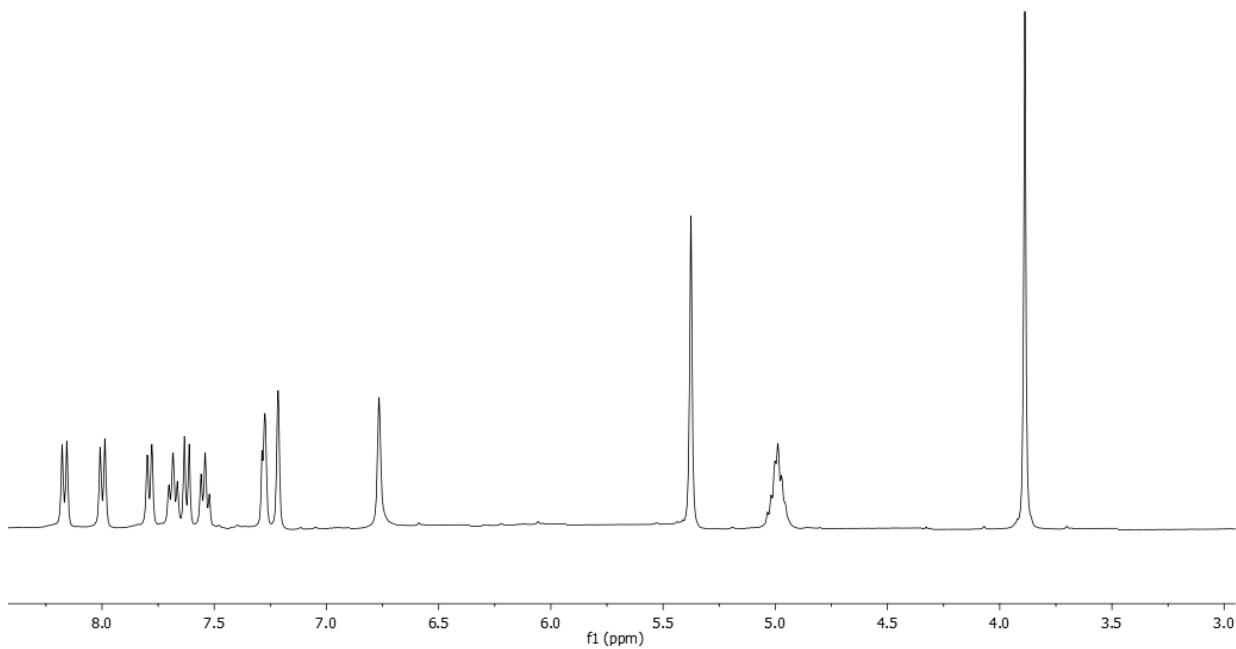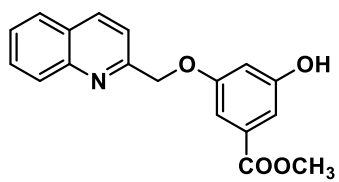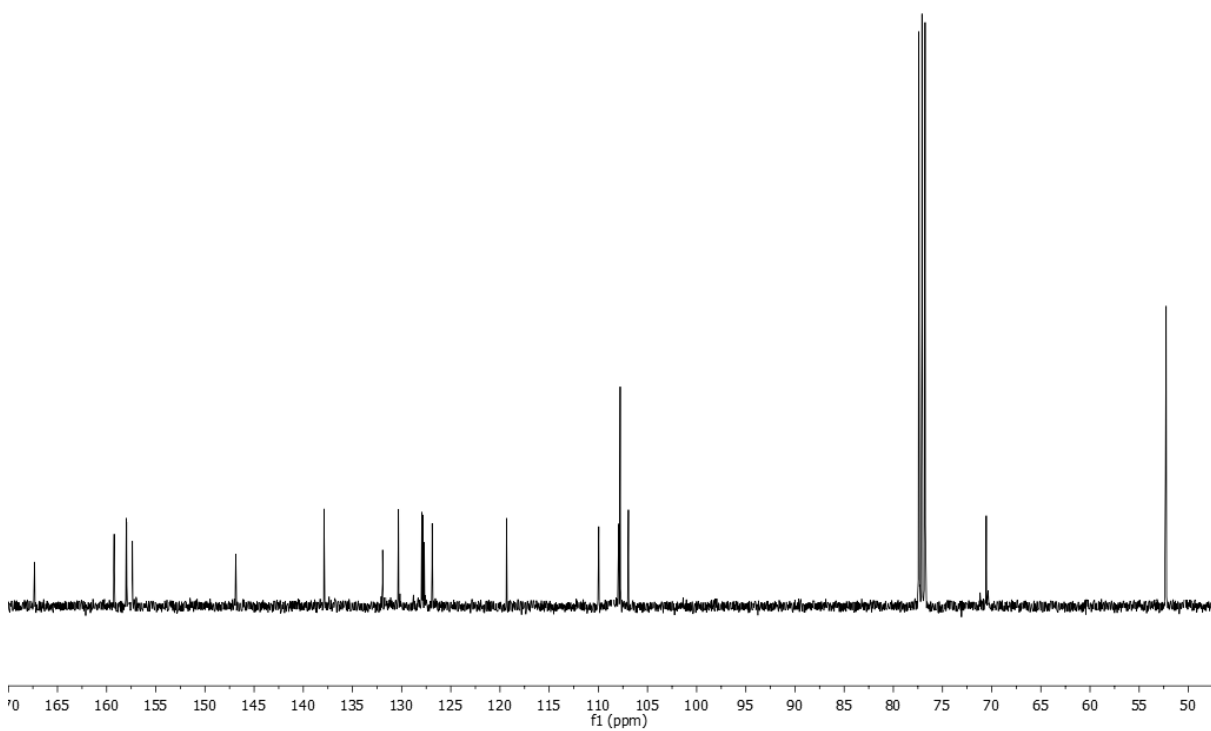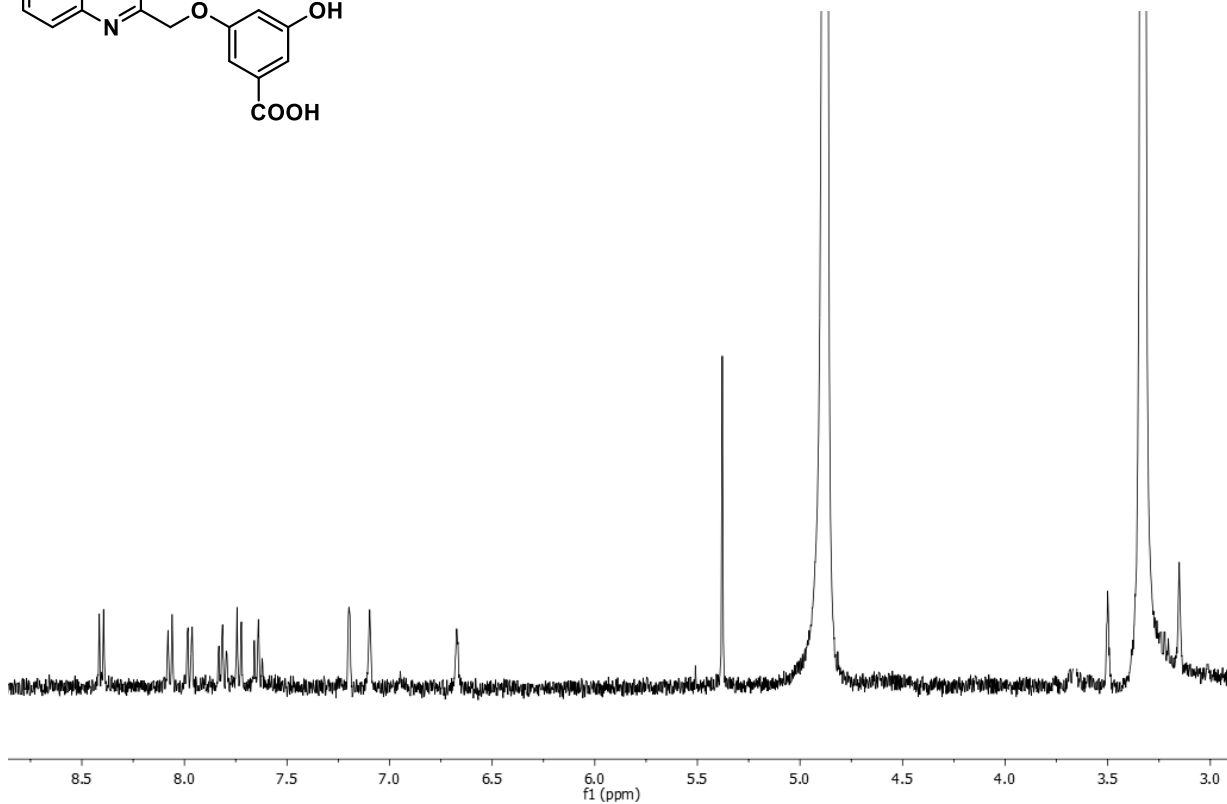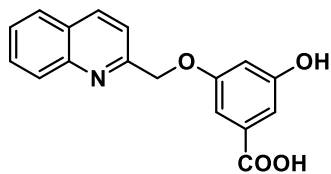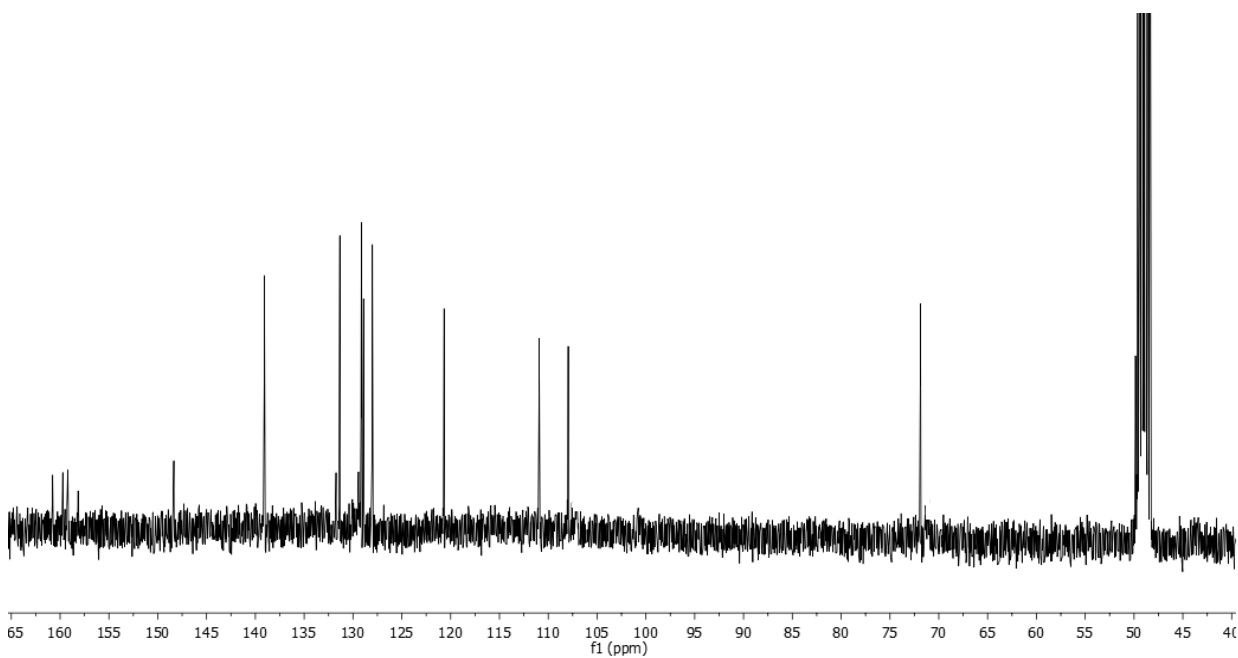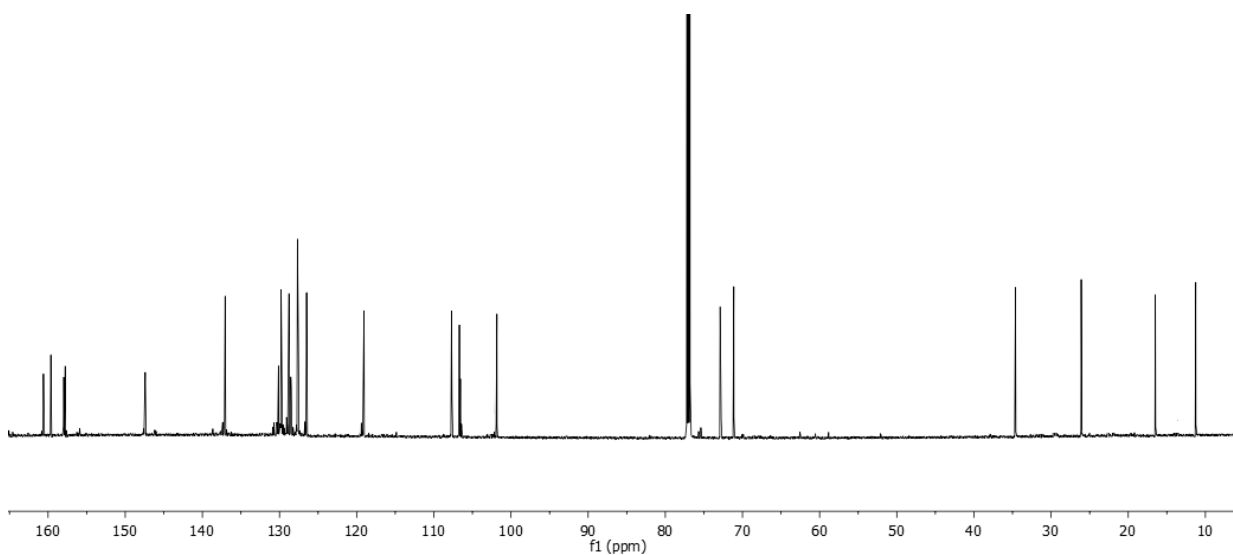
Experimental Information

^{1}H NMR (400 MHz, CDCl$_3$) of compound **54**
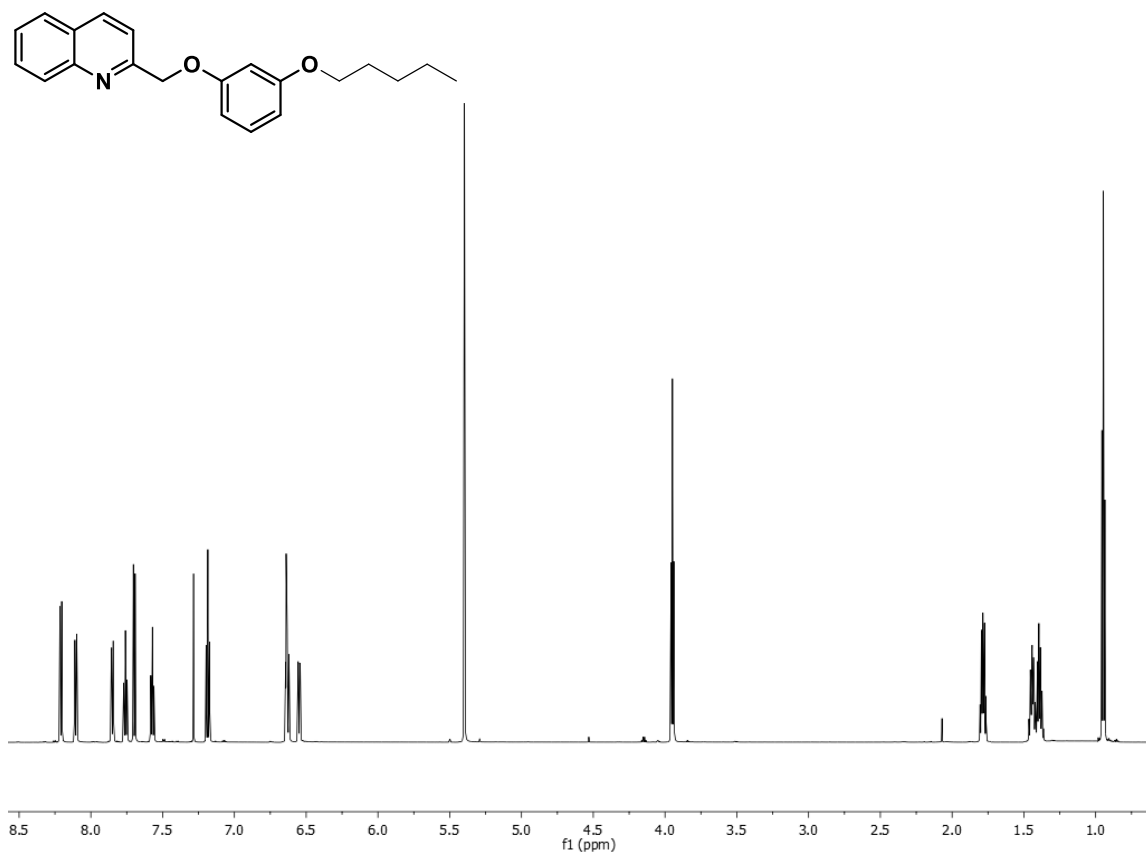
^{13}C NMR (100 MHz, CDCl$_3$) of compound **54**
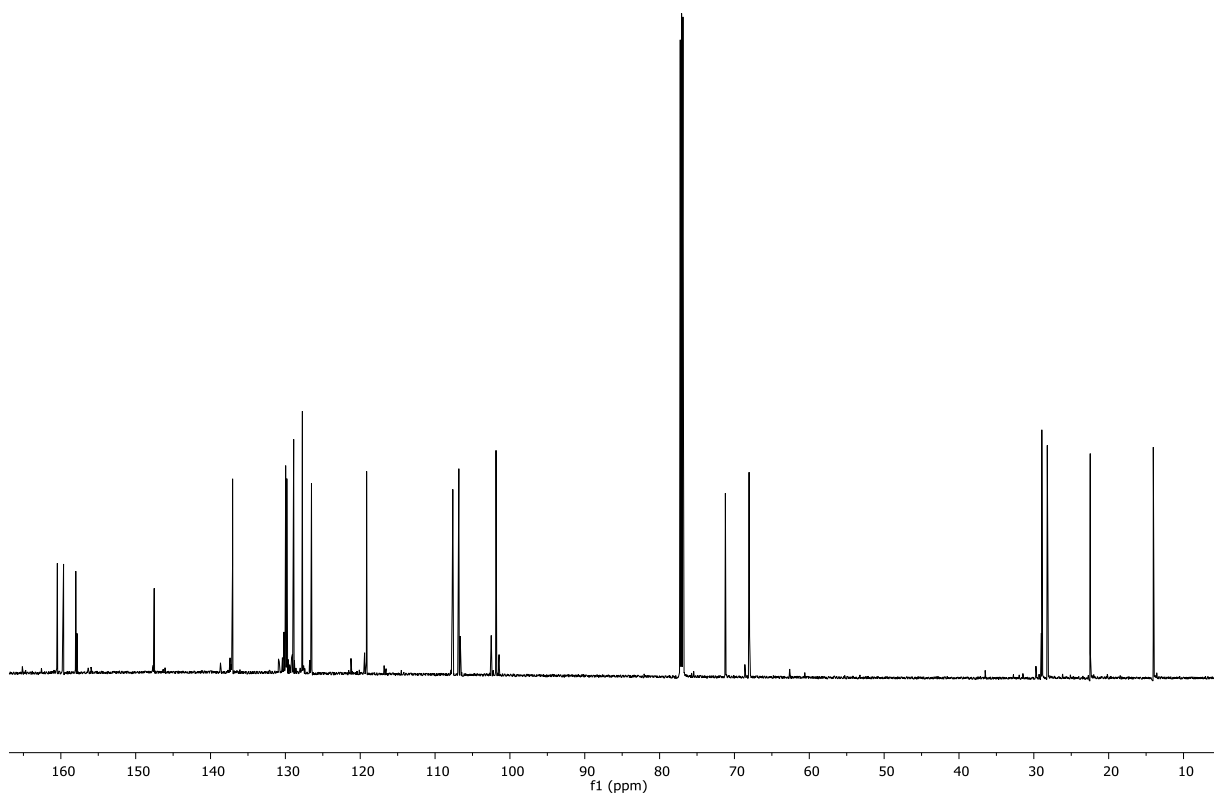
8.4. Biological Assays

Transactivation assay.

For FXR mediated transactivation, HepG2 cells were transfected with 100 ng of human pSG5-FXR, 100 ng of human pSG5-RXR, 200 ng of the reporter vector p(hsp27)-TK-LUC containing the FXR response element IR1 cloned from the promoter of heat shock protein 27 (hsp27) and with 100 ng of pGL4.70 (Promega), a vector encoding the human Renilla gene. To evaluate GPBAR1 mediated transactivation, HEK-293T cells were transfected with 200 ng of human pGL4.29 (Promega), a reporter vector containing a cAMP response element (CRE) that drives the transcription of the luciferase reporter gene luc2P, with 100 ng of pCMVSPORT6-human GPBAR1, and with 100 ng of pGL4.70. At 24 h post-transfection, cells were stimulated 18 h with 10 μM CDCA, TLCA and compounds **1-15.** After treatments, cells were lysed in 100 μL of lysis buffer (25 mM Tris-phosphate, pH 7.8; 2 mM DTT; 10% glycerol; 1% Triton X-100), and 20 μL of cellular lysate was assayed for luciferase activity using the luciferase assay system (Promega). Luminescence was measured using Glomax 20/20 luminometer (Promega). Luciferase activities were assayed and normalized with Renilla activities.

Human CysLT1 (LTD4) (h) (antagonist effect) Cellular Functional Assay.

These assays were performed at Eurofins Cerep-Panlabs (France).[22] The cells are suspended in DMEM buffer (Invitrogen), then distributed in microplates at a density of 3.104 cells/well. The fluorescent probe (Fluo4 Direct, Invitrogen) mixed with probenicid in HBSS buffer (Invitrogen) complemented with 20 mM Hepes (Invitrogen) (pH 7.4) is then added into each well and equilibrated with the cells for 60 min at 37°C then 15 min at 22°C. Thereafter, the assay plates are positioned in a microplate reader (CellLux, PerkinElmer) which is used for the addition of the test compound or HBSS buffer then 5

min later 0.1 nM LTD4 or HBSS buffer (basal control), and the measurements of changes in fluorescence intensity which varies proportionally to the free cytosolic Ca^{2+} ion concentration. The results are expressed as a percent inhibition of the control response to 0.1 nM LTD4. The standard reference antagonist is MK 571.

Dose-Response Curve.

To calculate the EC_{50} of FXR and GPBAR1, dose response curves were performed in HepG2 and HEK-293T cells transfected as described above and then treated with increasing concentrations of compounds **4-6**, **8-10** and **13-15** (from 0.5 to 50 µM). At 18 h post stimulations, cellular lysates were assayed for luciferase and Renilla activities using the Dual-Luciferase Reporter assay system (E1980, Promega). Luminescence was measured using Glomax 20/20 luminometer (Promega). Luciferase activities were normalized with Renilla activities. To calculate the IC_{50} of CysLT1R, dose response curves were performed at Eurofins Cerep-Panlabs (France).

Cell culture.

RAW264.7 cells were grown at 37 °C in D-MEM containing 10% FBS, 1% l-glutamine and 1% penicillin/streptomycin. Cells were regularly passaged to maintain exponential growth. Cell line was classically activated with LPS (100 nM, L2880; Sigma-Aldrich, St. Louis, MO), and exposed or not to **5**, **6** and **14** at the concentration of 0.1, 1, 5 and 10 µM for 16 h.

Real-Time PCR.

For cell culture total RNA was isolated from RAW264.7 cells using the TRIzol reagent according to the manufacturer's specifications (Life Technologies, Carlsbad CA). Total

RNA was further purified using Direct-zol™ RNA MiniPrep (Zymo Research, Irvine, CA), which includes an on-column DNase I treatment. The Zymo-Spin™ IIC Columns were included in the kit. After purification from genomic DNA by DNase-I treatment (Thermo Fisher Scientific, Waltam, MA), 1 μg of RNA from each sample was reverse-transcribed using random hexamer primers with Superscript-II (Thermo Fisher Scientific, Waltam, MA) in a 20 μl reaction volume; 10 ng cDNA were amplified in a 20 μl solution containing 200 nM of each primer and 10 μl of SYBR Select Master Mix (Thermo Fisher Scientific, Waltam, MA). All reactions were performed in triplicate using a Step One Plus machine (Applied Biosystem, Foster City CA). Primers were designed using the software PRIMER3 (https://bioinfo.ut.ee/primer3-0.4.0/) using published data obtained from the NCBI database.

The primer used were as following (forward and reverse):

Tnf-α (for CCAC CACGCTCTTCTGTCTA;

rev AGGGTCTGGGCCATAGAACT),

Il-1β (for GCTGAAAGCTCTCCACCTCA;

rev AGGCCACAGGTATTTTGTCG)

 Il-10 (for CCCAGAAATCAAGGAGCATT;

rev CTCTTCACCTGCT CCACTGC).

Statistical analysis.

The ANOVA followed by non parametric Mann-Whitney U test was used for statistical comparisons (*P < 0.05) using the Prism 6.0 software (GraphPad).

8.5. Physiochemical properties and pharmacokinetic characterization.

Solubility and LogD Measurements.

Each compound was dissolved in DMSO at the concentration of 10 mM. Then, ten microliters of the obtained solution were diluted either in 490 µL of PBS pH 7.4 or MeOH and maintained under agitation at 250 rpm for 24h at rt. Tubes were subsequently centrifuged for 5 min at 4000 rpm and 10 microliters of each sample were further diluted in 490 µL of MeOH and analyzed by LC-MS/MS. The ratio of mass signal area obtained in PBS and in organic solvent was then calculated and used to determine solubility of each compound.

LogD was estimated by dissolving 40 µL of selected compounds in 1960 µL of PBS pH 7.4/Octanol. After shaking the mix for 2 hours at rt, organic and aqueous phases were separated and 10 µl of each phase were withdrawn, diluted in 490 µL of MeOH and analyzed by LC-MSMS. Concentrations of products were determined by mass signal and LogD was calculated as the logarithm of the ratio of compounds concentrations in in octanol and PBS.

Metabolic Stability.

All incubations were performed under shaking at 37°C in a final volume of 0.5 mL, containing 50 mM potassium phosphate buffer (pH 7.4), all compounds were tested at the final concentration of 1 µM and 1% DMSO was used as vehicle. For microsomes assay, the incubation mixtures contained 0.15 mg of Human liver microsomes (Sigma-Aldrich, St. Louis, MO, USA) 5 mM $MgCl_2$, 1 mM NADPH, 5 mM glucose 6-phosphate, 0.4 U·mL−1 glucose 6-phosphate dehydrogenase. Aliquots were removed at 0, 5, 10, 20, 30, 40, 50, 60 min after microsomes addition. For S9 fraction analysis, the buffer contained 0.15 mg of S9 proteins (Sigma-Aldrich, St. Louis, MO, USA), 0.3 mM NADPH, 5.6 mM

glucose-6-phosphate, 0.6 units/ml glucose-6-phosphate dehydrogenase, 5.8 mM UDP-glucuronic acid, 0.05 mM acetyl-CoA, 0.5 mM dithiothreitol, 0.5 mM 3'-phosphoadenosine 5'-phosphosulfate, 1 mM glutathione, 0.2 mM acetyl carnitine, 4 units/ml carnitine acetyl transferase, 0.5 mM glycine, and 0.5 mM taurine and aliquots were removed at 0, 5, 15, 30, 45, 60, 90, 120, 150 min after S9 fraction addition. The reaction was stopped by adding 200 µL of ice-cold acetonitrile to withdrawn aliquots. After two hours, samples were centrifuged for 10 min at 10,000 rpm, and supernatants were subjected to LC-MS/MS analysis.

The slope of the linear regression of the curve obtained reporting the natural logarithm of compound area versus incubation time ($-k$) was used in the conversion to in vitro $t_{1/2}$ values by $t_{1/2} = -\ln(2)/k$. In vitro intrinsic clearance (Cl_{int} expressed as µL/min/mg) was calculated according to the following formula: Cl_{int} = volume of reaction (µL)/$t_{1/2}$ (min)/protein of liver microsomes (mg). The percentage of unmodified compound has been calculated assuming the peak area of the compound at time 0 min as 100%. Testosterone was used as a positive control for microsome and phase I enzymes, and 7-hydroxycoumarin was used as positive control for phase II enzymes.

8.6. Computational studies

Receptors and ligand preparation.

- **CysLT$_1$R.**

The crystal structure of the homo sapiens Cysteinyl leukotriene receptor 1 (PDB ID 6rz4)[98] was downloaded from the Protein Data Bank website. The soluble cytochrome b562 fragment, the co-crystallized ligand and water molecules were removed and the residue Gln274 was reconstructed. The missing 2 residues of ECL3 and the missing transmembrane helix 8 (TM8) were modeled using the Modeller 9.2 software package.[179,180] For TM8, the crystallographic structure of cysLT2 (PDB ID 6RZ6)[181] was employed as template and its secondary structure was confirmed using prediction tools PSIpred and Spider3. [182, 183] Residues protonation states were assigned in accordance with the most populated ones predicted by the H++ webserver [184] at pH 7.4. The final model was validated via 1 µs long molecular dynamics simulation. The protein was put in a box of size 10x10x12 nm and embedded in a lipid bilayer composed of cholesterol (CHL) and 1-parlmitoyl-2-oleoyl-sn-glycero-3-phosphocholine (POPC) with a 30:70 ratio using the CHARMM-GUI webserver. [185] For solvation, TIP3P water molecules were employed and a 0.150 mM concentration of NaCl was added to reach electrostatic neutrality. The simulation was performed using the Amber *ff14SB* and Lipid 17 force fields with the GROMACS 2020.4 software package. [186,187]

- **GPBAR1.**

GPBAR1 homology model reported in D'Amore *et al.*[144] was employed for docking calculations. The receptor was prepared as in Biagioli *et al.*[160]

Both the receptors were treated with the Protein Preparation Wizard [188] tool implemented in Maestro ver. 11.8.[189].

- **Ligands.**

The 3D structures of **compounds 40-54** were built using the Graphical User Graphical User Interface (GUI) of Maestro ver. 11.8. [189] The protonation state of **compounds 40-54** at pH 7.4 in water has been calculated using the Epik module.[190] Finally, **compounds 40-54** were then minimized using the OPLS 2005 force field through 2500 iteration steps of the Polak-Ribiere Conjugate Gradient (PRCG) [191] algorithm.

Docking calculations.

Preliminary docking calculations were performed using Glide and Autodock 4.2 [192,193] to reproduce the binding pose of the pranlukast ligand recently co-crystalized with $CysLT_1R$ (PDB ID 6rz4).[98] This redocking step allowed to identify the most suitable parameters and scoring function for docking of **compounds 40-54**. Considering the ability to reproduce the pranlukast crystallographic binding pose, Glide was finally employed for the docking calculations. The results were clustered and successively ranked according to the Glide Emodel and the Glide Score. Docking calculations of **compounds 40-54** on GPBAR1 were performed using the same approach described in *Biagioli et al.* [160]

In order to consider the ligand induced fit effect on the receptors' binding sites – rearrangement of residue side chains to improve interaction with the ligand -, we performed docking calculations on **5** in both GPBAR1 and $CysLT_1R$ using as structure the centroid of the most populated protein conformation during the MD calculations on the **5**/GPBAR1 and **5**/$CysLT_1R$ complex, respectively.

In detail, the docking procedure was carried out with the Glide software package, [189] using the Standard Precision (SP) algorithm of the GlideScore function [166] and the OPLS 2005 force field. [194] A grid box of $2.5 \times 1.6 \times 1.7$ nm for GPBAR1 receptor and one of $1.6 \times 2.0 \times 1.8$ nm for $CysLT_1R$ centered on the ligand binding cavity were created. A total amount of 100 poses was generated and the conformational sampling of the ligand

was enhanced by two times, as reported by the default setting of Glide. Docking conformations of **compounds 40-54** were then clustered based on their atomic RMSD. Globally, seven clusters were obtained and, among them, only the conformation included in the most populated cluster with both the Glide Emodel and GlideScore lowest-energy value was considered.

MD calculations.

MDs were performed with GROMACS suite ver. 2020.4, [195] using the Amber *ff14SB*, Lipid 17 and the General Amber Force Field (GAFF) parameters [186,196] for the protein, lipids and the ligands, respectively. The protein/ligand complexes were prepared as previously reported for CysLT$_1$R and GPBAR1 and embedded in a 30:70 CHL/POPC lipid bilayer of sizes 10x10nm. The resulting membrane was then solvated with TIP3P water and a 0.150 mM concentration of NaCl into a 10x10x12 nm box. The whole procedure was carried on using the CHARMM-GUI webserver. [185] The systems were minimized using the steepest descent algorithm in a two steps procedure. First, the protein and ligand heavy atoms were restrained, whereas water molecules and ions were left free and only the movement on the Z axis of hydroxyl group of CHL and the phosphate group of POPC was restrained. Afterward, the restraints were removed and a second round of minimization was performed. The systems were then gradually heated from 50 to 300 K using a stepwise approach of NVT/NPT simulations at fixed temperature, before increasing it by 50 K. Each NVT/NPT step lasted 1 ns. An initial restraint of 1000 kJ/mol at 50 K was applied on proteins, ligands and lipids as described for the minimization procedure. After each NVT/NPT cycle, the restraints were lowered by 160 kJ/mol. The Langevin dynamics integrator and the Berendsen barostat with semi-isotropic coupling at 1 atm were employed. After reaching 300 K, a preliminary production run of 10ns without

restraints was performed using the Langevin dynamics integrator and the Parrinello-Rahman barostat with semi-isotropic coupling at 1 atm. The same parameters were employed for the following production runs of 1 µs. In all these simulations, a time step integration of 2 fs. For the computation of electrostatic and Van der Waals interactions, the Particle-Mesh Ewald (PME) and the cutoff algorithms were used, respectively, with a threshold of 1.2 nm. The cluster analysis trajectory was carried out using the GROMACS gmx cluster tools with the GROMOS method [197] and a 0.2 nm cutoff.

WT-MetaD calculations.

 Well-tempered MetaD simulations were performed using the same protocol described for MD calculations. However, the GROMACS suite ver. 2020.4 was patched with the Plumed software package ver. 2.6.2 and the $C\alpha$ atoms of the protein structured parts (i.e. alpha helices, beta strands) were restrained around the initial conformation using a RMSD-based harmonic potential with constant 10000 kJ/mol and threshold 0.1 nm. As collective variable, the distance between the heavy atoms of the quinoline moiety and the C_β of CysLT$_1$R Arg79$^{2.60}$ was chosen. This distance CV was allowed to explore the values from 0 to 3.0 nm to limit the sampling of the free-energy landscape to the interior of the binding pocket. To do so, an upper wall with constant 10000 kJ/mol was placed at 3.0 nm of the distance CV to prevent the ligand from exiting the CysLT$_1$R cavity. A bias of 1 kJ/mol was deposited every 5 ps with a sigma of 0.05 nm and a bias factor of 15. The MetaD simulations were performed using 10 multiple walkers lasting 150 ns each, for a total of 1.5 µs of calculation.

MD trajectories were visualized using VMD software[198] and all figures were rendered by UCSF Chimera.[199]

REFERENCES

1. Newman D.J., Cragg G.M. Natural products as sources of new drugs over the 30 years from 1981 to 2010. *J Nat Prod*. 75(3):311-35 **2012**.

2. Srinivasa R. V. and Srinivas K. Modern drug discovery process: An in silico approach. *Journal of Bioinformatics and Sequence Analysis* Vol. 2(5), pp. 89-94, **2011**

3. Poupon R. "Primary Biliary Cirrhosis: A 2010 Update". *Journal of Hepatology*. 52 (5): 745–758 **2010**.

4. Hirschfield G.M., Gershwin M.E. "The Immunobiology and Pathophysiology of Primary Biliary Cirrhosis". *Annual Review of Pathology*. 8: 303–330 **2013**.

5. Dancygier, Henryk. Principles and Practice of Clinical Hepatology. Springer. pp. 895–. ISBN 978-3-642-04509-7. Retrieved 29 June **2010**.

6. Selmi C., Bowlus C.L., Gershwin L.E., Coppel R.L. "Primary Biliary Cirrhosis". *Lancet*. 377 (9777): 1600–1609 **2011**.

7. PBCers Organization. "Primary Biliary Cirrhosis Name Change Initiative"

8. Lindor K.D., Gershwin M.E., Poupon R., et al. "Primary Biliary Cirrhosis". *Hepatology*. 50 (1): 291–308 **2009**.

9. Boonstra K., Beuers U., Ponsioen C.Y. "Epidemiology of Primary Sclerosing Cholangitis and Primary Biliary Cirrhosis: A Systematic Review". *Journal of Hepatology*. 56 (5): 1181–1188 **2012**.

References

10. James O.F., Bhopal R., Howel D., et al. (1999). "Primary Biliary Cirrhosis Once Rare, Now Common in the United Kingdom?". Hepatology. 30 (2): 390–394. doi:10.1002/hep.510300213. PMID 10421645.

11. Dauphinee J.A.; Sinclair J.C. "Primary Biliary Cirrhosis". *Canadian Medical Association Journal*. 61 (1): 1–6 **1949**.

12. PBC Foundation (UK). "PBC Name Change". Retrieved 27 Jan **2017**.

13. Floreani A., Franceschet I., Cazzagon N. "Primary Biliary Cirrhosis: Overlaps with Other Autoimmune Disorders". *Seminars in Liver Disease*. 34 (3): 352–360 **2014**.

14. Liu J.Z., Almarri M.A., Gaffney D.J., et al "Dense Fine-Mapping Study Identifies New Susceptibility Loci for Primary Biliary Cirrhosis". *Nature Genetics*. 44 (10): 1137–1141 **2012**.

15. Juran B.D., Hirschfield G.M., Invernizzi P., et al. "Immunochip Analyses Identify a Novel Risk Locus for Primary Biliary Cirrhosis at 13q14, Multiple Independent Associations at Four Established Risk Loci and Epistasis Between 1p31 and 7q32 Risk Variants". *Human Molecular Genetics*. 21 (23): 5209–5221 **2012**.

16. Hitomi Y., et al. "POGLUT1, the putative effector gene driven by rs2293370 in primary biliary cholangitis susceptibility locus chromosome 3q13.33". *Sci Rep*. 9 (1): 102 **2019**.

17. Cheung A.C., Lapointe-Shaw L., Kowgier M., et al. "Combined ursodeoxycholic acid (UDCA) and fenofibrate in primary biliary cholangitis patients with incomplete UDCA response may improve outcomes". *Aliment Pharmacol Ther*. 43:283–93 **2016**.

18. "Nonalcoholic Fatty Liver Disease & NASH". *National Institute of Diabetes and Digestive and Kidney Diseases*. 7 November **2018**. Retrieved 2 April **2020**.

19. Chalasani N., Younossi Z., Lavine J.E., Charlton M., Cusi K., Rinella M., et al. "The diagnosis and management of nonalcoholic fatty liver disease: Practice guidance from the American Association for the Study of Liver Diseases" *Hepatology (Professional society guidelines)*. 67 (1): 328–357 **2018**.

20. Marjot, T; Moolla, A; Cobbold, JF; Hodson, L; Tomlinson, JW "Nonalcoholic Fatty Liver Disease in Adults: Current Concepts in Etiology, Outcomes, and Management". *Endocrine Reviews*. 41 (1): bnz009 **2020**.

21. Marchesini G, Petta S, Dalle Grave R "Diet, weight loss, and liver health in nonalcoholic fatty liver disease: Pathophysiology, evidence, and practice". *Hepatology*. 63 (6): 2032–43 **2016**.

22. Khan RS, Newsome PN "NAFLD in 2017: Novel insights into mechanisms of disease progression". *Nature Reviews. Gastroenterology & Hepatology*. 15 (2): 71–72 **2018**.

23. Neuschwander-Tetri BA "Non-alcoholic fatty liver disease". BMC Medicine. 15 (1): 45 **2017**.

24. European Association for the Study of the Liver (EASL); European Association for the Study of Diabetes (EASD); European Association for the Study of Obesity (EASO) "EASL-EASD-EASO Clinical Practice Guidelines for the management of non-alcoholic fatty liver disease". *Journal of Hepatology (Professional society guidelines)*. 64 (6): 1388–402 **2016**.

References

25. Iser D, Ryan M. "Fatty liver disease--a practical guide for GPs". *Australian Family Physician*. 42 (7): 444–7 **2013**.

26. Friedman SL, Neuschwander-Tetri BA, Rinella M, Sanyal AJ "Mechanisms of NAFLD development and therapeutic strategies". *Nature Medicine*. 24 (7): 908–922 **2018**.

27. AlKhater SA "Paediatric non-alcoholic fatty liver disease: an overview". *Obesity Reviews*. 16 (5): 393–405 **2015**.

28. Wong VW, Chan WK, Chitturi S, Chawla Y, Dan YY, Duseja A, et al. "Asia-Pacific Working Party on Non-alcoholic Fatty Liver Disease guidelines 2017-Part 1: Definition, risk factors and assessment". *Journal of Gastroenterology and Hepatology (Professional society guidelines)*. 33 (1): 70–85 **2018**.

29. "DB92 Non-alcoholic fatty liver disease". WHO. WHO. 18 June **2018**. Retrieved 2 October **2019**.

30. Rinella ME, Sanyal AJ "Management of NAFLD: a stage-based approach". *Nature Reviews. Gastroenterology & Hepatology*. 13 (4): 196–205 **2016**.

31. Tilg H, Moschen AR, Roden M "NAFLD and diabetes mellitus". *Nature Reviews. Gastroenterology & Hepatology*. 14 (1): 32–42 **2017**.

32. Younossi ZM, Koenig AB, Abdelatif D, Fazel Y, Henry L, Wymer M "Global epidemiology of nonalcoholic fatty liver disease-Meta-analytic assessment of prevalence, incidence, and outcomes". *Hepatology*. 64 (1): 73–84 **2016**.

References

33. Younossi Z, Anstee QM, Marietti M, Hardy T, Henry L, Eslam M, et al. "Global burden of NAFLD and NASH: trends, predictions, risk factors and prevention". *Nature Reviews. Gastroenterology & Hepatology*. 15 (1): 11–20 **2018**.

34. Wilson CH, Kumar S. "Caspases in metabolic disease and their therapeutic potential" *Cell Death & Differentiation* volume 25, pages1010–1024 **2018**

35. Musso G, Cassader M, Olivetti C, Rosina F, Carbone G, Gambino R "Association of obstructive sleep apnoea with the presence and severity of non-alcoholic fatty liver disease. A systematic review and meta-analysis". *Obesity Reviews*. 14 (5): 417–31 **2013**.

36. Friedman SL, Neuschwander-Tetri BA, Rinella M, Sanyal AJ "Mechanisms of NAFLD development and therapeutic strategies". *Nature Medicine*. 24 (7): 908–922 **2018.**

37. Ekstedt, M.; Hagstrom, H.; Nasr, P.; Fredrikson, M.; Stal, P.; Kechagias, S.; Hultcrantz, R. "Fibrosis Stage is the Strongest Predictor for Disease-Specific Mortality in NAFLD after up to 33 Years of Follow-Up". *Hepatology*, 61, 1547−1554 **2015**.

38. Romero FA, Jones CT, Xu Y, Fenaux M, and Halcomb RL. "The Race to Bash NASH: Emerging Targets and Drug Development in a Complex Liver Disease" *J. Med. Chem.*, 63, 5031−5073 **2020**.

39. Thorens B "Expression cloning of the pancreatic beta cell receptor for the gluco-incretin hormone glucagon-like peptide 1". *Proceedings of the National Academy of Sciences of the United States of America.* 89 (18): 8641–5 **1992**.

References

40. Dillon JS, Tanizawa Y, Wheeler MB, Leng XH, Ligon BB, Rabin DU, et al.. "Cloning and functional expression of the human glucagon-like peptide-1 (GLP-1) receptor". *Endocrinology*. 133 (4): 1907–10 **1993**.

41. Brubaker PL, Drucker DJ "Structure-function of the glucagon receptor family of G protein-coupled receptors: the glucagon, GIP, GLP-1, and GLP-2 receptors" *Receptors & Channels*. 8 (3–4): 179–88 **2002**.

42. Underwood CR, Garibay P, Knudsen LB, Hastrup S, Peters GH, Rudolph R, Reedtz-Runge S "Crystal structure of glucagon-like peptide-1 in complex with the extracellular domain of the glucagon-like peptide-1 receptor". *The Journal of Biological Chemistry*. 285 (1): 723–30 **2010**.

43. Song G, Yang D, Wang Y, de Graaf C, Zhou Q, Jiang S, et al. "Human GLP-1 receptor transmembrane domain structure in complex with allosteric modulators". *Nature*. 546 (7657): 312–315 **2017**.

44. Wootten D, Reynolds CA, Koole C, Smith KJ, Mobarec JC, Simms J, et al. "A Hydrogen-Bonded Polar Network in the Core of the Glucagon-Like Peptide-1 Receptor Is a Fulcrum for Biased Agonism: Lessons from Class B Crystal Structures". *Molecular Pharmacology*. 89 (3): 335–47 **2016**.

45. Wootten D, Reynolds CA, Smith KJ, Mobarec JC, Koole C, Savage EE, et al. "The Extracellular Surface of the GLP-1 Receptor Is a Molecular Trigger for Biased Agonism". *Cell.* 165 (7): 1632–1643 **2016**.

46. Yang D, de Graaf C, Yang L, Song G, Dai A, Cai X, et al "Structural Determinants of Binding the Seven-transmembrane Domain of the Glucagon-like

References

Peptide-1 Receptor (GLP-1R)". *The Journal of Biological Chemistry*. 291 (25): 12991–3004 **2016**.

47. Wootten D, Reynolds CA, Smith KJ, Mobarec JC, Furness SG, Miller LJ, et al. "Key interactions by conserved polar amino acids located at the transmembrane helical boundaries in Class B GPCRs modulate activation, effector specificity and biased signalling in the glucagon-like peptide-1 receptor". *Biochemical Pharmacology*. 118: 68–87 **2016**.

48. Drucker DJ, Philippe J, Mojsov S, Chick WL, Habener JF "Glucagon-like peptide I stimulates insulin gene expression and increases cyclic AMP levels in a rat islet cell line". *Proceedings of the National Academy of Sciences of the United States of America*. 84 (10): 3434–8 **1987**.

49. Holst JJ "Treatment of type 2 diabetes mellitus with agonists of the GLP-1 receptor or DPP-IV inhibitors". *Expert Opinion on Emerging Drugs*. 9 (1): 155–66 **2004**.

50. Michalik L, Auwerx J, Berger JP, Chatterjee VK, Glass CK, Gonzalez FJ, Grimaldi PA, Kadowaki T, Lazar MA, O'Rahilly S, Palmer CN, Plutzky J, Reddy JK, Spiegelman BM, Staels B, Wahli W "International Union of Pharmacology. LXI. Peroxisome proliferator-activated receptors". *Pharmacol. Rev*. 58 (4): 726–41 **2006**.

51. Dunning, Kylie R.; Anastasi, Marie R.; Zhang, Voueleng J.; Russell, Darryl L.; Robker, Rebecca L. "Regulation of Fatty Acid Oxidation in Mouse Cumulus-Oocyte Complexes during Maturation and Modulation by PPAR Agonists". *PLOS ONE*. 9 (2): e87327 **2014**.

52. Belfiore A, Genua M, Malaguarnera R. "PPAR-gamma Agonists and Their Effects on IGF-I Receptor Signaling: Implications for Cancer". *PPAR Res*. 2009: 830501 **2009**.

53. Berger J, Moller DE. "The mechanisms of action of PPARs". *Annu. Rev. Med*. 53: 409–35 **2002**.

54. Feige JN, Gelman L, Michalik L, Desvergne B, Wahli W "From molecular action to physiological outputs: peroxisome proliferator-activated receptors are nuclear receptors at the crossroads of key cellular functions". *Prog. Lipid Res*. 45 (2): 120–59 **2006**.

55. Yu S, Reddy JK). "Transcription coactivators for peroxisome proliferator-activated receptors". *Biochim. Biophys. Acta*. 1771 (8): 936–51 **2007**.

56. Hattori K, Naguro I, Runchel C, Ichijo H "The roles of ASK family proteins in stress responses and diseases". *Cell Communication and Signaling*. 7: 9 **2009**.

57. Nygaard G, Di Paolo JA, Hammaker D, Boyle DL, Budas G, Notte GT, et al. "Regulation and function of apoptosis signal-regulating kinase 1 in rheumatoid arthritis". *Biochemical Pharmacology*. 151: 282–290 **2018**.

58. Yoon KW, Cho JH, Lee JK, Kang YH, Chae JS, Kim YM, et al. "CIB1 functions as a Ca(2+)-sensitive modulator of stress-induced signaling by targeting ASK1". *PNAS*, vol. 106, no.41, 17389 –17394 **2009**.

59. Schreiner P, Neurath MF, Ng SC, El-Omar EM, Sharara AI, Kobayashi T, Hisamatsu T, Hibi T, Rogler G. "Mechanism-Based Treatment Strategies for IBD:

Cytokines, Cell Adhesion Molecules, JAK Inhibitors, Gut Flora, and More". *Inflamm Intest Dis*, 4, 79-96 **2019**.

60. Media medici/Shutterstock di Alila

61. Rampton DS, Phil D. "New treatments for inflammatory bowel disease". *World J Gastroenterol*; 4: 369-376 **1998**.

62. Sandborn WJ, Targan SR. "Biologic therapy of inflammatory bowel disease." *Gastroenterology*; 122: 1592-1608 **2002**.

63. Strober W, Fuss IJ, Blumberg RS. "Immunology of mucosalmodels of inflammation". *Ann Rev Immun*; 20: 495-549 **2002**

64. Landers CJ, Cohavy O, Misra R, Yang H, Lin Y, Braun J, Targan SR. "Selected loss of tolerance evidenced by Crohn's disease-associated immune responses to auto and microbial antigens". *Gastroenterology*; 123: 689-699 **2002**

65. Hyun JG, Mayer L "Mechanisms underlying inflammatorybowel disease" *Drug Discovery Today: Disease Mechanism*s Vol. 3, No. 4 **2006**

66. Madsen K. "Combining T cells and IL-10: A new therapy for Crohn's disease?" *Gastroenterology*; 123: 2140-2144 **2002**

67. Das KM, Farag SA. "Current medical therapy of inflammatory bowel disease". *World J Gastroenterol*; 6: 483-489 **2000**

68. Hendrickson BA., Gokhale R,. Cho JH. Clinical Aspects and Pathophysiology of Inflammatory Bowel Disease. *Clin Microbiol Rev.*, 15(1), 79-94 **2002**.

69. Kim DH, Cheon JH. Pathogenesis of Inflammatory Bowel Disease and Recent Advances in Biologic Therapies. *Immune Netw.*, 17, 25–40 **2017**.

70. Gadaleta RM, van Erpecum KJ, Oldenburg B, Willemsen ECL, Renooij W, Murzilli S, et al. Farnesoid X receptor activation inhibits inflammation and preserves the intestinal barrier in inflammatory bowel disease. *Gut,* , 60, 463–472 **2011**.

References

71. Meirer, K. et al. Inhibitors of the arachidonic acid cascade: interfering with multiple pathways. *Basic Clin. Pharmacol. Toxicol*., 114(1), 83-91 **2014**.

72. *Proceedings of the National Academy of Sciences of the United States of America.* 106 (41): 17389–94 **2009**.

73. Seol W, Choi HS, Moore DD. "Isolation of proteins that interact specifically with the retinoid X receptor: two novel orphan receptors". *Mol Endocrinol.* gennaio;9(1):72–85 **1995**.

74. Fiorucci, S.; Rizzo, G.; Donini, A.; Distrutti, E.; Santucci, L. "Targeting farnesoid X receptor for liver and metabolic disorders" *Trends in Molecular Medicine*, , 13(7):298-309 **2007**.

75. Goodwin B, Jones SA, Price RR, Watson MA, McKee DD, Moore LB, et al. "A regulatory cascade of the nuclear receptors FXR, SHP-1, and LRH-1 represses bile acid biosynthesis." *Mol Cell*.;6(3):517–26 **2000**.

76. Song K-H, Li T, Owsley E, Strom S, Chiang JYL. "Bile acids activate fibroblast growth factor 19 signaling in human hepatocytes to inhibit cholesterol 7alpha-hydroxylase gene expression". *Hepatology*.;49(1):297–305 **2009**.

77. The HDL Handbook (Third Edition), Biological Functions and Clinical Implications, Chapter MicroRNA Regulation of HDL Homeostasis XinghuiSunMark W.Feinberg **2017**

78. Makishima M, Okamoto AY, Repa JJ, Tu H, Learned RM, Luk A, et al. "Identification of a nuclear receptor for bile acids". *Science.*;284(5418):1362–5 **1999**.

79. Plass JRM, Mol O, Heegsma J, Geuken M, Faber KN, Jansen PLM, et al. "Farnesoid X receptor and bile salts are involved in transcriptional regulation of the gene encoding the human bile salt export pump". *Hepatology*.;35(3):589–96 **2002**.

80. Cariou B, Duran-Sandoval D, Kuipers F, Staels B. "Farnesoid X receptor: a new player in glucose metabolism?" *Endocrinology*.;146(3):981–3 **2005**.

81. Stojancevic M, Stankov K, Mikov M. "The impact of farnesoid X receptor activation on intestinal permeability in inflammatory bowel disease". *Can J Gastroenterol*.;26(9):631–7 **2012**.

82. Bailey AM, Zhan L, Maru D, Shureiqi I, Pickering CR, Kiriakova G, et al. "FXR silencing in human colon cancer by DNA methylation and KRAS signaling." *Am J Physiol Gastrointest Liver Physiol*.;306(1): G48–58 **2014**.

83. Rizzo, G.; et al. "The farnesoid X receptor promotes adipocyte differentiation and regulates adipose cell function in vivo". *Mol. Pharmacol*. 70, 1164-1173 **2006**.

84. Mencarelli, A.; et al. "Dissociation of intestinal and hepatic activities of FXR and LXRα supports metabolic effects of terminal ileum interposition in rodents". *Diabetes* 62, 3384-3393 **2013**.

85. Gai, Z. et al. "The effects of farnesoid X receptor activation on arachidonic acid metabolism, NF-κB signaling and hepatic inflammation." *Mol. Pharmacol*., 94, 802-811 **2018**.

86. Keitel, V. et al. "The G-protein coupled bile salt receptor TGR5 is expressed in liver sinusoidal endothelial cells". *Hepatology*, , 45, 695-704 **2007**.

References

87. Fiorucci S, Mencarelli A, Palladino G, Cipriani S. "Bile-acid-activated receptors: targeting TGR5 and farnesoid-X-receptor in lipid and glucose disorders" *REVIEW| VOLUME 30, ISSUE 11, P570-580* **2009**

88. Fiorucci, S.; Cipriani, S.; Baldelli, F.; Mencarelli, A. "Bile acid-activated receptors in the treatment of dyslipidemia and related disorders". P*rogress in Lipid Research*, , 49, 171-185 **2010**.

89. Watanabe et al. "Bile acids induce energy expenditure by promoting intracellular thyroid hormone activation". *Nature*, , 439, 484-489 **2006**.

90. Keitel, V. et al. "Expression and function of the bile acid receptor TGR5 in Kupffer cells". *Biochem. Biophys. Res. Commun*., 372, 78-84 **2008**.

91. Wallace, J.L. "Nitric oxide as a regulator of inflammatory processes". *Mem. Inst. Oswaldo Cruz*, 100(1): 5-9 **2005**.

92. Kida, T. et al. "Bile Acid Receptor TGR5 Agonism Induces NO Production and Reduces Monocyte Adhesion in Vascular Endothelial Cells". *Arteriosclerosis, Thrombosis and Vascular Biology*, , 33, 1663-1669 **2013**.

93. Guo, C.; Chen, W.D.; Wang, Y.D. "TGR5, Not Only a Metabolic Regulator." *Front Physiol*., 7:646 **2016**.

94. Alemi, F. et al. "The TGR5 receptor mediates bile acid-induced itch and analgesia". *J. Clin. Invest*. 123(4): 1513-1530 **2013**.

95. Back, M. Functional characteristics of cysteinyl-leukotriene receptor subtypes. *Life Sci*., 71, 611-622 **2002**.

96. Sarau, H.M. et al. Identification, molecular cloning, expression, and characterization of a cysteinyl leukotriene receptor. *Mol Pharmacol*., 56(6), 57-63 **1999**.

97. Proschak, E.; Heitel, P.; Kalinowsky, L.; Merk, D. Opportunities and Challenges for Fatty Acid Mimetics in Drug Discovery. *Journal of Medicinal Chemistry*, , 60, 5235-5266 **2007**.

98. Luginina A., Gusach A., Marin E., Mishin A., Brouillette R., Popov P.et al. "Structure-based mechanism of cysteinyl leukotriene receptor inhibition by antiasthmatic drugs" *Sci. Adv*.; 5 : eaax2518 **2019**.

99. Hui, Y.; Funk, C. D. "Cysteinyl leukotriene receptors". *Biochem. Pharmacol*, 64, 1549-1557 **2002**.

100. Savari, S.; Vinnakota, K.; Zhang, Y.; Sjolander, A. "Cysteinyl leukotrienes and their receptors: Bridging inflammation and colorectal cancer." *World J. Gastroenterol.*, 20(4): 968-977 **2014**.

101. Li, T.; Apte, U. "Bile Acid Metabolism and Signaling in Cholestasis, Inflammation, and Cancer." *Advances in Pharmacology*.; 74: 263–302 **2015**.

102. Rosini, G.; Cacchi, S.; Cagliati L. Chimica delle Sostanze Naturali. Complementi di Biochimica, Casa Editrice Ambrosiana, Milano, **1971**

103. Borgstrom, B.; Barrowman, J.A.; Lindstrom, M. "Roles of bile acids in intestinal lipid digestion and absorption", *Sterols and Bile Acids, Elsevier, Amsterdam*, , 405-425 **1985**.

104. Hofmann, A.F.; Mysels, K.J. "Bile Salts as Biological Surfactants", *Colloids and Surfaces*, , 30: 145-173 **1988**.

References

105. Russel, D.W.; Setchell, K.D.R. "Bile acid biosynthesis". *Biochemistry*, 31, 4737-4749 **1992**.

106. Chiang JYL. "Bile Acid Metabolism and Signaling." *Compr Physiol*. 3(3): 1191–1212 **2013**.

107. Chassaing B, Gewirtz AT, in *Physiology of the Gastrointestinal Tract* (Sixth Edition), Volume 1 **2018**

108. Parks, D.J. et al. "Bile acids: natural ligands for an orphan nuclear receptor" *Science*, , 284, 1365-1368 **1999**.

109. Kawamata, Y.; Fujii, R.; Hosoya, M.; et al. "A G Protein-coupled Receptor Responsive to Bile Acids". *J. Biol. Chem.*, 278, 9435–9440 **2003**.

110. Pellicciari R.; Fiorucci S.; Camaioni E.; Clerici C.; Costantino G.; Maloney P. R.; Morelli A.; Parks D. J.; Willson T. M. "6α-Ethyl-Chenodeoxycholic Acid (6-ECDCA), a Potent and Selective FXR Agonist Endowed with Anticholestatic Activity". *J. Med. Chem.*, , 45 (17), pp 3569–3572 **2002**.

111. Hohenester S., Oude-Elferink R.P.J., Beuers U. "Primary biliary cirrhosis". *Semin Immunopathol*. doi: 10.1007/s00281-009-0164-5 **2009**.

112. No authors listed. Review Clinical Review Report: Obeticholic Acid (Ocaliva): (Intercept Pharmaceuticals Canada, Inc.) Ottawa (ON): *Canadian Agency for Drugs and Technologies in Health*; **2017**

113. Ratziu V., Sanyal A.J., Loomba R., Rinella M., Harrison S., et al. "REGENERATE: Design of a pivotal, randomised, phase 3 study evaluating the

safety and efficacy of obeticholic acid in patients with fibrosis due to nonalcoholic steatohepatitis". *Contemp Clin Trials*. doi: 10.1016/j.cct.2019.06.017. **2019**.

114. De Marino S.; Carino A.; Masullo D.; Finamore C.; Sepe V.; Marchianò S. ; Di Leva F. S.; Limongelli V.; Fiorucci S.; Zampella A. "Epoxide functionalization on cholane side chains in the identification of G-protein coupled bile acid receptor (GPBAR1) selective agonists". *RSC Advances*, vol. 7, issue 52, pp. 32877-32885

115. Festa C, Renga B, D'Amore C, Sepe V, Finamore C, De Marino S, Carino A, Cipriani S, Monti MC, Zampella A, Fiorucci S. "Exploitation of cholane scaffold for the discovery of potent and selective farnesoid X receptor (FXR) and G-protein coupled bile acid receptor 1 (GP-BAR1) ligands". *J Med Chem*. 23;57(20):8477-95 **2014**.

116. Sepe V, Festa C, Renga B, Carino A, Cipriani S, Finamore C, Masullo D, del Gaudio F, Monti MC, Fiorucci S, Zampella A. "Insights on FXR selective modulation. Speculation on bile acid chemical space in the discovery of potent and selective agonists". *Scientific Reports* volume 6, Article number: 19008 **2016**.

117. De Marino S, Festa C, Sepe V, Zampella A. "Chemistry and Pharmacology of GPBAR1 and FXR Selective Agonists, Dual Agonists, and Antagonists". *Handb Exp Pharmacol*.;256:137-165 **2019**.

118. Festa C, De Marino S, Carino A, Sepe V, Marchianò S, Cipriani S, Di Leva FS, Limongelli V, Monti MC, Capolupo A, Distrutti E, Fiorucci S, Zampella A. "Targeting Bile Acid Receptors: Discovery of a Potent and Selective Farnesoid X Receptor Agonist as a New Lead in the Pharmacological Approach to Liver Diseases". *Frontiers in Pharmacology* (IF 4.225) Pub Date : **2017**-04-21

References

119. Sepe V, Renga B, Festa C, Finamore C, Masullo D, Carino A, Cipriani S, Distrutti E, Fiorucci S, Zampella A. "Investigation on bile acid receptor regulators. Discovery of cholanoic acid derivatives with dual G-protein coupled bile acid receptor 1 (GPBAR1) antagonistic and farnesoid X receptor (FXR) modulatory activity". *Steroids*. ;105:59-67 **2016**

120. Di Leva FS, Festa C, Renga B, Sepe V, Novellino E, Fiorucci S, Zampella A, Limongelli V. "Structure-based drug design targeting the cell membrane receptor GPBAR1: exploiting the bile acid scaffold towards selective agonism". *Scientific Reports* volume 5, Article number: 16605 **2015**

121. Sepe V, Distrutti E, Limongelli V, Fiorucci S, Zampella A. "Steroidal scaffolds as FXR and GPBAR1 ligands: from chemistry to therapeutical application". Future Medicinal Chemistry Vol. 7, No. 9

122. Sepe V, Renga B, Festa C, D'Amore C, Masullo D, Cipriani S, Di Leva FS, Monti MC, Novellino E, Limongelli V, Zampella A, Fiorucci S. "Modification on ursodeoxycholic acid (UDCA) scaffold. discovery of bile acid derivatives as selective agonists of cell-surface G-protein coupled bile acid receptor 1 (GP-BAR1)". *J Med Chem*. 25;57(18):7687-701 **2014**.

123. Sepe, V.; Festa, C.; Renga, B.; Carino, A.; Cipriani, S.; Finamore, C.; Masullo, D.; Del Gaudio, F.; Monti, M.C.; Fiorucci, S.; et al. "Insights on FXR Selective Modulation. Speculation on Bile Acid Chemical Space in the Discovery of Potent and Selective Agonists". *Sci. Rep.*, 6, 19008 **2016**

124. Renga, B.; Cipriani, S.; Carino, A.; Simonetti, M.; Zampella, A.; Fiorucci, S. "Reversal of Endothelial Dysfunction by GPBAR1 Agonism in Portal

References

Hypertension Involves a AKT/FOXOA1 Dependent Regulation of H2S Generation and Endothelin-1". *PLoS One* 10(11), e0141082 **2015**.

125. Distrutti, E.; Mencarelli, A.; Santucci, L.; Renga, B.; Orlandi, S.; et al. "The methionine connection: homocysteine and hydrogen sulfide exert opposite effects on hepatic microcirculation in rats". *Hepatology* 47, 659–667 **2008**.

126. Carino A, Cipriani S, Marchianò S, Biagioli M, Santorelli C, Donini A, Zampella A, Monti MC and Fiorucci S. "BAR502, a dual FXR and GPBAR1 agonist, promotes browning of white adipose tissue and reverses liver steatosis and fibrosis". *Scientific Reports | 7:42801* **2017**.

127. Kinzel, O.; Steeneck, C.; Schlüter, T.; Schulz, A.; Gege, C.; Hahn, U.; Hambruch, E.; Hornberger, M, et al. "Novel substituted isoxazole FXR agonists with cyclopropyl, hydroxycyclobutyl and hydroxyazetidinyl linkers: Understanding and improving key determinants of pharmacological properties." *Bioorg. Med. Chem. Lett*., 26, 3746-3753 **2016**.

128. Calkin A.C., Tontonoz P., "Transcriptional integration of metabolism by the nuclear sterol-activated receptors LXR and FXR" *Nat Rev Mol Cell Biol*. 13(4):213-24 **2012**

129. Fuchs M. "Non-Alcoholic Fatty Liver Disease: The Bile Acid-Activated Farnesoid X Receptor as an Emerging Treatment Target." *J Lipids*. 2012:934396, Article ID 934396 **2012**.

130. Lindor KD. "Farnesoid X receptor agonists for primary biliary cirrhosis" *Curr Opin Gastroenterol*. 27(3):285-8 **2011**

References

131. Adorini L, Pruzanski M, Shapiro D. "Farnesoid X receptor targeting ... steatohepatitis." *Drug Discov Today*. 17(17-18):988-97 **2012**

132. Kohli R et al. "High-fructose, medium chain trans fat diet induces liver fibrosis and elevates plasma coenzyme Q9 in a novel murine model of obesity and nonalcoholic steatohepatitis" *Hepatology*. 52(3):934-44. **2010**

133. Tully DC, Rucker PV, Chianelli D, Williams J, Vidal A, Alper PB, et al. "Discovery of Tropifexor (LJN452), a Highly Potent Non-bile Acid FXR Agonist for the Treatment of Cholestatic Liver Diseases and Nonalcoholic Steatohepatitis (NASH)". *Journal of Medicinal Chemistry*. 60 (24): 9960–9973 **2017**

134. Gege C., Kinzel O., Steeneck C., Schulz A., Kremoser C.. "Knocking on FXR's door: the "hammerhead"-structure series of FXR agonists - amphiphilic isoxazoles with potent in vitro and in vivo activities". *Curr. Top. Med. Chem.* **2014** doi: 10.2174/1568026614666141112094430

135. Hernandez E.D., Zheng L., Kim G., Fang B., Liu B., Valdez R.A., Dietrich W.F., Rucker P.V., Chianelli D., et al. "Tropifexor-Mediated Abrogation of Steatohepatitis and Fibrosis Is Associated With the Antioxidative Gene Expression Profile in Rodents". *Hepatol Commun* doi: 10.1002/hep4.1368. eCollection **2019**

136. Badman M.K., Chen J., Desai S., Vaidya S., Neelakantham S., Zhang J., Gan L., Danis K., Laffitte B., Klickstein L.B.. "Safety, Tolerability, Pharmacokinetics, and Pharmacodynamics of the Novel Non-Bile Acid FXR Agonist Tropifexor (LJN452) in Healthy Volunteers". *Clin Pharmacol Drug Dev.* **2020**. doi: 10.1002/cpdd.762. Epub 2019 Dec 10.

References

137. Meirer, K. et al. "Inhibitors of the arachidonic acid cascade: interfering with multiple pathways". *Basic Clin. Pharmacol. Toxicol.*, 114(1), 83-91 **2014**.

138. Smith LJ., Geller S, Ebright L, Glass M, and. Thyrum PT "Inhibition of Leukotriene D4-induced Bronchoconstriction in Normal Subjects by the Oral LTD4 Receptor Antagonist" lei 204,219 *Am Rev Respir Dis*; 141:988-992 **1990**

139. a)Yamaguchi T, Kohrog H, Honda I, Kawano O, Sugimoto M, Araki S and Ando M "A Novel Leukotriene Antagonist, ONO-1078, Inhibits and Reverses Human Bronchial Contraction Induced by Leukotrienes C4 and 04 and Antigen In Vitro" *Am Rev Respir Dis*; 148:823-828 **1912**; b) Baig S, Khan RA, Khan K and Rizvi N "Effectiveness and Quality of Life with Montelukast in Asthma – A double-blind randomized control trial" *Pak J Med Sci.* 35(3): 731–736 **2019**.

140. Bernstein PR. "Chemistry and Structure–Activity Relationships of Leukotriene Receptor Antagonists" *American Journal of Respiratory and Critical Care Medicine* Volume 157, Issue 6 **1998**

141. Van Inwegen RG., Khandwala A., Gordon R, Sonnino P., Coutts S. and Jolly S. "REV 5901: an orally effective peptidoleukotriene antagonist, detailed biochemical/pharmacological profile" *J. Pharmacol. Exp. Ther.*, 241 (1), pp. 117-124 **1987**

142. Savari, S.; Vinnakota, K.; Zhang, Y.; Sjolander, A. "Cysteinyl leukotrienes and their receptors: Bridging inflammation and colorectal cancer." *World J. Gastroenterol.*, 20(4): 968-977 **2014**.

143. Nielsen ST, Beninati L. and Chang J. "REV 5901 and Ly 171,883 protect rat gastric mucosa against ethanol-induced damage" *Agents and Actions,* vol. 21, 3/4 **1987**

References

144. D'Amore, C. et al. "Design, synthesis, and biological evaluation of potent dual agonists of nuclear and membrane bile acid receptors". *J. Med. Chem.* 57, 937–954 **2014**

145. Mi, L. Z. et al. "Structural basis for bile acid binding and activation of the nuclear receptor FXR". *Mol Cell.* 11, 1093–1100 **2003**

146. Finamore C, Baronissi G, Marchianò S, Di Leva FS, et al. "Introduction of Nonacidic Side Chains on 6-Ethylcholane Scaffolds in the Identification of Potent Bile Acid Receptor Agonists with Improved Pharmacokinetic Properties" *Molecules.* 16;24(6):1043 **2019**

147. Sepe, V.; Ummarino, R.; D'Auria, M.V.; et al. "Conicasterol E, a small heterodimer partner sparing farnesoid X receptor modulator endowed with a pregnane X receptor agonistic activity, from the marine sponge" *Theonella swinhoei.* *J. Med. Chem.* 55, 84-93 **2012.**

148. Alnouti, Y. "Bile Acid Sulfation: A Pathway of Bile Acid Elimination and Detoxification". *Toxicol. Sci.*, 108, 225–246 **2009**.

149. Anzini, M; Braile, C; Valenti, S; Cappelli, A; Vomero, S; Marinelli, L; Limongelli, V; Novellino, E; Betti, L; Giannaccini, G et al. "Ethyl 8-Fluoro-6-(3-nitrophenyl)-4H-imidazo[1,5-a][1,4]benzodiazepine-3-carboxylate as Novel, Highly Potent, and Safe Antianxiety Agent". *J. Med. Chem.*, 51, 4730–4743 **2008**.

150. Famiglini, V; La Regina, G; Coluccia, A; Pelliccia, S; Brancale, A; Maga, G; Crespan, E; Badia, R; Riveira-Muñoz, E; Esté, JA; et al. "Indolylaryl-sulfones Carrying a Heterocyclic Tail as Very Potent and Broad Spectrum HIV-1 Non-nucleoside Reverse Transcriptase Inhibitors." *J. Med. Chem.*, 57, 9945–9957 **2014**

References

151. Nuti E.; Casalini F.; Avramova SI.; Santamaria S.; Fabbi M.; Ferrini S.; Marinelli L.; La Pietra V.; Limongelli V.; Novellino E.; et al. "Potent Arylsulfonamide Inhibitors of Tumor Necrosis Factor- Converting Enzyme Able to Reduce Activated Leukocyte Cell Adhesion Molecule Shedding in Cancer Cell Models." *J. Med. Chem.*, 53, 2622–2635 **2010**.

152. Carino A.; Biagioli M.; Marchianò S.; Scarpelli P.; Zampella A.; Limongelli V.; Fiorucci S. "Disruption of TFG-SMAD3 Pathway by the Nuclear Receptor SHP Mediates the Antifibrotic Activities of BAR704, a Novel Highly Selective FXR Ligand". *Pharmacol. Res.*, 131, 17–31 **2018**.

153. Sepe V.; Marchianò S.; Finamore C.; Baronissi G.; Di Leva F. S.; Carino A.; Biagioli M.; Fiorucci C.; Cassiano C.; Monti M. C.; del Gaudio F.; Novellino E.; Limongelli V.; Fiorucci S.; Zampella A. "Novel Isoxazole Derivatives with Potent FXR Agonistic Activity Prevent Acetaminophen-Induces Liver Injury." *ACS Med. Chem. Lett.*, 10, 4, 407-412 **2019**

154. Cipriani S.; Carino A.; Masullo D.; Zampella A.; Distrutti E.; Fiorucci S. "Decoding the role of the nuclear receptor SHP in regulating hepatic stellate cells and liver fibrogenesis." *Sci. Rep.*, 7,41055 **2017**

155. Mitsunobu O, Yamada M. "Preparation of Esters of Carboxylic and Phosphoric Acid via Quaternary Phosphonium Salts". *BCSJ*.;40(10):2380–2 **1967**.

156. Di Leva FS; Festa C; D'Amore C; De Marino S.; Renga B; D'Auria M. V.; Novellino E; Limongelli V; Zampella A; Fiorucci S. "Binding mechanism of the farnesoid X receptor marine antagonist suvanine reveals a strategy to forestall drug

modulation on nuclear receptors. Design, synthesis, and biological evaluation of novel ligands". *J. Med. Chem.*, 56, 4701−4717 **2013**.

157. Kaplowitz, N. "Acetaminophen hepatoxicity: what do we know, what don't we know, and what do we do next?" *Hepatology*, 40, 23−26 **2004**.

158. McGill MR; Jaeschke H. "Metabolism and disposition of acetaminophen: recent advances in relation to hepatotoxicity and diagnosis." *Pharm. Res.*, 30, 2174−2187 **2013**.

159. Lee FY.; de Aguiar Vallim TQ.; Chong HK.; Zhang Y.; Liu Y.; Jones SA.; Osborne TF.; Edwards PA. "Activation of the farnesoid X receptor provides protection against acetaminophen-induced hepatic toxicity". *Mol. Endocrinol.*, 24, 1626−1636 **2010**.

160. Biagioli M, Carino A, Marchianò S, Roselli R, Di Giorgio C, Bordoni M, Fiorucci C, Sepe V, Conflitti P, Limongelli V, Distrutti E, Baldoni M, Zampella A, Fiorucci S. "Identification of cysteinyl-leukotriene-receptor 1 antagonists as ligands for the bile acid receptor GPBAR1". *Biochem Pharmacol*, 177, 113987 **2020**.

161. Sarau HM.; Ames RS.; Ellis C; Elshourbagy N; Foley JJ.; Schmidt DB.; Muccitelli RM.; Jenkins O.; Murdock PR.; Herrity NC et al. "Identification, molecular cloning, expression and characterization of a cysteinyl leukotriene receptor". *Mol. Pharmacol.*, 56, 657-663 **1999**.

162. Fiorillo B.; Sepe V.; Conflitti P.; Rosselli R.; Biagioli M.; Marchianò S.; De Luca P.; Baronissi G.; Rapacciuolo P.; Cassiano C.; Catalanotti B.; Zampella A.; Fiorucci S.; Limongelli V."Structural basis for developing multitarget compounds acting on Cysteinyl Leukotriene Receptor 1 and G-Protein coupled Bile Acid Receptor 1".*J.Med.Chem*. **2021** Submitted

163. Anzini M.; Valenti S.; Braile C.; Cappelli A.; Vomero S.; Alcaro S.; Ortuso F.; Marinelli, L.; Limongelli, V et al. "New Insight into the Central Benzodiazepine Receptor-Ligand Interactions: Design, Synthesis, Biological Evaluation, and Molecular Modeling of 3-Substituted 6-Phenyl-4H-imidazo[1,5-a][1,4]benzodiazepines and Related Compounds". *J Med Chem*, 54:5694-711 **2011**.

164. Limongelli V. "Ligand Binding Free Energy and Kinetics Calculation in 2020." *Wiley Interdiscip. Rev. Comput. Mol*. Sci. 10: e1455 **2020**.

165. Halgren TA.; Murphy RB.; Friesner RA.; Beard HS.; Frye LL.; Pollard WT.; Banks JL., "Glide: A New Approach for Rapid, Accurate Docking and Scoring. 2. Enrichment Factors in Database Screening", *J. Med. Chem.*, 47:1750–9 **2004**.

166. Friesner RA.; Banks JL.; Murphy RB.; Halgren TA.; Klicic JJ; Mainz DT.; Repasky MP.et al. "Glide: a new approach for rapid, accurate docking and scoring. 1. Method and assessment of docking accuracy. *J. Med. Chem.,* 47:1739–49 **2004**.

167. Yang F; Mao C; Guom L.; Lin J.; Ming Q.; Xiao P.; Wu X.; Shen O.; Guo S.; Shen D.; Lu R. et al "Structural basis of GPBAR activation and bile acid recognition". *Nature*, 587(7834):499-504 **2020**.

168. Chen G.; Wang X.; Ge Y.; Ma L.; Chen O.; Liu H.; Du Y.; Ye RD.; Hu H.; Ren R. "Cryo-EM structure of activated bile acids receptor TGR5 in complex with stimulatory G protein". *Signal Transduct Target Ther*., 5(1):142 **2020**.

169. Di Leva FS.; Festa C.; Carino A.; De Marino S.; Marchianò S.; Di Marino D.; Finamore C.; Monti M.C.; Zampella A.; Fiorucci S.; Limongelli V. "Discovery of ((1, 2, 4-oxadiazol-5-yl) pyrrolidin-3-yl) ureidyl derivatives as selective non-steroidal agonists of the G-protein coupled bile acid receptor-1". *Sci. Rep.,* 9: 43290 **2019**.

170. De Marino S; Carino A; Masullo D; Finamore C; Marachianò S; Cipriani S; Di Leva FS.; Catalanotti B.; Novellino E; Limongelli V; Fiorucci S; Zampella A "Hyodeoxycholic acid derivatives as liver X receptor α and G-protein-coupled bile acid receptor agonists" *Sci Rep.* 7:43290 **2017**.

171. Macchiarulo A; Gioiello A; Thomas C; Pols TWH.; Nuti R.; Ferrari C.; Giacchè N.; De Franco F.; Pruzanski M.; Auwerx J.; Schoonjans K.and Pellicciari R. "Probing the Binding Site of Bile Acids in TGR5." *ACS Med Chem Lett.* 4:1158-1162 **2013**.

172. Limongelli, V. et al. "Sampling protein motion and solvent effect during ligand binding." *Proc. Natl Acad. Sci. USA*, 109, 1467–1472 **2012**.

173. Casasnovas R.; Limongelli V.; Tiwary P.; Carloni P. and Parrinello M. "Unbinding kinetics of a p38 MAP kinase type II inhibitor from metadynamics simulations." *J. Am. Chem. Soc.*, 139, 4780–4788 **2017**.

174. Moraca F.; Amato J.; Ortuso F.; Artese A.; Pagano B.; Novellino E.; Alcaro S.; Parrinello M.; Limongelli V. "Ligand binding to telomeric G-quadruplex DNA investigated by funnel-metadynamics simulations". *Proc. Natl Acad. Soc. USA*, 114, E2136–E2145 **2017**.

175. Limongelli V.; Bonomi M.; Parrinello M. "Funnel metadynamics as accurate binding free-energy method". *Proc Natl Acad Sci U. S. A.*, 110, 6358-6363 **2013**.

176. Saleh N.; Ibrahim P.; Saladino G.; Gervasio FL.; Clark T. "An Efficient Metadynamics-Based Protocol To Model the Binding Affinity and the Transition State Ensemble of G-Protein-Coupled Receptor Ligands." *J Chem Inf Model*, 57(5):1210-1217 **2017**.

177. Raniolo S.; Limongelli V. "Ligand binding free-energy calculations with Funnel Metadynamics". *Nat Protoc*. 15: 2837-2866 **2020**.

References

178. Glide; Schrödinger, LLC: New York, NY, USA, **2018**.

179. Webb B.; Sali A. "Comparative Protein Structure Modeling Using MODELLER." *Current Protocols in Bioinformatics*, 5.6.1-5.6.37 **2016**

180. Fiser, a.; Do, R.K.; Sali, A. "Modeling of loops in protein structures" *Protein Sci.*, 9:1753-1773 **2000**.

181. Gusach A.; Luginina A.; Marin E.; et al. "Structural basis of ligand selectivity and disease mutations in cysteinyl leukotriene receptors" *Nat. Commun.,* 10:5573 **2019**

182. Buchan DWA. and Jones DT. "The PSIPRED Protein Analysis Workbench: 20 years on." *Nucleic Acids Res.*, 47:W402–W407 **2019**.

183. Heffernan R; Paliwal K; Lyons J.; Singh J.; Yang Y.; Zhou Y. "Single-sequence-based prediction of protein secondary structures and solvent accessibility by deep whole-sequence learning." *J. Comput. Chem.*, 39:2210–2216 **2018**.

184. Anandakrishnan R.; Aguilar B. and Onufriev AV. "H++ 3.0: automating pK prediction and the preparation of biomolecular structures for atomistic molecular modeling and simulations." *Nucleic Acids Res.*, 40:W537–W541 **2012**.

185. Jo S.; Kim T.; Iyer VG. and Im W. "CHARMM-GUI: A Web-based Graphical User Interface for CHARMM." *J. Comput. Chem.*, 29:1859-1865 **2008**.

186. Maier JA.; Martinez C.; Kasavajhala K.; Wickstrom L.; Hauser KE.; Simmerling C. "ff14SB: Improving the Accuracy of Protein Side Chain and Backbone Parameters from ff99SB." *J. Chem. Theory Comput.*, , 11:3696–3713 **2015**.

187. Abraham MJ. et al. "GROMACS: High performance molecular simulations through multilevel parallelism from laptops to supercomputers". *SoftwareX*, 1–2, 19–25 **2015**.

188. Sastry GM.; Adzhigirey M; Day T; Annabhimoju R; Sherman W "Protein and ligand preparation: parameters, protocols, and influence on virtual screening enrichments." *J. Comput. Aided Mol. Des*., 27:221-34 **2013**.

189. Schrödinger Release 2019-1: Maestro, New York, NY: Schrödinger, LLC, **2019**

190. Shelley JC.; Cholleti A; Frye LL.; Greenwood JR.; Timlin MR.; Uchimaya M "Epik: a software program for pKa prediction and protonation state generation for drug-like molecules." *J. Comput. Aided Mol. Des*., 21:681-91 **2007**.

191. Grippo L. and Lucidi S. "A globally convergent version of the Polak-Ribière conjugate gradient method." *Mathematical Programming*, 78:375–391 **1997**.

192. Huey R.; Morris GM.; Olson AJ. and Goodsell DS. "A Semiempirical Free Energy Force Field with Charge-Based Desolvation." *J. Computational Chemistry*, 28:1145-1152 **2007**.

193. Morris GM.; Huey R; Lindstrom W.; Sanner MF.; Belew RK.; Goodsell DS. and Olson AJ. "Autodock4 and AutoDockTools4: automated docking with selective receptor flexibility." *J. Computational Chemistry*, 16:2785-91 **2009**.

194. Banks JL.; Beard HS.; Cao Y.; Cho AE.; Damm W.; Farid R.; Felts AK.; Halgren TA.; Mainz DT.; Maple JR.; Murphy R.; et al. "Integrated Modeling Program, Applied Chemical Theory (IMPACT)." *J. Comput. Chem*., 26:1752-80 **2005**.

195. Pronk S.; Pall S.; Schulz R.; Larsson P.; Bjelkmar P.; Apostolov R.; Shirts MR. "GROMACS 4.5: A high-throughput and highly parallel open source molecular simulation toolkit." *Bioinformatics,* 29:845–854 **2013**.

196. Wang J.; Wolf RM.; Caldwell JW.; Kollman PA. and Case DA. "Development and testing of a general Amber force field". J. *Comput. Chem*., 25(9):1157-74 **2004**.

197. Daura X.; van Gunsteren WF; Jaun B.; Mark AE.; Gademann K.; Seebach D. "Peptide Folding: When Simulation Meets Experiment." *Angew. Chemie Int. Ed.*, 38 (1/2), 236-240 **1999**.

198. Humphrey W.; Dalke A. and Schulten K. "VMD - Visual Molecular Dynamics." *J. Molec. Graphics*, 14.1, 33-38 **1996**.

199. Pettersen EF.; Goddard TD.; Huang CC.; Couch GS.; Greenblatt DM.; Meng EC.; Ferrin TE. "UCSF Chimera—a visualization system for exploratory research and analysis." *J Comput Chem.*, 25(13):1605-12 **2004**.

ABBREVIATIONS

- **AMINOACIDS:**
  - Alanine (**Ala**)
  - Arginine (**Arg**)
  - Asparagine (**Asn**)
  - Aspartic acid (**Asp**)
  - Cysteine (**Cys**)
  - Glutamine (**Gln**)
  - Glutamic acid (**Glu**)
  - Glycine (**Gly**)
  - Histidine (**His**)
  - Isoleucine (**Ile**)
  - Leucine (**Leu**)
  - Lysine (**Lys**)
  - Methionine (**Met**)
  - Phenylalanine (**Phe**)
  - Proline (**Pro**)
  - Pyrrolysine (**Pyl**)
  - Serine (**Ser**)
  - Selenocysteine (**Sec**)
  - Threonine (**Thr**)
  - Tryptophan (**Trp**)
  - Tyrosine (**Tyr**)
  - Valine (**Val**)

- ATP-binding cassette-A1 (**ABCA1**)

- Absorption, distribution, metabolism, and excretion (**ADME**)

- Aldo-keto reductase family 1 member D1 (**AKR1D1**)

- Acetaminophen (**APAP**)

- Apolipoprotein A1 (**ApoA-I**)

- Apoptosis signal-regulating kinase 1 (**ASK1**)

- Adenosine triphosphate (**ATP**)

- Bile salt export pump (**BSEP**)

- Cholic acid (**CA**)

- Cyclic adenosine monophosphate (**cAMP**)

- C-terminal coiled-coil domain (**CCC**)

- Crohn's disease (**CD**)

- Chenodeoxycholic acid (**CDCA**)

- Intrinsic clearance (**Cl_{int}**)

- Calcium and integrin binding protein 1 (**CIB1**)

- Cyclooxygenase (**COX**)

- cAMP response element-binding protein (**CREB**)

- Cystathione-γ-lyase (**CSE**)

- Cysteinyl leukotriene receptor 1 (**$CysLT_1R$**)

- Deiodinase enzyme (**D2**)

- Deoxycholic acid (**DCA**)

- Di-isopropyl azodicarboxylate (**DIAD**)

- Dichloromethane (**CH_2Cl_2**)

- Di-isobutyl aluminium hydride (**DIBAL-H**)

- Extracellular domain (**ECD**)

Abbreviations

- Endothelial nitric oxide synthase enzyme (**eNOS**)

- Extracellular signal-regulated kinase (**Erk**)

- Endothelin (**ET**)

- 6-Ethylchenodeoxycholic acid (**6-ECDCA or INT-747 or obeticholic acid or**

- **OCA or OCAliva**)

- Food and drug administration (**FDA**)

- Fibroblast growth factor (**FGF-19**)

- Fibroblast growth factor receptor (**FGFR**)

- Fluorescence Resonance Energy Transfer (**FRET**)

- Farnesoid X receptor (**FXR**)

- Glucagon-like hormone (**GLP-1**)

- Glucagon-like peptide-1 receptor (**GLP1R**)

- Glycogen synthase kinase 3 beta (**GSK-3β**)

- Nucleotide guanosine triphosphate (**GTP**)

- High Density Lipoprotein (**HDL**)

- High-fat diet (**HFD**)

- Hepatocyte nuclear factor 4 alpha (**HNF4α**)

- Hydroperoxyl-eicosatetraenoic acid (**HPETE**)

- Inflammatory bowel disease (**IBD**)

- Intercellular Adhesion Molecule 1 (**ICAM-1**)

- Interferon (**IFN**)

- Interleukin (**IL**)

- c-Jun N-terminal kinase (**JNK**)

- 7-Ketolithocholic acid (**7-KLCA**)

- Lithocholic acid (**LCA**)

- Liquid chromatography-mass spectrometry (**LC-MS**)

- Ligand binding domain (**LDB**)

- Low density lipoprotein (**LDL**)

- Lithium borohydride (**LiBH$_4$**)

- Lithium Carbonate (**Li$_2$CO$_3$**)

- Lithium Bromide (**LiBr**)

- LJN452 (**Tropifexor**, **LMB763**)

- Lipoxygenases (**LO**)

- Liver Homolog Receptor-1 (**LRH-1**)

- Liver sinusoidal endothelial cell (**LSEC**)

- Leukotriene (**LT**)

- Mitogen-activated protein kinase (**MAPK**)

- Mitogen-activated protein kinase-kinase-kinase 5 (**MAP3K5**)

- Methanol (**MeOH, CH$_3$OH**)

- Sodium Boronhydride (**NaBH$_4$**)

- Non-alcoholic fatty liver (**NALF**)

- Non-alcoholic fatty liver disease (**NAFLD**)

- Sodium Hydroxyde (**NaOH**)

- Non-Alcoholic SteatoHepatitis (**NASH**)

- N-terminal coiled-coil domain (**NCC**)

- Nuclear receptor co-repressor 1 (**N-CoR**)

- Norepinephrine (**NE**)

- Nuclear factor kappa-light-chain-enhancer of activated B cells (**NF-κB**)

- Nitric oxide (**NO**)

- Nuclear Receptor (**NR**)

- The sodium taurocholate cotransporting polypeptide (**NTCP**)

- Organic anion transporting polypeptides (**OATPs**)

- The organic solute transporter alpha-beta (**OSTα-OSTβ**)

- Primary Biliary Cholangitis (**PBC**)

- Palladium Hydroxyde on Carbon (**Pd(OH)$_2$/C**)

- Protein kinase A (**PKA**)

- Protein kinase B (**PKB**)

- Peroxisome proliferator-activated receptor (**PPARs**)

- Triphenylphosphine (**PPh$_3$**)

- Peroxisome proliferator hormone response elements (**PPREs**)

- Rational drug design (**RDD**)

- Reverse transcriptase-polymerase chain reaction (**RT-PCR**)

- Retinoid-X-Receptor (**RXR**)

- Structure-based drug design (**SBDD**)

- Small heterodimer partner (**SHP**)

- non-synonymous single-nucleotide polymorphisms (**SNPs**)

- Steroid receptor coactivator 1 (**SRC-1**)

- Half-life (**t$_{1/2}$**)

- Transforming growth factor-beta (**TGF-β**)

- T-helper-1 (**Th1**)

- Tetrahydrofurane (**THF**)

- Taurolithocholic acid (**TLCA**)

- Transmembrane (**TM**)

- Transmembrane domain (**TMD**)

- Tumor factor-α (**TNF-α**)

- Thioredoxin (**Trx**)

- TNF-α receptor-associated factor 2 (**TRAF2**)

- ulcerative colitis (**UC**)

- Ursodeoxycholic acid (**UDCA**)

- Yeast Artificial Chromosome (**YAC**)

CURRICULUM VITAE
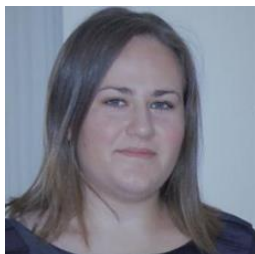
Giuliana Baronissi

University of Naples Federico II

giuliana.baronissi@unina.it

Giuliana Baronissi obtained a Master's Degree in Pharmacy in July 2017 at the University of Naples "Federico II", Department of Pharmacy and she discussed an experimental thesis entitled: « Epoxide functionalization on cholane side chains in the identification of G-protein coupled bile acid receptor (GPBAR1) selective agonists.»

In 2018 she entered the XXXIII cycle of the PhD program in Pharmaceutical Sciences, Dept. of Pharmacy in Naples. Her research is focused on Organic Chemistry, in particular her field of interest concerns the synthesis of steroidal and non-steroidal modulators of human receptors.

UNIVERSITY CAREER:

2018-present: PhD student in Pharmaceutical Sciences, University "Federico II", Naples.

2017: Master's Degree in Pharmacy.

PUBBLICATION

- Finamore C., Baronissi G., Marchianò S., Di Leva F. S., Carino A., Monti M. C., Limongelli V., Zampella A., Fiorucci S., Sepe V. Introduction of Nonacidic Side Chains on 6-Ethylcholane Scaffolds in the Identification of Potent Bile Acid Receptor Agonists with Improved Pharmacokinetic Properties *Molecules*. **2019** Mar 16;24(6):1043

- Sepe V.; Marchianò S.; Finamore C.; Baronissi G.; Di Leva F. S.; Carino A.; Biagioli M.; Fiorucci C.; Cassiano C.; Monti M. C.; del Gaudio F.; Novellino E.; Limongelli V.; Fiorucci S.; Zampella A. Novel Isoxazole Derivatives with Potent FXR Agonistic Activity Prevent Acetaminophen-Induces Liver Injury. *ACS Med. Chem. Lett.* **2019**, 10, 4, 407-412

- Fiorillo B., Sepe V., Conflitti P., Roselli R., Baronissi G., Cassiano C., Catalanotti B., Zampella A., Limongelli V., Fiorucci S. Structural basis for developing multitarget compounds acting on Cysteinyl Leukotriene Receptor 1 and G-Protein coupled Bile Acid Receptor 1. (**Manuscript in progress**)

-

POSTER AND ORAL COMMUNICATIONS

Poster communication:

- Design, synthesis and pharmacological characterization of novel potent non-steroidal agonists of the farnesoid X receptor - "Paul Ehrlich Euro-PhD Network & MuTaLig COST Action meeting 2019" – 13th June-15th June, Catanzaro, Italy
- Design and Synthesis of Novel Quinoline Derivatives for the Treatment of Inflammatory Bowel Disease. - 1st Virtual Symposium for Young Organic Chemists, 29th October and 3th-6th November 2020 on Twitter

Short Oral Communication:

Design, synthesis and pharmacological characterization of novel potent non-steroidal agonists of the farnesoid X receptor - "Paul Ehrlich Euro-PhD Network & MuTaLig COST Action meeting 2019" – 13th June-15th June, Catanzaro, Italy